



TRACING METABOLIC PATHWAYS
IN A SPECTRUM OF INHERITED DISEASES

disorders of the malate-aspartate shuttle
and rare hereditary anemias

Melissa H. Broeks

TRACING METABOLIC PATHWAYS IN A SPECTRUM OF INHERITED DISEASES

disorders of the malate-aspartate shuttle
and rare hereditary anemias

Melissa H. Broeks

Cover idea and design: Melissa, image generated using DALL-E 2 by OpenAI
Lay-out and thesis printing: Proefschrift-AIO.nl

ISBN: 978-94-93353-17-6

DOI: <https://doi.org/10.33540/876>

© M.H. Broeks, 2023. All rights reserved.

No part of this thesis may be reproduced, stored in a retrieval system or transmitted in any form or by any means without prior written permission from the author or, when appropriate, from the publisher.

Tracing metabolic pathways in a spectrum of inherited diseases

disorders of the malate-aspartate shuttle
and rare hereditary anemias

Het traceren van metabole routes in een spectrum van erfelijke ziekten

aandoeningen van de malaat-aspartaat shuttle en zeldzame
erfelijke bloedarmoedes
(met een samenvatting in het Nederlands)

Proefschrift

ter verkrijging van de graad van doctor aan de
Universiteit Utrecht
op gezag van de
rector magnificus, prof. dr. H.R.B.M. Kummeling,
ingevolge op het besluit van het college voor promoties
in het openbaar te verdedigen op

donderdag 12 oktober 2023 des middags te 12.15 uur

door

Melissa Henrike Broeks

geboren op 23 september 1994
te Zwolle

Promotor:

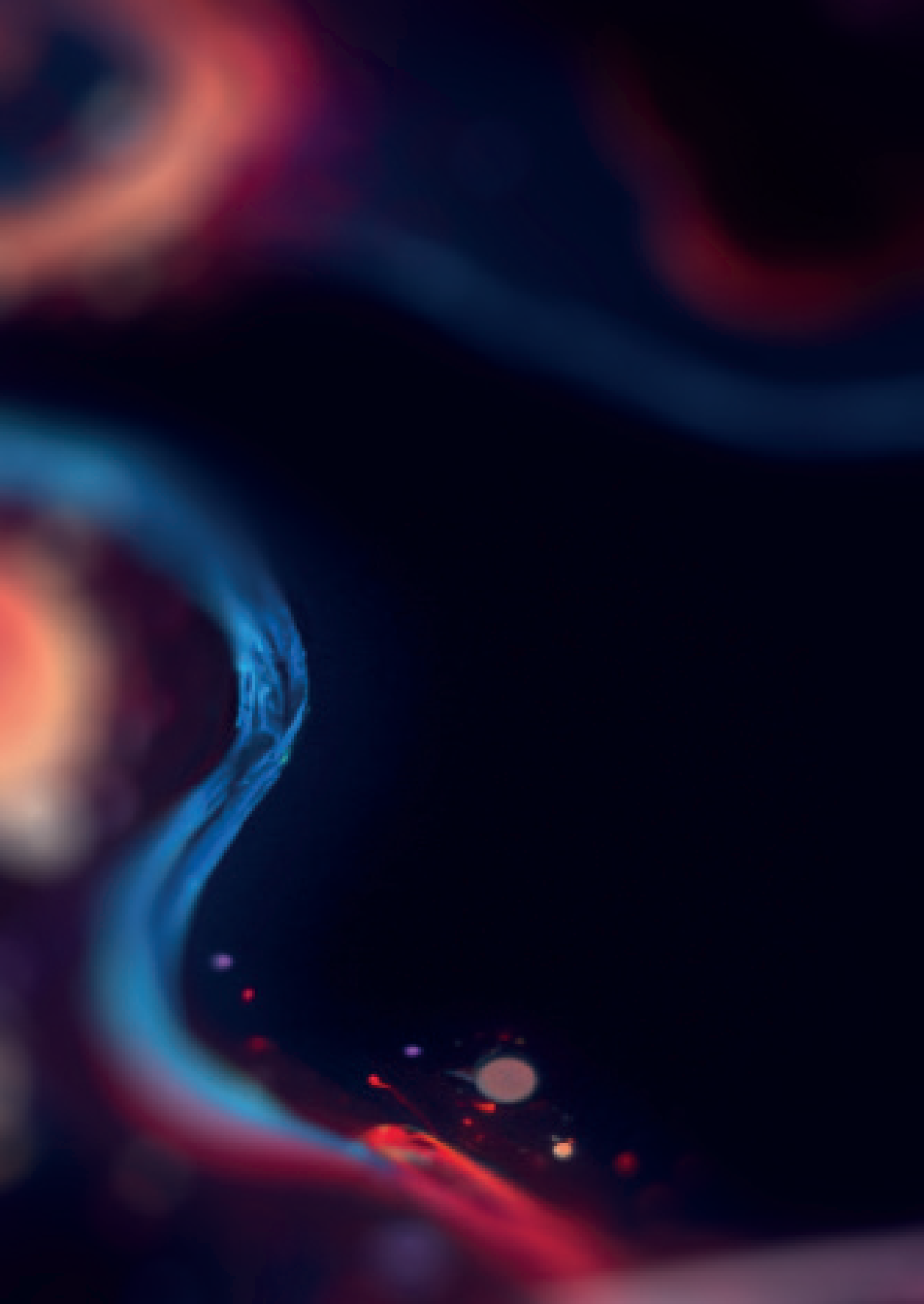
Prof. dr. N.M. Verhoeven-Duif

Copromotor:

Dr. J.J.M. Jans

Table of contents

Chapter 1	General introduction and thesis outline	7
Part I Pathophysiological insights into disorders of the malate-aspartate shuttle		
Chapter 2	MDH1 deficiency is a metabolic disorder of the malate-aspartate shuttle associated with early onset severe encephalopathy	25
Chapter 3	Inborn disorders of the malate-aspartate shuttle	49
Chapter 4	The malate-aspartate shuttle is important for <i>de novo</i> serine biosynthesis	79
Chapter 5	Pyruvate reverses the metabolic consequences of malate dehydrogenase 1 deficiency	117
Part II Metabolic phenotyping in rare hereditary anemia		
Chapter 6	Untargeted metabolic profiling in dried blood spots identifies disease fingerprint for pyruvate kinase deficiency	159
Chapter 7	Dried blood spot metabolomics reveals a metabolic fingerprint with diagnostic potential for Diamond Blackfan anaemia	177
Chapter 8	Metabolic fingerprint in hereditary spherocytosis correlates with red blood cell characteristics and clinical severity	199
Chapter 9	Summary and general discussion	231
Appendices	Nederlandse Samenvatting List of abbreviations List of publications Dankwoord Curriculum Vitae	261



Chapter 1

General introduction and thesis outline

A glance at metabolism

Metabolism is the set of life-sustaining biochemical reactions that form the basis of life as we know it.¹ Metabolism and metabolic processes are organized in a complex, layered network where enzymes, transporters, hormones, cells, and organs work together to enable us to grow, respond to our environment, and maintain our structural integrity. At a molecular level, nutrients are transformed into the molecular building blocks of proteins, lipids, and nucleic acids. In addition, molecular metabolic processes ensure the elimination of waste products, such as urea and water. Most importantly, metabolic processes produce the energy to drive a variety of biological functions, such as muscle contraction and neuronal excitation. Since metabolism is essential for life, metabolic dysfunction frequently coexists with disease. Understanding how metabolic processes change in disease may thus contribute to the treatment or prevention of a variety of diseases. Despite efforts to computationally reconstruct human metabolism into a genome-scale and whole-body organ-specific metabolic network,^{2,3} our current understanding of the human metabolic network remains incomplete. In addition, studying metabolism remains challenging due to the many unknowns about metabolites, enzymes, and their functions. One approach to improving our understanding of human metabolism is the systemic characterization of the human metabolome. The metabolome is the complete set of metabolites found within a cell, tissue, or biological sample and is the downstream product of the interaction between the genome and the environment. Since 2007, the Human Metabolome Project has cataloged known, expected, and predicted metabolites in the human metabolome database (HMDB).^{4,5} The systemic study of the metabolome - metabolite fingerprints that specific cellular processes leave behind - is also known as metabolomics. Hence, while genomics, transcriptomics, and proteomics reveal information about the set of gene products, metabolomics provides a readout that is more closely related to the biochemical functioning of cells and tissues (Figure 1). As a result, a snapshot provided by metabolomics is thought to contain valuable information that is closely tied to an organism's phenotype.

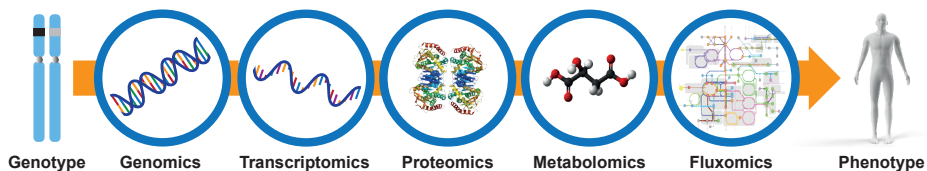


Figure 1. Omics layers between genotype and phenotype. The relationship between genotype and phenotype is hierarchically bridged by DNA, RNA, proteins, metabolites, and metabolite flux, which are profiled by genomics (and epigenomics), transcriptomics, proteomics, metabolomics, and fluxomics, respectively. Genomics identifies genes associated with disease, whereas other -omics provide downstream insights into pathophysiology. Fluxomics describes the dynamic activity of metabolic pathways.

Metabolomics

The metabolome encompasses small-molecules (50-1500 kDa) with a wide diversity in reactivity, structure, and concentration range. As a result, metabolomics analysis requires the use of instruments capable of analyzing these highly complex analytes in biological samples with high coverage and precision. Two examples of such sophisticated advanced analytical technologies are mass spectrometry (MS) and nuclear magnetic resonance (NMR) spectroscopy (Figure 2).⁶ However, due to the diverse physical properties of metabolites, no single analytical tool can measure all metabolites in a single analysis. Metabolomics strategies can be classified in two distinct types of approaches: targeted and untargeted metabolomics. Targeted metabolomics is the measurement of a predefined set of metabolites, whereas untargeted metabolomics is the comprehensive analysis of all measurable metabolites in a sample. This is followed by a metabolite identification step, in which m/z signals are matched to metabolites using databases such as the HMDB.⁵ Untargeted metabolomics is often hypothesis-generating in nature. Therefore, it can lead to the discovery of previously unknown and unexpected correlations between metabolites, yield novel disease biomarkers, or aid in novel pathophysiological insights.⁷ Due to its comprehensive nature, untargeted metabolomics generates biochemical fingerprints that can also be exploited for diseases that lack a single biomarker.^{8,9}

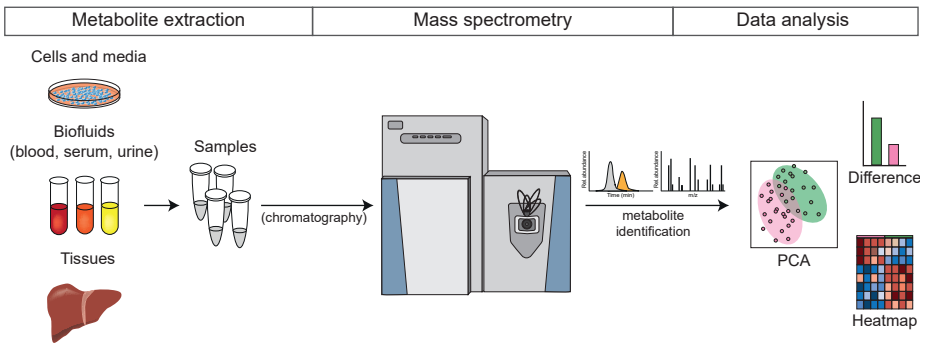


Figure 2. Metabolomics workflow. A metabolomics workflow consists of three basic steps: 1) Sample preparation: Metabolite extraction from cells, biofluids, and tissues includes the addition of cold organic solvents or freezing to denaturize enzymes. 2) Metabolite measurement: Chromatography physically separates analytes on a column prior to MS measurement, improving metabolome coverage and quantitative accuracy. MS detects metabolites with high sensitivity and resolution. 3) Data analysis: Raw MS data with mass peaks and intensities are converted to annotated metabolite data. Biological interpretation of metabolomics data through visualization techniques, such as clustered heatmaps, principal component analysis (which identifies linear combinations of metabolites that best differentiate samples), or individual metabolite changes.

Stable isotope resolved metabolomics

In the quest to decipher the human metabolome, concentration-based metabolic profiling is only part of the story. Since metabolites are continuously absorbed, synthesized, and degraded, the metabolome is very dynamic. In addition, many metabolic pathways intersect as the same metabolite participates in many pathways. For instance, glutamate is a common metabolite produced in the TCA cycle and glutaminolysis, which is utilized in a variety of other pathways, such as glutathione and amino acid synthesis. Stable isotope resolved metabolomics or tracer metabolomics is useful in delineating the contributions of different pathways to metabolite pools. The utilization of stable isotope-labeled nutrients, such as ^{13}C -glucose or ^{13}C -glutamine, allows for time-dependent analysis of downstream metabolite labeling (Figure 3).^{10,11} Subsequently, biological insights can be obtained by interpreting isotopic enrichment or integrating tracer data with computational models, known as ^{13}C -metabolic flux analysis.^{12,13} By combining metabolomics data and pathway activities in a complementary way, our understanding of metabolism in health and disease can greatly improve. This approach may be particularly beneficial for research and diagnostics in rare inherited diseases.

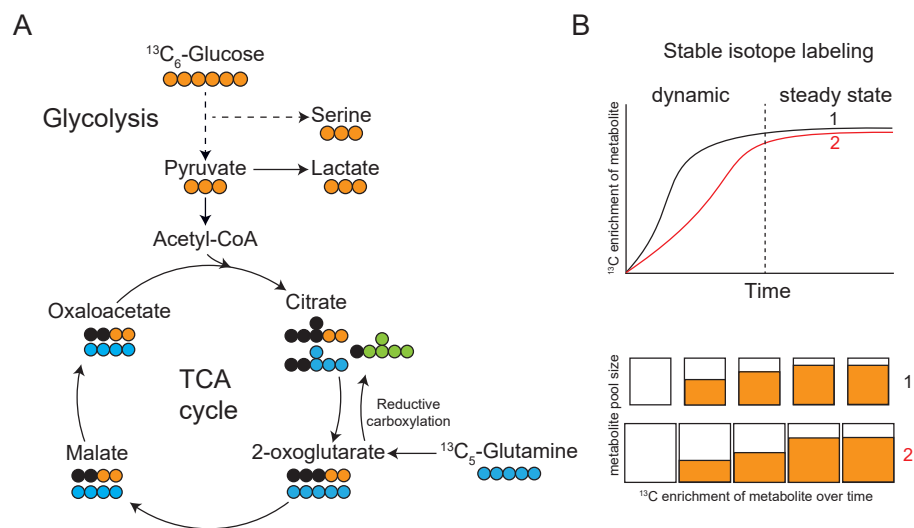


Figure 3. Stable isotope tracing to investigate the dynamics of metabolism. A. Carbon map of $^{13}\text{C}_6$ -Glucose (orange) and $^{13}\text{C}_5$ -Glutamine (blue for oxidative TCA cycle and green for reductive carboxylation) tracing in glycolysis and TCA cycle. Black dots represent unlabeled carbons. **B.** Upon introduction of a stable isotope tracer, metabolites downstream become labeled over time until the flux in and out of metabolite pools is balanced (metabolic steady state). The size of the metabolite pool influences the initial dynamic labeling because larger metabolite pools take longer to reach steady state (represented in condition 2).

A spectrum of inherited diseases

Inherited diseases are caused by a change in the DNA sequence that is inherited from the parents and is present in an individual at birth. Depending on their nature and genetic location, mutations in protein-encoding genes can result in missing or malfunctioning of proteins. The underlying genetic cause of inherited diseases frequently results in pediatric onset of disease, with clinical symptoms varying from mild to life-threatening. As a result, a significant number of children with an inherited disease die before the age of 5 years.^{14,15} While early detection is critical for disease management, diagnosing inherited diseases remains challenging and results in a long diagnostic odyssey for many patients.¹⁶ Nowadays, clinical diagnostic laboratories use next-generation sequencing techniques for whole-exome or whole-genome sequencing. This significantly improved the identification of disease-causing gene mutations as well as the discovery of novel genes associated with disease, thereby accelerating diagnostic procedures.¹⁷

Inherited metabolic diseases

Inherited metabolic diseases (IMDs) refer to diseases caused by a genetic variant that lead to disorders of metabolism. An IMD is broadly defined as “a disease with a primary genetic cause leading to a primary alteration of a biochemical pathway intrinsic to the specific biochemical, clinical, and pathophysiological features”.¹⁸ The majority of these cases are enzyme deficiencies due to mutations in individual genes. For example, in phenylketonuria (PKU), a common IMD in Northern-European countries, the enzymatic degradation of the amino acid phenylalanine is affected.¹⁹ Individual diseases are frequently rare to ultra-rare (<1 in 1,000,000),²⁰⁻²² but IMDs represent a heterogeneous group of over 1000 different disorders. The genetic spectrum of IMD varies from disorders of intermediary metabolism (e.g., amino acid or carbohydrate metabolism) to disorders of metabolic cell signaling (e.g., endocrine and neurotransmitter metabolism).^{18,23} As a consequence, the clinical recognition of IMD is challenged by heterogeneous clinical symptoms, including neurological, cardiac, ophthalmologic, metabolic, muscular-skeletal, and gastrointestinal symptoms.²⁴ Some diseases present with a more tissue-specific clinical phenotype, such as liver disease in citrin deficiency.²⁵

The quantification of specific metabolite classes, such as amino acids, acylcarnitines, and organic acids in body fluids, is frequently used to aid in the diagnosis of IMD patients. Changes in specific metabolite concentrations hint at a deficiency in specific enzymes or transporters. In the case of PKU, high levels of phenylalanine in the blood are indicative of the disease. Timely diagnosis is important for the significant number of IMDs that are amenable to treatment.^{26,27} Dietary treatment can

significantly improve clinical symptoms in many IMDs, as demonstrated by dietary phenylalanine restriction in PKU or low carbohydrate ketogenic diets in glycolysis-related defects.^{19,28} However, most treatments are aimed at improving quality of life through symptomatic or comfort treatment, which addresses secondary complications instead of the underlying disease cause. In order to develop a treatment rationale, pathophysiological knowledge is essential.

Untargeted metabolomics in inherited metabolic diseases

The increasing number of IMD poses an increasing clinical and diagnostic challenge. The current diagnostic platforms may fall short of efficiently covering a wide range of metabolites, and pathophysiological investigations are complicated due to the rarity of patients and the inherent scarcity of biological material. The application of metabolomics in the diagnosis and research of rare inherited diseases can be a valuable tool for identifying and characterizing disease, since only a small biological sample is needed to reveal data on thousands of metabolites. Recent developments demonstrated the potential of an untargeted metabolomics platform to screen clinical samples from patients with an IMD.^{29–32} The clinical utility of untargeted metabolomics as a novel or complementary screening tool holds promise for improved diagnostic accuracy and speed.^{33,34} In addition, untargeted metabolomics can play an important role in understanding pathophysiology for the development of therapeutic strategies.

Tracing metabolic pathways in a spectrum of inherited diseases

The overall aim of this thesis is to contribute to a better understanding of the pathophysiology of several rare inherited diseases using untargeted metabolomics in order to ultimately improve diagnostics and treatment. We apply state-of-the-art direct-infusion high resolution mass spectrometry (DI-HRMS)-based untargeted metabolomics to determine metabolic phenotypes in cells and patients (**chapters 2,5-8**) to identify pathophysiological leads (**chapters 4-8**) or aid in diagnostic interpretation (**chapters 2 & 7**). In addition, to gain pathophysiological insights, we combined metabolomics with stable isotope tracing *in vitro* (**chapters 4 & 5**). The work in this thesis focuses on improving our understanding of two groups of inherited diseases: *part 1* describes malate-aspartate shuttle disorders, and *part 2* describes rare hereditary anemias. All are considered IMDs, with the exception of the congenital red blood cell membrane disorder hereditary spherocytosis (HS), although the involvement of a structural component in the regulation of red blood cell metabolism provides an opening for metabolic investigation.^{35,36} Several aspects of these diseases are addressed in this thesis, including phenotypic recognition, molecular diagnostics, and pathophysiological insights.

PART 1 – Pathophysiological insights into disorders of the malate-aspartate shuttle

The malate-aspartate shuttle

The malate-aspartate shuttle (MAS) is a metabolic cycle that connects cytosolic redox metabolism to mitochondria and plays a crucial role in cellular energy metabolism.¹ Energy is gradually released from nutrients in food through cellular metabolic pathways that involve reduction and oxidation (redox) reactions. NAD(H) molecules are the pyridine nucleotide cofactors that serve as carriers to remove (oxidation) or provide (reduction) electrons from carbon compounds (Figure 4A).³⁷ Within central carbon metabolism, the enzymatic oxidation of carbon compounds in glycolysis and the tricarboxylic acid cycle (TCA) cycle reduce NAD⁺ to NADH (Figure 4B). The electrons from NADH are eventually consumed in the mitochondrial electron transport chain (ETC) to generate a proton gradient that drives ATP synthesis by oxidative phosphorylation. The presence of oxygen (O₂), which serves as the final electron acceptor, maintains oxidative phosphorylation. As cytosolic NADH molecules cannot enter the mitochondria, the MAS transports the redox equivalents from NADH to the mitochondrial matrix in an indirect way.^{38,39} The enzyme malate dehydrogenase 1 (MDH1) reduces cytosolic oxaloacetate to malate, which is then transported to the mitochondrial matrix and oxidized to oxaloacetate and NADH by MDH2 (Figure 4B). The proton gradient generated by ETC activity drives MAS activity. As a result, the MAS actively maintains the cytosolic NAD⁺/NADH ratio, which is important for the continuation of several metabolic pathways.

Inherited disorders of the MAS

Inherited disorders of the MAS include AGC2 (Citrin) deficiency (OMIM #603859)^{40,41}, AGC1 (Aralar) deficiency (OMIM #612949)^{42–46}, glutamate-oxaloacetate transaminase 2 (GOT2) deficiency (OMIM #618721)⁴⁷ and mitochondrial malate dehydrogenase (MDH2) deficiency (OMIM #617339)^{48–50}. In **chapter 2**, we report the first two patients with cytosolic MDH1 deficiency (OMIM #618959). Using untargeted metabolomics, we identified glycerol 3-phosphate as a biomarker in dried blood spots of patients with MDH1 deficiency, which can now be used to facilitate diagnostics. In **chapter 3**, we review and discuss the literature on clinical and biochemical similarities and differences among the reported MAS disorders to aid in their clinical recognition. Some of these MAS defects are, at least in part, amenable to targeted treatments such as a ketogenic diet. Interestingly, serine supplementation was found to be an effective treatment for GOT2 deficiency since patients had a secondary serine biosynthesis defect. In **chapter 4**, we investigate whether other MAS defects also lead to a secondary serine biosynthesis defect. We generated cell models with a

genetic disruption of all individual MAS components using Crispr/Cas9. Using stable isotope tracing experiments, we demonstrated that all MAS-deficient cells have impaired *de novo* serine biosynthesis, implying that patients with other MAS disorders may benefit from serine supplementation as well. Furthermore, we show that MAS-deficient cells have disturbed glycolysis and an increased flux to glycerol 3-phosphate. In **chapter 5**, we show in MDH1-deficient cells that these altered metabolite fluxes are restored by the addition of an electron acceptor, such as pyruvate or 2-ketobutyrate. In addition, disturbed glycolysis increases metabolite flux into the pentose phosphate pathway, resulting in ribitol accumulation in MDH1-deficient cells.

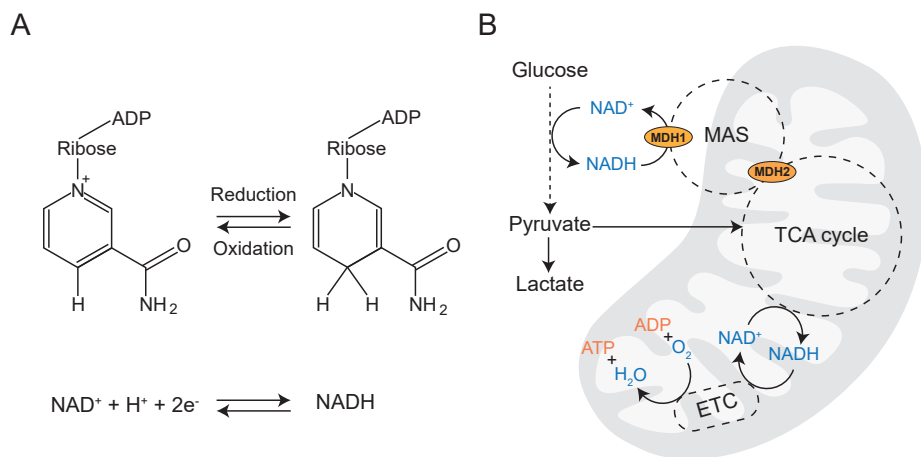


Figure 4. The malate-aspartate shuttle (MAS) in energy metabolism. A. reduction and oxidation reactions of nicotinamide adenine nucleotide (NAD). **B.** Glycolysis, the breakdown of glucose in ten enzymatic steps in the cytosol, and the citric acid or tricarboxylic acid (TCA) cycle, an important connecting hub for many metabolic pathways in the mitochondria, are two major metabolic pathways that rely on the NAD⁺/NADH ratio. The MAS transports cytosolic NADH to the mitochondria to eventually generate ATP in the electron transport chain (ETC), where the electrons from NADH are transferred to oxygen, the final electron acceptor.

PART 2 – Metabolic phenotyping in rare hereditary anemias

Red blood cell metabolism

Red blood cells (RBCs) are the most abundant cells in the human body (~83%), and approximately 2.4 million new erythrocytes (mature RBCs) are produced per second in human adults.⁵¹ The primary function of the RBC is to enable respiration in tissues by supplying oxygen and removing carbon dioxide through gas exchange in the lungs. Since RBCs transport oxygen, the most important component of the RBC is the specialized oxygen-binding protein hemoglobin. In order to accommodate maximum space for hemoglobin, RBCs extrude their nuclei and other cellular organelles (mitochondria, Golgi apparatus, and endoplasmic reticulum) during the maturation process (Figure 6A). While RBCs play a vital role in providing energy for metabolic functions, the RBC itself only has limited metabolic activity due to the lack of organelles. RBCs primarily rely on anaerobic glycolysis (Embden-Meyerhof pathway) for energy production, which is required to maintain their shape and deformability (i.e., the capacity to deform) for passage through capillaries and splenic sinuses (Figure 5).⁵²⁻⁵⁴ In addition, to maintain a favorable antioxidant defense, they rely on activity of the pentose phosphate pathway (hexose monophosphate shunt). A unique feature of RBC metabolism is the Rapoport-Luebering shunt, which uses ~25% of glucose to produce 2,3-bisphosphoglycerate (2,3-DPG), a metabolite that lowers hemoglobin's oxygen affinity, thereby favoring oxygen release to tissues.⁵⁵

Hereditary anemia

Anemia is defined as a condition in which the blood's oxygen transport capacity is decreased due to a low number of RBCs or a low hemoglobin concentration. Rare hereditary anemias (RHA) are a group of heterogeneous disorders caused by either an intrinsic RBC defect or erythropoietic defects that result in increased decay or impaired synthesis of the RBC, respectively.⁵⁶ Typical RHA symptoms include fatigue, shortness of breath, palpitations, enlargement of the spleen, muscle pain, and jaundice, and they can range in severity from mild to life-threatening. Based on clinical manifestations and morphological RBC alterations, RHA can be classified into four types⁵⁷: 1) RBC enzyme defects, such as glucose 6-phosphate dehydrogenase deficiency and pyruvate kinase deficiency (PKD)⁵⁸; 2) hemoglobin disorders, such as thalassemia and sickle cell disease (SCD); 3) hyporegenerative anemias, such as Diamond-Blackfan anemia (DBA) and congenital dyserythropoietic anemia (CDA); 4) RBC membrane defects caused by either altered membrane structural organizations, such as hereditary spherocytosis (HS) and hereditary elliptocytosis⁵⁹, or alterations in membrane transport functions, such as hereditary stomatocytosis/hereditary xerocytosis (HX)⁶⁰ (Figure 6).

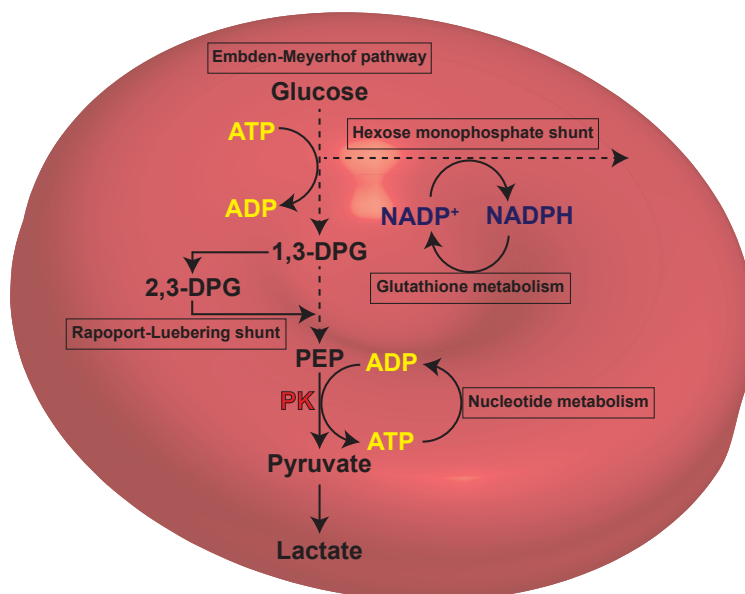


Figure 5. Main metabolic pathways of the red blood cell. The Embden-Meyerhof pathway (anaerobic glycolysis) produces ATP, which drives membrane pumps involved in the RBC's flexibility and integrity. Pyruvate kinase (PK) generates ATP by converting phosphoenolpyruvate (PEP) to pyruvate. The Rapoport-Luebering Shunt is a bypass step of glycolysis that produces 2,3-diphosphoglycerate (2,3-DPG), which regulates hemoglobin's oxygen affinity. The hexose monophosphate shunt or pentose phosphate pathway generates NADPH, which is required for the maintenance of reduced glutathione in antioxidant metabolism. The RBC's nucleotide metabolism contributes to the maintenance of energy balance.

Treatment for RHA depends on the specific condition and the severity of the symptoms. Supportive treatments such as blood transfusions or splenectomy (removal of the spleen) have significantly improved patient survival and quality of life. Other types of RHA require medications to increase RBC production, and in severe cases, a bone marrow transplant may be necessary. However, these treatments remain suboptimal and invalidate patients suffering from anemia. Early diagnosis and effective treatment are essential for managing RHA and improving patient outcomes, but there are still significant gaps in our understanding of clinical heterogeneity, genotype-phenotype correlations, and pathophysiology.⁶¹⁻⁶³ Hence, there is a need for more functional tools that accelerate diagnostic procedures and the investigation of disease and treatment response. Untargeted metabolomics, which functionally approaches the layer between genotype and phenotype, may provide important insights that aid in diagnostic procedures, delineate metabolic disease phenotypes, and improve understanding of pathophysiology. Importantly, metabolic insights can provide key insights for developing therapeutic options for various forms of RHA.^{64,65} In this thesis, we focused on three genetically and clinically heterogeneous types of anemia: PKD, DBA, and HS.

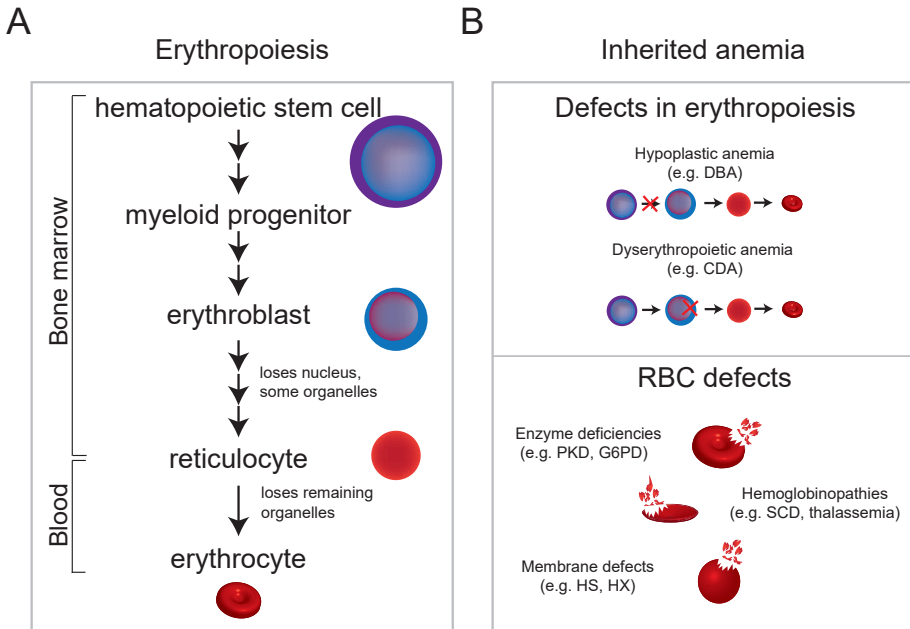


Figure 6. Erythropoiesis and inherited anemia. **A.** Simplified scheme of erythropoiesis. Erythropoiesis starts in the bone marrow with lineage commitment of pluripotent myeloid progenitor cells and differentiation into immature erythroid progenitors. Later stages of development include the formation of erythroblasts, which mature into reticulocytes by extruding their nuclei and other organelles. The final stage is reticulocyte maturation into an erythrocyte, where it acquires its biconcave shape through extensive membrane remodeling. **B.** A schematic overview of inherited anemias. Defects in erythropoiesis result in a lower number of mature RBCs. RBC defects cause abnormal RBCs, which are destroyed prematurely.

Pyruvate kinase deficiency

PKD is an RBC glycolytic enzyme defect with an estimated prevalence of 1 in 20,000-3,000,000.⁶⁶⁻⁶⁸ The disorder is mostly caused by autosomal recessive inherited missense mutations in the *PKLR* gene, which encodes for both liver and RBC pyruvate kinase. Pyruvate kinase catalyzes the conversion of phosphoenolpyruvate to pyruvate while simultaneously generating ATP (Figure 5). As a result, PKD causes ATP depletion and decreased RBC survival due to premature RBC destruction primarily in the liver or spleen.⁵⁸ In addition, glycolytic intermediates such as 2,3-DPG accumulate. Characteristic laboratory findings include decreased hemoglobin, reticulocytosis, and elevated unconjugated bilirubin. The clinical phenotype of PKD ranges from well-compensated hemolytic anemia to severe hemolysis and hydrops fetalis.^{69,70} Clinical symptoms include pallor, jaundice, dark urine, fatigue, splenomegaly, gallstones, and cholecystitis. Treatment is mainly supportive and consists of erythrocyte transfusions to maintain adequate hemoglobin levels.

Severely affected patients may require (partial) splenectomy or hematopoietic stem cell transplantation.⁷¹ Novel treatments are aimed at restoring PK activity. The allosteric PK enzyme activator mitapivat demonstrated significant clinical benefit in clinical trials, where it was shown to significantly upregulate PK, increase ATP production, and decrease 2,3-DPG levels.⁶⁵ Its capability to enhance erythrocyte ATP production may be promising as a new therapeutic for several other RHAs as well, including thalassemia and sickle cell disease.⁶⁵

Diamond Blackfan anemia

Diamond Blackfan anemia (DBA) is a rare congenital erythroblastopenia that is part of the inherited bone marrow failure syndromes.⁷² The disorder is classified as a ribosomopathy since the majority of the underlying molecular defects encompass ribosomal protein genes and thereby affect ribosome biogenesis.⁷³ Mutations in *RPS19* account for ~25% of DBA cases, but mutations have also been identified in many other RP genes, including *RPL5*, *RPL11*, *RPL35A*, *RPS7*, *RPS10*, *RPS24*, and *RPS26I*.^{72,73} In a few patients, the disease is caused by mutations in *GATA1*, an erythroid transcription factor, or *TSR2*, a ribosome maturation factor.^{74,75} Ribosomes are the molecular machines that translate messenger RNA (mRNA) into proteins. Although ribosome biogenesis is a ubiquitous and important cellular process, ribosome defects in DBA selectively impact erythropoiesis but not the differentiation of other hematopoietic lineages.⁷⁶ The underlying molecular mechanisms linking ribosome defects and defective erythropoiesis remain to be fully understood, but it is thought to be due in part to tissue-specific sensitivity to p53 pathway activation in response to ribosome stress.^{77,78} Clinically, DBA is characterized by hypoplastic anemia, congenital malformations, and a predisposition to cancer. Treatment consists of glucocorticoid administration and erythrocyte transfusions, although both have significant toxicity and long-term consequences.^{79,80} Currently, the only curative treatment for the bone marrow failure in DBA is allogenic hematopoietic stem cell transplantation.⁸¹

Hereditary spherocytosis

Hereditary spherocytosis (HS) is caused by mutations in genes encoding for one of the many membrane- or cytoskeletal proteins (α -spectrin (SPTA1), b-spectrin (SPTB), ankyrin (ANK1), band 3 (SLC4A1), and protein 4.2 (EPB42)), and has a prevalence of 1:2000 to 1:5000.^{59,82} The RBC membrane proteins regulate flexibility and deformability, which are required for the RBC's physiological cell function while traversing the circulatory system and specifically the capillary network. As a result of affected membrane stability and deformability, RBCs become spheroidal, leading to premature splenic sequestration and hemolysis.⁸³ Central to the stability and

functional regulation of the RBC membrane is band 3, an anion transporter that accounts for up to 25% of the cell membrane surface. Band 3 is thought to bind the glycolytic enzyme glyceraldehyde 3-phosphate dehydrogenase (GAPDH) in a competitive binding with deoxygenated hemoglobin, directing glucose metabolism between glycolysis and the pentose phosphate pathway in response to metabolic needs.^{35,36} Partly due to its genetic heterogeneity, HS is also clinically highly heterogeneous.⁸⁴ Clinical symptoms include anemia, jaundice, splenomegaly, and cholelithiasis.⁸³ Similar to PKD, treatment consists of regular erythrocyte transfusions and (partial) splenectomy in severe cases.^{83,85} Interestingly, HS has been linked with decreased PK activity, potentially opening a therapeutic option for PK activation in HS as well.⁸⁶

Metabolic phenotyping in rare hereditary anemias

To address some of the challenges in the diagnostic evaluation and clinical characterization of RHA, we introduced untargeted metabolomics as a novel investigative tool. In **chapter 6**, we evaluated the diagnostic application of metabolomics in anemia and presented proof-of-principle that we could confirm or rule out the diagnosis of PKD based on a metabolic fingerprint using a predictive machine learning model. Furthermore, the metabolic fingerprint, established for 22 patients, revealed known and unknown metabolites in the context of PKD, providing leads for future investigations. In **chapter 7**, we also used machine learning to predict the diagnosis of DBA patients based on their metabolic fingerprints. In addition, the metabolic fingerprints of 18 DBA patients were compared to those of patients with congenital dyserythropoietic anemia, a clinically and diagnostically similar disease. Furthermore, we demonstrated that untargeted metabolomics data in DBA patients reveals a different metabolic signature for different treatment modalities, implying that it could be a useful tool for investigating treatment response. In **chapter 8**, the metabolic fingerprint of 35 patients with HS revealed decreased levels of 2,3-DPG, prompting further pathophysiological investigation in light of recent advances in PK activation. In addition, we shed light on several associations of the metabolic fingerprint with clinical phenotypic heterogeneity.

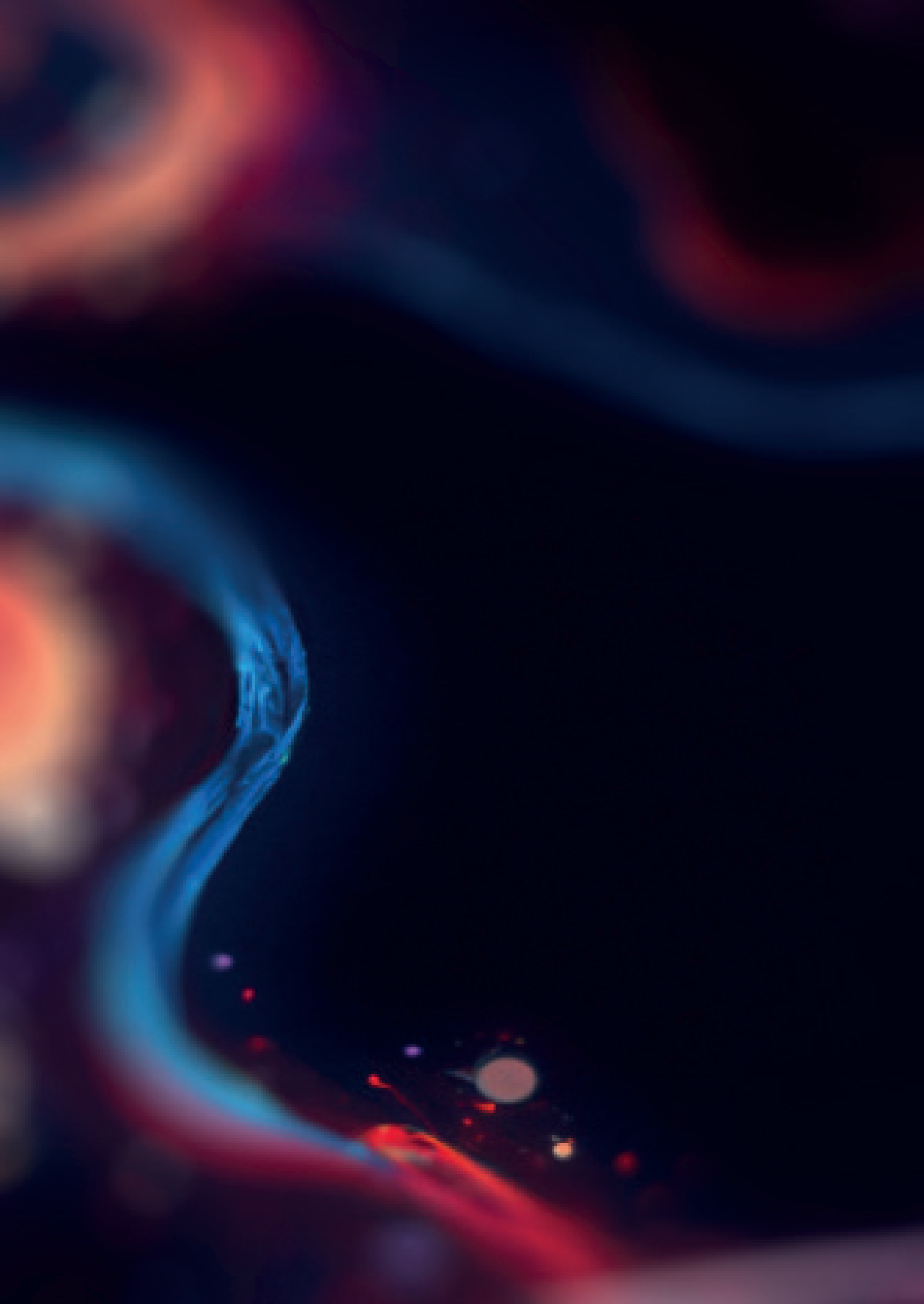
REFERENCES

1. Judge A, Dodd MS. Metabolism. *Essays Biochem.* 2020;64(4):607-647.
2. Brunk E, Sahoo S, Zielinski DC, et al. Recon3D: A Resource Enabling A Three-Dimensional View of Gene Variation in Human Metabolism. *Nat Biotechnol.* 2018;36(3):272.
3. Thiele I, Sahoo S, Heinken A, et al. Personalized whole-body models integrate metabolism, physiology, and the gut microbiome. *Mol Syst Biol.* 2020;16(5):e8982.
4. Wishart DS. Proteomics and the human metabolome project. *Expert Rev Proteomics.* 2007;4(3):333-335.
5. Wishart DS, Guo AC, Oler E, et al. HMDB 5.0: the Human Metabolome Database for 2022. *Nucleic Acids Res.* 2022;50(D1):D622-D631.
6. Ren JL, Zhang AH, Kong L, Wang XJ. Advances in mass spectrometry-based metabolomics for investigation of metabolites. *RSC Adv.* 2018;8(40):22335-22350.
7. Sandlers Y. The future perspective: metabolomics in laboratory medicine for inborn errors of metabolism. *Transl Res.* 2017;189:65-75.
8. Abela L, Spiegel R, Crowther LM, et al. Plasma metabolomics reveals a diagnostic metabolic fingerprint for mitochondrial aconitase (ACO2) deficiency. Dzeja P, ed. *PLoS One.* 2017;12(5):e0176363.
9. Saffari A, Cannet C, Blaschek A, et al. 1H-NMR-based metabolic profiling identifies non-invasive diagnostic and predictive urinary fingerprints in 5q spinal muscular atrophy. *Orphanet J Rare Dis.* 2021;16(1).
10. Buescher JM, Antoniewicz MR, Boros LG, et al. A roadmap for interpreting 13C metabolite labeling patterns from cells. *Curr Opin Biotechnol.* 2015;34:189-201.
11. Balcells C, Foguet C, Tarragó-Celada J, de Atauri P, Marin S, Cascante M. Tracing metabolic fluxes using mass spectrometry: Stable isotope-resolved metabolomics in health and disease. *TrAC Trends Anal Chem.* 2019;120:115371.
12. Jang C, Chen L, Rabinowitz JD. Metabolomics and Isotope Tracing. *Cell.* 2018;173(4):822-837.
13. Antoniewicz MR. A guide to metabolic flux analysis in metabolic engineering: Methods, tools and applications. *Metab Eng.* 2021;63:2-12.
14. Wojcik MH, Schwartz TS, Yamin I, et al. Genetic disorders and mortality in infancy and early childhood: delayed diagnoses and missed opportunities. *Genet Med 2018 2011.* 2018;20(11):1396-1404.
15. Kingsmore SF, Henderson A, Owen MJ, et al. Measurement of genetic diseases as a cause of mortality in infants receiving whole genome sequencing. *npj Genomic Med 2020 51.* 2020;5(1):1-10.
16. Pogue RE, Cavalcanti DP, Shanker S, et al. Rare genetic diseases: update on diagnosis, treatment and online resources. *Drug Discov Today.* 2018;23(1):187-195.
17. Fernandez-Marmiesse A, Gouveia S, Couce ML. NGS Technologies as a Turning Point in Rare Disease Research , Diagnosis and Treatment. *Curr Med Chem.* 2018;25(3):404-432.
18. Ferreira CR, Rahman S, Keller M, et al. An international classification of inherited metabolic disorders (ICIMD). *J Inherit Metab Dis.* 2021;44(1):164-177.
19. van Spronsen FJ, Blau N, Harding C, Burlina A, Longo N, Bosch AM. Phenylketonuria. *Nat Rev Dis Prim.* 2021;7(1).
20. Richter T, Nestler-Parr S, Babela R, et al. Rare Disease Terminology and Definitions-A Systematic Global Review: Report of the ISPOR Rare Disease Special Interest Group. *Value Health.* 2015;18(6):906-914.
21. Hee SW, Willis A, Tudur Smith C, et al. Does the low prevalence affect the sample size of interventional clinical trials of rare diseases? An analysis of data from the aggregate analysis of clinicaltrials.gov. *Orphanet J Rare Dis.* 2017;12(1).
22. Frederiksen SD, Avramović V, Maroilley T, Lehman A, Arbour L, Tarailo-Graovac M. Rare disorders have many faces: in silico characterization of rare disorder spectrum. *Orphanet J Rare Dis.* 2022;17(1):1-18.

23. Ferreira CR, van Karnebeek CDM, Vockley J, Blau N. A proposed nosology of inborn errors of metabolism. *Genet Med*. 2019;21(1):102-106.
24. Saudubray JM, Garcia-Cazorla A. Inborn Errors of Metabolism Overview: Pathophysiology, Manifestations, Evaluation, and Management. *Pediatr Clin North Am*. 2018;65(2):179-208.
25. Saheki T, Moriyama M, Funahashi A, Kuroda E. Agc2 (Citrin) deficiency—from recognition of the disease till construction of therapeutic procedures. *Biomolecules*. 2020;10(8):1-17.
26. Van Karnebeek CDM, Stockler S. Treatable inborn errors of metabolism causing intellectual disability: A systematic literature review. *Mol Genet Metab*. 2012;105(3):368-381.
27. Hoytema van Konijnenburg EMM, Wortmann SB, Koelewijn MJ, et al. Treatable inherited metabolic disorders causing intellectual disability: 2021 review and digital app. *Orphanet J Rare Dis* 2021. 2021;16(1):1-35.
28. Scholl-Bürgi S, Höller A, Pichler K, Michel M, Haberlandt E, Karall D. Ketogenic diets in patients with inherited metabolic disorders. *J Inherit Metab Dis*. 2015;38(4):765-773.
29. Miller MJ, Kennedy AD, Eckhart AD, et al. Untargeted metabolomic analysis for the clinical screening of inborn errors of metabolism. *J Inherit Metab Dis*. 2015;38(6):1029-1039.
30. KLM C, LAJ K, E van der H, et al. Next-generation metabolic screening: targeted and untargeted metabolomics for the diagnosis of inborn errors of metabolism in individual patients. *J Inherit Metab Dis*. 2018;41(3):337-353.
31. Haijes HA, Willemsen M, van der Ham M, et al. Direct Infusion Based Metabolomics Identifies Metabolic Disease in Patients' Dried Blood Spots and Plasma. *Metabolites*. 2019;9(1):12.
32. Bonte R, Bongaerts M, Demirdas S, et al. Untargeted Metabolomics-Based Screening Method for Inborn Errors of Metabolism using Semi-Automatic Sample Preparation with an UHPLC-Orbitrap-MS Platform. *Metabolites*. 2019;9(12):289.
33. Almontashiri N, Zha L, Young K, et al. Clinical Validation of Targeted and Untargeted Metabolomics Testing for Genetic Disorders: A 3 Year Comparative Study. *Sci Rep*. 2020;10(1):9382.
34. Liu N, Xiao J, Gijavanekar C, et al. Comparison of Untargeted Metabolomic Profiling vs Traditional Metabolic Screening to Identify Inborn Errors of Metabolism. *JAMA Netw open*. 2021;4(7):e2114155.
35. Lewis IA, Campanella ME, Markley JL, Low PS. Role of band 3 in regulating metabolic flux of red blood cells. *Proc Natl Acad Sci U S A*. 2009;106(44):18515-18520.
36. Issaian A, Hay A, Dzieciatkowska M, et al. The interactome of the N-terminus of band 3 regulates red blood cell metabolism and storage quality. *Haematologica*. 2021;106(11):2971-2985.
37. Hosios AM, Matthew GVH. The redox requirements of proliferating mammalian cells. *J Biol Chem*. 2018;293(20):7490-7498.
38. Borst P. Hydrogen transport and transport metabolites. In: *Funktionelle Und Morphologische Organisation Der Zelle*. Springer Berlin Heidelberg; 1963:137-162.
39. Dawson AG. Oxidation of cytosolic NADH formed during aerobic metabolism in mammalian cells. *Trends Biochem Sci*. 1979;4(8):171-176.
40. Kobayashi K, Sinasac DS, Iijima M, et al. The gene mutated in adult-onset type II citrullinaemia encodes a putative mitochondrial carrier protein. *Nat Genet*. 1999;22(2):159-163.
41. Saheki T, Kobayashi K. Mitochondrial aspartate glutamate carrier (citrin) deficiency as the cause of adult-onset type II citrullinemia (CTLN2) and idiopathic neonatal hepatitis (NICCD). *J Hum Genet*. 2002;47(7):333-341.
42. Wibom R, Lasorsa FM, Töhönen V, et al. AGC1 deficiency associated with global cerebral hypomyelination. *N Engl J Med*. 2009;361(5):489-495.
43. Falk MJ, Li D, Gai X, et al. AGC1 Deficiency Causes Infantile Epilepsy, Abnormal Myelination, and Reduced N-Acetylaspartate. *JIMD Rep*. 2014;14:77-85.

44. Kavanaugh BC, Warren EB, Baytas O, et al. Longitudinal MRI findings in patient with SLC25A12 pathogenic variants inform disease progression and classification. *Am J Med Genet Part A*. 2019;179(11):2284-2291.
45. Pfeiffer B, Sen K, Kaur S, Pappas K. Expanding Phenotypic Spectrum of Cerebral Aspartate-Glutamate Carrier Isoform 1 (AGC1) Deficiency. *Neuropediatrics*. 2020;51(2):160-163.
46. Saleh M, Helmi M, Yacop B. A novel nonsense gene variant responsible for early infantile epileptic encephalopathy type 39: Case report. *Pakistan J Biol Sci*. 2020;23(7):973-976.
47. van Karnebeek CDM, Ramos RJ, Wen XY, et al. Bi-allelic GOT2 Mutations Cause a Treatable Malate-Aspartate Shuttle-Related Encephalopathy. *Am J Hum Genet*. 2019;105(3):534-548.
48. Ait-El-Mkadem S, Dayem-Quere M, Gusic M, et al. Mutations in MDH2, Encoding a Krebs Cycle Enzyme, Cause Early-Onset Severe Encephalopathy. *Am J Hum Genet*. 2017;100(1):151-159.
49. Laemmle A, Steck AL, Schaller A, et al. Triheptanoin – Novel therapeutic approach for the ultra-rare disease mitochondrial malate dehydrogenase deficiency. *Mol Genet Metab Reports*. 2021;29:100814.
50. Ticci C, Nesti C, Rubegni A, et al. Bi-allelic variants in MDH2: Expanding the clinical phenotype. *Clin Genet*. 2022;101(2):260-264.
51. Nemkov T, Reisz JA, Xia Y, Zimring JC, D'Alessandro A. Red blood cells as an organ? How deep omics characterization of the most abundant cell in the human body highlights other systemic metabolic functions beyond oxygen transport. *Expert Rev Proteomics*. 2018;15(11):855-864.
52. Weed RI, LaCelle PL, Merrill EW. Metabolic dependence of red cell deformability. *J Clin Invest*. 1969;48(5):795-809.
53. Danielczok JG, Terriac E, Hertz L, et al. Red blood cell passage of small capillaries is associated with transient Ca²⁺-mediated adaptations. *Front Physiol*. 2017;8:979.
54. Koralkova P, Van Solinge WW, Van Wijk R. Rare hereditary red blood cell enzymopathies associated with hemolytic anemia – pathophysiology, clinical aspects, and laboratory diagnosis. *Int J Lab Hematol*. 2014;36(3):388-397.
55. MACDONALD R. Red cell 2,3-diphosphoglycerate and oxygen affinity. *Anaesthesia*. 1977;32(6):544-553.
56. Risinger M, Emberesh M, Kalfa TA. Rare Hereditary Hemolytic Anemias: Diagnostic Approach and Considerations in Management. *Hematol Oncol Clin North Am*. 2019;33(3):373-392.
57. Russo R, Marra R, Rosato BE, Iolascon A, Andolfo I. Genetics and Genomics Approaches for Diagnosis and Research Into Hereditary Anemias. *Front Physiol*. 2020;11:613559.
58. Van Wijk R, Van Solinge WW. The energy-less red blood cell is lost: erythrocyte enzyme abnormalities of glycolysis. *Blood*. 2005;106(13):4034-4042.
59. Da Costa L, Galimand J, Fenneteau O, Mohandas N. Hereditary spherocytosis, elliptocytosis, and other red cell membrane disorders. *Blood Rev*. 2013;27(4):167-178.
60. Andolfo I, Alper SL, De Franceschi LD, et al. Multiple clinical forms of dehydrated hereditary stomatocytosis arise from mutations in PIEZO1. *Blood*. 2013;121(19):3925-3935.
61. Grace RF, Bianchi P, van Beers EJ, et al. Clinical spectrum of pyruvate kinase deficiency: data from the Pyruvate Kinase Deficiency Natural History Study. *Blood*. 2018;131(20):2183-2192.
62. Bianchi P, Fermo E, Lezon-Geyda K, et al. Genotype-phenotype correlation and molecular heterogeneity in pyruvate kinase deficiency. *Am J Hematol*. 2020;95(5):472-482.
63. Yang L, Shu H, Zhou M, Gong Y. Literature review on genotype-phenotype correlation in patients with hereditary spherocytosis. *Clin Genet*. 2022;102(6):474-482.
64. Grace RF, Rose C, Layton DM, et al. Safety and Efficacy of Mitapivat in Pyruvate Kinase Deficiency. *N Engl J Med*. 2019;381(10):933-944.
65. Al-Samkari H, van Beers EJ. Mitapivat, a novel pyruvate kinase activator, for the treatment of hereditary hemolytic anemias. *Ther Adv Hematol*. 2021;12:1-11.
66. Beutler E, Gelbart T. Estimating the prevalence of pyruvate kinase deficiency from the gene frequency in the general white population. *Blood*. 2000;95(11):3585-3588.

67. Carey PJ, Chandler J, Hendrick A, et al. Prevalence of pyruvate kinase deficiency in a northern European population in the north of England. *Blood*. 2000;96(12):4005-4006.
68. Secrest MH, Storm M, Carrington C, et al. Prevalence of pyruvate kinase deficiency: A systematic literature review. *Eur J Haematol*. 2020;105(2):173-184.
69. Ferreira P, Morais L, Costa R, et al. Hydrops fetalis associated with erythrocyte pyruvate kinase deficiency. *Eur J Pediatr*. 2000;159(7):481-482.
70. Al-Samkari H, van Beers EJ, Kuo KHM, et al. The variable manifestations of disease in pyruvate kinase deficiency and their management. *Haematologica*. 2020;105(9):2229-2239.
71. Grace RF, Barcellini W. Management of pyruvate kinase deficiency in children and adults. *Blood*. 2020;136(11):1241-1249.
72. da Costa LM, Marie I, Leblanc TM. Diamond-Blackfan anemia. *Hematol Am Soc Hematol Educ Progr*. 2021;2021(1):353-360.
73. Ulirsch JC, Verboon JM, Kazerounian S, et al. The Genetic Landscape of Diamond-Blackfan Anemia. *Am J Hum Genet*. 2018;103(6):930-947.
74. Klar J, Khalfallah A, Arzoo PS, Gazda HT, Dahl N. Recurrent GATA1 mutations in Diamond-Blackfan anaemia. *Br J Haematol*. 2014;166(6):949-951.
75. Gripp KW, Curry C, Olney AH, et al. Diamond-Blackfan anemia with mandibulofacial dystostosis is heterogeneous, including the novel DBA genes TSR2 and RPS28. *Am J Med Genet Part A*. 2014;164(9):2240-2249.
76. Khajuria RK, Munschauer M, Ulirsch JC, et al. Ribosome Levels Selectively Regulate Translation and Lineage Commitment in Human Hematopoiesis. *Cell*. 2018;173(1):90-103.e19.
77. Horos R, von Lindern M. Molecular mechanisms of pathology and treatment in Diamond Blackfan Anaemia. *Br J Haematol*. 2012;159(5):514-527.
78. Le Goff S, Boussaid I, Floquet C, et al. p53 activation during ribosome biogenesis regulates normal erythroid differentiation. *Blood*. 2021;137(1):89-102.
79. Vlachos A, Ball S, Dahl N, et al. Diagnosing and treating Diamond Blackfan anaemia: results of an international clinical consensus conference. *Br J Haematol*. 2008;142(6):859-876.
80. Berdoukas V, Nord A, Carson S, et al. Tissue iron evaluation in chronically transfused children shows significant levels of iron loading at a very young age. *Am J Hematol*. 2013;88(11):E283-E285.
81. Peffault De Latour R, Peters C, Gibson B, et al. Recommendations on hematopoietic stem cell transplantation for inherited bone marrow failure syndromes. *Bone Marrow Transplant*. 2015;50(9):1168-1172.
82. Andolfo I, Russo R, Gambale A, Iolascon A. New insights on hereditary erythrocyte membrane defects. *Haematologica*. 2016;101(11):1284-1294.
83. Perrotta S, Gallagher PG, Mohandas N. Hereditary spherocytosis. *Lancet (London, England)*. 2008;372(9647):1411-1426.
84. Van Vuren A, Van Der Zwaag B, Huisjes R, et al. The Complexity of Genotype-Phenotype Correlations in Hereditary Spherocytosis: A Cohort of 95 Patients: Genotype-Phenotype Correlation in Hereditary Spherocytosis. *HemaSphere*. 2019;3(4):e276.
85. Iolascon A, Andolfo I, Barcellini W, et al. Recommendations regarding splenectomy in hereditary hemolytic anemias. *Haematologica*. 2017;102(8):1304-1313.
86. Andres O, Loewecke F, Morbach H, et al. Hereditary spherocytosis is associated with decreased pyruvate kinase activity due to impaired structural integrity of the red blood cell membrane. *Br J Haematol*. 2019;187(3):386-395.



Chapter 2

MDH1 deficiency is a metabolic disorder of the malate-aspartate shuttle associated with early onset severe encephalopathy

Melissa H. Broeks^{1*}, Hanan E. Shamseldin^{2*}, Amal Alhashem³, Mais Hashem², Firdous Abdulwahab², Tarfa Alshedi², Iman Alobaid², Fried J.T. Zwartkruis⁴, Denise Westland¹, Sabine Fuchs⁵, Nanda M. Verhoeven-Duif¹, Judith J.M. Jans^{1#}, Fowzan S. Alkuraya^{2#}

¹ Section Metabolic Diagnostics, Department of Genetics, University Medical Center Utrecht, 3584 EA Utrecht, The Netherlands.

² Department of Genetics, King Faisal Specialist Hospital and Research Center, Riyadh 12713, Saudi Arabia

³ Department of Pediatrics, Prince Sultan Military Medical City, Riyadh 11159, Saudi Arabia.

⁴ Center for Molecular Medicine, Department of Molecular Cancer Research, University Medical Center Utrecht, 3584 CX Utrecht, The Netherlands.

⁵ Section Metabolic Diseases, Department of Child Health, Wilhelmina Children's Hospital, University Medical Center Utrecht, 3584 EA Utrecht, The Netherlands

*#These authors contributed equally to this work.

ABSTRACT

The reversible oxidation of L-malate to oxaloacetate is catalyzed by NAD(H)-dependent malate dehydrogenase (MDH). MDH plays essential roles in the malate–aspartate shuttle and the tricarboxylic acid cycle. These metabolic processes are important in mitochondrial NADH supply for oxidative phosphorylation. Recently, bi-allelic mutations in mitochondrial MDH2 were identified in patients with global developmental delay, epilepsy and lactic acidosis. We now report two patients from an extended consanguineous family with a deleterious variant in the cytosolic isoenzyme of MDH (MDH1). The homozygous missense variant in the NAD⁺-binding domain of *MDH1* led to severely diminished MDH protein expression. The patients presented with global developmental delay, epilepsy and progressive microcephaly. Both patients had normal concentrations of plasma amino acids, acylcarnitines, lactate, and urine organic acids. To identify the metabolic consequences of MDH1 deficiency, untargeted metabolomics was performed on dried blood spots (DBS) from the patients and in MDH1 knockout HEK293 cells that were generated by Crispr/Cas9. Increased levels of glutamate and glycerol 3-phosphate were found in DBS of both patients. In MDH1 KO HEK293 cells, increased levels of glycerol 3-phosphate were also observed, as well as increased levels of aspartate and decreased levels of fumarate. The consistent finding of increased concentrations of glycerol 3-phosphate may represent a compensatory mechanism to enhance cytosolic oxidation of NADH by the glycerol-*P*-shuttle. In conclusion, MDH1 deficiency is a new metabolic defect in the malate–aspartate shuttle characterized by a severe neurodevelopmental phenotype with elevated concentrations of glycerol 3-phosphate as a potential biomarker.

Keywords: malate-aspartate shuttle, MDH1, MDH2, glycerol 3-phosphate, microcephaly

INTRODUCTION

Malate dehydrogenase 1 (MDH1), an NAD(H)-dependent enzyme, is a part of the malate-aspartate shuttle (MAS). MAS is important for intracellular NAD(H) redox homeostasis as it transfers reducing equivalents across the mitochondrial membrane. NAD(H) itself cannot pass the mitochondrial inner membrane (Figure 1). Cytosolic and mitochondrial NAD⁺/NADH pools are independent from each other, and a proper balance of redox state per compartment is important for cell proliferation and cell growth.^{1,2} A constant supply of cytosolic NAD⁺ is required to sustain glycolysis via glyceraldehyde-3-phosphate dehydrogenase.¹ Replenishing cytosolic NAD⁺ occurs via the reversible reduction of oxaloacetate to L-malate by MDH1.³ Oxidation of L-malate to oxaloacetate by MDH2 occurs in mitochondria as part of both the MAS and tricarboxylic acid (TCA) cycle. This reaction generates NADH for the electron transport chain. The two MDH isoenzymes act in conjunction with four additional components: the cytosolic and the mitochondrial aspartate aminotransferases, and two mitochondrial carriers: the malate-oxoglutarate carrier and the aspartate glutamate carrier (AGC). The latter exists in two isoforms that are expressed in a tissue-specific manner; AGC1 is mainly expressed in the brain and AGC2 in the liver.⁴

Although both MDH enzymes have a high degree of three-dimensional structure conservation, they share a sequence-level homology of only ~20-25% and display different kinetics.^{5,6} Expression of MDH1 correlates with high aerobic metabolic demands in a tissue-specific manner. The most abundant expression is in the heart, skeletal muscle and brain, and to a lesser extent in smooth muscle and kidney, with low expression in the liver.⁶⁻⁸ MDH2 has a similar tissue-specific expression pattern as MDH1, which is consistent with the fact that they work co-operatively in the MAS to transport NADH across the mitochondrial membrane.⁸

Since malate dehydrogenase plays a central role in metabolism via the MAS and the TCA cycle, it is a well-studied enzyme. Senescence is associated with decreased MDH1 activity.⁹ Conversely, MDH1 depletion has been shown to induce senescence.⁹ The role of MDH1 in the nucleus has been studied less. Upon glucose deprivation, MDH1 facilitates the binding of p53 to the promotor of downstream genes.¹⁰ Other studies of MDH1 in the context of human diseases have been limited to oncology. It has been noted that MDH1 activity correlates with the malignant potential of certain cancers, e.g. lung.¹¹ This is thought to be mediated by glycolytic-related ATP production.

No human disease-causing mutations in MDH1 have been reported to date; however, genetic diseases in the four other MAS components are known. The first disease

reported was associated with mutations in *AGC2* (or *SLC25A13*). Patients presented with hyperammonemia and hepatic encephalopathy-like symptoms (OMIM #603471, #605814).^{12,13} Subsequently, *AGC1* (or *SLC25A12*) deficiency was described in patients presenting with global developmental delay, encephalopathy and hypotonia (OMIM #612949).^{14,15} A deficiency in the mitochondrial aspartate aminotransferase *GOT2* leads to a similar phenotype as *AGC1* deficiency, with additional hyperammonemia and lactic acidosis.¹⁶ The fourth defect was recently discovered in *MDH2*. This defect is also characterized by global developmental delay, epilepsy and lactic acidosis (OMIM #617339).¹⁷ Here we report a deficiency in *MDH1* as the fifth MAS defect. Two patients from an extended consanguineous family were identified with a pathogenic homozygous *MDH1* variant. They both presented with a neurological phenotype that includes global developmental delay, epilepsy and progressive microcephaly.

RESULTS

Clinical history

Index patient 1 is a 25-month-old Saudi boy. He was born prematurely at 32 weeks following an uneventful pregnancy. He spent 3 weeks in the NICU mainly for weight management, during which he required a blood transfusion. At age 13 months, the pediatrician noted a global developmental delay and progressive microcephaly (OFC was 35.5 cm at 3 m of age, -3.6 SD). He was able to roll over but not to sit or crawl and his babbling was minimal. There was episodic up-rolling of the eyes suggestive of seizures. At 14 months of age, physical examination revealed microcephaly (OFC 41.5 cm, -4.6 SD), poor growth with length of 70 cm (-2.7 SD) and weight of 8.75 kg (3rd centile), dysmorphic facies (tall forehead, depressed nasal bridge, prominent infraorbital creases, long philtrum, open mouth and everted lower lip), axial hypotonia and hypertonia of the extremities with hyperactive reflexes. EEG revealed a hypsarrhythmia pattern confirming the clinical suspicion of epilepsy. MRI brain showed partial agenesis of predominately the splenium of the corpus callosum, prominent ventricles, and mild hypoplasia of the inferior vermis and pons. He was started on antiepileptic medications with only partial response. His healthy consanguineous parents (Figure 2A for pedigree) had experienced recurrent miscarriages. His 4-year-old female cousin (Figure 2B) had a similar phenotype, with severe global developmental delay (walking at 3 years and a vocabulary of only a few words at 4 years of age), epilepsy (controlled with antiepileptic medication, Table 1), microcephaly (OFC 47 cm, -2 SD), and similar facial dysmorphisms (Figure 2B). Her brain MRI showed mild shortening of the corpus callosum and a normal pons and ventricles. Chromosomal microarray and exome sequencing following the routine diagnostic pipeline did not yield a cause for the clinical phenotype, nor did plasma amino acid, acylcarnitine, lactate, and urine organic acid analysis in both patients.

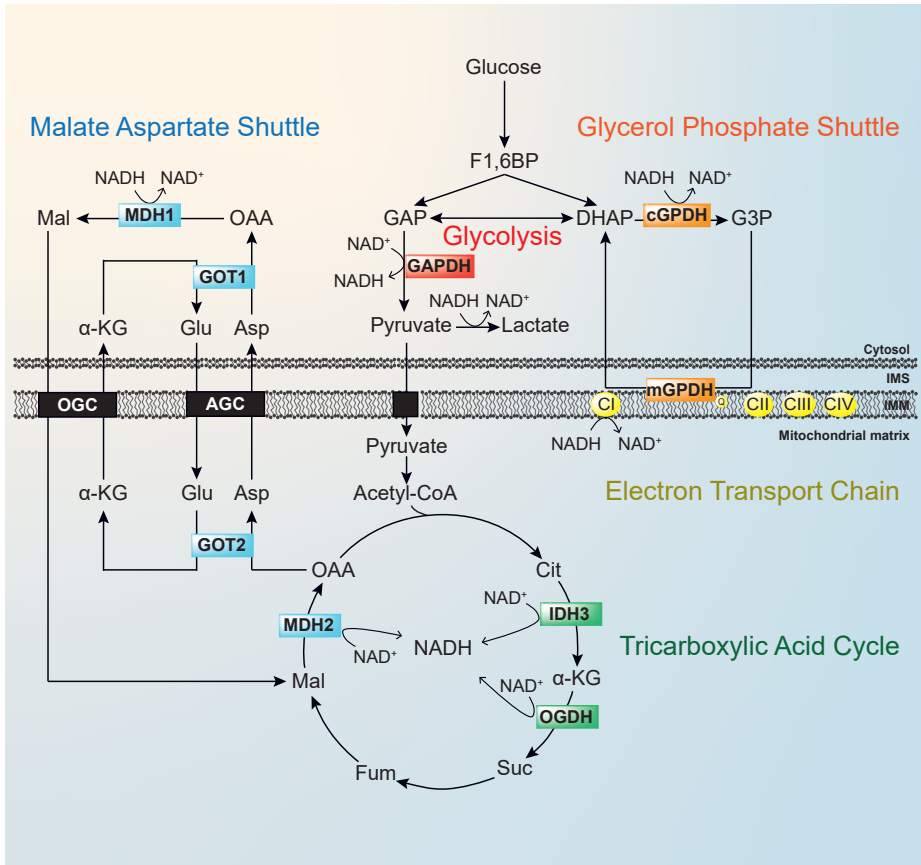


Figure 1. Schematic overview of oxidative glucose metabolism and NAD(H) redox shuttles. NADH generated in the cytosol needs to be shuttled across the mitochondrial membrane, using NAD(H) redox shuttles. During glycolysis, fructose-1,6-bisphosphate (F1,6BP) is converted into glyceraldehyde-3-phosphate (GAP) and dihydroxyacetone phosphate (DHAP). The lower part of glycolysis converts GAP to pyruvate, generating NADH via glyceraldehyde-3-phosphate dehydrogenase (GAPDH). Cytosolic NADH is mainly shuttled into mitochondria via the malate-aspartate shuttle, which requires the action of cytosolic and mitochondrial malate dehydrogenase (MDH1 and MDH2). Other components are cytosolic and mitochondrial glutamate aspartate transaminase (GOT1 and GOT2), the mitochondrial aspartate-glutamate carriers (AGC1 and AGC2), and the malate-oxoglutarate carrier (OGC). Pyruvate is converted into acetyl-CoA, which then enters the tricarboxylic acid cycle. The tricarboxylic acid cycle generates NADH from isocitrate dehydrogenase (IDH2), oxoglutarate dehydrogenase (OGDH), and also includes MDH2. Electrons of these mitochondrial NADH dehydrogenases enter the electron transport chain at the level of complex I (CI). In the glycerol phosphate shuttle, DHAP from glycolysis is further reduced to glycerol 3-phosphate (G3P) by cytosolic G3P dehydrogenase (cGPDH). Electrons from the reconversion to DHAP by mitochondrial GPDH enter the electron transport chain at the level of the quinol pool (Q). *Mal*, malate; *OAA*, oxaloacetate; *α -KG*, alpha-ketoglutarate; *Glu*, glutamate; *Asp*, aspartate; *Cit*, citrate; *Suc*, succinate; *Fum*, fumarate; *CII*, complex II (succinate dehydrogenase); *CIII*, complex III; *CIV*, complex IV; *NADH*, nicotinamide adenine dinucleotide (reduced form); *NAD⁺*, nicotinamide adenine dinucleotide (oxidized form); *IMS*, intermembrane space; *IMM*, inner mitochondrial membrane.

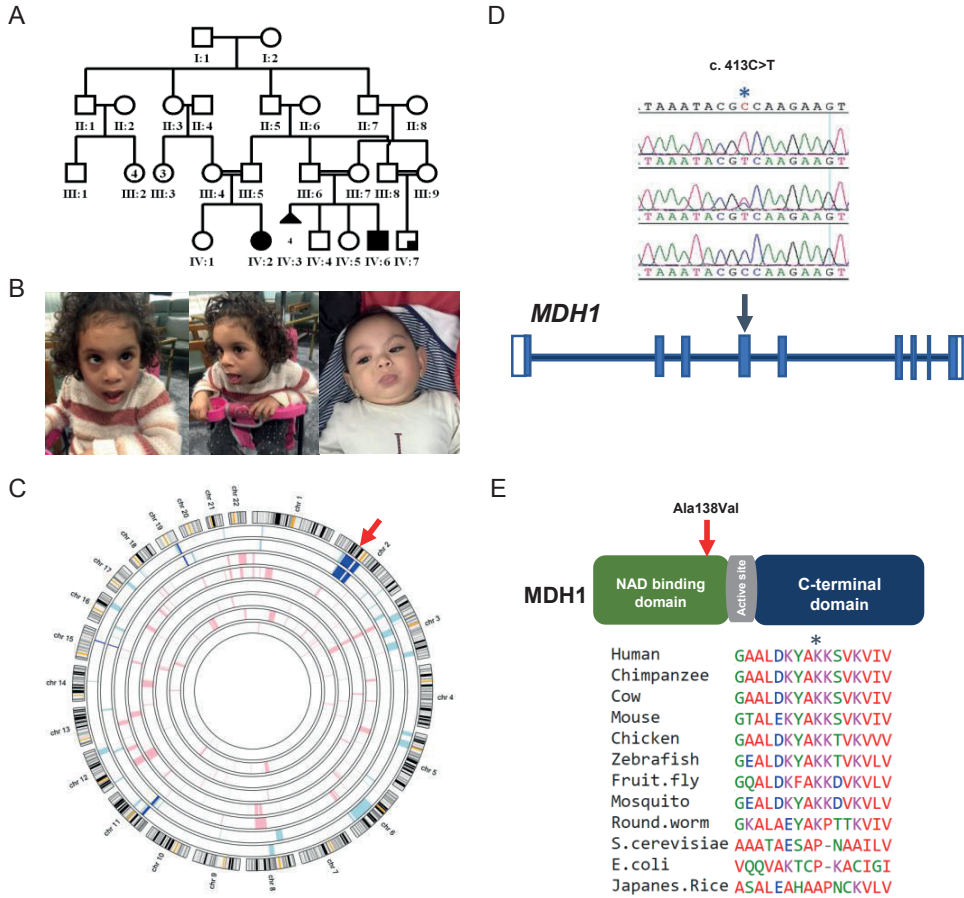


Figure 2. **A.** Pedigree of the affected family. **B.** Clinical photographs of the two affected individuals. **C.** Autozygome analysis using Agilent ideogram showing the candidate autozygome in dark blue. **D.** Sequence chromatogram of the variant (top tracing corresponds to a homozygous patient, middle corresponds to a carrier and bottom corresponds to normal control) shown and its location on a cartoon of MDH1. **E.** Degree of conservation of the affected amino acid residue.

WES results

We enrolled both individuals and their parents with informed consent under an IRB-approved research protocol (RAC#2080006) to identify the underlying cause of their likely autosomal recessive condition. We performed autozygome analysis as described before,²⁰ which revealed four autozygous intervals that were exclusively shared by the two affected individuals (Figure 2C). We also proceeded with whole exome sequencing on the index patient and filtered the resulting variants by the coordinates of the candidate autozygome as described before.²¹ Only one homozygous variant was identified that was absent both in gnomAD and in a local database of ~2,300 ethnically matched exomes: *MDH1*:NM_001199111:c.413C>T (Figure 2D). The resulting missense variant p.Ala138Val replaces an absolutely conserved alanine (down to yeast and rice) in the NAD⁺-binding domain (Figure 2E). This variant segregated with the phenotype in a fully penetrant autosomal recessive fashion within the family.

MDH1 deficiency leads to aberrations in MAS-related metabolites

To study the potential pathogenicity of the *MDH1* variant, we assessed protein expression levels. MDH1 protein level was greatly reduced compared to controls in both lymphoblastoid cells (80%) and fibroblasts (70%) derived from both affected individuals (Figure 3). We then aimed to identify the metabolic consequences of MDH1 deficiency. To this end, MDH1 knockout HEK293 cells were generated by Crispr/Cas9 (Figure S1). Since the MAS plays an integral role in TCA and amino acid metabolism, compounds from both metabolic pathways were analyzed in dried bloodspots (DBS) and in MDH1 knockout cells. Targeted LC-MS/MS analysis revealed high concentrations of glutamate and a decreased glutamine/glutamate ratio compared to controls (Figures 4A and 4B) in DBS, but not in the KO cell lysates (Figure S2). In addition, analysis of MDH1 KO cell lysates revealed an increase in aspartate and a decrease in fumarate levels (Figures 4C and 4D), findings that were not observed in DBS (data not shown). No clear differences were found in concentrations of other TCA cycle intermediates, with the exception of low malate levels in one of the KO cell lysates (Figure S3).

Table 1. Clinical presentation of patients with MDH1 deficiency.

Clinical and genetic findings		
Origin	Saudi Arabia	Saudi Arabia
Family	Family-1	Family-1
Age	2.5 years	4 years
Sex	Male	Female
Consanguinity	yes	yes
ID on the pedigree	(IV:6)	(IV:2)
Genetic variant	MDH1:NM_001199111::c.413C>T:p. Ala138Val	MDH1:NM_001199111::c.413C>T:p. Ala138Val
Zygoty	Homozygous	Homozygous
NICU	Product of 32 week, birth weight 1.4 kg, admitted at NICU for 7 days, discharged home with 2 kg weight, one week later, readmitted with respiratory distress, found to have mild acidosis, had repeated visit to the hospital because of respiratory distress	No NICU admission
Growth parameters	OFC 41.5 cm (-4.6 SD), length 70 cm (-2.7 SD) and weight 8.75 kg (3 rd centile)	OFC 47 cm (-2 SD)
Age at which growth parameters were taken	14 months	4 years
Developmental History	Global developmental delay	Global developmental delay
Dysmorphic Features	Microcephaly, plagiocephaly, bulbous nose, deep eyes, frontal bossing, micrognathia, strabismus	Microcephaly, plagiocephaly, bulbous nose, deep eyes, frontal bossing, micrognathia, strabismus
Ophthalmology	Normal retina	NA
Hematology	Normal CBC	Normal CBC
EEG	Consistent with epileptic encephalopathy, similar to hypsarrhythmic pattern	Normal

Table 1. Continued

Clinical and genetic findings		
Brain MRI	<p>Thinning and hypogenesis of the corpus callosum predominately the splenium. There is paucity of the white matter mainly in the posterior region with prominent peri-cerebral CSF spaces with asymmetry of the lateral ventricle predominantly prominent on the left side and posterior horn representing ex vacuo dilatation. There is mildly hypoplastic inferior vermis with mild pontine hypoplasia.</p>	<p>Sagittal T1 revealed mild short corpus callosum, however, revealed normal signal intensity Axial T2 revealed mildly short corpus callosum, however, it shows normal signal intensity Axial T2 revealed normal myelination process which could be compatible with the age of the patient. 3D SPGR revealed no gross cortical abnormalities. Normal configuration of the brainstem. The pituitary gland revealed normal size and signal intensity with no gross abnormality seen within hypothalamus region.</p>
Laboratory findings	<p>Tandem MS urine GCMS, ammonia and lactate was within normal limits.</p>	<p>Tandem MS: normal, URO: normal, lactate: 2.3, ammonia: normal</p>
Diagnosis	<p>Severe progressive microcephaly, global developmental delay and epilepsy.</p>	<p>Severe developmental delay and microcephaly</p>
Medications	<p>Topamax 37.5 mg p.o. b.i.d and Clonazepam 0.1 mg p.o. b.i.d.</p>	-

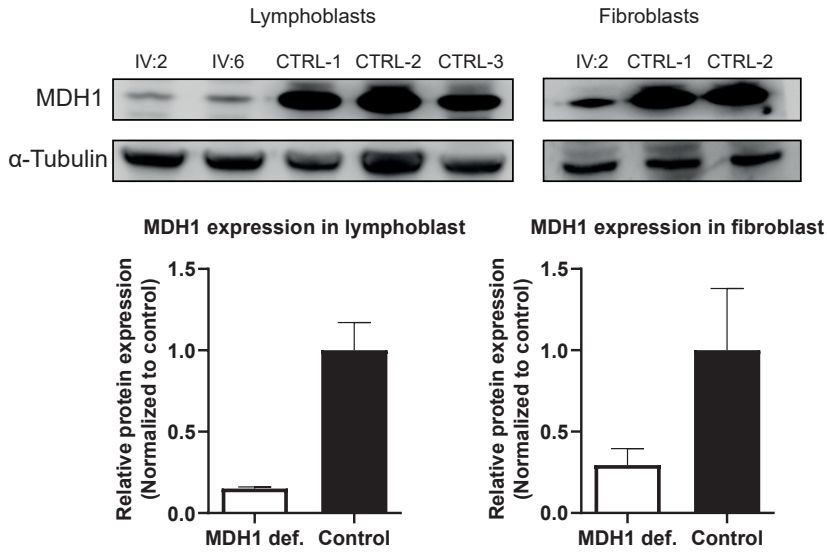


Figure 3. Western blot analysis of MDH1 in protein extracts from LCL as well as fibroblast cells from the affected individuals compared to controls. Relative MDH1 expression is shown as mean \pm SD for both patients and controls 1 and 3 in lymphoblasts. For fibroblasts, relative expression is shown as mean \pm SD for technical triplicates of the patient, and individual datapoints for both controls.

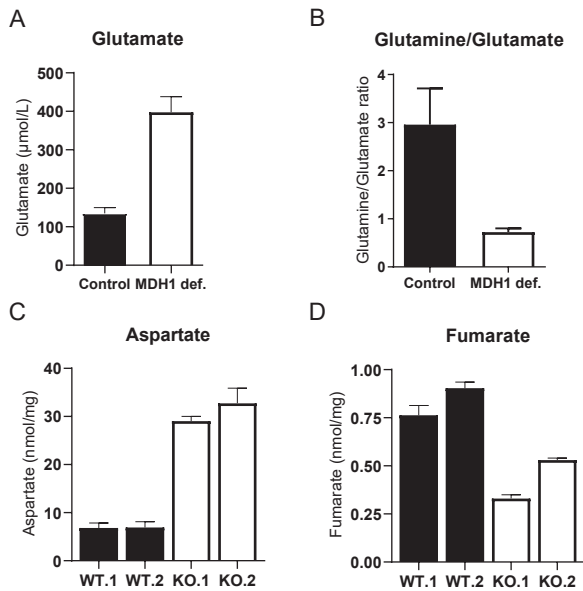


Figure 4. MDH1 deficiency leads to aberrations in MAS-related metabolites. **A.** Glutamate concentration and **B.** Glutamine/Glutamate ratio in dried bloodspots (Control $n=3$, MDH1 def. $n=2$). Data are presented as mean \pm SD. **C.** Aspartate and **D.** Fumarate concentrations in MDH1 HEK293 cells (WT $n=2$, KO $n=2$). Data are presented as mean \pm SD for technical triplicates.

Untargeted metabolomics reveals increased levels of glycerol 3-phosphate

To map additional biochemical consequences of MDH1 deficiency, we performed untargeted metabolomics in both DBS and MDH1 knockout HEK293 cells using direct-infusion mass spectrometry. Untargeted metabolomics revealed increased concentrations of a metabolite corresponding in mass with glycerol 3-phosphate (glycerol 3-*P*) in DBS of both individuals compared to controls (Figure 5A). All other metabolites with Z-scores above 2.5 are listed in supplemental Table 1. Similarly, increased levels of glycerol 3-*P* were found in MDH1 KO HEK293 cells when compared to controls (Figure 5B). However, since direct-infusion mass spectrometry does not distinguish between isomers, the identification of glycerol 3-*P* is limited, as beta-glycerophosphoric acid (glycerol 2-*P*) has the same mass. To this end, these findings were validated using targeted measurements of glycerol 3-*P*. In DBS of both individuals high concentrations of glycerol 3-*P* were found compared to control (Figure 5C), but in cell lysates the difference between MDH1 KO and controls was no longer significant (Figure 5D).

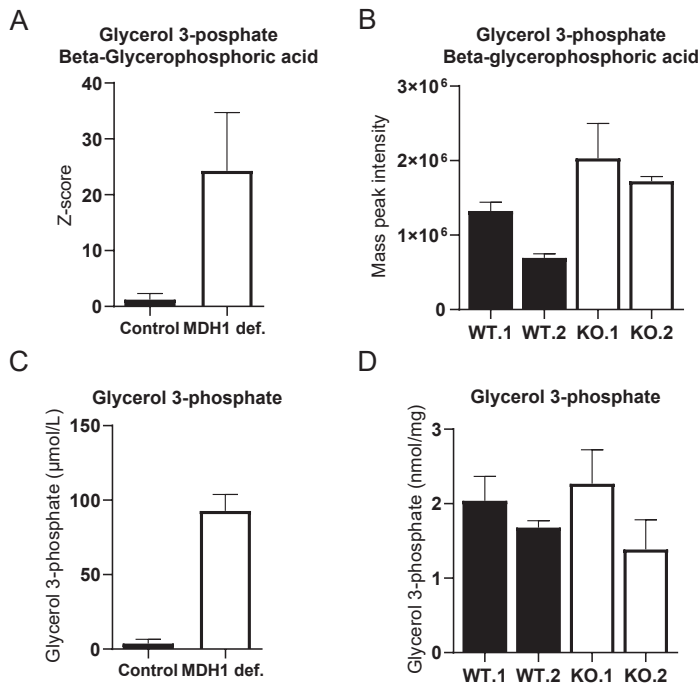


Figure 5. Untargeted metabolomics revealed increased levels of glycerol 3-phosphate. **A.** Z-scores annotated for glycerol 3-phosphate and beta-glycerophosphoric acid in dried blood spots (Control $n=3$; MDH1 def. $n=2$). **B.** Raw mass peak intensities annotated for glycerol 3-phosphate and beta-glycerophosphoric acid in MDH1 HEK293 cells (WT $n=2$, KO $n=2$). **C.** Glycerol 3-phosphate concentration in dried blood spots (Control $n=3$; MDH1 def. $n=2$) and **D.** MDH1 HEK293 cells. Data from MDH1 HEK293 cells are presented as mean \pm SD for technical triplicates.

DISCUSSION

We report a family with a neurodevelopmental disorder characterized by global developmental delay, epilepsy and progressive microcephaly and a homozygous MDH1 candidate causal variant. This neurological phenotype highly resembles the phenotype that was observed in patients with MDH2 and other MAS deficiencies and might, thus, well represent the clinical consequences of this group of disorders. A notable exception is that we did not find lactic acidemia in our patients. Since MDH1 and MDH2 are localized into different subcellular compartments, this is not surprising. Lactic acidemia is often a characteristic of mitochondrial dysfunction, caused by compensatory ATP-production via glycolysis.²² Lactic acidemia is expected in MDH2 deficiency given its role linked to the mitochondrial electron transport chain,¹⁷ but might not be seen in MDH1 deficiency because of hampered glycolysis.

The mechanism of how MDH1 deficiency may cause the observed neurodevelopmental phenotype is unclear. Both children presented with global developmental delay, progressive microcephaly, epilepsy, axial hypotonia and hypertonia of the extremities. The combination of these clinical symptoms suggests underlying problems in the central nervous system. This is further supported by the abnormal findings on neuroimaging and would be consistent with the important role of the MAS in neurons.²³

One of the biochemical findings in dried blood spots (DBS) of both patients was the elevated level of glutamate. In addition, increased levels of a bile acid (3-oxo-4,6-choladienoic acid, Table S1) were found. Since primary functions of the liver include breakdown of amino acids and the production and excretion of bile acids, these findings might indicate subclinical liver problems in the patients. The regulation of MAS enzymes and transporters also have an important influence on glutamate metabolism in the brain.^{23–25} Although glutamate cannot cross the blood-brain barrier, the increased glutamate levels in the blood may reflect similar metabolic consequences as in the brain. Glutamate acts as an important excitatory neurotransmitter in the brain.²⁶ Neurons are able to synthesize glutamate from its local precursor α -ketoglutarate via GOT1, using aspartate as nitrogen source.^{27,28} The supply of cytosolic α -ketoglutarate for this transamination reaction occurs via the malate-oxoglutarate carrier, which exchanges cytosolic malate for mitochondrial α -ketoglutarate. However, to drive this exchange, sufficient cytosolic malate is required. A deficiency in MDH1 might decrease cytosolic malate availability. In addition, glutamate homeostasis may be affected in these cells. Disturbances in glutamate homeostasis are also seen in patients with epilepsy, in which a rise in extracellular glutamate levels has been observed.^{29,30} Since both children presented with clinical symptoms of epilepsy, the increased glutamate

levels in dried blood spots of the patients may be associated with the neurological clinical phenotype of MDH1 deficiency.

In contrast, no clear differences of glutamate concentration were found in our MDH1 KO HEK cell model compared to control. This is probably due to the fact that cell culture simply reflects metabolites from a single cell type, whereas dried blood spots reflect metabolites from multiple tissues.

Further analysis of the MDH1 KO cells identified two interesting phenomena: increased aspartate levels and decreased fumarate levels. Aspartate is essential for protein synthesis as well as for purine and pyrimidine biosynthesis.³¹ Increased levels of aspartate were also previously identified in a MDH1 KO model of Jurkat cells.³² Transamination of aspartate to oxaloacetate by GOT1 has been shown to support generation of malate via MDH1.³³ In MDH1 deficiency, oxaloacetate cannot be converted into malate, which may result in accumulation of its precursor aspartate. The decreased levels of fumarate in MDH1 KO cells might also indicate a disruption in several pathways. Cytosolic fumarate is transported into mitochondria to be recycled for cytosolic aspartate via the TCA cycle and MAS enzymes and transporters. A defect in recycling cytosolic aspartate, which is a precursor for malate in the MAS, might be compensated via increased conversion of fumarate to malate. Cytosolic malate have been shown to be essential for the transport of glutamate into mitochondria via the AGC,³⁴ since malate is also a precursor of mitochondrial aspartate via oxaloacetate. In addition, transport of malate in mitochondria is important for pyruvate oxidation and feeding in the TCA cycle. The identified metabolic consequences of MDH1 deficiency involve metabolites that are directly linked to both substrates of MDH1. However, since transporters and enzymes of the MAS, TCA and also the urea cycle share overlapping metabolic mechanisms involving MDH1, these biochemical aberrations may reflect a more complex mechanism. Future work regarding functional pathway analysis is required to elucidate the exact role of these metabolites in MDH1 deficiency.

Using untargeted metabolomics we were able to discover a potential biomarker for this new deficiency. Increased levels of glycerol 3-phosphate (glycerol 3-*P*) were revealed in DBS of both patients compared to controls. The accumulation of glycerol 3-*P* may be a logical consequence of MDH1 deficiency. Glycerol 3-*P* is an oxidative product of the cytosolic NADH-dependent glycerol 3-phosphate dehydrogenase (GPDH) and is part of the glycerol-phosphate (glycerol-*P*) shuttle (Figure 1). This shuttle functions similarly to the MAS to mediate the cytosolic oxidation of NADH, but is mainly involved in triglyceride synthesis via regulation of cytosolic glycerol 3-*P* availability.³⁵ The glycerol-*P* shuttle has a variable expression

over tissues, with highest expression in brown adipose tissue.³⁶ There is also evidence of glycerol-*P* shuttle activity in the central nervous system, with probably a more dominant role for the glycerol-*P* shuttle in astrocytes than in neurons.³⁷⁻³⁹ Increased levels of glycerol 3-*P* may be caused by increased GPDH activity due to high cytosolic NADH levels, which may partly compensate the consequences of MDH1 deficiency.

In conclusion, we propose that MDH1 deficiency is a new defect in the MAS causing a neurological phenotype. The elevated concentrations of glycerol-3-*P* in DBS of both patients suggest a potential role for glycerol 3-*P* as a biomarker in this novel metabolic disorder.

ACKNOWLEDGEMENTS

We thank the patients and families for their enthusiastic participation. We also thank the Genotyping and Sequencing Core Facilities at KFSHRC for their technical help. We also thank Marjolein Bosma, Birgit Schiebergen-Bronckhorst, Johan Gerrits and Yuen Fung Tang for their technical assistance. This work was supported by King Salman Center for Disability Research (85721 to FSA) and Metakids (2017-075 to JJMJ).

CONFLICT OF INTEREST STATEMENT

The authors declare no conflict of interest

MATERIALS AND METHODS

Human subjects

Patients, parents and other available relatives were recruited under an IRB-approved research protocol (KFSRHC RAC #2080006) with informed consent. Venous blood was collected in EDTA tubes for DNA extraction and sodium heparin tubes for LCL establishment. A skin biopsy was also obtained from one patient for fibroblast culture. Bloodspots from both patients and three healthy controls were collected on a Guthrie card filter paper blood spot card and shipped from Saudi Arabia to the Netherlands. Dried bloodspots (DBS) were stored at -80 °C until analysis in a zip lock bag containing a silica gel bag.

Cell culture, protein extraction and western blot of affected cells

Affected and control fibroblasts and Lymphoblastoid cell lines (LCL) were cultured in Minimum Essential Medium Eagle (Sigma-Aldrich, M-5650) and RPMI (Thermo Fisher Scientific, 22400-089) media, respectively. Both media were supplemented with 15% v/v heat inactivated fetal bovine serum (Thermo Fisher Scientific, Cat. No. 16140071),

1% v/v L- glutamine, and 1% v/v penicillin and streptomycin. Both cell types were cultured in a humidified, 5% CO₂ atmosphere at 37 °C. Protein extraction for western blot of patient cell lines was performed using RIPA buffer (Sigma-Aldrich, Cat. No. R0278) and protease inhibitor (Thermo Fisher Scientific, Cat No. 78438). Western blot was performed on affected and control protein extracts using a rabbit anti-MDH1 polyclonal antibody (Thermo Fisher Scientific, Cat. No. PA5-50446; diluted 1:1000). A mouse anti-alpha Tubulin monoclonal antibody (Abcam Cat. No. ab7291; diluted 1:1000) was used as loading control.

Generation of MDH1-knockout HEK293T cells by CRISPR-Cas9

HEK293T cells were transiently transfected with pSpCas9(BB)-2A-GFP (PX458), encoding a sgRNA targeting *MDH1* (sgRNA1 : ATTTATCTAAGGCTGCACCC, or sgRNA2: CTTCTTGGCGTATTTATCTA). GFP-positive cells were sorted using a FACSaria II flow cytometer (BD) and plated in 10-cm dishes. Colonies were picked from these plates after 1 week and checked for the absence of MDH1 by western blot analysis using a mouse anti-MDHC (H6) monoclonal antibody (Santa Cruz cat. sc-166879; diluted 1:5000). A mouse anti-β-Catenin monoclonal antibody (BD Biosciences Cat. 610154; diluted 1:5000) was used as loading control.

Cell culture of HEK293T cells

Dulbecco's Modified Eagle Medium (DMEM), high glucose, GlutaMAX™, pyruvate (Cat. No. 31966); fetal bovine serum (FBS; Cat. No. 10270); penicillin-streptomycin (P/S (10,000 U/mL); Cat. No. 15140) and trypsin-ethylenediaminetetraacetic acid (trypsin-EDTA (0.5%), no phenol red; Cat. No. 15400) were purchased from Gibco™ (Thermo Fisher Scientific). HEK293T cells were cultured in 75 cm² filter cap flasks in a humidified, 5% CO₂ atmosphere at 37 °C. They were cultured in DMEM, high glucose, GlutaMAX™, pyruvate (with 10% (v/v) heat-inactivated FBS and 1% P/S (v/v)). Cells were passaged upon reaching confluence and medium was refreshed every 48 hours.

Collection of cell lysates for metabolomics

MDH1 WT and KO HEK293 cells were plated in 6-well plates and cultured until full confluency. Medium was refreshed 24 hours after plating and 24 hours before cell collection. Cell collection was done by washing cells with cold PBS (4 °C), followed by cell scraping in 1 ml ice-cold methanol. Next, methanol samples were transferred into 1.5 ml Eppendorf tubes, centrifuged (16,200 g for 10 min at 4 °C), and then supernatants were transferred to new 1.5 ml Eppendorf tubes. The samples were evaporated at 40 °C under a gentle stream of nitrogen until complete dryness, and reconstituted with 500 µl of UPLC-grade methanol (room temperature). The reconstituted samples were stored at -80 °C until analysis was performed.

Targeted metabolomics by LC-MS/MS

Amino acids

To quantify amino acids in DBS and cell lysates, we adapted the UPLC-MS/MS method that was previously described.¹⁸ The range of calibrators were adapted to our samples' concentrations. Furthermore, quality control samples that resembled the concentrations of our samples were used. No further adaptations were needed for sample preparation or analysis of the amino acids. The assay was performed for technical triplicates and data were corrected for total protein concentration.

TCA cycle intermediates

The quantification of TCA cycle intermediates in cell lysates was performed using a Q-Exactive HF High-resolution mass spectrometer. Chromatographic separation was achieved by injecting 5 μ l sample on an Sunshell RP-Aqua column (3 x 150 mm, 2.6 μ m; ChromaNik Technologies Inc., Osaka, Japan). The flow rate remained constant at 0.6 ml/min; column temperature was maintained at 40 °C and the autosampler at 10 °C. Solvent A consisted of 0.1% formic acid (v/v) dissolved in ultrapure H₂O and solvent B was 0.1% formic acid (v/v) dissolved in acetonitrile. The mobile phase gradient (%B) was as follows: 0-2.75 min isocratic 0% B; 2.75-3.5 min linear gradient from 0% to 70% B; 3.5-6.5 min isocratic 70% B; 6.5-6.7 min linear gradient from 70% to 0% B; 6.7-10 min isocratic 0% B for column equilibration.

The internal standard solution consisted of ²H₃-pyruvate, ²H₃-lactate, ²H₄-citrate, ²H₄-2-oxoglutarate, ²H₄-succinate, ²H₄-fumarate, ²H₃-malate (Sigma-Aldrich, Denmark). Calibration standards were prepared with internal standards in the concentration range of 0.15 – 100 μ M. 20 μ l internal standard solution was added to 0.5 ml methanol cell extract, evaporated with nitrogen and reconstituted in a mixture of 25 μ l 0.1% NaOH and 25 μ l 10mg/ml O-(2,3,4,5,6-pentafluorobenzyl)hydroxylamine dissolved in ultrapure H₂O. Samples were derivatized in a thermomixer at 1000 rpm for 30 minutes.

Samples were detected in full scan negative ionisation mode with a scan range of 70-400 m/z and a resolution of 240000. Parameters for negative ESI were as follows: capillary voltage = 4 kV, capillary temperature = 300 °C, automatic gain control target = 1e6, sheath gas = 50, aux gas = 20, spare gas = 0, S-lens RF level = 65. Peak integration was performed using TraceFinder software (Thermo Scientific). The concentration of each analyte was calculated using the calibration curve. The assay was performed for technical triplicates of cell lysates and data were corrected for total protein concentration.

Glycerol 3-phosphate

Quantification of glycerol 3-phosphate in DBS and cell lysates was performed on a Thermo Q-Exactive HF liquid chromatography system (Thermo Scientific, Bremen, Germany). Samples were prepared by taking a 3-mm punch from each DBS and adding 500 μ l methanol absolute ULC/MS (Biosolve BV, Valkenswaard, The Netherlands), followed by a 20-minute ultrasonication step. For cell lysates from HEK293 cells, 500 μ l sample was used. Calibration standards were prepared with internal standards in the concentration range of 0.24–290 μ M. 20 μ l of $^{13}\text{C}_3$ -Lactate internal standard (1 mM) was added to 500 μ l methanol sample extract or 50 μ l standard dilutions. Next, the samples were evaporated under a gentle flow of nitrogen at 40 °C and reconstituted in 30% Methanol/Milli-Q water. Chromatographic separation was performed on a Dionex ultimate 3000 quaternary UHPLC (Thermo Scientific, Germering, Germany) equipped with a refrigerated autosampler (15 °C) and a column heater (55 °C) using a Synergi Hydro-RP 80A column (250 mm x 2 mm i.d., 4 μ m; Phenomenex (Macclesfield, Cheshire, UK)). The following eluents were used: solvent A contained 10% methanol (v/v) and 750 mg/L octylammonium acetate (w/v) dissolved in water provided by a Millipore system; solvent B contained 90% methanol (v/v) and 750 mg/L octylammonium acetate (w/v). The gradient elution was as follows: 0–7.0 min isocratic 20% B, 7.0–8.5 min linear from 20% to 100% B, 8.5–11.5 min isocratic 100% B, and 11.5–12.0 min linear from 100% to 20% B, with 12.0–15 min for initial conditions of 20% B for column equilibration. The flow rate remained constant at 0.5 ml/min. Injection volume was 5 μ l. The octylammonium acetate was made by dissolving 0.1 mol of octylamine (12.9 g) and 0.1 mol of concentrated acetic acid (6 g) in 100 ml of diethyl ether on an ethanol/dry ice bath. The cooled solution was constantly mixed with a magnetic stirrer. After the octylammonium acetate salt crystallized, the ether was removed and the solid crystals were washed twice with 50 ml of n-hexane. Before preparation of the HPLC eluents, the octylammonium acetate was frozen at -20 °C. Sodium L-lactate- $^{13}\text{C}_3$ solution 45–55 % (w/w) in H_2O , octylamine, and L-Glycerol 3-phosphate lithium salt were purchased from Sigma-Aldrich. Acetic acid (>99% purity) was purchased from Merck, Sharpe & Dohme BV.

Detection of glycerol 3-phosphate was performed using a Q-Exactive HF mass spectrophotometer (Thermo Scientific, Bremen, Germany) with an ESI source operating in full scan negative ionisation mode. Parameters for ESI-MS analysis in negative ion mode were as follows: scan range 70 to 600 m/z with a resolution of 120,000, AGC target: $1e6$, maximum IT: 200 ms, capillary voltage: 4 kV, capillary temperature: 300 °C, sheath gas: 50, aux gas: 20, sweep gas: 0, S-lens RF level: 65. Quantification m/z for the compounds measured in the negative ion mode were as follows: $^{13}\text{C}_3$ -lactate: 92.03448 m/z , glycerol 3-phosphate: 171.0064 m/z . Data were

acquired and processed using Thermo Scientific Xcalibur v 4.1.31.9 and Tracefinder v.4.1. The assay was performed for technical triplicates of cell lysates and data were corrected for total protein concentration.

Direct-infusion-based metabolomics

A non-quantitative direct-infusion high-resolution mass spectrometry metabolomics method was used as previously described.¹⁹ In brief, dried blood spots (DBS) from 30 different Dutch controls, 3 Saudi Arabic controls and both patients were measured in a single batch. A 3-mm punch was made from each DBS and 140 µl working solution was added, followed by a 20-minute ultrasonication step. For cell lysates from HEK293 cells, 70 µl cell working solution was added to 70 µl of cell lysate in methanol. Both DBS and cell lysate samples were diluted with 60 µl 0.3% formic acid (Emsure, Darmstadt, Germany). Next, the solutions were filtered using a methanol preconditioned 96-well filter plate (Acro prep, 0.2 µm GHP, NTRL, 1 ml well; Pall Corporation, Ann Arbor, MI, USA) and a vacuum manifold. The sample filtrate was collected in a 96-well plate (Advion, Ithaca, NY, USA).

Samples were analyzed using a TriVersa NanoMate system (Advion, Ithaca, NY, USA) controlled by Chipsoft software (version 8.3.3, Advion). Data acquisition was performed using Xcalibur software (version 3.0, Thermo Scientific, Waltham, MA, USA). A peak-calling pipeline, developed in R-programming language, annotated the raw mass spectrometry data according to the Human Metabolome DataBase (HMDB).

For each annotated mass peak in the DBS samples, the deviation of the intensities of the sample of interest compared to the control samples was indicated by a Z-score. This Z-score was calculated by: $Z\text{-score} = (\text{intensity patient sample} - \text{mean intensity control samples}) / \text{standard deviation intensity control samples}$. Next, metabolites were identified as increased when Saudi Arabic controls had a Z-score below 2.5 and patients had Z-scores above 2.5. The list of increased metabolites is displayed in Table S1, sorted from highest to lowest mean Z-score.

REFERENCES

- Hanse EA, Ruan C, Kachman M, Wang D, Lowman XH, Kelekar A. Cytosolic malate dehydrogenase activity helps support glycolysis in actively proliferating cells and cancer. *Oncogene*. 2017;36(27):3915-3924.
- Olguín-Albuerne M, Morán J. Redox Signaling Mechanisms in Nervous System Development. *Antioxidants Redox Signal*. 2018;28(18):1603-1625.
- Webb LE, Hill EJ, Banaszak LJ. Conformation of Nicotinamide Adenine Dinucleotide Bound to Cytoplasmic Malate Dehydrogenase. *Biochemistry*. 1973;12(25):5101-5109.
- Palmieri L, Pardo B, Lasorsa FM, et al. Citrin and aralar1 are Ca²⁺-stimulated aspartate/glutamate transporters in mitochondria. *EMBO J*. 2001;20(18):5060-5069.
- Birktoft JJ, Fu Z, Carnahan GE, Rhodes G, Roderick SL, Banaszak LJ. Comparison of the molecular structures of cytoplasmic and mitochondrial malate dehydrogenase. *Biochem Soc Trans*. 1989;17(2):301-304.
- Joh T, Takeshima H, Tsuzuki T, et al. Cloning and sequence analysis of cDNAs encoding mammalian cytosolic malate dehydrogenase. Comparison of the amino acid sequences of mammalian and bacterial malate dehydrogenase. *J Biol Chem*. 1987;262(31):15127-15131.
- Tanaka T, Inazawa J, Nakamura Y. Molecular cloning and mapping of a human cDNA for cytosolic malate dehydrogenase (MDH1). *Genomics*. 1996;32(1):128-130.
- Lo ASY, Liew CT, Ngai SM, et al. Developmental regulation and cellular distribution of human cytosolic malate dehydrogenase (MDH1). *J Cell Biochem*. 2005;94(4):763-773.
- Lee SM, Dho SH, Ju SK, Maeng JS, Kim JY, Kwon KS. Cytosolic malate dehydrogenase regulates senescence in human fibroblasts. *Biogerontology*. 2012;13(5):525-536.
- Lee SM, Kim JH, Cho EJ, Youn HD. A nucleocytoplasmic malate dehydrogenase regulates p53 transcriptional activity in response to metabolic stress. *Cell Death Differ*. 2009;16(5):738-748.
- Zhang B, Tornmalm J, Widengren J, Vakifahmetoglu-Norberg H, Norberg E. Characterization of the role of the Malate dehydrogenases to lung tumor cell survival. *J Cancer*. 2017;8(11):2088-2096.
- Saheki T, Kobayashi K. Mitochondrial aspartate glutamate carrier (citrin) deficiency as the cause of adult-onset type II citrullinemia (CTLN2) and idiopathic neonatal hepatitis (NICCD). *J Hum Genet*. 2002;47(7):333-341.
- Song YZ, Deng M, Chen FP, et al. Genotypic and phenotypic features of citrin deficiency: Five-year experience in a Chinese pediatric center. *Int J Mol Med*. 2011;28(1):33-40.
- Wibom R, Lasorsa FM, Töhönen V, et al. AGC1 deficiency associated with global cerebral hypomyelination. *N Engl J Med*. 2009;361(5):489-495.
- Falk MJ, Li D, Gai X, et al. AGC1 Deficiency Causes Infantile Epilepsy, Abnormal Myelination, and Reduced N-Acetylaspartate. *JIMD Rep*. 2014;14:77-85.
- van Karnebeek CDM, Ramos RJ, Wen XY, et al. Bi-allelic GOT2 Mutations Cause a Treatable Malate-Aspartate Shuttle-Related Encephalopathy. *Am J Hum Genet*. 2019;105(3):534-548.
- Ait-El-Mkadem S, Dayem-Quere M, Gusic M, et al. Mutations in MDH2, Encoding a Krebs Cycle Enzyme, Cause Early-Onset Severe Encephalopathy. *Am J Hum Genet*. 2017;100(1):151-159.
- Prinsen HCMT, Schiebergen-Bronkhorst BGM, Roeleveld MW, et al. Rapid quantification of underivatized amino acids in plasma by hydrophilic interaction liquid chromatography (HILIC) coupled with tandem mass-spectrometry. *J Inherit Metab Dis*. 2016;39(5):651-660.
- Haijes HA, Willemsen M, van der Ham M, et al. Direct Infusion Based Metabolomics Identifies Metabolic Disease in Patients' Dried Blood Spots and Plasma. *Metabolites*. 2019;9(1):12.
- Alkuraya FS. Discovery of rare homozygous mutations from studies of consanguineous pedigrees. *Curr Protoc Hum Genet*. 2012;75(SUPPL.75):6.12.1-6.12.13.
- Alkuraya FS. The application of next-generation sequencing in the autozygosity mapping of human recessive diseases. *Hum Genet*. 2013;132(11):1197-1211.

22. McInnes J. Mitochondrial-associated metabolic disorders: Foundations, pathologies and recent progress. *Nutr Metab.* 2013;10(1):63.
23. McKenna MC, Waagepetersen HS, Schousboe A, Sonnewald U. Neuronal and astrocytic shuttle mechanisms for cytosolic-mitochondrial transfer of reducing equivalents: Current evidence and pharmacological tools. *Biochem Pharmacol.* 2006;71(4):399-407.
24. Gruetter R, Adriany G, Choi IY, Henry PG, Lei H, Öz G. Localized in vivo ¹³C NMR spectroscopy of the brain. *NMR Biomed.* 2003;16(67):313-338.
25. Malik P, McKenna MC, Tildon JT. Regulation of malate dehydrogenases from neonatal, adolescent, and mature rat brain. *Neurochem Res.* 1993;18(3):247-257.
26. McKenna MC. The glutamate-glutamine cycle is not stoichiometric: Fates of glutamate in brain. *J Neurosci Res.* 2007;85(15):3347-3358.
27. Palaiologos G, Hertz L, Schousboe A. Evidence that Aspartate Aminotransferase Activity and Ketodicarboxylate Carrier Function Are Essential for Biosynthesis of Transmitter Glutamate. *J Neurochem.* 1988;51(1):317-320.
28. Pardo B, Rodrigues TB, Contreras L, et al. Brain glutamine synthesis requires neuronal-born aspartate as amino donor for glial glutamate formation. *J Cereb Blood Flow Metab.* 2011;31(1):90-101.
29. During MJ, Spencer DD. Extracellular hippocampal glutamate and spontaneous seizure in the conscious human brain. *Lancet.* 1993;341(8861):1607-1610.
30. Cavus I, Kasoff WS, Cassaday MP, et al. Extracellular metabolites in the cortex and hippocampus of epileptic patients. *Ann Neurol.* 2005;57(2):226-235.
31. Lane AN, Fan TWM. Regulation of mammalian nucleotide metabolism and biosynthesis. *Nucleic Acids Res.* 2015;43(4):2466-2485.
32. Birsoy K, Wang T, Chen WW, Freinkman E, Abu-Remaileh M, Sabatini DM. An Essential Role of the Mitochondrial Electron Transport Chain in Cell Proliferation Is to Enable Aspartate Synthesis. *Cell.* 2015;162(3):540-551.
33. Gaude E, Schmidt C, Gammage PA, et al. NADH Shuttling Couples Cytosolic Reductive Carboxylation of Glutamine with Glycolysis in Cells with Mitochondrial Dysfunction. *Mol Cell.* 2018;69(4):581-593.e7.
34. Rasmussen UF, Rasmussen HN. Human quadriceps muscle mitochondria: A functional characterization. *Mol Cell Biochem.* 2000;208(1-2):37-44.
35. Mráček T, Drahota Z, Houštěk J. The function and the role of the mitochondrial glycerol-3-phosphate dehydrogenase in mammalian tissues. *Biochim Biophys Acta - Bioenerg.* 2013;1827(3):401-410.
36. Ohkawa KI, Vogt MT, Farber E. Unusually high mitochondrial alpha glycerophosphate dehydrogenase activity in rat brown adipose tissue. *J Cell Biol.* 1969;41(2):441-449.
37. Nguyen NHT, Bråthe A, Hassel B. Neuronal uptake and metabolism of glycerol and the neuronal expression of mitochondrial glycerol-3-phosphate dehydrogenase. *J Neurochem.* 2003;85(4):831-842.
38. Ramos M, Del Arco A, Pardo B, et al. Developmental changes in the Ca²⁺-regulated mitochondrial aspartate-glutamate carrier aralar1 in brain and prominent expression in the spinal cord. *Dev Brain Res.* 2003;143(1):33-46.
39. McKenna MC, Tyson Tildon J, Stevenson JH, Boatright R, Huang S. Regulation of energy metabolism in synaptic terminals and cultured rat brain astrocytes: Differences revealed using aminooxyacetate. *Dev Neurosci.* 1993;15(3-5):320-329.

SUPPLEMENTARY MATERIAL

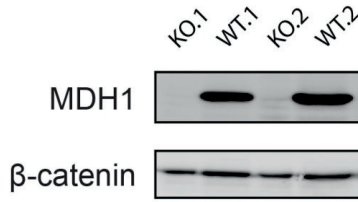


Figure S1. Western Blot analysis showing malate dehydrogenase 1 (MDH1) and beta-catenin expression in wildtype (WT) and knockout (KO) clones.

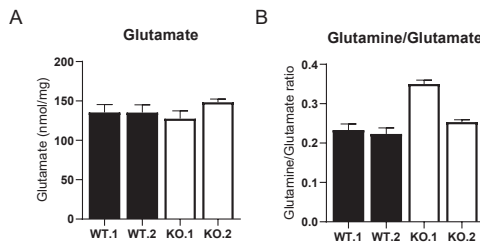


Figure S2. A. Glutamate concentration in *MDH1* HEK293 WT and KO clones. **B.** Glutamine/Glutamate ratio in *MDH1* HEK293 WT and KO clones. Data are presented as mean ± SD for technical triplicates.

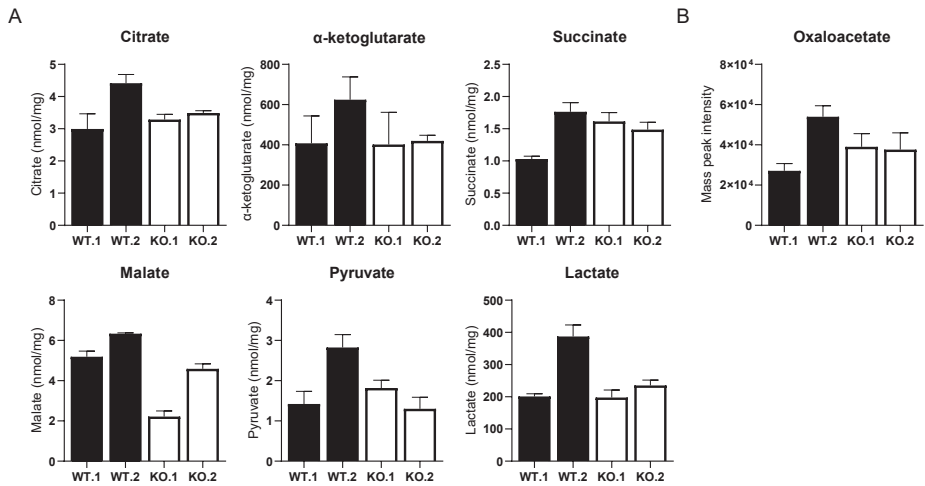
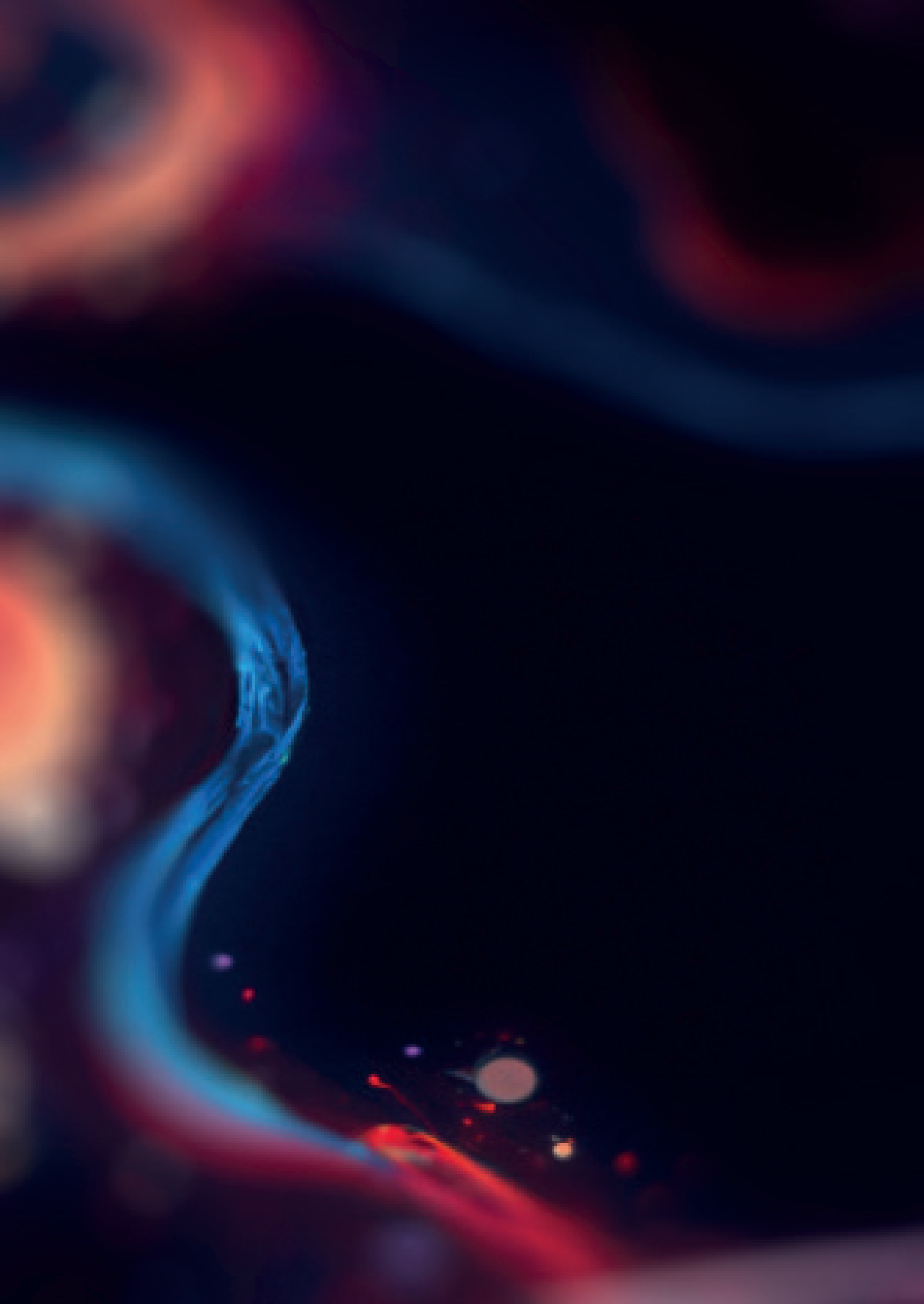


Figure S3. A. Concentration of intermediates of the tricarboxylic acid cycle in *MDH1* HEK293 WT and KO clones. **B.** Raw mass peak intensities annotated for oxaloacetic acid in *MDH1* HEK293 cells. Data are presented as mean ± SD for technical triplicates.

Table S1. Z-scores for compounds identified in DBS of two patients with MDH1 deficiency (P1 and P2).

	Compound name	P1.1	P1.2	P2.1	P2.2	Mean
1	MG(0:0/18:2(9Z,12Z)/0:0); MG(18:2(9Z,12Z)/0:0/0:0)	25.8	42.3	49.2	41.4	39.7
2	3-Oxo-4,6-choladienoic acid	21.6	34.2	39.1	41.9	34.2
3	CPA(16:0/0:0)	19.0	30.5	34.6	37.6	30.4
4	Glycerol 3-phosphate; Beta-Glycerophosphoric acid	34.6	28.7	12.7	21.2	24.3
5	5,6-Epoxy-8,11,14-eicosatrienoic acid; 8,9-Epoxyeicosatrienoic acid; 14R,15S-EpETrE; 15(S)-HETE; 14,15-Epoxy-5,8,11-eicosatrienoic acid; 11,12-Epoxyeicosatrienoic acid; 8-HETE; 16(R)-HETE; 11(R)-HETE; 20-Hydroxyeicosatetraenoic acid; 12-HETE; 18-Hydroxyarachidonic acid; 9-HETE; 11,12-EpETrE; 5-HETE; 19(S)-HETE; 10-HETE; 13-HETE; 17-HETE; 12 Hydroxy arachidonic acid; Arachidonate	50.8	8.9	10.4	8.6	19.7
6	Cervonoyl ethanolamide	8.4	18.3	13.3	13.8	13.5
7	LPA(P-16:0e/0:0)	8.2	17.9	13.0	14.3	13.4
8	MG(0:0/18:1(11Z)/0:0); MG(0:0/18:1(9Z)/0:0); MG(18:1(11Z)/0:0/0:0); MG(18:1(9Z)/0:0/0:0)	7.2	15.7	11.0	14.4	12.1
9	Neurine	8.8	9.7	10.2	19.4	12.0
10	MG(0:0/20:3(11Z,14Z,17Z)/0:0); MG(0:0/20:3(5Z,8Z,11Z)/0:0); MG(0:0/20:3(8Z,11Z,14Z)/0:0); MG(20:3(11Z,14Z,17Z)/0:0/0:0); MG(20:3(5Z,8Z,11Z)/0:0/0:0); MG(20:3(8Z,11Z,14Z)/0:0/0:0);	11.8	10.4	8.2	8.8	9.8
11	2-Arachidonylglycerol; MG(0:0/20:4(8Z,11Z,14Z,1 7Z)/0:0); MG(20:4(5Z,8Z,11Z,14Z)/0:0/0:0); MG(20:4(8Z,11Z,14Z,17Z)/0:0/0:0);	10.3	8.7	8.3	7.1	8.6
12	Inosinic acid; Inosine 2'-phosphate	9.0	6.2	10.3	5.2	7.7
13	Threonic acid	6.5	5.9	8.3	6.1	6.7
14	13S-hydroxyoctadecadienoic acid; Alpha- dimorphelic acid; 9,10-Epoxyoctadecenoic acid; 12,13-EpOME; 9-HODE	4.7	3.4	7.2	10.4	6.4
15	Diacetylspermine	16.0	2.5	3.1	2.7	6.1
16	MG(0:0/14:0/0:0); MG(14:0/0:0/0:0)	5.8	6.2	6.3	2.3	5.2
17	PE(P-16:0e/0:0)	11.2	2.7	2.4	2.2	4.7
18	MG(0:0/16:1(9Z)/0:0); MG(16:1(9Z)/0:0/0:0)	4.8	5.2	5.5	2.5	4.5
19	CPA(18:2(9Z,12Z)/0:0)	4.8	3.8	5.1	2.9	4.1
20	Glyceric acid; L-Glyceric acid	2.1	2.4	2.5	8.0	3.7
21	Hypoxanthine	2.4	2.1	2.3	7.7	3.6
22	Ribitol; D-Arabitol; L-Arabitol	2.9	2.6	3.5	4.9	3.5
23	N-Decanoylglycine	3.7	2.0	2.9	3.8	3.1
24	7b-Hydroxy-3-oxo-5b-cholanoic acid; MG(0:0/22:6(4Z,7 Z,10Z,13Z,16Z,19Z)/0:0) MG(22:6(4Z,7Z,10Z,13Z,16Z,19Z)/0:0/0:0)	2.4	2.7	4.1	2.4	2.9



Chapter 3

Inborn disorders of the malate-aspartate shuttle

Melissa H. Broeks¹, Clara D.M. van Karnebeek^{2,4,5}, Ronald J.A. Wanders³,
Judith J.M. Jans^{1,5*}, Nanda M. Verhoeven-Duif^{1,5*}

¹ Department of Genetics, Section Metabolic Diagnostics, University Medical Center Utrecht, Utrecht, The Netherlands

² Departments of Pediatrics, Amsterdam University Medical Center, Amsterdam, The Netherlands

³ Departments of Pediatrics and Laboratory Medicine, Laboratory Genetic Metabolic Diseases, Amsterdam University Medical Center, University of Amsterdam, Amsterdam, The Netherlands

⁴ Department of Pediatrics, Amalia Children's Hospital, Radboud Center for Mitochondrial Diseases, Radboud University Medical Center, Nijmegen, The Netherlands

⁵ On behalf of 'United for Metabolic Diseases', The Netherlands

*Authors contributed equally

ABSTRACT

Over the last few years, various inborn disorders have been reported in the malate- aspartate shuttle (MAS). The MAS consists of four metabolic enzymes and two transporters, one of them having two isoforms that are expressed in different tissues. Together they form a biochemical pathway that shuttles electrons from the cytosol into mitochondria, as the inner mitochondrial membrane is impermeable to the electron carrier NADH. By shuttling NADH across the mitochondrial membrane in the form of a reduced metabolite (malate), the MAS plays an important role in mitochondrial respiration. In addition, the MAS maintains the cytosolic NAD⁺/NADH redox balance, by using redox reactions for the transfer of electrons. This explains why the MAS is also important in sustaining cytosolic redox-dependent metabolic pathways, such as glycolysis and serine biosynthesis. The current review provides insights into the clinical and biochemical characteristics of MAS deficiencies. To date, five out of seven potential MAS deficiencies have been reported. Most of them present with a clinical phenotype of infantile epileptic encephalopathy. Although not specific, biochemical characteristics include high lactate, high glycerol 3-phosphate, a disturbed redox balance, TCA abnormalities, high ammonia and low serine, which may be helpful in reaching a diagnosis in patients with an infantile epileptic encephalopathy. Current implications for treatment include a ketogenic diet, as well as serine and vitamin B6 supplementation.

Keywords: AGC1; AGC2; GOT2; MDH1; MDH2; NAD(H); inborn metabolic disorder; malate-aspartate shuttle; redox

INTRODUCTION

In the last few years, several inherited metabolic disorders (IMDs) affecting the malate-aspartate shuttle (MAS) have been discovered. The MAS is a redox shuttle which plays an essential and indispensable role in the redox balance both in mitochondria as well as the cytosol. Nutrients that enter the cytosol are oxidized in metabolic pathways by many different enzymes that use NAD^+ as a cofactor. These metabolic pathways generate cytosolic reducing equivalents in the form of NADH which need to enter the mitochondrion to be used for energy production. As the inner mitochondrial membrane is impermeable to NADH molecules, the MAS transports the cytosolic reducing equivalents, or electrons, from the cytosol across the membrane.¹ Eventually, electrons are supplied to the electron transport chain in the form of NADH for ATP production. Simultaneously, the MAS regenerates cytosolic NAD^+ . This cytosolic NADH re-oxidation system maintains the highly compartmentalized NAD^+/NADH balance, which is essential for cellular energy metabolism and is also the driving force for NAD^+ -dependent reactions in the cytosol for instance in the biosynthesis of serine.² The MAS is thus a redox shuttle that supports oxidative pathways as well as oxidative phosphorylation.³

The MAS is particularly important for the central nervous system,⁴ where it is also involved in the synthesis of aspartate and glutamate for neurotransmission.⁵ The fact that patients with a deficiency in one of the components of the MAS present with predominant neurological signs and symptoms emphasizes the importance of the MAS for neurological functioning.⁶⁻¹² Early infantile epileptic encephalopathy is a common phenotype observed in patients with a defect in the MAS but is currently attributed to over 80 different genetic diseases in the OMIM database¹³ and over 30 in the IEMbase.¹⁴ Since these clinical phenotypes are unspecific, insights into the clinical and biochemical phenotypes of MAS deficiencies could help narrowing down the differential diagnosis.

In this literature review the clinical phenotypes and biochemical characteristics of the different MAS deficiencies identified up to now will be discussed. These MAS deficiencies are, at least in part, amenable to targeted treatments, making early diagnosis important. In order to gain additional insight in the MAS and MAS disorders, biochemical clues and possible biochemical mechanisms linking the clinical phenotypes will be explored.

Historical perspective

In 1949, Friedkin and Lehninger proved that NADH links key metabolic pathways and processes such as the citric acid cycle and mitochondrial ATP synthesis,^{15,16} setting the path to the discovery that ATP synthesis and NADH oxidation by oxygen are coupled. Later work showed that these processes are linked to proton translocation across the inner mitochondrial membrane, and led to the concept of a protonmotive force (about 200 mV) driving chemiosmotically ATP synthesis.¹⁷ A key requirement for mitochondrial NADH oxidation is the continuous entry of reducing equivalents such as NADH into the mitochondria. However, the pioneer experiments of Kennedy and Lehninger with isolated mitochondria,¹⁸ led to the conclusion that cytosolic NADH is not directly oxidized by isolated rat-liver mitochondria, indicating that mitochondrial membranes are impermeable to NADH.¹⁹ Consequently, NADH had to be re-oxidized in the cytosol, reducing another acceptor that could permeate into mitochondria.¹ In 1962, Piet Borst postulated that reducing equivalents could be shuttled across the mitochondrial membrane by using substrate cycles involving malate and aspartate, thus formulating the malate-aspartate cycle.^{20,21} Today, the MAS is a well-established mitochondrial electron shuttle.^{22–24} An excellent historical and personal perspective of the MAS has been published recently by its discoverer, Piet Borst.²⁵

Enzymes and transporters of the Malate-Aspartate Shuttle

Four enzymes and two mitochondrial carriers cooperate to transport reducing equivalents across the inner mitochondrial membrane (Figure 1). Enzymes of the MAS include cytosolic and mitochondrial NAD(H)-dependent malate dehydrogenase (EC 1.1.1.37; respective encoding genes, *MDH1* and *MDH2*), as well as cytosolic and mitochondrial aspartate aminotransferase (EC 2.6.1.1; respective encoding genes, *GOT1* and *GOT2*). The two mitochondrial carriers are the oxoglutarate/malate carrier (OGC; gene *SLC25A11*) and the two isoforms of the aspartate-glutamate carrier, AGC1 (also known as Aralar; gene *SLC25A12*) or AGC2 (also known as Citrin; gene *SLC25A13*).

The MAS components are mainly expressed in high-energy demanding tissues, such as the brain, heart and liver, reflecting their critical roles in energy production. Malate dehydrogenases, aspartate aminotransferases and OGC show relatively high expression in the brain, heart and skeletal muscle.²⁶ Isoforms of AGC are expressed in a tissue-specific manner.²⁷ Whereas AGC1 is highly expressed in the brain, heart, central nervous system and skeletal muscle, AGC2 is only abundant in the epithelial lining of the intestine and in the liver.^{27–29} Both isoforms are regulated by cytosolic calcium.²⁷ MDH2 is more ubiquitously expressed than other MAS genes, probably reflecting its direct involvement in the TCA cycle. Not every MAS gene is expressed in all the tissues. In liver, AGC2, MDH2, GOT1 and GOT2 are strongly expressed, but

MDH1 and OGC have low expression.²⁶ Some tissues, such as the lung, have low expression of all MAS genes.

The MAS can be considered to start in the cytosol with the reduction of oxaloacetate to malate by MDH1, which is obligatory coupled to the oxidation of NADH to NAD⁺, thus regenerating NAD⁺ in the cytosol. Malate can enter the mitochondrial matrix by an electroneutral antiporter mechanism that exchanges malate for mitochondrial matrix 2-oxoglutarate, which is mediated by the OGC.^{24,30} Next, malate is re-oxidized in the mitochondrial matrix by MDH2 and NAD⁺ to yield NADH and oxaloacetate. In this way, reducing equivalents are introduced into the mitochondria without passage of NADH across mitochondrial membranes. The oxaloacetate produced in the mitochondrial matrix can be converted to aspartate by transamination by the pyridoxal phosphate-dependent enzyme GOT2, using glutamate as the amino group donor and as the source of the 2-oxoglutarate that is exchanged for malate by OGC. Mitochondrial aspartate is then exported to the cytosol across the inner mitochondrial membrane by the Aralar or Citrin carriers (AGC isoforms), in exchange for cytosolic glutamate and a proton. The electrogenic nature of the glutamate/aspartate antiporting mechanism implies that AGC is essentially irreversible, at least under energized conditions.^{31,32} Lastly, cytosolic oxaloacetate is regenerated by transamination from aspartate to cytosolic 2-oxoglutarate by GOT1 (Figure 1), regenerating the cytosolic glutamate needed for exchange with aspartate.

The role of the Malate-Aspartate Shuttle in metabolism

A major role of the MAS in metabolism is the net transfer of NADH over the inner mitochondrial membrane for oxidative phosphorylation. Simultaneously, the MAS maintains the cytosolic redox state by balancing the NAD⁺/NADH ratio via regeneration of NAD⁺. NAD⁺ is an important cofactor that serves as a carrier for the net removal of electrons from metabolites (oxidation).³³ NAD⁺ impacts metabolism in several ways, both directly as well as via the NAD⁺/NADH ratio.³⁴ Indeed, the absolute NAD⁺-pool plays a key role in cellular signaling, transcriptional regulation and DNA damage repair via protein and nucleic acid modifications, since NAD⁺ is the driving force behind different enzymes including the various members of the sirtuins family as well as the different poly (ADP)-ribose polymerases (PARPs).^{35,36} In these reactions NAD⁺ is not reduced to NADH but instead converted into other metabolites. On the other hand, the NAD⁺/NADH ratio determines the preferred direction of reactions that are NAD(H)-dependent. In general, cells favor a high cytosolic NAD⁺/NADH ratio (~500-1000) which drives oxidative pathways, whereas the mitochondrial NAD⁺/NADH ratio is much lower (~5-10).^{34,37,38} Transfer of cytosolic reducing equivalents to the electron transport chain (ETC) against this 10-100 fold difference in NAD⁺/

NADH ratio, as mediated by the MAS, is energetically unfavorable. It can only take place because the electrogenic AGC is driven by the electrical potential gradient across the inner mitochondrial membrane (~200 mV), which is generated by proton pumping coupled to the electron transport chain.²⁴ Thus, MAS activity is intimately linked to electron transport through the respiratory chain. In addition, AGC1-mediated cytosolic calcium sensing has recently been shown to be essential for the control of oxidative phosphorylation by regulating mitochondrial pyruvate supply, as demonstrated in a knockout mouse model in which the mitochondrial calcium transporter was deleted.³⁹

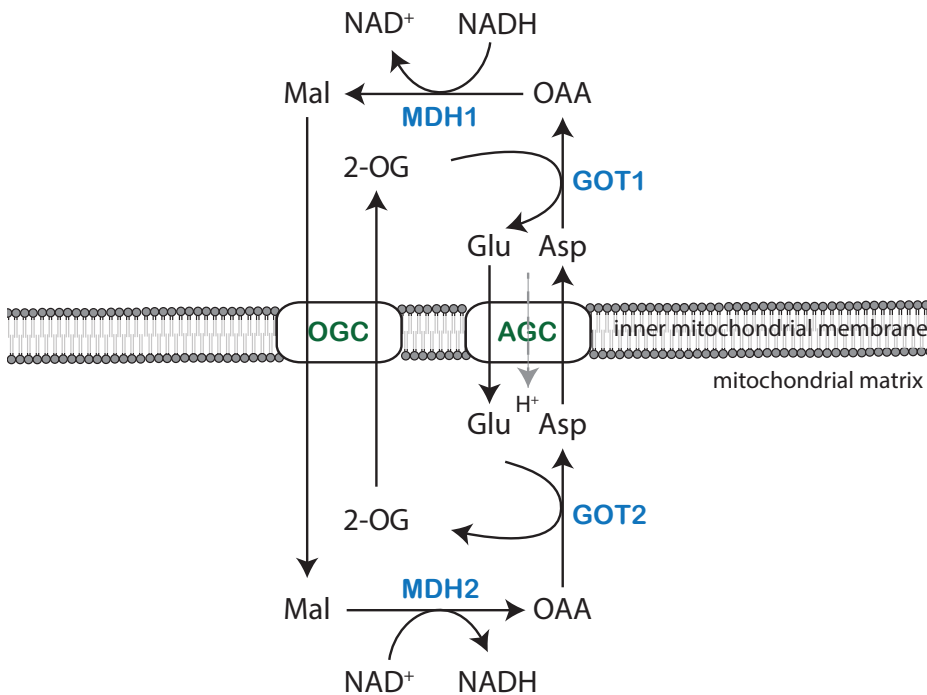


Figure 1. The Malate-Aspartate shuttle. Cytosolic malate dehydrogenase (MDH1) transfers the reducing equivalents from NADH to oxaloacetate (OAA). This reaction generates malate (Mal) and replenishes cytosolic NAD⁺. Cytosolic malate is then transported across the inner mitochondrial membrane via the malate-2-oxoglutarate carrier (OGC), which exports 2-oxoglutarate (2-OG) from the mitochondrial matrix into the cytosol simultaneously. Next, malate is re-oxidized by mitochondrial MDH2 to form oxaloacetate and NADH. Oxaloacetate is transaminated into aspartate (Asp) by mitochondrial aspartate aminotransferase (GOT2). This transamination reaction uses cytosolic glutamate (Glu) as nitrogen donor, which is converted into 2-oxoglutarate. Mitochondrial aspartate is transported across the inner mitochondrial membrane via the aspartate-glutamate carrier (AGC) in exchange for cytosolic glutamate and a proton (H⁺). Lastly, aspartate is converted into oxaloacetate by cytosolic aspartate aminotransferase (GOT1) to maintain malate-aspartate shuttle activity.

Metabolic flux through NAD^+ -dependent pathways affects cytosolic and mitochondrial NAD^+/NADH ratios. Glycolysis is an important NAD^+ -dependent pathway that both affects and is affected by the cytosolic NAD^+/NADH ratio. For glycolysis to continue, a high NAD^+/NADH ratio is required for the conversion of glyceraldehyde 3-phosphate into 1,3-bisphosphoglycerate by glyceraldehyde 3-phosphate dehydrogenase (GAPDH, EC 1.2.1.12), in which NAD^+ is converted into NADH .^{40,41} Re-oxidation of NADH can either be accomplished via the conversion of pyruvate to lactate by lactate dehydrogenase (LDH, EC 1.1.1.27) or by the conversion of oxaloacetate into malate by MDH1 (Figure 2). Converting glucose into lactate consumes and regenerates an equal amount of NAD^+ ,^{33,37} and additionally results in the production of 2 ATP molecules per glucose molecule. However, re-oxidation of NADH via MDH1, and the subsequent transfer of reducing equivalents to the ETC, coupled with the transfer of pyruvate across the mitochondrial membrane and its subsequent full oxidation to CO_2 and H_2O , results in the production of 36 ATP molecules per glucose molecule. Therefore, re-oxidation of NADH via the MAS provides more energy as it supports both glycolysis and mitochondrial respiration.⁴² In addition, sufficient NAD^+ -regeneration is also necessary for oxidative synthesis of nucleotides and amino acids, such as serine. The first step of serine biosynthesis is catalyzed by phosphoglycerate dehydrogenase (PHGDH, EC 1.1.1.95), another NAD^+ -dependent enzyme. The synthesis of serine from glucose, includes two oxidative steps catalyzed by GAPDH and PHGDH, requiring two molecules of NAD^+ . Therefore, other metabolic pathways that need serine, including synthesis of cysteine, glycine, but also one-carbon metabolism, indirectly require NAD^+ .³⁷ The MAS plays an essential role in redox balance and consequently in the continuation of the metabolic pathways mentioned above.

Next to their roles in cellular redox balance, some of the MAS enzymes play a role in anabolic and catabolic processes. Via transamination of oxaloacetate and glutamate by GOT2, the MAS is involved in the synthesis of aspartate. Whereas a cycle of the MAS as discussed above only results in a net transfer of electrons, *de novo* synthesis of aspartate can take place if oxaloacetate is supplied via pyruvate carboxylase. However, the major source of aspartate is oxidative glutamine metabolism. Here, glutamine carbons enter the TCA cycle as 2-oxoglutarate, which is further oxidized into oxaloacetate via MDH2.⁴³ Oxaloacetate is then further converted to aspartate via GOT2. Inhibition of the ETC impairs aspartate biosynthesis via a drop in the mitochondrial NAD^+/NADH ratio, which implies that mitochondrial respiration sustains aspartate biosynthesis.^{43,44} Aspartate is essential for cell proliferation, as it is a precursor for purine and pyrimidine synthesis. In liver, aspartate is also involved in the urea cycle. Thus, the MAS is important for aspartate synthesis by providing its precursor oxaloacetate via MDH2 followed by transport of aspartate to the cytosol by AGC, thereby impacting several other metabolic pathways.

The glycerol 3-phosphate shuttle

An alternative shuttle linked to the MAS via transfer of redox equivalents may be of importance if MAS activity is deficient.^{1,45} In addition to the MAS, the glycerol 3-phosphate shuttle also transfers cytosolic reducing equivalents into the ETC. In 1958, two independent groups proposed the glycerol 3-phosphate shuttle, also known as the glycerophosphate (GP) shuttle.^{46,47} In this shuttle, cytosolic glycerol 3-phosphate dehydrogenase (GPD1, EC 1.1.1.8) transfers reducing equivalents of NADH to dihydroxyacetone phosphate with concomitant formation of glycerol 3-phosphate (G3P) and NAD⁺ (Figure 2). Via the enzyme GPD2 (EC 1.1.5.3), which is bound to the cytosolic face of the mitochondrial inner membrane, G3P is re-oxidized into dihydroxyacetone phosphate, whilst flavin adenine dinucleotide (FAD) is reduced to FADH₂. FADH₂ then transfers two electrons to ubiquinone (coenzyme Q), reducing it to ubiquinol, which subsequently enters the ETC at complex III. Two GPD enzymes form the GP shuttle, of which GPD2 is rate-limiting. Mammalian GPD2 is mainly expressed in brown adipose tissue, muscle and brain, with a lower expression in liver and heart.⁴⁸ Various glycolytic cells have expression of the GP-shuttle, including beta-pancreatic cells.^{49–51} Whereas the MAS connects glycolysis, the TCA cycle and the ETC, the GP-shuttle acts as a connection between glycolysis, glycerol metabolism and ETC.⁴⁸

Inborn disorders of the Malate-Aspartate Shuttle

Like the majority of IEM, MAS deficiencies form a group of rare diseases, with only a few reported patients. The most common disorder is AGC2 or citrin deficiency, which occurs at a relatively high frequency in Japan and Southeast Asia. The molecular basis of this deficiency was identified in 1999.⁵² A few years later, the role of the AGC2 isoform AGC1, or aralar, was reported in a mouse model and the first patient with AGC1 deficiency was reported in 2009.^{9,53} MDH2 deficiency was first described in 2017 and in 2019 deficiencies in GOT2 and MDH1 were published.^{6–8} No deficiencies in GOT1 and OGC have been reported to date.

As all MAS genes are highly expressed in brain, it is not surprising that the majority of MAS deficiencies affect the central nervous system. Deficiencies in GOT2, MDH1, MDH2 and AGC1 all present with early infantile epileptic encephalopathy, with abnormalities in myelination, hypoplasia and atrophy in the central nervous system. Since AGC2 is only expressed in liver, AGC2 deficiency leads to a more liver-specific disease. Table 1 comprises published data composed of biochemical and phenotypical findings. Because of the distinct phenotype of AGC2 deficiency compared to the other four MAS deficiencies, AGC2 was excluded from a more comprehensive overview of the neurological phenotypes, which is provided in Table 2.

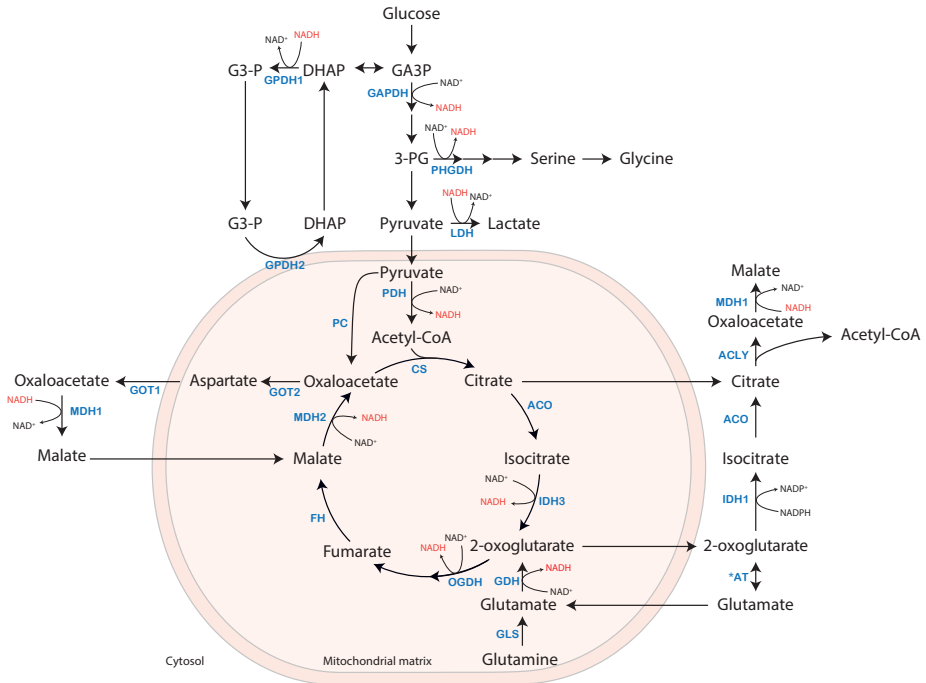


Figure 2. Malate-Aspartate Shuttle in cellular redox metabolism. Schematic view of cellular redox metabolism involving glycolysis, serine biosynthesis, the tricarboxylic acid (TCA) cycle, the malate -aspartate shuttle and glycerol-3 phosphate shuttle. In glycolysis, cytosolic NADH is generated by the oxidation of glyceraldehyde 3-phosphate (GA3P) by glyceraldehyde 3-phosphate dehydrogenase (GAPDH). GA3P can be isomerized into dihydroxyacetone phosphate (DHAP), which is converted into glycerol 3-phosphate (G3-P) by glycerol 3-phosphate dehydrogenase 1 (GPDH1) as part of the glycerol 3 phosphate shuttle. Serine biosynthesis branches from glycolysis at the level of 3-phosphoglycerate (3-PG), which is oxidized by phosphoglycerate dehydrogenase (PHGDH). Pyruvate is oxidized to lactate by lactate dehydrogenase (LDH), to sustain glycolysis by NAD⁺-regeneration. Pyruvate in the mitochondria is converted to either Acetyl-CoA by pyruvate dehydrogenase (PDH) to enter the TCA cycle, or oxaloacetate by pyruvate carboxylase (PC) for the *de novo* synthesis of aspartate via glutamate-oxaloacetate transaminase (GOT2). Within the TCA cycle NADH is generated via isocitrate dehydrogenase 3 (IDH3), oxoglutarate dehydrogenase (OGDH), and malate dehydrogenase 2 (MDH2). Malate in the TCA cycle is either derived from the conversion of fumarate or can be supplied from the cytosol via activity of the malate-aspartate shuttle. Citrate, exported from the mitochondria, is converted to oxaloacetate by ATP citrate lyase (ACLY), which in turn can be converted to malate via malate dehydrogenase 1 (MDH1). Malate can enter the mitochondria via the malate-2-oxoglutarate carrier or citrate carrier. Additional abbreviations: ACO, aconitase; *AT, aminotransferases; CS, citrate synthetase; FH, fumarate hydratase; GDH, glutamate dehydrogenase; GLS, glutaminase.

MDH1 deficiency

Two cousins from a highly consanguineous family were identified with a pathogenic homozygous variant in the NAD⁺-binding domain of *MDH1*.⁶ Both patients presented with an early neurological phenotype of global developmental delay, epilepsy and progressive microcephaly (Tables 1 and 2). In addition, dysmorphic features such as plagiocephaly, a bulbous nose, deep eyes, micrognathia and strabismus were present in both patients. Epilepsy in one of the patients was controlled using antiepileptic medication. Magnetic resonance imaging (MRI) of the brain in one patient revealed partial agenesis of predominantly the splenium of the corpus callosum, prominent ventricles, and mild hypoplasia of the inferior vermis and pons. The other patient's brain MRI showed mild shortening of the corpus callosum and a normal pons and ventricles. In both individuals amino acids, acylcarnitines and lactate levels in plasma were normal, as were organic acids in urine. A definite diagnosis was made by exome sequencing. Further biochemical investigations in dried blood spots of the patients revealed increased levels of glutamate and G3P, suggesting that G3P may be a biomarker for MDH1 deficiency. Additional investigations at the cellular level revealed decreased levels of fumarate and increased levels of aspartate in MDH1 KO HEK293 cells compared to control.

The increased levels of G3P in dried blood spots may provide mechanistic insights in MDH1 deficiency. As described above, GPD1 is a cytosolic enzyme that, similar to MDH1, is part of a NADH redox shuttle to recycle cytosolic NAD⁺. Although the GP shuttle is less efficient in ATP production than the MAS, it is potentially suitable as a compensatory mechanism for generating cytosolic NAD⁺ in MDH1 deficiency. As mitochondrial GPD2 is the rate-limiting step of the GP shuttle, increased activity of the GP shuttle may lead to accumulation of G3P in cytosol. In addition, untargeted metabolomics analysis in dried blood spots of the patients revealed increased levels of unsaturated fatty acids, which may also serve as an additional cytosolic NAD⁺-recycling mechanism.⁵⁴

Table 1. Biochemical and clinical findings in inborn disorders of the malate-aspartate shuttle based on published data.

Disorder (OMIM) protein; gene	High tissue expression	Clinical phenotype	Biochemical	N	Reference
MDH1 deficiency (618959) Malate dehydrogenase 1; <i>MDH1</i>	Brain, skeletal muscle, heart, kidney	Global developmental delay infantile epileptic encephalopathy microcephaly	Plasma: Lactate ≈ Dried blood spots: Glutamate ↑, Glycerol 3 Phosphate ↑	2	Broeks et al., 2019 ⁶
MDH2 deficiency (617339) Malate dehydrogenase 2; <i>MDH2</i>	Brain, skeletal muscle, heart, liver	Global developmental delay infantile epileptic encephalopathy hypotonia	Plasma: Lactate ↑, Lactate/Pyruvate ratio ↑ Urine: Malate ↑, Fumarate ↑, Succinate (N) CSF: Lactate ↑ MRS in brain: Lactate ↑ Fibroblasts: Malate/Citrate ratio ↑, Fumarate/Citrate ratio ↑, RC-CI activity ↓ Muscle biopsy: RC-CV activity ↓ (N) Liver biopsy: RC-CV activity ↓	3	Ait-EH-Mkadem et al., 2017 ⁷
GOT2 deficiency (618721) Aspartate aminotransferase 2; <i>GOT2</i>	Brain, skeletal muscle, heart, kidney, liver	Infantile epileptic encephalopathy progressive microcephaly	Plasma: Lactate ↑, Ammonia ↑, Citrulline ↑, Serine ↓	4	Van Karnebeek et al., 2019 ⁸
AGC1 deficiency (612949) Aralar; <i>SLC25A12</i>	Brain, skeletal muscle, heart	Global developmental delay infantile epileptic encephalopathy hypotonia	Plasma: Lactate ≈ ↑ CSF: Lactate ≈ ↑ MRS in brain: N-acetyl aspartate ↓, Myo-inositol ↑, Lactate ≈ ↑, Choline ≈ ↑ Muscle biopsy: RC activity (N), ATP production (substrates Glu+Mal/Suc) ↓	5	Wibom et al., 2009 ⁹ ; Falk et al., 2014 ¹⁰ ; Kavanaugh et al., 2019 ¹² ; Pfeiffer et al., 2020 ¹¹
Citrin deficiency (603859/605814) Citrin; <i>SLC25A13</i>	Liver, kidney, small intestine	CTLN2: Hepatic encephalopathy, associated with neuropsychiatric symptoms. NICCD: Neonatal intrahepatic cholestasis with or without failure to thrive and dyslipidemia	Plasma: Ammonia ↑, Citrulline ↑, Arginine ↑, Threonine/Serine ratio ↑, Pancreatic secretory trypsin inhibitor ↑ Liver biopsy: ASS activity ↓	> 100	Kobayashi et al., 1999 ⁵² ; Yasuda et al., 2000 ⁵⁵ ; Ohura et al., 2001 ^{56,57} , etc.

≈ around normal levels; ↑ increased levels; ↓ decreased levels; (N) normal; CSF cerebrospinal fluid; MRS magnetic resonance spectroscopy; RC respiratory chain; CI complex I; CV complex V; ASS argininosuccinate synthetase; GOT glutamic oxaloacetic transaminase; AGC aspartate glutamate carrier; CTLN2 adult-onset type II citrullinemia; NICCD neonatal intrahepatic cholestasis caused by citrin deficiency.

Table 2. Comprehensive overview of malate-aspartate shuttle deficiencies presenting with a clinical neurological phenotype (based on published data, HPO database⁵⁸ and OMIM database⁵⁹).

Clinical features	HPO ID	Deficiency			
		MDH1	MDH2	GOT2	AGC1
		n=2	n=3	n=4	n=5
Failure to thrive	HP:0001508		2/3	4/4	
Microcephaly	HP:0000252	2/2		4/4	3/5
Ocular					
Strabismus	HP:0000486	2/2	2/3		
Retinitis pigmentosa	HP:0008035		1/3		
Gastro-intestinal					
Constipation	HP:0002019		2/3		1/5
Feeding difficulties	HP:0011968			4/4	
Neurological					
<i>Developmental</i>					
Global developmental delay	HP:0001263	2/2	3/3	4/4	4/5
Intellectual disability, severe	HP:0010864			2/4	1/5
Intellectual disability, profound	HP:0002187			2/4	
Absent speech	HP:0001344	1/2	2/3	4/4	4/5
<i>Epilepsy</i>					
Epileptic encephalopathy	HP:0200134	2/2	3/3	4/4	5/5
Seizures	HP:0001250	2/2	3/3	4/4	5/5
<i>Tonus abnormalities</i>					
Dystonia	HP:0001332		2/3		
Hyporeflexia	HP:0001265		1/3		
Infantile axial hypotonia	HP:0009062	1/2	3/3		
Severe muscular hypotonia	HP:0006829			4/4	5/5
Hypertonia	HP:0001276	1/2			1/5
Spastic quadriplegia	HP:0002510			2/4	1/5
Spastic paraparesis	HP:0002313			2/4	
Hyperreflexia	HP:0001347	1/2		2/4	1/5
Hyporeflexia	HP:0001265		1/3		
Pyramidal signs	HP:0007256		2/3		
Non-ambulatory	HP:0002540		2/3	3/4	3/5
<i>Movement disorder</i>					
Dyskinesia	HP:0100660		1/3		

Table 2. Continued

Clinical features	HPO ID	Deficiency			
		MDH1	MDH2	GOT2	AGC1
		n=2	n=3	n=4	n=5
<i>Neuro-imaging (MRI/MRS)</i>					
Cerebral atrophy	HP:0002059		2/3	3/4	4/4
Cerebellar atrophy	HP:0001272		1/3		1/4
Delayed myelination	HP:0012448		1/3		3/4
Cerebral hypomyelination	HP:0006808				3/4
Hypoplasia of the pons	HP:0012110	1/2			
Hypoplasia of corpus callosum	HP:0002079	2/2	1/3	3/4	1/4
Inferior vermis hypoplasia	HP:0007068	1/2		3/4	
Multicystic encephalomalacia	HP:0040197			1/4	
High myoinositol in brain by MRS	HP:0025460				3/3
Elevated brain lactate level by MRS	HP:0012707		2/3		2/4
Reduced brain N-acetyl aspartate level by MRS	HP:0012708				3/3

Findings from other studies provide supporting or additional biochemical insights in case of a defect in MDH1. These findings include accumulation of aspartate which was found in three different experimental models: after knockdown of MDH1 in PANC-1 cells, in MDH1 KO HEK293 cells and in a MDH1 KO model of Jurkat cells.^{6,43,60} In addition, accumulation of oxaloacetate and decreased levels of malate were reported in MDH1 knockdown PANC-1 cells. Furthermore, a knockdown model of MDH1 in fibroblasts showed a decreased NAD⁺/NADH ratio⁶¹. These fibroblasts had a senescent phenotype with a low-proliferative state, suggesting a role for decreased MDH1 activity in cellular senescence.⁶¹ Secondary consequences of MDH1 deficiency include a decreased ratio between reduced and oxidized glutathione (GSH/GSSG) as was observed in MDH1 KD PANC-1 cells. MDH1 was suggested to play a role in antioxidant defense by supporting NADPH production via malic enzyme.⁶² All together these findings suggest that MDH1 deficiency could lead to increased oxidative stress by disruption of both NAD⁺/NADH and NADPH/NADP⁺ balances.

MDH2 deficiency

To date, MDH2 deficiency has been reported in three unrelated subjects.⁷ Patients presented with bi-allelic MDH2 variants as identified by exome sequencing. The phenotypes of these patients were characterized by early-onset generalized hypotonia,

psychomotor delay, and refractory epilepsy, accompanied by elevated lactate in the blood and cerebrospinal fluid (Table 1 and 2). Additional clinical findings shared by two of three patients included failure to thrive, obstinate constipation, dystonia and strabismus. Epileptic seizure frequency decreased in response to a ketogenic diet in two of three patients. Brain MRI showed nonspecific findings including atrophy of the anterior part of the corpus callosum, delayed myelination of the frontal white matter, and cortical, frontal, and parietal atrophy. Repeat brain MRI in a second patient showed delayed myelination of the genu of the corpus callosum and cortical and subcortical atrophy of the frontal lobes. For the last patient, marked cerebral and cerebellar atrophy were observed. Urinary organic acid analysis revealed increased levels of malate and fumarate in two of three patients, whereas succinate levels were normal in all patients. One of the patients had also increased concentrations of urinary ketone bodies, lactate, pyruvate and 3-methylglutaconic acid. An important note for diagnostics is that MDH2-individuals can show nearly normal concentrations of urinary organic acids in a non-metabolic decompensation state.

No clear biomarkers were identified in patients with MDH2 deficiency, but additional insights from MDH2 KO cells have revealed increased intracellular levels of malate and fumarate.⁶³ High concentrations of malate and fumarate can trigger an hypoxia response.⁶⁴ Eventually, this can lead to inactivation of the PDH complex, pyruvate accumulation in the cytosol and consequently increased lactate formation.⁶⁵ Another consequence of the hypoxia response is an increase in glutamine catabolism that feeds in the 2-oxoglutarate pool.⁶⁶ When mitochondrial pyruvate import is impaired, TCA cycle activity can be maintained via oxidative glutamine metabolism, as glutamine-derived malate can be converted into pyruvate via malic enzyme 2.⁶⁷ Furthermore, glutamine may also undergo reductive carboxylation to support fatty acid biosynthesis. To this end, glutamine-derived 2-oxoglutarate is then carboxylated by the mitochondrial NADP-linked enzyme isocitrate dehydrogenase (IDH2) to produce isocitrate, which is, after conversion into citrate, exported from the mitochondrial matrix into the cytosol where citrate can be cleaved into both oxaloacetate and acetyl-CoA via the cytosolic enzyme citrate lyase.⁶⁷ Similar to MDH1, activation of MDH2 also indirectly supports fatty acid biosynthesis in adipocytes by increasing intracellular NADPH levels via malic enzyme.⁶⁸ Thus, these findings suggest that MDH2 deficiency might affect MAS and TCA cycle substrates, but also glutathione dependent antioxidant defense via decreased NADPH and glutamine levels.

GOT2 deficiency

Four patients with GOT2 deficiency from three independent families have been reported.⁸ Homozygous and compound heterozygous *GOT2* variants were identified

using exome sequencing. All patients presented with similar clinical features including progressive microcephaly, epileptic encephalopathy and failure to thrive (Table 1 and 2). Additional phenotypic features included feeding difficulties, hypotonia, frequent infections, intellectual and motor disabilities, such as spastic paraparesis and severe spastic quadriplegia. MRI brain scan showed multicystic encephalomalacia and wide cerebral atrophy for one of the patients. In addition, two of four patients revealed mild cerebral atrophy with a hypoplastic vermis and a thin corpus callosum. Brain MRI in the last patient showed (mainly frontoparietal) cerebral atrophy, asymmetric dilated lateral ventricles, hypoplastic vermis and hypoplasia of the corpus callosum. Biochemically, patients had high plasma lactate and hyperammonemia. All patients had normal urinary organic acids and plasma acylcarnitines. In addition, amino acids in plasma were normal in three of the four patients. Low serine levels and high citrulline levels were found in one of the patients. This finding was followed up by additional functional analysis of serine biosynthesis in patients' fibroblasts and GOT2 KO HEK293 cells. These studies revealed that *de novo* serine biosynthesis was impaired which prompted institution of a new therapeutic option involving serine supplementation in two patients. In addition, these patients were given pyridoxine supplementation to boost residual enzyme activity. The epilepsy and overall neurodevelopmental status in these patients were serine and pyridoxine responsive.

Impaired *de novo* serine biosynthesis may provide mechanistic insights in GOT2 deficiency. Since the first step of serine synthesis is catalyzed by the NAD⁺-dependent enzyme 3-phosphoglycerate dehydrogenase, a secondary serine synthesis defect may occur as a consequence of cytosolic NAD⁺/NADH imbalance. The notion that GOT2 deficiency can cause an overall deficiency in the MAS and thereby decrease the cytosolic NAD⁺/NADH ratio, is supported by a GOT2 knockdown model in pancreatic cancer cells that had impaired net transfer of cytosolic NADH into mitochondria.⁶⁹ The addition of glycerol in cultured GOT2 KO HEK293 cells, as an attempt to restore the NAD⁺/NADH balance through the GP shuttle, was not sufficient to correct the impaired serine biosynthesis.⁸ This suggests that the MAS is the predominant NADH shuttle in HEK293 cells. This is in line with the finding that G3P was not increased in MDH1 HEK293 cells.⁶ Interestingly, pyruvate supplementation restored serine biosynthesis *in vitro*,⁸ presumably by correcting the NAD⁺/NADH balance. However, since increasing pyruvate may result in increased lactate formation this may not be suitable for treatment. To circumvent glycolytic NADH production, and consequently lactate accumulation in the cytosol, the authors suggested a diet low in carbohydrates, high in fat, and supplementation with ketone bodies.

Hyperammonemia and hypercitrullinemia in patients with a GOT2 deficiency point to a secondary defect of the urea cycle. In GOT2 deficiency, mitochondrial aspartate production from oxaloacetate is decreased, as supported by findings in GOT2 knockdown cells.⁷⁰ GOT2 is closely linked to the urea cycle via the production of aspartate, which reacts with citrulline to form argininosuccinate. A lack of aspartate will lead to accumulation of citrulline and dysfunction of the urea cycle. Thus, the hyperammonemia and hypercitrullinemia as observed in GOT2 deficient patients can be explained by a deficient aspartate provision to the cytosol. Hyperammonemia may also have consequences for the TCA cycle, since glutamate plays an important role in ammonia detoxification by forming glutamine.⁷¹ The high levels of ammonia can thereby deplete TCA cycle intermediates by withdrawing 2-oxoglutarate for the formation of glutamate and consequently glutamine. This can contribute to dysregulation of the TCA cycle. Thus, a deficiency in GOT2 may affect redox homeostasis, MAS substrates, the urea cycle as well as the TCA cycle.

AGC1 (Aralar/SLC25A12) deficiency

AGC1 deficiency is also known as Aralar deficiency. Five patients from four unrelated families with AGC1 deficiency have been reported. The phenotype of the first three reported patients, including two siblings, is characterized by severe infantile-onset encephalopathy with epilepsy, global developmental delay, generalized hypotonia and abnormal myelination, accompanied by reduced cerebral N-acetyl aspartate (NAA) content (Table 1 and 2).^{9,10} In addition, two of three patients had frequent infections. A fourth patient presented with a similar phenotype, with the exception that this patient had normal myelination and absence of microcephaly or dysmorphic features.¹¹ MRI findings included cerebral volume loss, delayed myelination, bilateral symmetric abnormal signal in the putamina,⁹ global lack of myelination in the cerebral hemispheres, and a slightly smaller than normal putamen and globus pallidus.¹⁰ The cerebellum, brainstem, and thalami were essentially normal. Lactate was reported normal to mildly elevated in these four patients. A fifth patient was identified with compound heterozygous variants at the age of 12 years.¹² The clinical phenotype of this patient was characterized by small stature, microcephaly, dysmorphic features, early-onset global developmental delay, severe intellectual disability (non-verbal), hypotonia, epilepsy, non-ambulatory spastic quadriplegia albeit a happy disposition. Neuroimaging findings indicated cerebral atrophy with early hypomyelination, but were more consistent with a leukodystrophy of the leuko-axonopathy category. A lactate peak was found upon MRS, which may have reflected the ongoing seizures at that time. Seizures of all patients were successfully controlled with medication. The oldest patient was free of seizures between the age of 3 and 12 years, without medical seizure control.¹² For the first reported patient treatment with a ketogenic

diet was published, reporting improved psychomotor development and eye contact as well as increased alertness.^{9,72} After 20 months on the diet, the patient remained seizure free and neuro-imaging showed increased brain volume, as well as improved myelination. Subsequently, another patient was published in whom ketogenic diet was successful in terms of seizure control.¹¹ These reports suggest the ketogenic diet as a viable therapeutic option for AGC1 deficiency.⁷⁶

Recently, an alternative to a ketogenic diet was explored in a mouse model, by administering β -hydroxybutyrate (B-OHB), the main metabolic product in a ketogenic diet.⁷³ B-OHB was able to boost aspartate and NAA synthesis in neurons and myelin proteins in brain from the Aralar-KO mice. NAA is produced from aspartate and acetyl-CoA by the enzyme aspartate-N-acetyltransferase.⁷⁴ As the B-OHB dependent recovery of aspartate and NAA did not require lowering of carbohydrates, this treatment may provide an alternative therapy and deserves further investigation.

At first, reduced levels of neuronal-generated NAA have been proposed to contribute to the observed hypomyelination in AGC1 deficiency,^{9,10,72} in which NAA would be a precursor for myelin lipid synthesis. However, one of the patients had normal myelination.¹¹ In addition, in one of the reports serial MRI findings were less characteristic of a primary or permanent hypomyelinating disorder, pointing to AGC1 deficiency as a leukodystrophy of the leuko-axonopathy category.¹² Therefore, the observed hypomyelination was later suggested to be secondary to neuronal dysfunction, which argues against AGC1 deficiency as a primary hypomyelinating disease.⁷⁵ This conclusion was supported by the results of studies in mice which showed that the degeneration of neuronal processes in AGC1 deficiency occurred independent of hypomyelination.⁷⁶ Moreover, an increase in aspartate and NAA after B-OHB administration in Aralar-KO mice was also not associated with myelin recovery.⁷³ In addition, studies in mice in which both the NAA synthesizing enzyme (NAT8L) as well as the NAA hydrolyzing enzyme (aspartoacylase, ASPA) were inactivated, revealed no abnormalities in myelination, despite undetectable NAA levels.⁷⁷

Another interesting observation is the variable presence of lactic acidemia in the reported cases. A proposed mechanism for lactic acidemia in patients with AGC1 deficiency is a secondary form of mitochondrial dysfunction, due to the inability of the MAS to transfer reducing equivalents across the mitochondrial membrane. A drastic decrease in respiration was found in AGC1 deficient mouse brain tissue when using malate plus glutamate as substrate.⁵³ Still, 12% of residual activity persisted, which may be explained by the presence of other glutamate carriers (GC1,

GC2), which also transport glutamate into mitochondria for respiration. In line with this, analysis of brain extracts from AGC1-deficient mice revealed a striking 86% decrease in the levels of aspartate, but only a modest 25% decrease in glutamate.⁷⁸ Interestingly, the most prominent drop in amino acid concentrations was observed for glutamine and serine with decreases of 77% and 75% compared to control, respectively. This may suggest that AGC1 deficiency, similar to GOT2 deficiency, may be associated with a secondary serine synthesis deficiency as a consequence of a dysfunctional MAS and a cytosolic NAD⁺/NADH imbalance.

AGC2 (Citrin/SLC25A13) deficiency

AGC2 or citrin deficiency is the most extensively described and studied MAS deficiency (Table 1). Over hundred patients have been reported, often in East Asia.^{79,80} AGC2 deficiency can manifest in several stages of life, dependent on age. In newborns or infants it can present as neonatal intrahepatic cholestasis (citrin deficiency, NICCD), in older children as failure to thrive and dyslipidemia (citrin deficiency, FTTDCD), and in adults as recurrent hyperammonemia with neuropsychiatric symptoms in citrullinemia type II (CTLN2).

NICCD was discovered in neonates suffering from cholestasis and multiple amino acidemia including citrulline, threonine, methionine, lysine, arginine, tyrosine, serine and phenylalanine.^{57,81} Some of these may be detected in newborn screening, including citrulline, tyrosine, methionine and phenylalanine, and a decreased ratio of alanine/citrulline.⁸² Other biochemical abnormalities were hypoproteinemia, galactosemia, and hypoglycemia.^{57,81,83,84} Further symptoms include diffuse fatty liver with hepatomegaly and parenchymal cellular infiltration with hepatic fibrosis (cirrhosis), decreased coagulation factors (echinocytosis), elevated bilirubin (bilirubinemia), hemolytic anemia and variable liver dysfunction. Most patients showed clinical improvement between 6 and 12 months upon treatment with a diet containing fat-soluble vitamin supplementation, lactose-free therapeutic formulas and/or medium-chain triglyceride enriched therapeutic formulas.^{56,85} However, some may develop cirrhosis or severe infections, or may later develop symptoms of adult-onset citrin deficiency.^{79,83}

FTTDCD has been proposed as a post-NICCD phenotype before the onset of CTLN2.⁸⁶ Some children were found to have laboratory and/or clinical abnormalities after NICCD. Clinical symptoms included growth restriction, hypoglycemia, pancreatitis, but also severe fatigue and impaired quality of life.⁸⁷ Laboratory abnormalities included dyslipidemia manifesting as higher levels of triglyceride and total- and LDL-cholesterols, but lower levels of HDL-cholesterol.⁸⁶ Other findings were an

increased lactate-to pyruvate ratio, higher levels of urinary oxidative stress markers, and marked abnormalities in tricarboxylic acid cycle metabolites.^{88,89} Often FTTDCD is characterized by the patient's preference for protein-rich and/or lipid-rich foods and aversion to carbohydrate-rich foods.

CTLN2 patients also have a particular preference for protein-rich and/or lipid-rich foods, such as beans and peanuts.⁷⁹ Clinical symptoms of CTLN2 patients are characterized by recurring episodes of hyperammonemia and neurologic and psychotic symptoms that closely resemble those of hepatic encephalopathy or genetic urea cycle disorders, including nocturnal delirium, aberrant behaviors (aggression, irritability, and hyperactivity), delusions, disorientation, restlessness, drowsiness, loss of memory, flapping tremor, convulsive seizures, and coma.⁷⁹ In general, the onset is sudden, usually between the ages of 20 and 40. The age of patients diagnosed varies from 11 to 70 years with a mean age of 34.4 years.⁵⁵ Although prognosis is bad, liver transplantation is the most effective therapy, preventing episodic hyperammonemia and eliminating the preference for protein-rich foods.⁹⁰⁻⁹² Pancreatitis, hyperlipidemia, and hepatoma are major complications of CTLN2.⁹¹ Biochemical abnormalities of CTLN2 patients include citrullinemia, abnormal liver enzymes, low albumin, increased serum triglycerides and decreased activity of argininosuccinate synthetase (ASS) in the liver (however, normal levels of ASS1 in other tissues).

Since the major function of the AGC is to supply aspartate to the cytosol, AGC2 deficiency causes a deficiency of cytosolic aspartate in the liver. A lack of aspartate limits synthesis of proteins and nucleotides, resulting in hypoproteinemia in NICCD. In addition, lack of aspartate for the ASS reaction causes accumulation of citrulline and eventually hyperammonemia.⁷⁹ Beans and peanuts are the most prominent dietary sources of aspartate and asparagine, which might be the reason why CTLN2 patients show extraordinary liking for beans and peanuts. Administration of sodium pyruvate with L-arginine proved effective in treatment of a 13- and 73-year old citrin-deficient patient.^{93,94} Arginine was shown to be effective in lowering blood ammonia in hyperammonemic patients, potentially via urea cycle enzymes.⁹⁵ Administration of sodium pyruvate may increase the cytosolic NAD⁺/NADH ratio, which activates ureagenesis, as demonstrated in mice.⁹⁶

Komatsu et al. hypothesized that the hepatic steatosis observed in patients with CTLN2 may result from a compensatory upregulation of the citrate-malate shuttle. This shuttle catalyzes the net transfer of acetyl-CoA from mitochondria to the cytosol, to promote fatty acid synthesis.²³ In addition to the transfer of acetyl-CoA, the pathway

regenerates cytosolic NAD^+ via MDH1.⁶² An increase in cytosolic citrate and acetyl-CoA, may result in an overproduction of fatty acids in hepatocytes and contribute to hyperlipidemia.⁹⁷ In addition, since the GP shuttle exerts low expression in liver, glycerol and G3P accumulation can also contribute to hyperlipidemia. Increased levels of urine glycerol and G3P have been observed in patients with FTTDCD.⁹⁸

DISCUSSION

The current review presents an overview of clinical and biochemical aspects of the known genetic MAS deficiencies. Due to the expression pattern of the different MAS components, most of the MAS deficiencies affect the central nervous system and present with a neurological phenotype. An exception is AGC2 deficiency, which presents with a primary hepatic phenotype due to its liver-specific expression. MAS deficiencies with a neurological phenotype include MDH1, MDH2, GOT2 and AGC1. Common clinical features in these disorders are epilepsy, hypotonia and global developmental delay (Table 2). In addition, MDH1, GOT2 and AGC1 deficiencies present with microcephaly. Common MRI findings include an affected corpus callosum in MDH1, MDH2 and GOT2 deficiencies. The most striking finding in AGC1 deficiency is delayed or hypomyelination.

As one of the major roles of the MAS is to maintain redox homeostasis, a dysfunctional MAS will result in a disturbed NAD^+/NADH -redox balance. Indeed, in all reported MAS deficiencies a disturbed redox balance is reflected by different flux through other redox dependent pathways. These pathways include the GP shuttle and the conversion of pyruvate to lactate, which are both directly connected to the cytosolic NAD^+/NADH balance.^{37,46} Increased activities of glycerol phosphate dehydrogenase and lactate dehydrogenase result in regeneration of NAD^+ (Figure 2). Interestingly, both in MDH1 and AGC1 deficiencies, lactate was normal to slightly increased in plasma. In MDH1 deficiency, GP shuttle activity appears increased, as G3P levels were high in blood (Table 1).⁶ In AGC1 deficiency, increased activity of the GP shuttle has also been suggested,⁹⁹ especially since a clear increase in lactate production is lacking. Since astrocytes in the brain lack AGC1,^{78,100} it is postulated that the glycerol phosphate shuttle is the main NADH redox shuttle in astrocytes. Moreover, the lack of or only slight increase in lactate may be explained by the fact that mainly the unaffected astrocytes are responsible for lactate production.⁹⁹

In contrast to the presumed absence of increased lactate levels in MDH1 and AGC1 deficiencies, patients with MDH2 and GOT2 deficiency present with a clear lactic

acidosis (Table 1). Both MDH2 and GOT2 enzymes are located in the mitochondria and are functionally coupled to the TCA cycle and ATP production, thus, defects in these enzymes can result in overall mitochondrial dysfunction. Mitochondrial dysfunction is often partly compensated by increased glycolytic ATP production, leading to increased conversion of glucose to pyruvate as glycolytic end-point, with secondary conversion of pyruvate to lactate. Supporting this notion, high levels of urinary pyruvate were observed in MDH2 deficiency. However, GOT2 deficiency appears to result in low levels of pyruvate, as observed in KO HEK293 cells. This may indicate disturbed glycolysis in GOT2 deficiency as an additional consequence of redox imbalance, the enzyme GAPDH being dependent on NAD⁺/NADH ratio. Although overall glycolytic flux may be decreased in GOT2 deficiency, high levels of lactate are likely the result of increased pyruvate to lactate conversion due to increased NADH levels in the cytosol.

Disturbed redox homeostasis also affects other NAD(H)-dependent metabolic pathways like serine biosynthesis (Figure 2). This has been experimentally demonstrated to occur in GOT2 deficiency,⁸ and low serine levels were found in brains of AGC1 deficient mice.⁷⁸ Serine is a non-essential amino acid and a precursor of essential compounds including phosphatidylserine, sphingomyelin, glycine and D-serine. Genetic defects in serine biosynthesis illustrate that this pathway is the main source of serine in the brain, as dietary sources are typically not sufficient to compensate for these defects.¹⁰¹ Interestingly, defects in any of the three enzymes involved in the *de novo* serine biosynthetic pathway mainly present with a neurological phenotype. Clinical characteristics include microcephaly, developmental delay, irritability, feeding difficulties, poor psychomotor development, spastic tetraplegia, epilepsy, nystagmus, brain atrophy, and hypomyelination. The diseases are biochemically characterized by low serine and glycine in CSF and blood in fasting state.¹⁰² Many of the clinical characteristics overlap with the clinical phenotype of MAS deficiencies, including microcephaly, epilepsy, developmental delay, poor psychomotor development and hypomyelination (Table 2). This may support the notion that part of the clinical phenotype is due to a secondary serine biosynthesis defect, especially as oral L-serine supplementation ameliorated the neurologic phenotype in GOT2 deficiency.

Next to the expected disturbed redox homeostasis, a dysfunctional MAS also affects aspartate and glutamate. As demonstrated in AGC1 deficiency, lack of cytosolic aspartate leads to a reduction of N-acetylaspartate and subsequently cerebral hypomyelination may occur. As GOT2 is responsible for aspartate production, N-acetylaspartate may also be low in this defect, but was not reported in GOT2

deficient patients. In AGC2 deficiency, similar to GOT2 deficiency, a lack of cytosolic aspartate leads to substrate reduction for the urea cycle. In both deficiencies aspartate cannot react with citrulline in the urea cycle, causing accumulation of citrulline (Table 1). In addition, impaired activity of the urea cycle to dispose toxic ammonia leads to hyperammonemia. As MAS activity is required for aspartate synthesis by GOT2, MAS activity is also necessary for glutamate synthesis by GOT1 in the brain.^{4,5} A deficiency in MAS can therefore affect the availability of glutamate for neurotransmission, potentially contributing to the epileptic phenotype seen in these deficiencies.¹⁰³

A viable option for treatment of MAS deficiencies is provided by a ketogenic diet, which was shown to be effective in MDH2 and AGC1 deficiency.^{7,11,72} MAS deficiencies lead to inefficient use of glucose by neurons, since the decreased NAD⁺/NADH ratio prevents pyruvate from entering the TCA cycle by reducing it to lactate. A ketogenic diet contains ketone bodies that serve as an alternative to glucose as fuel for the brain. Therefore, a ketogenic diet can bypass the NAD⁺-dependent glycolytic metabolic pathways, and may be a beneficial therapeutic option in MAS deficiencies. Interestingly, serine supplementation might also ameliorate some of the neurological phenotypes in MAS deficiencies, as proven to be effective in GOT2 deficiency. In addition, vitamin B6 supplementation is advocated in GOT2 deficiency, as the residual enzyme activity might deplete other vitamin B6-dependent enzymes from their cofactor.

Although a ketogenic diet can bypass NAD⁺-dependent glycolytic metabolic pathways, a recent report demonstrated a novel approach to alleviate the intracellular redox balance.¹⁰⁴ A well-known method *in vitro* to correct the intracellular NAD⁺/NADH redox imbalance is the conversion of pyruvate into lactate, however this would not work well in patients as this would lead to an even further increase in lactate levels.⁸ Hence, a fusion protein of bacterial lactate oxidase and catalase was constructed, LOXCAT, which was able to convert lactate and oxygen into pyruvate and water.¹⁰⁴ As proof-of-principle they demonstrated that the lactate/pyruvate ratio in medium could be lowered, hence intra-cellularly. In addition, LOXCAT had alleviated intracellular NAD⁺/NADH redox imbalance in heart and brain of mice with metformin induced complex I inhibition. In the context of MAS deficiencies, which have a low cytosolic NAD⁺/NADH ratio, this invention holds great promise.¹⁰⁵

Important to note is that, since the MAS is essential for the brain, most reported deficiencies are hypomorphic in nature with residual enzyme activity. It is expected that complete inactivity of the MAS components are lethal in humans, as

demonstrated by homozygous knockouts of MDH1, MDH2, GOT1, GOT2 in mice.^{8,106,107} For GOT1 and OGC no deficiencies in humans have been reported yet. However, in the older order Amish population, a rare in-frame 3 bp deletion in GOT1 that was strongly associated with low serum aspartate aminotransferase activity was observed in heterozygous state. Functional studies showed that the mutant recombinant protein had no enzyme activity. No individuals with homozygosity for this deletion were found, suggesting that complete loss of function of GOT1 is indeed not compatible with life.¹⁰⁸ Expected biochemical effects of GOT1 deficiency could be extrapolated from knockout and knockdown studies in cells, in which increased levels of aspartate were reported.^{43,70} Allelic variants of OGC have been identified in paragangliomas, in which tumor tissue showed absence of the protein.¹⁰⁹ Interestingly, loss of MDH2 was also associated with pheochromocytoma and paraganglioma.⁶³ Knockdown of SLC25A11 in mouse chromaffin cells showed low 2-oxoglutarate and increased aspartate and glutamate. The cells acquired metastatic properties, which suggested that SLC25A11 can act as a tumor-suppressor gene.¹⁰⁹ Other expected biochemical effects of OGC deficiency could be extrapolated from SLC25A11 knockdown in A549 cells, in which levels of fumarate, malate, citrate, NADH and ATP were decreased.¹¹⁰

CONCLUSION

The current review provides insights into the biochemical and clinical characteristics of MAS deficiencies. Many of these deficiencies have no specific markers to support clinical diagnosis. The disturbed redox homeostasis in MAS deficiencies affects multiple redox dependent pathways, with complex consequences due to compartment- and tissue-specific expression of the MAS components. In general, biochemical clues for MAS deficiencies include high lactate, high glycerol 3-phosphate, a disturbed redox balance, TCA abnormalities, high ammonia and low serine. Although not specific, these profiles may narrow down the long differential diagnosis of possible IMDs causing infantile epileptic encephalopathies.¹¹¹ Interestingly, implications for treatment of MAS deficiencies are offered by the study of GOT2 deficiency, in which it was demonstrated that a cytosolic redox imbalance leads to a secondary serine biosynthesis defect and serine supplementation exerted a significant clinical benefit. Other treatment possibilities may include vitamin B6 supplementation (cofactor for GOT2) and a ketogenic diet. Pyruvate supplementation or other redox-correcting supplements may be interesting potential treatments for future research. All together, these IMD of MAS expands the list of treatable intellectual disabilities.¹¹² Future studies are needed to reveal more specific biomarkers and to obtain more insights in the pathophysiological mechanisms of MAS deficiencies.

REFERENCES

1. Dawson AG. Oxidation of cytosolic NADH formed during aerobic metabolism in mammalian cells. *Trends Biochem Sci.* 1979;4(8):171-176.
2. Xiao W, Wang RS, Handy DE, Loscalzo J. NAD(H) and NADP(H) Redox Couples and Cellular Energy Metabolism. *Antioxidants Redox Signal.* 2018;28(3):251-272.
3. Kauppinen RA, Sihra TS, Nicholls DG. Aminooxyacetic acid inhibits the malate-aspartate shuttle in isolated nerve terminals and prevents the mitochondria from utilizing glycolytic substrates. *BBA - Mol Cell Res.* 1987;930(2):173-178.
4. McKenna MC, Waagepetersen HS, Schousboe A, Sonnewald U. Neuronal and astrocytic shuttle mechanisms for cytosolic-mitochondrial transfer of reducing equivalents: Current evidence and pharmacological tools. *Biochem Pharmacol.* 2006;71(4):399-407.
5. Pardo B, Contreras L, Satrústegui J. De novo Synthesis of Glial Glutamate and Glutamine in Young Mice Requires Aspartate Provided by the Neuronal Mitochondrial Aspartate-Glutamate Carrier Aralar/AGC1. *Front Endocrinol (Lausanne).* 2013;4:149.
6. Broeks MH, Shamseldin HE, Alhashem A, et al. MDH1 deficiency is a metabolic disorder of the malate-aspartate shuttle associated with early onset severe encephalopathy. *Hum Genet.* 2019;138(11-12):1247-1257.
7. Ait-EI-Mkadem S, Dayem-Quere M, Gusic M, et al. Mutations in MDH2, Encoding a Krebs Cycle Enzyme, Cause Early-Onset Severe Encephalopathy. *Am J Hum Genet.* 2017;100(1):151-159.
8. van Karnebeek CDM, Ramos RJ, Wen XY, et al. Bi-allelic GOT2 Mutations Cause a Treatable Malate-Aspartate Shuttle-Related Encephalopathy. *Am J Hum Genet.* 2019;105(3):534-548.
9. Wibom R, Lasorsa FM, Töhönen V, et al. AGC1 deficiency associated with global cerebral hypomyelination. *N Engl J Med.* 2009;361(5):489-495.
10. Falk MJ, Li D, Gai X, et al. AGC1 Deficiency Causes Infantile Epilepsy, Abnormal Myelination, and Reduced N-Acetylaspartate. *JIMD Rep.* 2014;14:77-85.
11. Pfeiffer B, Sen K, Kaur S, Pappas K. Expanding Phenotypic Spectrum of Cerebral Aspartate-Glutamate Carrier Isoform 1 (AGC1) Deficiency. *Neuropediatrics.* 2020;51(2):160-163.
12. Kavanaugh BC, Warren EB, Baytas O, et al. Longitudinal MRI findings in patient with SLC25A12 pathogenic variants inform disease progression and classification. *Am J Med Genet Part A.* 2019;179(11):2284-2291.
13. Online Mendelian Inheritance in Man, OMIM®. Johns Hopkins University, Baltimore M. Phenotypic Series PS308350.
14. Lee JY, Wasserman WW, Hoffmann GF, Van Karnebeek CDM, Blau N. Knowledge base and mini-expert platform for the diagnosis of inborn errors of metabolism. *Genet Med.* 2018;20(1):151-158.
15. Friedkin M, Lehninger AL. Esterification of inorganic phosphate coupled to electron transport between dihydrodiphosphopyridine nucleotide and oxygen. *J Biol Chem.* 1949;178:611-623.
16. Lehninger AL. Esterification of inorganic phosphate coupled to electron transport between dihydrodiphosphopyridine nucleotide and oxygen. II. *J Biol Chem.* 1949;178:625-644.
17. Mitchell P. Coupling of phosphorylation to electron and hydrogen transfer by a chemi-osmotic type of mechanism. *Nature.* 1961;191(4784):144-148.
18. KENNEDY EP, LEHNINGER AL. Oxidation of fatty acids and tricarboxylic acid cycle intermediates by isolated rat liver mitochondria. *J Biol Chem.* 1949;179(2):957-972.
19. Lehninger AL. Phosphorylation coupled to oxidation of dihydrodiphosphopyridine nucleotide. *J Biol Chem.* 1951;190(1):345-359.
20. Borst P. The aerobic oxidation of reduced diphosphopyridine nucleotide formed by glycolysis in ehrlich ascites-tumour cells. *BBA - Biochim Biophys Acta.* 1962;57(1):270-282.
21. Borst P. Hydrogen transport and transport metabolites. In: *Funktionelle Und Morphologische Organisation Der Zelle.* Springer Berlin Heidelberg; 1963:137-162.

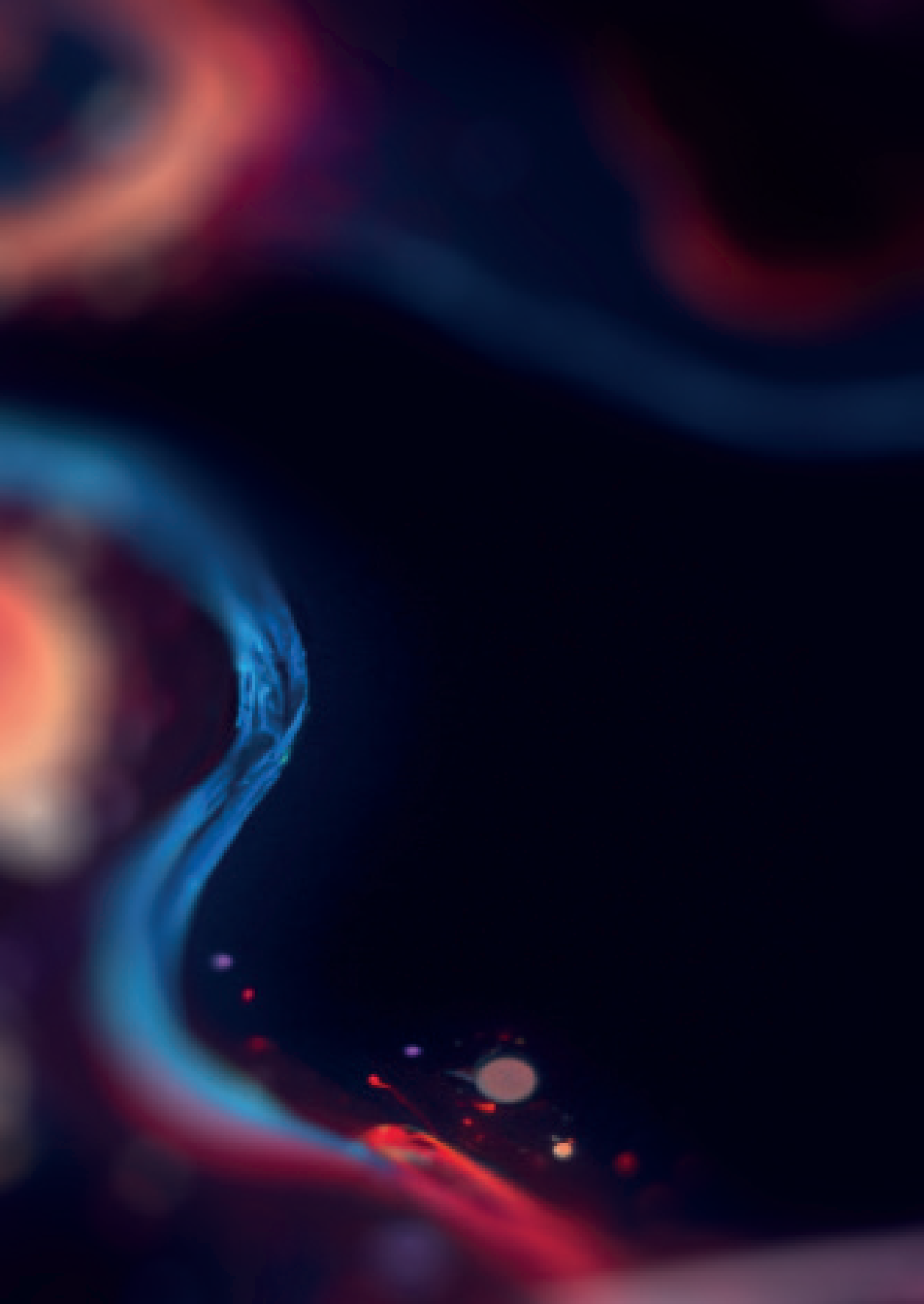
22. LaNoue KF, Williamson JR. Interrelationships between malate-aspartate shuttle and citric acid cycle in rat heart mitochondria. *Metabolism*. 1971;20(2):119-140.
23. Meijer AJ, van Dam K. The metabolic significance of anion transport in mitochondria. *BBA Rev Bioenerg*. 1974;346(3-4):213-244.
24. Safer B. The metabolic significance of the malate aspartate cycle in heart. *Circ Res*. 1975;37(5):527-533.
25. Borst P. The malate-aspartate shuttle (Borst cycle): How it started and developed into a major metabolic pathway. *IUBMB Life*. 2020;72(11):2241-2259.
26. Uhlén M, Fagerberg L, Hallström BM, et al. Tissue-based map of the human proteome. *Science*. 2015;347(6220):1260419.
27. Palmieri L, Pardo B, Lasorsa FM, et al. Citrin and aralar1 are Ca²⁺-stimulated aspartate/glutamate transporters in mitochondria. *EMBO J*. 2001;20(18):5060-5069.
28. Iijima M, Jalil A, Begum L, et al. Pathogenesis of adult-onset type II citrullinemia caused by deficiency of citrin, a mitochondrial solute carrier protein: Tissue and subcellular localization of citrin. *Adv Enzyme Regul*. 2001;41(1):325-342.
29. Amoedo ND, Punzi G, Obre E, et al. AGC1/2, the mitochondrial aspartate-glutamate carriers. *Biochim Biophys Acta - Mol Cell Res*. 2016;1863(10):2394-2412.
30. Sluse FE, Ranson M, Liébecq C. Mechanism of the Exchanges Catalysed by the Oxoglutarate Translocator of Rat-Heart Mitochondria: Kinetics of the Exchange Reactions between 2-Oxoglutarate, Malate and Malonate. *Eur J Biochem*. 1972;25(2):207-217.
31. LaNoue KF, Tischler ME. Electrogenic characteristics of the mitochondrial glutamate aspartate antiporter. *J Biol Chem*. 1974;249(23):7522-7528.
32. Lanoue KF, Meijer AJ, Brouwer A. Evidence for electrogenic aspartate transport in rat liver mitochondria. *Arch Biochem Biophys*. 1974;161(2):544-550.
33. Lunt SY, Vander Heiden MG. Aerobic Glycolysis: Meeting the Metabolic Requirements of Cell Proliferation. *Annu Rev Cell Dev Biol*. 2011;27(1):441-464.
34. Goodman RP, Calvo SE, Mootha VK. Spatiotemporal compartmentalization of hepatic NADH and NADPH metabolism. *J Biol Chem*. 2018;293(20):7508-7516.
35. Houtkooper RH, Pirinen E, Auwerx J. Sirtuins as regulators of metabolism and healthspan. *Nat Rev Mol Cell Biol*. 2012;13(4):225-238.
36. Bai P, Cantó C. The role of PARP-1 and PARP-2 enzymes in metabolic regulation and disease. *Cell Metab*. 2012;16(3):290-295.
37. Hosios AM, Matthew GVH. The redox requirements of proliferating mammalian cells. *J Biol Chem*. 2018;293(20):7490-7498.
38. Williamson DH, Lund P, Krebs HA. The redox state of free nicotinamide-adenine dinucleotide in the cytoplasm and mitochondria of rat liver. *Biochem J*. 1967;103(2):514-527.
39. Szibor M, Gizatullina Z, Gainutdinov T, et al. Cytosolic, but not matrix, calcium is essential for adjustment of mitochondrial pyruvate supply. *J Biol Chem*. 2020;295(14):4383-4397.
40. Mochizuki S, Neely JR. Control of glyceraldehyde-3-phosphate dehydrogenase in cardiac muscle. *J Mol Cell Cardiol*. 1979;11(3):221-236.
41. Kobayashi K, Neely JR. Control of maximum rates of glycolysis in rat cardiac muscle. *Circ Res*. 1979;44(2):166-175.
42. Hanse EA, Ruan C, Kachman M, Wang D, Lowman XH, Kelekar A. Cytosolic malate dehydrogenase activity helps support glycolysis in actively proliferating cells and cancer. *Oncogene*. 2017;36(27):3915-3924.

43. Birsoy K, Wang T, Chen WW, Freinkman E, Abu-Remaileh M, Sabatini DM. An Essential Role of the Mitochondrial Electron Transport Chain in Cell Proliferation Is to Enable Aspartate Synthesis. *Cell*. 2015;162(3):540-551.
44. Sullivan LB, Gui DY, Hosios AM, Bush LN, Freinkman E, Vander Heiden MG. Supporting Aspartate Biosynthesis Is an Essential Function of Respiration in Proliferating Cells. *Cell*. 2015;162(3):552-563.
45. Palmieri F. The mitochondrial transporter family (SLC25): Physiological and pathological implications. *Pflügers Arch Eur J Physiol*. 2004;447(5):689-709.
46. Estabrook RW, Sacktor B. alpha-Glycerophosphate oxidase of flight muscle mitochondria. *J Biol Chem*. 1958;233(4):1014-1019.
47. Bücher T, Klingenberg M. Wege des Wasserstoffs in der lebendigen Organisation. *Angew Chemie*. 1958;70(17-18):552-570.
48. Mráček T, Drahota Z, Houštěk J. The function and the role of the mitochondrial glycerol-3-phosphate dehydrogenase in mammalian tissues. *Biochim Biophys Acta - Bioenerg*. 2013;1827(3):401-410.
49. MacDonald MJ, Warner TF, Pellett JR. Increased Mitochondrial Glycerol Phosphate Dehydrogenase Activity in Insulinomas of Two Hypoglycemic Infants*. *J Clin Endocrinol Metab*. 1983;57(3):662-664.
50. Chretien D, Rustin P, Bourgeron T, Rötig A, Saudubray JM, Munnich A. Reference charts for respiratory chain activities in human tissues. *Clin Chim Acta*. 1994;228(1):53-70.
51. Mráček T, Pecinová A, Vrbáček M, Drahota Z, Houštěk J. High efficiency of ROS production by glycerophosphate dehydrogenase in mammalian mitochondria. *Arch Biochem Biophys*. 2009;481(1):30-36.
52. Kobayashi K, Sinasac DS, Iijima M, et al. The gene mutated in adult-onset type II citrullinaemia encodes a putative mitochondrial carrier protein. *Nat Genet*. 1999;22(2):159-163.
53. Jalil MA, Begumi L, Contreras L, et al. Reduced N-acetylaspartate levels in mice lacking aralar, a brain- and muscle-type mitochondrial aspartate-glutamate carrier. *J Biol Chem*. 2005;280(35):31333-31339.
54. Kim W, Deik A, Gonzalez C, et al. Polyunsaturated Fatty Acid Desaturation Is a Mechanism for Glycolytic NAD⁺ Recycling. *Cell Metab*. 2019;29(4):856-870.e7.
55. Yasuda T, Yamaguchi N, Kobayashi K, et al. Identification of two novel mutations in the SLC25A13 gene and detection of seven mutations in 102 patients with adult-onset type II citrullinemia. *Hum Genet*. 2000;107(6):537-545.
56. Ohura T, Kobayashi K, Abukawa D, et al. A novel inborn error of metabolism detected by elevated methionine and/or galactose in newborn screening: Neonatal intrahepatic cholestasis caused by citrin deficiency. *Eur J Pediatr*. 2003;162(5):317-322.
57. Ohura T, Kobayashi K, Tazawa Y, et al. Neonatal presentation of adult-onset type II citrullinemia. *Hum Genet*. 2001;108(2):87-90.
58. Köhler S, Carmody L, Vasilevsky N, et al. Expansion of the Human Phenotype Ontology (HPO) knowledge base and resources. *Nucleic Acids Res*. 2019;47(D1):D1018-D1027.
59. Amberger JS, Hamosh A. Searching online mendelian inheritance in man (OMIM): A knowledgebase of human genes and genetic phenotypes. *Curr Protoc Bioinforma*. 2017;58:1.2.1-1.2.12.
60. Wang YP, Zhou W, Wang J, et al. Arginine Methylation of MDH1 by CARM1 Inhibits Glutamine Metabolism and Suppresses Pancreatic Cancer. *Mol Cell*. 2016;64(4):673-687.
61. Lee SM, Dho SH, Ju SK, Maeng JS, Kim JY, Kwon KS. Cytosolic malate dehydrogenase regulates senescence in human fibroblasts. *Biogerontology*. 2012;13(5):525-536.
62. Kim EY, Kim WK, Kang HJ, et al. Acetylation of malate dehydrogenase 1 promotes adipogenic differentiation via activating its enzymatic activity. *J Lipid Res*. 2012;53(9):1864-1876.
63. Cascón A, Comino-Méndez I, Currás-Freixes M, et al. Whole-exome sequencing identifies MDH2 as a new familial paraganglioma gene. *J Natl Cancer Inst*. 2015;107(5):djv053.
64. Pollard PJ, Brière JJ, Alam NA, et al. Accumulation of Krebs cycle intermediates and over-expression of HIF1 α in tumours which result from germline FH and SDH mutations. *Hum Mol Genet*. 2005;14(15):2231-2239.

65. Papandreou I, Cairns RA, Fontana L, Lim AL, Denko NC. HIF-1 mediates adaptation to hypoxia by actively downregulating mitochondrial oxygen consumption. *Cell Metab.* 2006;3(3):187-197.
66. Heiden MGV, Cantley LC, Thompson CB. Understanding the warburg effect: The metabolic requirements of cell proliferation. *Science (80-)*. 2009;324(5930):1029-1033.
67. Yang C, Ko B, Hensley CT, et al. Glutamine oxidation maintains the TCA cycle and cell survival during impaired mitochondrial pyruvate transport. *Mol Cell.* 2014;56(3):414-424.
68. Kim EY, Han BS, Kim WK, Lee SC, Bae KH. Acceleration of adipogenic differentiation via acetylation of malate dehydrogenase 2. *Biochem Biophys Res Commun.* 2013;441(1):77-82.
69. Yang H, Zhou L, Shi Q, et al. SIRT 3-dependent GOT 2 acetylation status affects the malate-aspartate NADH shuttle activity and pancreatic tumor growth. *EMBO J.* 2015;34(8):1110-1125.
70. Allen EL, Ulanet DB, Pirman D, et al. Differential Aspartate Usage Identifies a Subset of Cancer Cells Particularly Dependent on OGDH. *Cell Rep.* 2016;17(3):876-890.
71. Hakvoort TBM, He Y, Kulik W, et al. Pivotal role of glutamine synthetase in ammonia detoxification. *Hepatology.* 2017;65(1):281-293.
72. Dahlin M, Martin DA, Hedlund Z, Jonsson M, Von Döbeln U, Wedell A. The ketogenic diet compensates for AGC1 deficiency and improves myelination. *Epilepsia.* 2015;56(11):e176-e181.
73. Pérez-Liébana I, Casarejos MJ, Alcaide A, et al. bOHB protective pathways in Aralar-Ko neurons and brain: An alternative to ketogenic diet. *J Neurosci.* 2020;40(48):9293-9305.
74. Lu ZH, Chakraborty G, Ledeen RW, Yahya D, Wu G. N-Acetylaspartate synthase is bimodally expressed in microsomes and mitochondria of brain. *Mol Brain Res.* 2004;122(1):71-78.
75. Wolf NI, Van Der Knaap MS. AGC1 deficiency and cerebral hypomyelination. *N Engl J Med.* 2009;361(20):1997-1998.
76. Ramos M, Pardo B, Llorente-Folch I, Saheki T, del Arco A, Satrústegui J. Deficiency of the mitochondrial transporter of aspartate/glutamate aralar/AGC1 causes hypomyelination and neuronal defects unrelated to myelin deficits in mouse brain. *J Neurosci Res.* 2011;89(12):2008-2017.
77. Maier H, Wang-Eckhardt L, Hartmann D, Gieselmann V, Eckhardt M. N-acetylaspartate synthase deficiency corrects the myelin phenotype in a canavan disease mouse model but does not affect survival time. *J Neurosci.* 2015;35(43):14501-14516.
78. Pardo B, Rodrigues TB, Contreras L, et al. Brain glutamine synthesis requires neuronal-born aspartate as amino donor for glial glutamate formation. *J Cereb Blood Flow Metab.* 2011;31(1):90-101.
79. Saheki T, Kobayashi K. Mitochondrial aspartate glutamate carrier (citrin) deficiency as the cause of adult-onset type II citrullinemia (CTLN2) and idiopathic neonatal hepatitis (NICCD). *J Hum Genet.* 2002;47(7):333-341.
80. Tabata A, Sheng JS, Ushikai M, et al. Identification of 13 novel mutations including a retrotransposal insertion in SLC25A13 gene and frequency of 30 mutations found in patients with citrin deficiency. *J Hum Genet.* 2008;53(6):534-545.
81. Tazawa Y, Kobayashi K, Ohura T, et al. Infantile cholestatic jaundice associated with adult-onset type II citrullinemia. *J Pediatr.* 2001;138(5):735-740.
82. Tang CF, Liu SC, Feng Y, et al. [Newborn screening program and blood amino acid profiling in early neonates with citrin deficiency]. *Zhonghua er ke za zhi = Chinese J Pediatr.* 2019;57(10):797-801.
83. Tomomasa T, Kobayashi K, Kaneko H, et al. Possible clinical and histologic manifestations of adult-onset type II citrullinemia in early infancy. *J Pediatr.* 2001;138(5):741-743.
84. Naito E, Ito M, Matsuura S, et al. Type II citrullinaemia (citrin deficiency) in a neonate with hypergalactosaemia detected by mass screening. *J Inherit Metab Dis.* 2002;25(1):71-76.
85. Hayasaka K, Numakura C, Toyota K, Kimura T. Treatment with lactose (galactose)-restricted and medium-chain triglyceride-supplemented formula for neonatal intrahepatic cholestasis caused by citrin deficiency. *JIMD Rep.* 2012;2:37-44.
86. Song YZ, Deng M, Chen FP, et al. Genotypic and phenotypic features of citrin deficiency: Five-year experience in a Chinese pediatric center. *Int J Mol Med.* 2011;28(1):33-40.

87. Okano Y, Kobayashi K, Ihara K, et al. Fatigue and quality of life in citrin deficiency during adaptation and compensation stage. *Mol Genet Metab.* 2013;109(1):9-13.
88. Nagasaka H, Okano Y, Tsukahara H, et al. Sustaining hypercitrullinemia, hypercholesterolemia and augmented oxidative stress in Japanese children with aspartate/glutamate carrier isoform 2-citrin-deficiency even during the silent period. *Mol Genet Metab.* 2009;97(1):21-26.
89. Nagasaka H, Komatsu H, Inui A, et al. Circulating tricarboxylic acid cycle metabolite levels in citrin-deficient children with metabolic adaptation, with and without sodium pyruvate treatment. *Mol Genet Metab.* 2017;120(3):207-212.
90. Kasahara M, Ohwada S, Takeichi T, et al. Living-related liver transplantation for type II citrullinemia using a graft from heterozygote donor. *Transplantation.* 2001;71(1):157-159.
91. Ikeda S, Yazaki M, Takei Y, et al. Type II (adult onset) citrullinaemia: clinical pictures and the therapeutic effect of liver transplantation. *J Neurol Neurosurg Psychiatry.* 2001;71(5):663-670.
92. Yazaki M, Hashikura Y, Takei YI, et al. Feasibility of auxiliary partial orthotopic liver transplantation from living donors for patients with adult-onset type II citrullinemia. *Liver Transplant.* 2004;10(4):550-554.
93. Mutoh K, Kurokawa K, Kobayashi K, Saheki T. Treatment of a citrin-deficient patient at the early stage of adult-onset type II citrullinaemia with arginine and sodium pyruvate. *J Inherit Metab Dis.* 2008;31 Suppl 2:S343-S347.
94. Yazaki M, Kinoshita M, Ogawa S, et al. A 73-year-old patient with adult-onset type II citrullinemia successfully treated by sodium pyruvate and arginine. *Clin Neurol Neurosurg.* 2013;115(8):1542-1545.
95. Imamura Y, Kobayashi K, Shibata T, et al. Effectiveness of carbohydrate-restricted diet and arginine granules therapy for adult-onset type II citrullinemia: A case report of siblings showing homozygous SLC25A13 mutation with and without the disease. *Hepatol Res.* 2003;26(1):68-72.
96. Moriyama M, Li MX, Kobayashi K, et al. Pyruvate ameliorates the defect in ureogenesis from ammonia in citrin-deficient mice. *J Hepatol.* 2006;44(5):930-938.
97. Komatsu M, Yazaki M, Tanaka N, et al. Citrin deficiency as a cause of chronic liver disorder mimicking non-alcoholic fatty liver disease. *J Hepatol.* 2008;49(5):810-820.
98. Moriyama M, Fujimoto Y, Rikimaru S, et al. Mechanism for increased hepatic glycerol synthesis in the citrin/mitochondrial glycerol-3-phosphate dehydrogenase double-knockout mouse: Urine glycerol and glycerol 3-phosphate as potential diagnostic markers of human citrin deficiency. *Biochim Biophys Acta - Mol Basis Dis.* 2015;1852(9):1787-1795.
99. Juaristi I, García-Martín ML, Rodrigues TB, Satrústegui J, Llorente-Folch I, Pardo B. ARALAR/AGC1 deficiency, a neurodevelopmental disorder with severe impairment of neuronal mitochondrial respiration, does not produce a primary increase in brain lactate. *J Neurochem.* 2017;142(1):132-139.
100. Ramos M, Del Arco A, Pardo B, et al. Developmental changes in the Ca²⁺-regulated mitochondrial aspartate-glutamate carrier aralar1 in brain and prominent expression in the spinal cord. *Dev Brain Res.* 2003;143(1):33-46.
101. Van Der Crabben SN, Verhoeven-Duif NM, Brilstra EH, et al. An update on serine deficiency disorders. *J Inherit Metab Dis.* 2013;36(4):613-619.
102. El-Hattab AW. Serine biosynthesis and transport defects. *Mol Genet Metab.* 2016;118(3):153-159.
103. Cavus I, Kasoff WS, Cassaday MP, et al. Extracellular metabolites in the cortex and hippocampus of epileptic patients. *Ann Neurol.* 2005;57(2):226-235.
104. Patgiri A, Skinner OS, Miyazaki Y, et al. An engineered enzyme that targets circulating lactate to alleviate intracellular NADH:NAD⁺ imbalance. *Nat Biotechnol.* 2020;38(3):309-313.
105. Wanders RJA, Karnebeek CDM, Jans JJM, Verhoeven NM, Houten SM. News and views. *J Inherit Metab Dis.* 2020;43(4):647-650.
106. International Mouse Phenotyping Consortium. IMPC | International Mouse Phenotyping Consortium. IMPC.
107. Dickinson ME, Flenniken AM, Ji X, et al. High-throughput discovery of novel developmental phenotypes. *Nature.* 2016;537(7621):508-514.

108. Shen H, Damcott C, Shuldiner SR, et al. Genome-wide association study identifies genetic variants in GOT1 determining serum aspartate aminotransferase levels. *J Hum Genet.* 2011;56(11):801-805.
109. Buffet A, Morin A, Castro-Vega LJ, et al. Germline Mutations in the Mitochondrial 2-Oxoglutarate/Malate Carrier SLC25A11 Gene Confer a Predisposition to Metastatic Paragangliomas. *Cancer Res.* 2018;78(8):1914-1922.
110. Lee JS, Lee H, Lee SSH, et al. Loss of SLC25A11 causes suppression of NSCLC and melanoma tumor formation. *EBioMedicine.* 2019;40:184-197.
111. van Karnebeek CDM, Sayson B, Lee JJY, et al. Metabolic Evaluation of Epilepsy: A Diagnostic Algorithm With Focus on Treatable Conditions. *Front Neurol.* 2018;9:1016.
112. van Karnebeek CD, Stockler S. Treatable Inborn Errors of Metabolism Causing Intellectual Disability: A Review and Diagnostic Approach. In: *ELS.* John Wiley & Sons, Ltd; 2014.



Chapter 4

The malate-aspartate shuttle is important for *de novo* serine biosynthesis

Melissa H. Broeks¹, Nils W.F. Meijer¹, Denise Westland¹, Marjolein Bosma¹,
Johan Gerrits¹, Clara D.M. van Karnebeek^{2,3}, Ronald J.A. Wanders³, Fried J.T. Zwartkruis⁴,
Nanda M. Verhoeven-Duif^{1*} & Judith J.M. Jans^{1*}

¹ Department of Genetics, Section Metabolic Diagnostics, University Medical Center Utrecht, Lundlaan 6, 3584 EA Utrecht, The Netherlands

² Emma Center for Personalized Medicine, Departments of Pediatrics and Human Genetics, Amsterdam University Medical Center, Meibergdreef 9, 1105 AZ Amsterdam, The Netherlands

³ Departments of Pediatrics and Laboratory Medicine, Laboratory Genetic Metabolic Diseases, Amsterdam University Medical Center, University of Amsterdam, Meibergdreef 9, 1105 AZ Amsterdam, The Netherlands

⁴ dLAB, Center for Molecular Medicine, University Medical Center Utrecht, Universiteitsweg 100, 3584 CG, Utrecht, The Netherlands

* These authors contributed equally

ABSTRACT

The malate-aspartate shuttle (MAS) is a redox shuttle that transports reducing equivalents across the inner mitochondrial membrane, while recycling cytosolic NADH to NAD⁺. We genetically disrupted each MAS component to generate a panel of MAS-defective HEK293 cell lines in which we performed [U-¹³C]-glucose tracing. MAS-defective cells had diminished serine biosynthesis, which strongly correlated with the lactate M+3/pyruvate M+3 ratio (reflective of the cytosolic NAD⁺/NADH ratio), consistent with the NAD⁺-dependency of phosphoglycerate dehydrogenase in the serine synthesis pathway. MDH1-deficient cells were most severely affected, whereas OGC- and MDH2-deficient cells were less affected. Overall, we demonstrated that the MAS is important for *de novo* serine biosynthesis, implying that serine supplementation could be used as a therapeutic strategy for MAS defects and possibly other redox disorders.

Keywords: malate-aspartate shuttle, NADH shuttle, malate dehydrogenase, glutamate-oxaloacetate transaminase, aspartate-glutamate carrier, oxoglutarate-malate carrier, isotope-tracer analysis, serine biosynthesis, glycolysis, metabolomics, metabolism

INTRODUCTION

The cellular NAD⁺/NADH ratio is an important regulator for metabolic activity, as cellular oxidation reactions require the net transfer of electrons to an electron acceptor, such as NAD⁺, to yield NADH. The electrons of NADH are consumed in the mitochondrial electron transport chain (ETC) to drive ATP synthesis, coupling cellular oxidation reactions to oxidative phosphorylation. Since cytosolic NADH cannot cross the inner mitochondrial membrane, reducing equivalents from NADH are indirectly transported to the mitochondrial matrix via the malate-aspartate shuttle (MAS) or directly to the ETC via the glycerol 3-phosphate shuttle.¹⁻⁴ Simultaneously, these shuttles regenerate cytosolic NAD⁺, facilitating the continuation of cytosolic oxidative pathways such as glycolysis.

The MAS is the main metabolic redox shuttle in the human body and its components are most strongly expressed in high-energy-demanding tissues such as the brain, heart, kidney and liver. The biochemical steps of the MAS, catalyzed by four enzymes and two transporters, have a net result of shuttling redox equivalents from cytosolic NADH to the mitochondrial matrix. First, cytosolic malate dehydrogenase 1 (MDH1) oxidizes NADH by reducing oxaloacetate to malate (Figure 1A). The oxoglutarate-malate carrier (OGC, *SLC25A11*) catalyzes the transport of cytosolic malate and intramitochondrial 2-oxoglutarate in electroneutral exchange over the inner mitochondrial membrane. Next, mitochondrial MDH2 reduces NAD⁺ by oxidizing malate to oxaloacetate as part of the tricarboxylic acid (TCA) cycle in the mitochondrial matrix. Mitochondrial glutamate-oxaloacetate transaminase 2 (GOT2) transaminates oxaloacetate and glutamate to synthesize aspartate and 2-oxoglutarate. The aspartate glutamate carrier (AGC1/ Aralar, *SLC25A12*, brain isoform; AGC2/ Citrin, *SLC25A13*, liver isoform) exchanges mitochondrial aspartate for cytosolic glutamate and a proton. To close the MAS cycle, GOT1 transaminates cytosolic aspartate and 2-oxoglutarate to oxaloacetate and glutamate.

Disorders of the MAS are rare inherited metabolic diseases. Currently, reported MAS disorders include AGC2 (Citrin) deficiency (OMIM #603859),^{5,6} AGC1 (Aralar) deficiency (OMIM #612949),⁷⁻¹¹ GOT2 deficiency (OMIM #618721),¹² MDH2 deficiency (OMIM #617339)¹³⁻¹⁵ and MDH1 deficiency (OMIM #618959).¹⁶ Most patients affected by a MAS disorder clinically present with infantile epileptic encephalopathy,^{17,18} or in the case of a deficiency of the liver-specific mitochondrial carrier citrin, with hepatic encephalopathy.¹⁹

Previously, it was demonstrated that the disturbed NAD⁺/NADH ratio in GOT2 deficiency hampered the flux of *de novo* serine biosynthesis, of which the first enzymatic step is catalyzed by NAD⁺-dependent phosphoglycerate dehydrogenase

(PHGDH). This finding paved the way to the effective treatment of neurological symptoms by a combination of pyridoxine and serine supplementation.¹² Therefore, we hypothesized that all MAS defects lead to a secondary serine biosynthesis defect. To study this on a cellular level, we generated a comprehensive panel of HEK293 cell lines with genetic disruption of the individual MAS components. Here, we demonstrate that all MAS defects result in a lower cytosolic NAD⁺/NADH ratio, which disturbs glycolysis and diminishes *de novo* serine biosynthesis.

RESULTS

MAS defects have reduced *de novo* serine and glycine biosynthesis

To study MAS defects on a cellular level, we generated a comprehensive panel of HEK293 cell lines with genetic disruptions of the MAS-enzymes (*GOT1*, *MDH1*, *MDH2* and *GOT2*) and transporters (OGC: *SLC25A11* and AGC: *SLC25A12* & *SLC25A13*), which included cell lines with a knockout of both AGC genes (Figures 1A and S1A-B). Transfected cell lines that did not result in the absence of protein were included as the corresponding WT for the respective MAS components, resulting in a total of 33 HEK293 cell lines (Figure S1A). To study whether MAS defects lead to diminished serine and glycine biosynthesis, we performed [U-¹³C]-glucose isotopic tracing experiments in all cell lines, as serine and glycine are synthesized *de novo* from the glycolytic intermediate 3-phosphoglycerate (3-PG) (Figures 1A-B). After 8 hours of incubation with [U-¹³C]-glucose, ¹³C₃-serine and ¹³C₂-glycine concentrations were most strongly decreased in MDH1 KO cells, followed by AGC, GOT1, GOT2, OGC and MDH2 KO cells when compared to control cells (Figures 1C and S2C-D). At that time, differences in unlabeled serine and glycine concentrations between KO and WT cells were negligible (Figures S2A-B), indicating that the altered *de novo* labeling of serine and glycine over this time course was not due to altered serine and glycine uptake in KO cells. A decrease in the fractional enrichment of ¹³C₃-serine and ¹³C₂-glycine further confirmed the diminished *de novo* serine and glycine biosynthesis in all MAS KO cells (Figure 1D), with serine and glycine biosynthesis being only partially hampered in OGC and MDH2 KO cells. Overall, these findings demonstrate that all MAS-defective cells display decreased *de novo* serine and glycine biosynthesis.

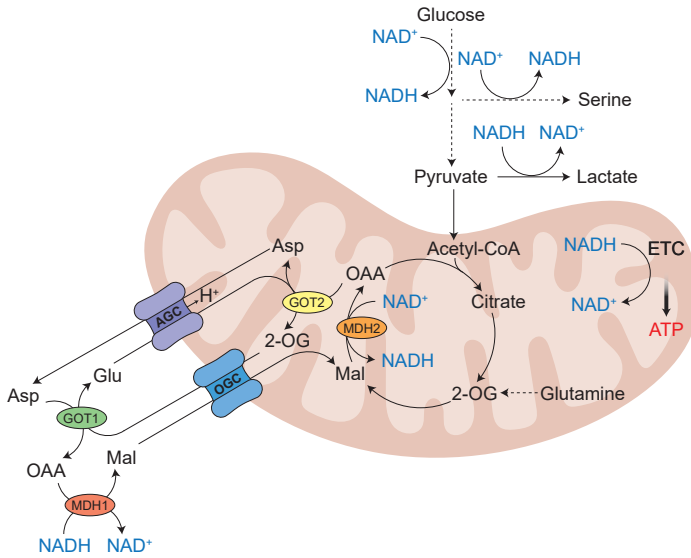
MAS defects lead to disturbed cytosolic NAD⁺/NADH ratio and constrained glycolysis

To investigate the underlying mechanism of diminished *de novo* serine biosynthesis in MAS-defective cells, we used direct-infusion high-resolution mass spectrometry (DI-HRMS) to further analyze the intracellular metabolomes of cells incubated with

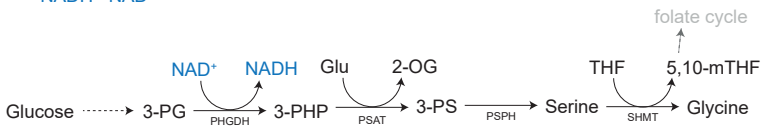
[U-¹³C]-glucose for 8 hours. One of the enzymatic steps in glycolysis prior to the formation of the serine biosynthesis precursor 3-PG is the NAD⁺-driven oxidation of glyceraldehyde 3-phosphate (GA3P) to 1,3-bisphosphoglycerate by glyceraldehyde 3-phosphate dehydrogenase (GAPDH) (Figure 2A). Since GAPDH becomes rate-limiting when the NAD⁺/NADH ratio is low, we expect that in MAS-defective cells metabolites upstream of GAPDH accumulate and metabolites downstream of GAPDH decrease. Indeed, fructose 1,6-bisphosphate M+6 and glyceraldehyde 3-phosphate (GA3P) M+3 (indistinguishable by DI-HRMS from fructose 2,6-bisphosphate M+6 and dihydroxyacetone phosphate (DHAP) M+3, respectively; Table S1) were increased in all MAS-defective cells compared to controls, with the exception of MDH2 KO (Figures 2B and S3A-B). In addition, glycerol synthesis branches from glycolysis upstream of GAPDH. In this pathway, glycerol phosphate dehydrogenase (GPD1) regenerates NAD⁺ by converting DHAP to glycerol 3-phosphate (G3P), which is then converted to glycerol (Figure 2A). Both relative levels and fractional enrichment of G3P M+3 were increased in all MAS KO cells compared to controls, implying that the abundant availability of intermediates in the first steps of glycolysis leads to an increased flux into the glycerol synthesis pathway in MAS-defective cells (Figures 2C and S3C).

Downstream of GAPDH, 3-PG M+3 levels (and 2-phosphoglycerate M+3, indistinguishable by DI-HRMS) were most markedly decreased in OGC, GOT2 and AGC KO cells compared to controls (Figures 2B and S3B). Furthermore, both relative levels and fractional enrichment of the glycolytic end-product pyruvate M+3 were decreased in all KO cells compared to controls (Figures 2B and S3B), indicating a decrease in [U-¹³C]-glucose flux to pyruvate M+3 in all MAS-defective cells. In addition, lactate M+3 levels were most prominently decreased in OGC, GOT2 and AGC KO cells (Figure 2B). The enzymatic conversion of pyruvate to lactate is catalyzed by lactate dehydrogenase (LDH), and this reaction is in equilibrium with the cytosolic NAD⁺/NADH ratio (Figure 2A).^{20,21} The lactate/pyruvate ratio thus reflects the free cytosolic NAD⁺/NADH ratio, with a higher lactate/pyruvate ratio indicating a lower NAD⁺/NADH ratio. To determine whether MAS-defective cells have an altered cytosolic NAD⁺/NADH ratio, we analyzed the labeled and unlabeled lactate/pyruvate ratio. We found no differences in the lactate M+0/pyruvate M+0 ratio (Figure S3D), and the total (labeled and unlabeled) lactate/pyruvate ratio was only slightly increased in MAS-defective cells (Figure S3E). However, the lactate M+3/pyruvate M+3 ratios were strikingly increased in all MAS KO cells compared to controls (Figure 2D). MDH1 KO cells had the highest lactate M+3/pyruvate M+3 ratio, followed by AGC, GOT1, GOT2, OGC and MDH2 KO cells in decreasing order. Together, these findings indicate that a disturbed cytosolic NAD⁺/NADH ratio disrupts glycolysis at the level of GAPDH in all MAS-defective cells, resulting in decreased flux from glucose to the lower part of glycolysis as well as serine biosynthesis.

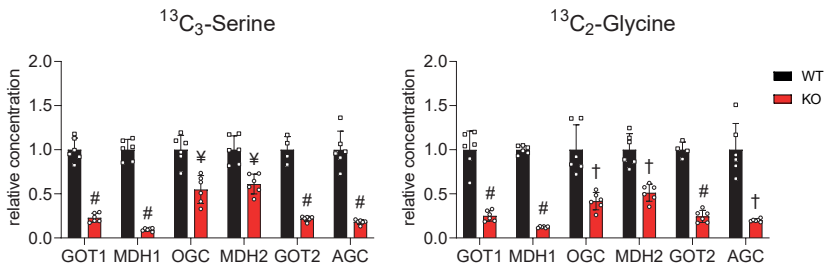
A



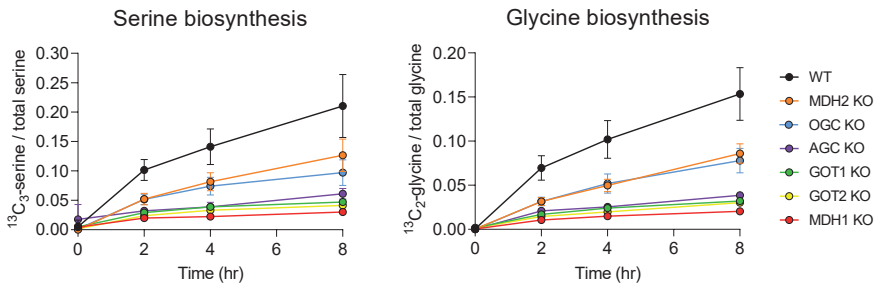
B



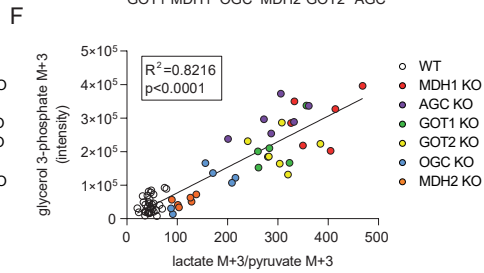
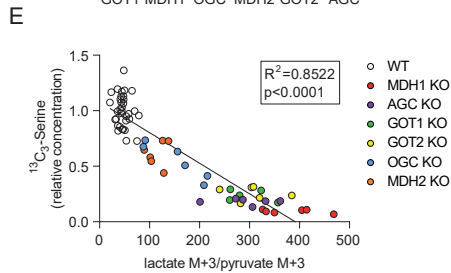
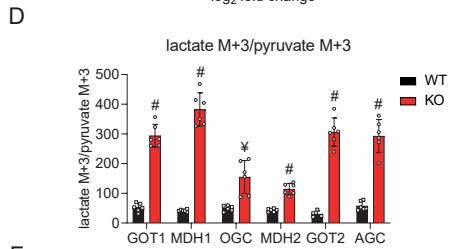
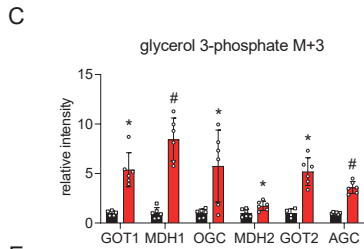
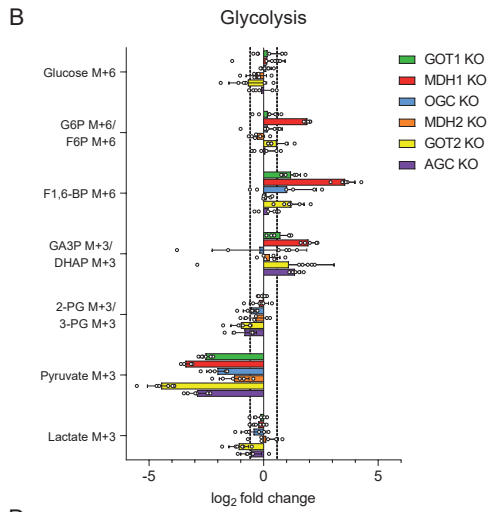
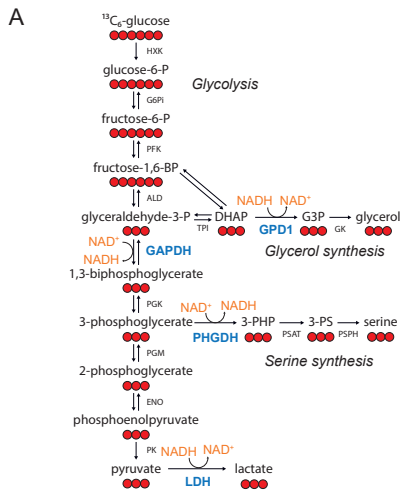
C



D



< **Figure 1. MAS defects have reduced *de novo* serine and glycine biosynthesis. (A and B)** A schematic representation of glycolysis, *de novo* serine and glycine biosynthesis, the tricarboxylic acid (TCA) cycle and the malate-aspartate shuttle (MAS). Glycolysis and subsequently serine biosynthesis from the glycolytic intermediate 3-phosphoglycerate (3-PG) depend on the cytosolic NAD⁺/NADH ratio. Both pyruvate to lactate conversion and the MAS regenerate cytosolic NAD⁺. The MAS and the TCA cycle are intimately connected via mitochondrial MDH2, which transfers the reducing equivalents from malate onto NAD⁺ to generate NADH. NADH is used to generate ATP in the electron transport chain (ETC). OAA, oxaloacetate; Asp, aspartate; Glu, glutamate; Mal, malate; 2-OG, 2-oxoglutarate; 3-PHP, 3-phosphohydroxypyruvate; 3-PS, 3-phosphoserine; THF, tetrahydrofolate; 5,10-mTHF, 5,10-methyleneTHF. **(C)** ¹³C₃-serine and ¹³C₂-glycine concentrations after an 8-hour incubation with [U-¹³C]-glucose. Concentrations in KO cells are expressed relative to controls. **(D)** Fractional labeling of serine and glycine from [U-¹³C]-glucose in MAS KO HEK293 cells incubated for 2, 4 and 8 hours [WT (*n* = 34), KO (*n* = 6 for each)]. Data shown are mean ± SD of three biological replicates from two independent experiments. Parametric unpaired t-tests were followed by Holm-Sidak's multiple comparisons test to compare each KO to its corresponding WT. The adjusted p-values are indicated as **p*<0.05, †*p*<0.01, ‡*p*<0.001, #*p*<0.0001.



< Figure 2. MAS defects lead to constrained glycolysis and disturbed cytosolic NAD⁺/NADH, which is correlated with serine and glycerol 3-phosphate synthesis from glucose. (A) A schematic illustrating [U-¹³C]-glucose labeling in glycolysis and branching pathways. DHAP, dihydroxyacetone phosphate; G3P, glycerol 3-phosphate; 3-PHP, 3-phosphohydroxypyruvate; 3-PS, 3-phosphoserine. **(B)** log₂ fold change of intracellular ¹³C₆-glucose-derived glycolytic intermediates after 8 hours measured by DI-HRMS. The fold change was calculated by dividing the intensity of the KO by the geometric mean of intensities of experimentally matched controls. The log₂ of the fold change is shown (*n* = 6 for each KO) and the dotted line indicates a fold change of ± 1.5. Glucose 6-phosphate (G6P)/Fructose-6-phosphate (F6P) isomers include a.o. myo-inositol phosphates, mannose phosphates, tagatose phosphates and isomers of fructose 1,6-bisphosphate (F1,6BP) include bisphosphates. Pyruvate has the same *m/z* as malonic semialdehyde and lactate as hydroxypropionic acid, glyceraldehyde, dihydroxyacetone and methoxyacetic acid. Additional isobaric compounds are listed in Table S1. GA3P, glyceraldehyde 3-phosphate; 2-PG and 3-PG, 2- and 3-phosphoglycerate. **(C and D)** Relative intensity of glycerol 3-phosphate M+3 (isomer = beta-glycerophosphoric acid M+3) **(C)** and lactate M+3/pyruvate M+3 ratio **(D)** in MAS WT and KO cells following an 8-hour incubation with ¹³C₆-glucose (*n* = 4-6). Data shown are mean ± SD of three biological replicates from two independent experiments and expressed as relative intensities to corresponding controls. Parametric unpaired t-tests were followed by Holm-Sidak's multiple comparisons test to compare each KO to its corresponding WT. The adjusted p-values are indicated as **p*<0.05, ¥*p*<0.01, †*p*<0.001, #*p*<0.0001. **(E and F)** Correlation of the relative ¹³C₃-serine concentration **(E)** and glycerol 3-phosphate M+3 (isomer = beta-glycerophosphoric acid M+3) intensity **(F)** with the lactate M+3/pyruvate M+3 ratio in MAS WT and KO cells displayed with Pearson correlation coefficients.

The cytosolic NAD⁺/NADH ratio in MAS defects correlates with serine and glycerol 3-P synthesis from glucose

Since the activity of both glycolysis and the serine biosynthesis pathway depends on the free cytosolic NAD⁺/NADH ratio, we studied the association between the lactate/pyruvate ratio, reflecting the cytosolic NAD⁺/NADH ratio, and the levels of synthesized serine and glycerol 3-phosphate in MAS-defective cells. Interestingly, the lactate M+3/pyruvate M+3 ratio strongly correlated with both the relative ¹³C₃-serine (*R*²=0.8522, *p*<0.0001) (Figure 2E) and G3P concentrations (*R*²=0.8216, *p*<0.0001) (Figure 2F), and they also correlated with each other (*R*²=0.7105, *p*<0.0001) (Figure S3F). We found no correlation between the lactate M+0/pyruvate M+0 ratio and ¹³C₃-serine or G3P and only a weak correlation between the total lactate/pyruvate ratio and ¹³C₃-serine (*R*²=0.2693, *p*<0.0001) (Figure S3G). These findings illustrate that the low cytosolic NAD⁺/NADH ratio in MAS defects is quantitatively associated with the synthesis of serine and G3P from glucose and provide further evidence for the association between the MAS and cytosolic NAD⁺-dependent pathways.

Most MAS defects affect flux through the NAD⁺-regenerating enzyme MDH1

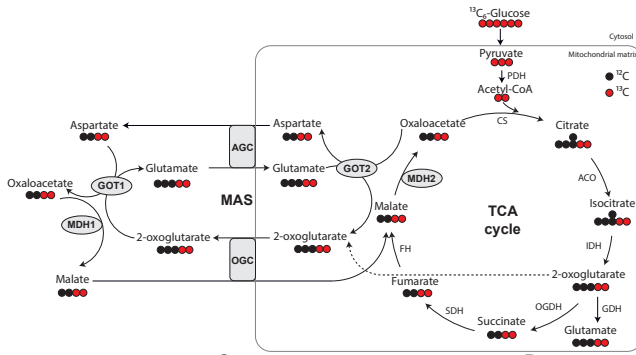
Since the MAS is linked to the TCA cycle via MDH2, we studied the consequences of MAS defects on TCA cycle and MAS fluxes. Total levels and the fraction of M+2 intermediates labeled in the first round of the TCA cycle and the MAS, as determined by DI-HRMS after 8 hours of incubation with [U-¹³C]-glucose, provided further insights into these metabolic flux in MAS-defective cells (Figure 3A). As MDH2 generates oxaloacetate that subsequently reacts with acetyl-CoA to form citrate, loss of MDH2 results in depletion of oxaloacetate and consequently citrate. When compared to controls and other MAS defective cells, MDH2 KO cells had the lowest citrate levels, as well as increased levels of acetyl-CoA M+2 (reflected by an increased conversion to acetylcarnitine M+2) (Figures 3B-G, S4C, S4J and S4K). As a result, MDH2 KO cells had a decreased fractional enrichment of all M+2 TCA cycle intermediates (Figure 3E), indicating low oxidative TCA cycle activity from pyruvate. To assess whether pyruvate M+3 was diverted to anaplerotic routes in MDH2 KO cells, we examined the enrichment of M+3 isotopologues, formed by pyruvate carboxylation (malate, fumarate, citrate, aspartate) or the second round of the TCA cycle (succinate) (Figure S4A). The relative increase in fumarate and malate M+3 compared to succinate M+3 indicates the increased carboxylation of pyruvate in MDH2 KO cells (Figure S4L).²² In addition, despite lower total intensities (Figure S4O), the fractional enrichment of M+3 isotopologues within the total labeled pools of aspartate, malate, fumarate and citrate was relatively increased in MDH2 KO cells compared to controls (Figures S4M-N), indicating a relative (but not absolute) increase in pyruvate anaplerosis. Overall, these findings indicate that pyruvate entry into the TCA cycle is blocked in MDH2 KO cells, diverting it to alternative pathways.

MAS defects, with the exception of MDH2, are not intrinsic TCA cycle defects. Hence, the low citrate levels in all other MAS-defective cells are consistent with constrained glycolysis and decreased pyruvate M+3 (Figures 2B, 3B-G and S4C). In the TCA cycle, citrate M+2 is converted to 2-oxoglutarate M+2, which is then converted to either mitochondrial succinate M+2 by OGDH or mitochondrial glutamate M+2 by GDH, or is exchanged for malate by the OGC in the MAS (Figure 3A). As expected, loss of OGC results in decreased 2-oxoglutarate levels as well as decreased fractional enrichment of 2-oxoglutarate M+2 due to impaired export to the cytosol (Figure 3D). Interestingly, total and M+2 fractional enrichment of 2-oxoglutarate were also decreased in GOT1, MDH1, GOT2 and AGC KO cells when compared to controls, suggesting that 2-oxoglutarate export is also diminished in these cells (Figures 3B, 3C, 3F, 3G and S4D). In addition, total malate and the fractional enrichment of malate M+2 were decreased in MDH1, GOT1, OGC, GOT2 and AGC KO cells (Figures 3B-D, 3F,

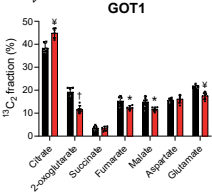
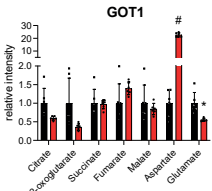
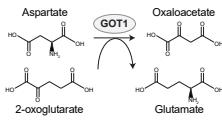
3G and S4G). Malate, as the cytosolic exchange partner for 2-oxoglutarate in the MAS, is formed by MDH1. The decreased fractional enrichment of malate M+2 in MDH1 KO cells is thus presumably due to the decreased malate formation in the cytosol as a result of the primary defect and not due to the decreased formation of malate in the mitochondrion by fumarate hydratase. The similar decrease in GOT1, GOT2 and AGC KO cells indicates that cytosolic malate M+2 formation is also decreased in these MAS defects, collectively indicating that decreased malate M+2 formation by MDH1 leads to impaired exchange with 2-oxoglutarate M+2 in MAS-defective cells.

The impaired exchange of malate and 2-oxoglutarate in defects other than the OGC KO is likely due to the fact that all other defects cause impaired flux through the MAS prior to the OGC. Defects in GOT2 and AGC both result in low total aspartate levels due to diminished synthesis and export to the cytosol, respectively (Figures 3F and 3G). Accordingly, both GOT2 and AGC KO cells had decreased fractional enrichment of aspartate M+2 (Figures 3F, 3G and S4H). In contrast, total aspartate was strikingly increased in GOT1, MDH1 and OGC KO cells, corresponding to the localization of defects downstream of aspartate (Figures 3B-D and S4H). Aspartate accumulation indicates a lower flux through GOT1, as GOT1 converts aspartate to oxaloacetate in the cytosol, while simultaneously converting 2-oxoglutarate to glutamate (Figures 3A and 3B). Indeed, the fractional enrichment of glutamate M+2 was decreased in GOT1 and MDH1 KO cells, but also in GOT2 and AGC KO cells with low aspartate levels (Figures 3B, 3C, 3F, 3G and S4I), indicating that the conversion of 2-oxoglutarate M+2 to glutamate M+2 by GOT1 is decreased. Total glutamate levels were decreased in GOT1, MDH1 and OGC KO cells (Figures 3B-D and S4I), possibly due to decreased availability of 2-oxoglutarate in the case of OGC KO. Collectively, these findings indicate that a defect in the MAS cycle from GOT2 via AGC and GOT1 to MDH1 results in hampered metabolite flux through MDH1. Consequently, the ability to regenerate NAD^+ is decreased, which may explain the most severely disturbed NAD^+/NADH ratios in these MAS-defective cells.

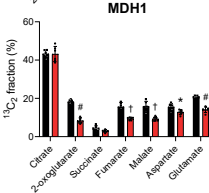
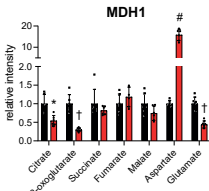
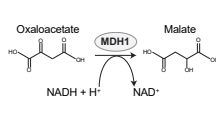
A



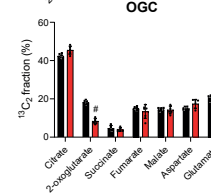
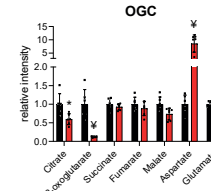
B



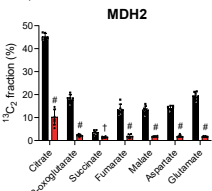
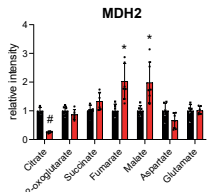
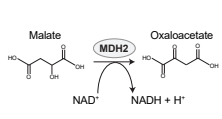
C



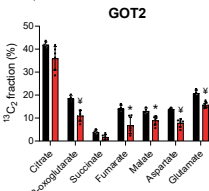
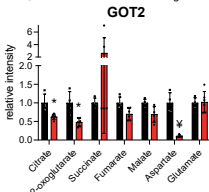
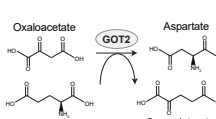
D



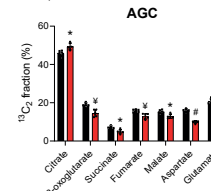
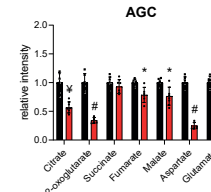
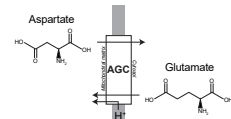
E



F



G



< **Figure 3. Most MAS defects affect flux through the NAD⁺-regenerating enzyme MDH1.** (A) Schematic of [U-¹³C]-glucose labeling in the first round of the TCA cycle and MAS. (B-G) Reaction schemes of the biochemical reaction of (B) GOT1, (C) MDH1, (D) OGC, (E) MDH2, (F) GOT2 and (G) AGC followed by the summed intensity of labeled and unlabeled TCA and MAS intermediates expressed relative to control and as fractional enrichment of M+2 isotopologues following an 8-hour incubation with [U-¹³C]-glucose (n = 4-6). Isobaric compounds are listed in Table S1. Data shown are mean ± SD of three biological replicates from two independent experiments. Parametric unpaired t-tests were followed by Holm-Sidak's multiple comparisons test to compare each KO to its corresponding WT. The adjusted p-values are indicated as *p<0.05, †p<0.01, ‡p<0.001, #p<0.0001.

DISCUSSION

The malate-aspartate shuttle (MAS) is an important redox shuttle that transports reducing equivalents across the inner mitochondrial membrane and maintains the cytosolic NAD⁺/NADH ratio. Although this pathway has been intensively studied, a comprehensive systematic analysis in a single cell system has not been performed before. In this study, we demonstrated that serine biosynthesis, an NAD⁺-dependent metabolic pathway, was disturbed after genetic disruption of each element of the MAS due to a low NAD⁺/NADH ratio impacting glycolysis. Cells with a deficiency in MDH1 were most severely affected, whereas OGC- and MDH2-deficient cells were less affected. Our data further supports the notion that the severity of cytosolic redox imbalance in MAS defects depends on the metabolite flux through the NAD⁺-regenerating enzyme MDH1.

Our study provides important insights into the role of the MAS in serine biosynthesis. Serine is a precursor for many metabolites, including glycine, cysteine, tryptophan, phosphatidyl-L-serine, sphingolipids, purine, porphyrins and glyoxylate, but is also a major donor of one-carbon units for the folate pool by the conversion of serine to glycine. A defect in *de novo* serine biosynthesis was initially demonstrated in a patient with a GOT2 deficiency. Following functional analysis of serine biosynthesis in patients' fibroblasts and GOT2 KO HEK293 cells, a new therapeutic option involving serine supplementation improved the epilepsy and neurodevelopmental status in two patients.¹² Here, we showed that other MAS-defective cells have defective serine biosynthesis as well, implying that the successful therapeutic implementation of serine supplementation might be extended beyond GOT2 to other MAS disorders with a neurological phenotype.

We additionally showed that the cytosolic NAD⁺/NADH ratio, which shifts pyruvate to lactate rather than to CO₂ and H₂O via PDH and the citric acid cycle,²³ strongly

correlated with serine biosynthesis activity in MAS-defective cells. The strong correlation between the NAD^+/NADH ratio and serine synthesis suggests that other disorders with a low cytosolic NAD^+/NADH ratio, such as complex I deficiency and other (genetic) mitochondrial disorders characterized by ETC dysfunction,^{24,25} may have a serine biosynthesis defect as well. Indeed, NAD^+ -availability is important for serine biosynthesis.²³ In addition, it has been shown that complex I inhibition, resulting in a low cytosolic NAD^+/NADH ratio, similarly constrains the serine biosynthesis flux from glucose that was restored upon addition of the electron acceptor 2-ketobutyrate.²⁴ Moreover, studies in cells with defective mitochondrial respiration revealed impaired one-carbon unit production,²⁶ thereby affecting folate metabolism. This is consistent with folate deficiencies occurring in patients with serine biosynthesis defects.²⁷ Part of the clinical phenotype in MAS disorders may be due to a folate deficiency as well. In addition, NAD^+ -repletion might warrant further investigation as a therapeutic intervention for MAS disorders.²⁸

Since the MAS supports glycolysis by regulating the cytosolic NAD^+/NADH ratio,^{3,29,30} each MAS defect demonstrated a decrease in flux from glucose to pyruvate. In addition, we found that glucose flux toward glycerol 3-phosphate increased, which may increase cytosolic NAD^+ when the cytosolic NAD^+/NADH ratio is decreased.³¹ Whether the glycerol phosphate shuttle plays a compensatory role in MAS defects remains to be investigated. However, recent work demonstrated that the MAS and glycerol phosphate shuttle may become saturated, driving aerobic glycolysis,³² which is in line with the strong correlation between glycolysis-derived lactate/pyruvate ratio and glycerol 3-phosphate synthesis in MAS-defects. In addition, the accumulation of glyceraldehyde 3-phosphate and/or dihydroxyacetone phosphate in MAS defects may result in the inhibition of the irreversible mGPDH, due to competitive inhibition in the substrate-binding pocket and by product inhibition, respectively.³³

The underlying pathophysiological mechanism depends on the individual MAS defect. Each MAS-defect results in varying MAS-metabolite concentrations, with low concentrations of these MAS-metabolites limiting MAS activity.³⁴ Lower metabolite flux through GOT1, either by the intrinsic defect or by low aspartate levels due to upstream defects, results in low oxaloacetate and subsequently metabolite flux through the NAD^+ -regenerating enzyme MDH1. As such, fueling MAS-metabolite concentrations, e.g. via aspartate supplementation, has been demonstrated to restore a low NAD^+/NADH ratio in case of mitochondrial dysfunction.^{29,35} Hence, the lower metabolite flux through MDH1 in GOT2, AGC, GOT1 and MDH1 KO cells decreases its NAD^+ -regenerating capacity, resulting in the most prominent drop in cytosolic NAD^+/NADH ratio in these cells, whereas the OGC and MDH2 KO cells were less affected.

The exact pathophysiological mechanisms involved in OGC and MDH2 defects require further research; however, based on our study, we can speculate about potential mechanisms. Although OGC deficiency primarily affects the exchange of 2-oxoglutarate and malate, the disturbed NAD^+/NADH ratio and increased aspartate concentration indicate that GOT1 flux is also affected. However, other transporters may partially compensate for the impaired exchange of 2-oxoglutarate and malate in OGC deficiency, such as the dicarboxylate transporter (DIC, *SLC25A10*), which allows malate to enter the mitochondria in exchange for phosphate, and the oxodicarboxylate carrier (ODC, *SLC25A21*), which exchanges 2-oxoadipate for mitochondrial 2-oxoglutarate.^{36,37} In addition, the citrate carrier (CIC, *SLC25A1*) can exchange mitochondrial citrate for malate, contributing to malate import as well as the potential extramitochondrial 2-oxoglutarate production via isocitrate and cytosolic isocitrate dehydrogenase. MDH2 deficiency, however, completely disrupted the entry of glucose-derived pyruvate into the TCA cycle and MAS. The cytosolic NAD^+/NADH imbalance in MDH2 KO cells may be the result of impaired respiratory chain activity due to disruption of TCA cycle oxidative activity. Since the unidirectional AGC is driven by the proton-motive force of the respiratory chain,³⁸ impaired respiratory chain activity may then hamper MAS activity.^{39–41} Fumarate and malate accumulation suggest that MDH2-defective cells compensate for this by increasing glutamine consumption to fuel the TCA cycle. In addition, glutamine can be converted to citrate via reductive carboxylation, which can then be cleaved into acetyl-CoA and oxaloacetate by citrate lyase.⁴² MDH1 can then convert oxaloacetate to malate to regenerate NAD^+ , which may compensate to some extent for the disturbed NAD^+/NADH ratio. Furthermore, relatively more pyruvate carboxylation to form oxaloacetate may contribute to the flux through MDH1, resulting in only a minor effect on the cytosolic NAD^+/NADH ratio in MDH2 KO cells.

In conclusion, we demonstrated that all MAS-defective HEK293 cells have disrupted glycolysis, resulting in increased glycerol synthesis from the glycolytic intermediate dihydroxyacetone-phosphate. Despite clear differences in metabolic alterations between the various defects, all MAS defects have a lower cytosolic NAD^+/NADH ratio that restricts serine biosynthesis. As serine supplementation benefits GOT2-deficient patients, further investigations into the use of serine as a therapeutic option for patients with a (partially) defective MAS are worthwhile.

Limitations of the study

The main message of our study is that serine supplementation may be considered as a therapeutic strategy for patients with MAS disorders. We acknowledge that our *in vitro* system poses several limitations, including the use of a single cell line.

Clearly, there is potential for additional cell lines or *in vivo* models that recapitulate the neurological phenotype of MAS disorders to further study the physiological relevance of our findings. In addition, we did not perform addback experiments with catalytically active or inactive enzymes to determine whether effects are due to the loss of the enzyme or loss of its activity, although we had a catalytic dead enzyme of GOT2 that demonstrated the same metabolic results as the KO with absence of GOT2. Furthermore, rescue experiments with pyruvate and 2-ketobutyrate could further strengthen the causal link between the loss of MAS-enzymes, the NAD⁺/NADH ratio and serine biosynthesis.

Author Contributions

J.J.M.J., N.M.V., F.J.T.Z., R.J.A.W., C.D.M.K., and M.H.B. were involved in conceptualization and design of the study. D.W. and F.J.T.Z generated the Crispr/Cas9 KO cell lines. D.W. performed the metabolic tracing experiments. M.H.B., N.W.F., M.B. and J.G. performed mass spectrometry and data processing. M.H.B. performed data and statistical analysis and wrote the manuscript. All authors helped with the editing of the manuscript.

Acknowledgements

We thank Susan Zwakenberg for her technical assistance. This work was supported by Metakids (2017-075 to J.J.M.J) and Stofwisselkracht (2019 to N.M.V.).

Declaration of Interests

The authors declare no competing interests

STAR★METHODS

KEY RESOURCES TABLE

REAGENT or RESOURCE	SOURCE	IDENTIFIER
Antibodies		
Mouse anti-CMDH1 (clone H-6) (monoclonal)	Santa Cruz biotechnology	Cat#sc-166879; RRID: AB_10609257
Rabbit anti-GOT1 (clone E4A40) (monoclonal)	Cell signaling	Cat#34423; RRID: AB_2799052
Rabbit anti-GOT2 (polyclonal)	Bethyl Laboratories	Cat#A304-356A; RRID: AB_2620551
Mouse anti-SLC25A11 (clone E-2) (monoclonal)	Santa Cruz Biotechnology	Cat#sc-515593
Mouse anti-Aralar (clone B-2) (monoclonal)	Santa Cruz Biotechnology	Cat#sc-271056; RRID: AB_10608837
Mouse anti-Citrin (clone D-7) (monoclonal)	Santa Cruz Biotechnology	Cat#sc-393303
Rabbit anti-MDH2 (polyclonal)	Cell signaling	Cat#8610; RRID: AB_10841300
Mouse anti-Vinculin (clone 7F9) (monoclonal)	Santa Cruz Biotechnology	Cat#sc-73614; RRID: AB_1131294
Rabbit anti-Citrate synthetase (polyclonal)	Abcam	Cat#Ab96600; RRID: AB_10678258
Goat anti-Rabbit IgG H&L (HRP) (polyclonal)	Abcam	Cat#Ab6721; RRID: AB_955447
Goat anti-Mouse IgG H&L (HRP) (polyclonal)	Jackson ImmunoResearch	Cat#115-035-146; RRID: AB_2307392
Bacterial and virus strains		
Subcloning Efficiency™ DH5α Competent Cells	Invitrogen	Cat#18265017
Chemicals, peptides, and recombinant proteins		
Dulbecco's Modified Eagle Medium, high glucose, GlutaMAX™ supplement, pyruvate	ThermoFisher Scientific	Cat#10569010
Fetal Bovine Serum (FBS)	ThermoFisher Scientific	Cat#10270106
Penicillin-Streptomycin (10,000 U/ml)	ThermoFisher Scientific	Cat#15140122
Trypsin-EDTA (0.5%), no phenol red	ThermoFisher Scientific	Cat#15400054
Dulbecco's Phosphate buffer saline (PBS)	Lonza	Cat#17513F
DMEM, no glucose	ThermoFisher	Cat#11966025
Methanol Absolute, ULC/MS grade	Biosolve	Cat#13684102
Formic acid 99% ULC/MS – CC/SFC	Biosolve	Cat#06914143
Acetonitrile ULC/MS – CC/SFC	Biosolve	Cat#01204102
Ammonium formate ULC/MS – CC/SFC	Biosolve	Cat#01984156
5-Sulfosalicylic acid dihydrate	Merck	Cat#247006
D-Glucose (U-13C6, 99%)	Cambridge Isotope Laboratories, Inc.	Cat#CLM-1396-PK
L-Serine	Sigma-Aldrich	Cat#S4500
L-Serine (13C3, 99%)	Cambridge Isotope Laboratories, Inc.	Cat#CLM-1574-H-PK

REAGENT or RESOURCE	SOURCE	IDENTIFIER
L-Serine (13C3, 99%; 15N, 99%)	Cambridge Isotope Laboratories, Inc.	Cat#CNLM-474-H-PK
Glycine	Merck	Cat#100590
Glycine (13C2, 97-99%)	Cambridge Isotope Laboratories, Inc.	Cat#CLM-1017-PK
Glycine (13C2, 99%; 15N, 99%)	Cambridge Isotope Laboratories, Inc.	Cat#CNLM-1673-H-PK
Labeled amino acids standards set A	Cambridge Isotope Laboratories, Inc.	Cat#NSK-A
Labeled amino acids standards set B	Cambridge Isotope Laboratories, Inc.	Cat#NSK-B
L-Aspartic acid	Sigma-Aldrich	Cat#A9256
DL-Aspartic acid (2,3,3-D3, 98%)	Cambridge Isotope Laboratories, Inc.	Cat#DLM-832-PK
D-Glutamic acid	Merck	Cat#100291
DL-Glutamic acid (2,4,4-D3, 98%)	Cambridge Isotope Laboratories, Inc.	Cat#DLM-335-PK
Pyruvic acid sodium salt	Fluka (chemika)	Cat#15990
Lactic acid sodium salt	Sigma-Aldrich	Cat#71716
Citric acid dihydrate	Merck	Cat#106448
Alpha-ketoglutaric acid sodium salt	Sigma-Aldrich	Cat#K2010
Succinic acid	Sigma-Aldrich	Cat#398055
Fumaric acid	Fluka (Chemika)	Cat#47900
DL-Malic acid	Sigma-Aldrich	Cat#M0875
Sodium Pyruvate (D3,97-98%)	Cambridge Isotope Laboratories, Inc.	Cat#DLM-6068-PK
Sodium L-Lactate (3,3,3-D3, 98%)	Cambridge Isotope Laboratories, Inc.	Cat#DLM-9071-PK
Citric acid (2,2,4,4-D4,98%)	Cambridge Isotope Laboratories, Inc.	Cat#DLM-3487-PK
Alpha-ketoglutaric acid (3,3,4,4,-D4, 90%)	Cambridge Isotope Laboratories, Inc.	Cat#DLM-6201-PK
Succinic acid (2,2,3,3-D4, 98%)	Cambridge Isotope Laboratories, Inc.	Cat#DLM-584-PK
Fumaric acid (D4, 98%)	Cambridge Isotope Laboratories, Inc.	Cat#DLM-7654-PK
DL-Malic acid (2,3,3-D3, 98%)	Cambridge Isotope Laboratories, Inc.	Cat#DLM-9045-PK
Protease inhibitor cocktail	Sigma-Aldrich	Cat#11697498001
NuPAGE™ LDS Sample Buffer (4x)	Invitrogen	Cat#NP0007
1,4-dithiothreitol (DTT)	Sigma-Aldrich	Cat#10197777001
NuPAGE™ 4 to 12%, Bis-Tris, 1.0-1.5 mm, Mini Protein Gels	Invitrogen	Cat#NP0323BOX
Novex™ Sharp Pre-stained Protein Standard	ThermoFisher Scientific	Cat#LC5800
NuPAGE™ MOPS SDS Running Buffer (20x)	Invitrogen	Cat#NP0001
NuPAGE™ Transfer buffer (20x)	Invitrogen	Cat#NP0006
Immobilon®-P PVDF membrane	Merck	Cat#IPVH00010

REAGENT or RESOURCE	SOURCE	IDENTIFIER
SuperSignal™ West Pico PLUS Chemiluminescent Substrate	ThermoFisher	Cat#34580
T4 DNA ligase	New England BioLabs	Cat#M0202L
BbsI	New England BioLabs	Cat#R0539S
X-tremeGENE™ 9 DNA Transfection Reagent	Merck	Cat#6365809001
Gibco™ Opti-Mem™ 1 Reduced Serum Medium	Fisher Scientific	Cat#12087549
<i>Pfu</i> DNA Polymerase	Promega	Cat#M7745
dNTP Mix (10 mM each)	ThermoFisher Scientific	Cat#R0193
Critical commercial assays		
Pierce™ BCA Protein Assay Kit	ThermoFisher Scientific	Cat#23225
QIAprep Spin Miniprep Kit	Qiagen	Cat#27106
Jetstar Plasmid Maxiprep Kit	ITK Diagnostics	Cat#LN2400008
QIAamp DNA Micro Kit	Qiagen	Cat#56304
QIAquick Gel Extraction Kit	Qiagen	Cat#28706
CloneJET PCR Cloning Kit	Fisher Scientific	Cat#10809720
Experimental models: Cell lines		
Human: HEK293T cells	ATCC	CRL-3216
Oligonucleotides		
#1 GOT1 Forward: CCATTCTCCAGCATATCGCA	IDT	N/A
#2 GOT1 Reverse: TTGGCAGATACTCGTGATTT	IDT	N/A
#3 GOT1 Forward: CACGAGTATCTGCCAATCCT	IDT	N/A
#1 MDH1 Reverse: ATTTATCTAAGGCTGCACCC	IDT	N/A
#2 MDH1 Reverse: CTCTTGCGGTATTATCTA	IDT	N/A
#3 MDH1 Reverse: GGTACCTTAACTGACTTCT	IDT	N/A
#1 SLC25A11 Forward: GTGCTGTTTGAGCGCCTGAC	IDT	N/A
#2 SLC25A11 Forward: CTTATCCGCATGACTGCCGA	IDT	N/A
#1 MDH2 Reverse: GGTGTTGAACAGTCTGCC	IDT	N/A
#2 MDH2 Forward: ATCATTCCAGGCATGACCC	IDT	N/A
#3 MDH2 Reverse: GGTGGCCACAATCGTGGCAT	IDT	N/A
#1 GOT2 Forward: ATCGCGCCGCTTCCACCC	IDT	N/A
#2 GOT2 Forward: TGCCCTGCGCCACAATCCA	IDT	N/A
#1 SLC25A13 Reverse: GCCTAATCCAAAGACTGTGG	IDT	N/A
#2 SLC25A13 Reverse: AATCCAAAGACTGTGGAAT	IDT	N/A
#1 SLC25A12 Forward: AGGAGTAGCTGATCAAACCA	IDT	N/A
#2 SLC25A12 Forward: GTAGCTGATCAAACCAAGGA	IDT	N/A
Recombinant DNA		
pSpCas9(BB)-2A-GFP (PX458)	Addgene	Cat#48138
Software and algorithms		
R-programming	In-house pipeline for peak-calling	https://github.com/UMCUGenetics/DIMS
MassLynx (version 4.2)	Waters	N/A

REAGENT or RESOURCE	SOURCE	IDENTIFIER
Exactive Tune Software (version 2.9.0)	Thermo Fisher Scientific	BRE0012262
Chipsoft (version 8.3.1)	Advion Biosciences	N/A
Xcalibur (version 4.1)	Thermo Fisher Scientific	BRE0011868
TraceFinder (version 4.1)	Thermo Fisher Scientific	XCALI-64767
GraphPad Prism	GraphPad Software	N/A
Adobe Illustrator CC 2015	Adobe	N/A
Other		
Sanger Sequencing	Macrogen	N/A
Xevo-TQ MS triple quadrupole MS	Waters	N/A
Acquity UPLC BEH Amide column	Waters	N/A
Van Guard UPLC BEH Amide pre-column	Waters	N/A
TriVersa NanoMate	Advion	TV-NMT
ESI A chip	Advion	HD_A_384
Q-Exactive Plus Orbitrap	Thermo Fisher Scientific	0726030
Q-Exactive HF Orbitrap	Thermo Fisher Scientific	0726041
UltiMate 3000 Dual Gradient UHPLC	Thermo Fisher Scientific	5040.0066
Sunshell RP-Aqua column 3.0x150mm, 2.6µm	ChromaNik Technologies	CR6371

RESOURCE AVAILABILITY

Lead contact

Further information and requests for resources and reagents should be directed to and will be fulfilled by the Lead Contact, Judith J.M. Jans (j.j.m.jans@umcutrecht.nl)

Materials availability

This study did not generate any unique reagents.

Data and Code availability

The underlying datasets of $^{13}\text{C}_3$ -serine and $^{13}\text{C}_2$ -glycine concentrations and DI-HRMS data have been uploaded to Mendeley Data and are available at: <https://doi.org/10.17632/sd575642jm.1>

EXPERIMENTAL MODEL AND SUBJECT DETAILS

Cell lines

HEK293T cells were maintained in DMEM, high glucose, GlutaMAX™, pyruvate with 10% (v/v) heat-inactivated FBS and 1% P/S (v/v) in a humidified, 5% CO₂ atmosphere at 37 °C. Cells were passaged upon reaching confluence. For isotope tracer experiments, cells were incubated with DMEM, no glucose (and no pyruvate) with 1 % P/S (v/v) and 25 mM D-Glucose (U-13C6, 99%). Dulbecco's Modified Eagle Medium (DMEM), high glucose, GlutaMAX™, pyruvate; DMEM, no glucose; fetal bovine serum (FBS); penicillin-streptomycin (P/S (10,000 U/ml) and trypsin-ethylenediaminetetraacetic acid (Trypsin-EDTA (0.5%), no phenol red) were purchased from Gibco™ (ThermoFisher Scientific). D-Glucose (U-13C6, 99%) was purchased from Cambridge Isotope Laboratories, Inc.

METHOD DETAILS

Generation of HEK293 KO cell lines using CRISPR/Cas9

To investigate the cellular pathophysiological mechanisms of MAS defects, we used CRISPR/Cas9 to create human embryonic kidney (HEK293) cell lines with a genetic disruption in each MAS-gene (*GOT1*, *MDH1*, *SLC25A11*, *MDH2*, *GOT2* and *SLC25A12+SLC25A13*). HEK293T cells were transiently transfected with pSpCas9(BB)-2A-GFP (PX458), encoding sgRNA targeting MAS genes. GFP-positive cells were

sorted using a FACSaria II flow cytometer (BD) and plated in 10-cm dishes. After 1 week, colonies were picked from these plates and knockout candidates were selected via western blot. GOT1, MDH1, OGC, MDH2, GOT2 and AGC were absent at the protein level (Figure S1A). Cell lines treated with Crispr/Cas9 but without successful knockout were considered corresponding wild-type cell lines and used as a control in the experiments. A total of 33 different cell lines were used.

Isotope tracing and metabolite extraction in HEK293 cells

WT and KO HEK293 cells were seeded at a density of 300,000 cells per well in six-well dishes in parallel and grown to ~80-90% confluency. The medium was refreshed 24 hours before the start of the experiment. Cells were incubated in [U- ^{13}C]-glucose-containing medium for 2,4 and 8 hours (Figure S1B), then washed with 2 ml cold PBS (4 °C). Cells were harvested by scraping them twice in 0.25 ml pre-chilled 100% methanol (-80 °C), whereafter the cell lysate was collected. After centrifuging the 0.5 ml cell lysate/methanol-mixture (16,200 g, 10 min, 4 °C), the supernatant was transferred to a new 1.5 ml Eppendorf tube. The supernatant was stored at -80 °C until further analysis.

Liquid chromatography-mass spectrometry analysis of serine and glycine

The concentrations of serine, glycine, $^{13}\text{C}_3$ -serine and $^{13}\text{C}_2$ -glycine in the cell lysate/methanol samples from isotope tracing experiments were determined using LC-MS/MS. The internal standard (IS) solution consisted of ^{15}N , $^{13}\text{C}_3$ -serine and ^{15}N , $^{13}\text{C}_2$ -glycine (Cambridge Isotope Laboratories, Inc.) in 5% (w/v) sulfosalicylic acid. Calibration curves were prepared within the following ranges: serine (0-100 μM), glycine (0-500 μM), $^{13}\text{C}_3$ -serine (0-10 μM), $^{13}\text{C}_2$ -glycine (0-50 μM). In addition, two quality controls with either high or low concentrations serine and glycine were prepared from a mixture of cell lysates. Solvent A consisted of 10 mM ammonium formate in 85% acetonitrile and 0.15% formic acid, and solvent B of 10 mM ammonium formate in ultrapure H_2O containing 0.15% formic acid, pH 3.0. To a 10 μl methanol sample, 10 μl IS and 140 μl solvent A were added. Samples were vortexed, centrifuged for 5 min at 13,000 rpm in an Eppendorf centrifuge and subsequently all of the supernatant was transferred to a 96-wells plate (Waters). Samples were analyzed using a Xevo-TQ MS triple quadrupole mass spectrometer with an ESI source and an Acquity UPLC system. Chromatographic separation was achieved by injecting 5 μl of sample on an Acquity UPLC BEH Amide column (2.1 x 100 mm, 1.7 μm ; Waters) with a Van Guard™ UPLC BEH Amide pre-column (2.1 x 5 mm, 1.7 μm). The flow rate was set to 0.4 mL/min and the column temperature was maintained at 35 °C. Initial conditions were 100% solvent A. After 1 min the mobile phase gradient (%B) was set in the

following protocol: 1.0-1.1 min linear gradient from 0 to 5.9% B; 1.1-2.0 min linear gradient from 5.9 to 17.6% B; 2.0-3.0 min linear gradient from 17.6 to 29.4% B; 3.0-3.1 min linear gradient from 29.4 to 0% B; 3.1-4.5 min isocratic 0% B. Parameters for ESI-MS analysis in positive ionmode were as follows: capillary voltage 1.0 kV, source temperature = 150 °C, desolvation temperature = 550 °C, cone gas flow = 50 L/hr, collision gas flow=0.15 ml/min, desolvation gas flow = 1000 L/hr. Collision energy and cone voltage were optimized for each component and dwell time was set automatically. Peak integration and data analysis were performed using Waters MassLynx v4.2 software. The concentration for each analyte was calculated by a linear regression analysis of the peak area/IS area using the calibration curve. Technical triplicates of cell lysates were measured and concentrations were normalized to total protein concentrations obtained by the Pierce BCA protein assay. To account for interrun and experimental day variation, data are expressed relative to experimental controls measured within the same run.

Direct infusion mass spectrometry analysis for isotopologue identification

The cell lysate/methanol-samples collected after an 8-hour incubation with [U-¹³C]-glucose were diluted 10 times in methanol. 70 µl cell working solution (as previously described⁴³) and 60 µl 0.3% formic acid (Emsure, Darmstadt, Germany) were added to 70 µl of diluted cell lysate/methanol sample. The solutions were filtered using a methanol preconditioned 96-well filter plate (Acro prep, 0.2 µm GHP, NTRL, 1 ml well; Pall Corporation, Ann Arbor, MI, USA) and a vacuum manifold, after which the sample filtrate was collected in a 96-well plate (Advion, Ithaca, NY, USA). Direct-infusion high-resolution mass spectrometry (DI-HRMS) metabolomics was performed as previously described.⁴³ Samples were analyzed using a TriVersa NanoMate system (Advion, Ithaca, NY, USA) controlled by Chipsoft software (version 8.3.3, Advion), mounted on a Q-Exactive Plus high-resolution mass spectrometer (Thermo Scientific). 13 µl sample was automatically aspirated and injected through nozzles on an ESI-chip (Advion) using nitrogen gas (0.5 psi, voltage = 1.6 kV), and measured in positive and negative ion mode for 3.0 min. Parameters were: scan range = 70-600 m/z, resolution = 140,000 at 200 m/z, automatic gain control target = 3e6, capillary temperature = 275 °C, S-lens RF level = 70. Data acquisition was performed using Xcalibur software (version 3.0, Thermo Scientific, Waltham, MA, USA). A peak-calling pipeline, developed in R-programming language, annotated the raw mass spectrometry data according to the Human Metabolome DataBase (HMDB, version 3.6) with a range of 2 ppm (<https://github.com/UMCUGenetics/DIMS>). Only endogenously relevant metabolite features (according to HMDB) with the following adduct ions were selected: [M+H]⁺, [M+Na]⁺, [M+K]⁺ (positive mode), [M-H]⁻ and [M+Cl]⁻ (negative

mode). As DI-HRMS is unable to separate isomers, the resulting mass peak intensities consist of the summed intensities of these isomers. In order to extract isotopologues of metabolites from the resulting data, the theoretical m/z value for the annotated metabolite in the negative or ionization mode was used to determine the expected m/z of the ^{13}C labeled metabolite. Potential isobaric compounds are listed in Table S1. All samples were measured in a single run.

Different isotopologues - molecules with different isotopic compositions - are formed as a result of increasing labeling of metabolites with each round of the TCA cycle. The fractional enrichment of each isotopologue is calculated as a percentage of the sum of all possible isotopologues. Isotopologues range from $M+0$ to $M+n$ (1-6), in which $M+0$ reflects the unlabeled ^{12}C carbons and $M+n$ the labeled ^{13}C carbons. For control cell lines, total label incorporation from $[\text{U-}^{13}\text{C}]$ -glucose in glycolysis ranged between ~70-95% after 8 hours (Figure S3B). For the TCA cycle, ~70% of citrate became labeled, whereas the label incorporation of $[\text{U-}^{13}\text{C}]$ -glucose for 2-oxoglutarate, glutamate, fumarate, malate was ~35% (Figure S4B).

Liquid chromatography-mass spectrometry analysis of TCA intermediates

Cells were seeded in six-well plates and grown to confluency in 2 ml DMEM with 10% FBS and 1% P/S. The medium was refreshed 24 hours before harvesting and metabolite extraction was performed as described above. The concentrations of TCA cycle intermediates were determined using LC-MS/MS. The internal standard solution consisted of $^2\text{H}_3$ -pyruvate, $^2\text{H}_3$ -lactate, $^2\text{H}_4$ -citrate, $^2\text{H}_4$ -2-oxoglutarate, $^2\text{H}_4$ -succinate, $^2\text{H}_4$ -fumarate, $^2\text{H}_3$ -malate (Sigma-Aldrich, Denmark). Calibration standards were prepared with internal standards in the concentration range of 0.15 – 100 μM . 20 μl internal standard solution was added to 0.5 ml methanol cell extract, evaporated with nitrogen and reconstituted in a mixture of 25 μl 0.1% NaOH and 25 μl 10mg/ml O-(2,3,4,5,6-pentafluorobenzyl)hydroxylamine dissolved in ultrapure H_2O . Samples were derivatized in a thermomixer at 1000 rpm for 30 min. Samples were analyzed using a Q-Exactive HF High resolution mass spectrometer. Chromatographic separation was achieved by injecting 5 μl sample onto a Sunshell RP-Aqua column (3 x 150 mm, 2.6 μm ; ChromaNik Technologies Inc., Osaka, Japan). The flow rate remained constant at 0.6 ml/min, the column temperature was maintained at 40 $^\circ\text{C}$ and the autosampler at 10 $^\circ\text{C}$. Solvent A consisted of 0.1% formic acid (v/v) dissolved in ultrapure H_2O and solvent B of 0.1% formic acid (v/v) dissolved in acetonitrile. The mobile phase gradient (%B) was as follows: 0-2.75 min isocratic 0% B; 2.75-3.5 min linear gradient from 0% to 70% B; 3.5-6.5 min isocratic 70% B; 6.5-6.7 min linear gradient from 70% to 0% B; 6.7-10 min isocratic 0% B for column equilibration. Samples were detected in full

scan negative ionisation mode with a scan range of 70-400 m/z and a resolution of 240000. Parameters for negative ESI were as follows: capillary voltage = 4 kV, capillary temperature = 300 °C, automatic gain control target = 1e6, sheath gas = 50, aux gas = 20, spare gas = 0, S-lens RF level = 65. TraceFinder software (Thermo Scientific) was used for peak integration. The concentration of each analyte was calculated using the calibration curve. Technical triplicates of cell lysates were measured and concentrations were normalized to total protein concentrations obtained by the Pierce BCA protein assay. To account for interrun and experimental day variation, data are expressed relative to experimental controls measured within the same run.

Liquid chromatography-mass spectrometry analysis of aspartate and glutamate

Cells were seeded in six-well plates and grown to confluency in 2 ml DMEM with 10% FBS and 1% P/S. The medium was refreshed 24 hours before harvesting and metabolite extraction was performed as described above. To quantify aspartate and glutamate, we adapted the UPLC-MS/MS method that was previously described for the quantification of amino acids in plasma.⁴⁴ The range of calibrators and quality controls were adapted according to the concentration range of amino acids within cell lysates. Technical triplicates of cell lysates were measured and concentrations were normalized to total protein concentrations obtained by the Pierce BCA protein assay. To account for interrun and experimental day variation, data are expressed relative to experimental controls measured within the same run.

Western blot

Cells were collected in Radioimmunoprecipitation assay (RIPA) buffer containing 0.05 M Tris, 0.15 M NaCl, 1% NP-40, 0.5% sodium deoxycholate and 0.1% SDS with a protease inhibitor cocktail (1:200, Sigma Aldrich) and 2 mM phosphatase inhibitor NaF. Samples were agitated for 30 min at 4 °C, followed by centrifugation (14,000 g, 10 min, 4 °C), and collection of the supernatant, which was stored at -80 °C until further analysis. The BCA Protein Assay Kit (Pierce) was used to determine the protein concentration. Samples were prepared for western blot by protein denaturation at 98 °C for 5 min in LDS Sample Buffer (ThermoFisher Scientific) and DTT (Sigma Aldrich). A NuPage 4-12% pre-cast gel (ThermoFisher Scientific) was assembled in an electrophoresis cell (Xcell, sure-lock mini cell, Novex, Invitrogen) with running buffer (ThermoFisher Scientific). After samples were loaded on the gel, proteins were separated by gel electrophoresis for 60 min at 200 V. The separated proteins were transferred from the gel to a PVDF membrane (Sigma Aldrich) in transfer buffer (ThermoFisher Scientific) for 60 min at 30 V. After a 1-hour blocking step in 5% (w/v) milk, the PVDF membrane was incubated overnight at 4 °C with primary antibodies

diluted in 1% (w/v) milk. The membrane was incubated with secondary antibodies in 0.5% (w/v) milk for 1 hour at room temperature. Protein bands were visualized using SuperSignal™ West Pico plus chemiluminescent substrate (ThermoFisher Scientific).

Mitochondrial isolation for western blot

Cells were grown to ~80-90% confluency in 10-cm culture dishes in 10 ml DMEM with 10% FBS and 1% P/S. Prior to cell collection, cells were washed with 5 ml cold PBS (4 °C). Cells were harvested by scraping them in 10 ml cold PBS (4 °C), whereafter the cell lysate/PBS mixture was centrifuged (800 rpm, 5 min, RT). The supernatant was discarded and the cell pellet was resuspended in 1 ml cold isolation medium (250 mM sucrose, 10 mM Tris, 1 mM EGTA and 0.1 mg/ml digitonin, pH 7.6) and incubated on ice for 3 min. The cell suspension was then homogenized with 10 up-and-down strokes of a Teflon pestle mounted on a motor overhead at 750 rpm. Centrifugation (800 g, 5 min, 4 °C) of the homogenate separated the cytosolic fraction with mitochondria (supernatant) from other cell structures and membranes. The supernatant was transferred to a new Eppendorf cup. A second centrifugation step (10,000 g, 10 min, 4 °C) separated the cytosolic fraction (supernatant) from the mitochondria (pellet). The mitochondrial pellet was dissolved in ultrapure H₂O and samples were stored at -80 °C until further analysis. Sample preparation for western blot was the same as for total cell lysates.

QUANTIFICATION AND STATISTICAL ANALYSIS

Peak intensities were extracted from LC-MS data as described above in the corresponding method. GraphPad Prism (V9.3.0) was used for statistical analysis. p-values were determined using unpaired, two-tailed Student's t tests, corrected for multiple comparisons with the Holm-Sidak method. Data are presented as mean ± standard deviation (SD). An adjusted p-value of <0.05 was considered statistically significant.

REFERENCES

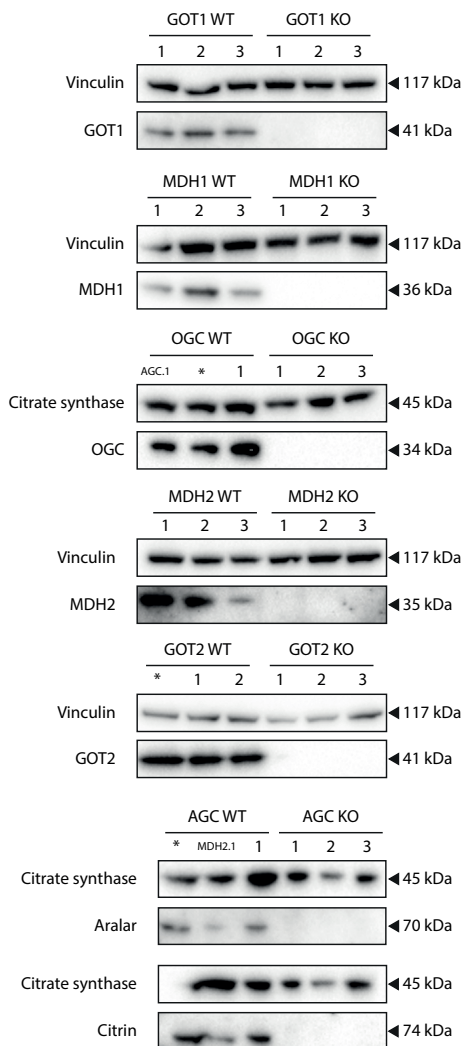
1. Borst P. The aerobic oxidation of reduced diphosphopyridine nucleotide formed by glycolysis in ehrlich ascites-tumour cells. *BBA - Biochim Biophys Acta*. 1962;57(1):270-282.
2. Borst P. Hydrogen transport and transport metabolites. In: *Funktionelle Und Morphologische Organisation Der Zelle*. Springer Berlin Heidelberg; 1963:137-162.
3. Dawson AG. Oxidation of cytosolic NADH formed during aerobic metabolism in mammalian cells. *Trends Biochem Sci*. 1979;4(8):171-176.
4. Borst P. The malate–aspartate shuttle (Borst cycle): How it started and developed into a major metabolic pathway. *IUBMB Life*. 2020;72(11):2241-2259.
5. Kobayashi K, Sinasac DS, Iijima M, et al. The gene mutated in adult-onset type II citrullinaemia encodes a putative mitochondrial carrier protein. *Nat Genet*. 1999;22(2):159-163.
6. Saheki T, Kobayashi K. Mitochondrial aspartate glutamate carrier (citrin) deficiency as the cause of adult-onset type II citrullinemia (CTLN2) and idiopathic neonatal hepatitis (NICCD). *J Hum Genet*. 2002;47(7):333-341.
7. Wibom R, Lasorsa FM, Töhönen V, et al. AGC1 deficiency associated with global cerebral hypomyelination. *N Engl J Med*. 2009;361(5):489-495.
8. Falk MJ, Li D, Gai X, et al. AGC1 Deficiency Causes Infantile Epilepsy, Abnormal Myelination, and Reduced N-Acetylaspartate. *JIMD Rep*. 2014;14:77-85.
9. Kavanaugh BC, Warren EB, Baytas O, et al. Longitudinal MRI findings in patient with SLC25A12 pathogenic variants inform disease progression and classification. *Am J Med Genet Part A*. 2019;179(11):2284-2291.
10. Pfeiffer B, Sen K, Kaur S, Pappas K. Expanding Phenotypic Spectrum of Cerebral Aspartate-Glutamate Carrier Isoform 1 (AGC1) Deficiency. *Neuropediatrics*. 2020;51(2):160-163.
11. Saleh M, Helmi M, Yacop B. A novel nonsense gene variant responsible for early infantile epileptic encephalopathy type 39: Case report. *Pakistan J Biol Sci*. 2020;23(7):973-976.
12. van Karnebeek CDM, Ramos RJ, Wen XY, et al. Bi-allelic GOT2 Mutations Cause a Treatable Malate-Aspartate Shuttle-Related Encephalopathy. *Am J Hum Genet*. 2019;105(3):534-548.
13. Ait-El-Mkadem S, Dayem-Quere M, Gusic M, et al. Mutations in MDH2, Encoding a Krebs Cycle Enzyme, Cause Early-Onset Severe Encephalopathy. *Am J Hum Genet*. 2017;100(1):151-159.
14. Laemmle A, Steck AL, Schaller A, et al. Triheptanoin – Novel therapeutic approach for the ultra-rare disease mitochondrial malate dehydrogenase deficiency. *Mol Genet Metab Reports*. 2021;29:100814.
15. Ticci C, Nesti C, Rubegni A, et al. Bi-allelic variants in MDH2: Expanding the clinical phenotype. *Clin Genet*. 2022;101(2):260-264.
16. Broeks MH, Shamseldin HE, Alhashem A, et al. MDH1 deficiency is a metabolic disorder of the malate–aspartate shuttle associated with early onset severe encephalopathy. *Hum Genet*. 2019;138(11-12):1247-1257.
17. Broeks MH, van Karnebeek CDM, Wanders RJA, Jans JJM, Verhoeven-Duif NM. Inborn disorders of the malate aspartate shuttle. *J Inherit Metab Dis*. 2021;44(4):792-808.
18. Pardo B, Herrada-Soler E, Satrustegui J, Contreras L, Del Arco A. AGC1 Deficiency: Pathology and Molecular and Cellular Mechanisms of the Disease. *Int J Mol Sci*. 2022;23(1):528.
19. Saheki T, Moriyama M, Funahashi A, Kuroda E. Agc2 (Citrin) deficiency—from recognition of the disease till construction of therapeutic procedures. *Biomolecules*. 2020;10(8):1-17.
20. Bücher T, Klingenberg M. Wege des Wasserstoffs in der lebendigen Organisation. *Angew Chemie*. 1958;70(17-18):552-570.
21. Williamson DH, Lund P, Krebs HA. The redox state of free nicotinamide-adenine dinucleotide in the cytoplasm and mitochondria of rat liver. *Biochem J*. 1967;103(2):514-527.

22. Buescher JM, Antoniewicz MR, Boros LG, et al. A roadmap for interpreting ¹³C metabolite labeling patterns from cells. *Curr Opin Biotechnol.* 2015;34:189-201.
23. Luengo A, Li Z, Gui DY, et al. Increased demand for NAD⁺ relative to ATP drives aerobic glycolysis. *Mol Cell.* 2021;81(4):691-707.e6.
24. Thompson Legault J, Strittmatter L, Tardif J, et al. A Metabolic Signature of Mitochondrial Dysfunction Revealed through a Monogenic Form of Leigh Syndrome. *Cell Rep.* 2015;13(5):981-989.
25. Titov D V., Cracan V, Goodman RP, Peng J, Grabarek Z, Mootha VK. Complementation of mitochondrial electron transport chain by manipulation of the NAD⁺/NADH ratio. *Science.* 2016;352(6282):231-235.
26. Gui DY, Sullivan LB, Luengo A, et al. Environment Dictates Dependence on Mitochondrial Complex I for NAD⁺ and Aspartate Production and Determines Cancer Cell Sensitivity to Metformin. *Cell Metab.* 2016;24(5):716-727.
27. Pope S, Artuch R, Heales S, Rahman S. Cerebral folate deficiency: Analytical tests and differential diagnosis. *J Inherit Metab Dis.* 2019;42(4):655-672.
28. Zapata-Perez R, Wanders RJA, Van Karnebeek CDM, Houtkooper RH. NAD⁺ homeostasis in human health and disease. *EMBO Mol Med.* 2021;13(7):e13943.
29. Gaude E, Schmidt C, Gammage PA, et al. NADH Shuttling Couples Cytosolic Reductive Carboxylation of Glutamine with Glycolysis in Cells with Mitochondrial Dysfunction. *Mol Cell.* 2018;69(4):581-593.e7.
30. Hanse EA, Ruan C, Kachman M, Wang D, Lowman XH, Kelekar A. Cytosolic malate dehydrogenase activity helps support glycolysis in actively proliferating cells and cancer. *Oncogene.* 2017;36(27):3915-3924.
31. Liu S, Fu S, Wang G, et al. Glycerol-3-phosphate biosynthesis regenerates cytosolic NAD⁺ to alleviate mitochondrial disease. *Cell Metab.* 2021;33(10):1974-1987.e9.
32. Wang Y, Stancliffe E, Fowle-Grider R, et al. Saturation of the mitochondrial NADH shuttles drives aerobic glycolysis in proliferating cells. *Mol Cell.* 2022;82(17):3270-3283.e9.
33. Yeh JI, Chinte U, Du S. Structure of glycerol-3-phosphate dehydrogenase, an essential monotopic membrane enzyme involved in respiration and metabolism. *Proc Natl Acad Sci U S A.* 2008;105(9):3280-3285.
34. Meijer AJ, Van Woerkom GM, Williamson JR, Tager JM. Rate limiting factors in the oxidation of ethanol by isolated rat liver cells. *Biochem J.* 1975;150(2):205-209.
35. Ilic N, Birsoy K, Aguirre AJ, et al. PIK3CA mutant tumors depend on oxoglutarate dehydrogenase. *Proc Natl Acad Sci U S A.* 2017;114(17):E3434-E3443.
36. Fiermonte G, Dolce V, Palmieri L, et al. Identification of the human mitochondrial oxodicarboxylate carrier. Bacterial expression, reconstitution, functional characterization, tissue distribution, and chromosomal location. *J Biol Chem.* 2001;276(11):8225-8230.
37. Johnson RN, Chappell JB. The transport of inorganic phosphate by the mitochondrial dicarboxylate carrier. *Biochem J.* 1973;134(3):769-774.
38. Lanoue KF, Meijer AJ, Brouwer A. Evidence for electrogenic aspartate transport in rat liver mitochondria. *Arch Biochem Biophys.* 1974;161(2):544-550.
39. Birsoy K, Wang T, Chen WW, Freinkman E, Abu-Remaileh M, Sabatini DM. An Essential Role of the Mitochondrial Electron Transport Chain in Cell Proliferation Is to Enable Aspartate Synthesis. *Cell.* 2015;162(3):540-551.
40. Sullivan LB, Gui DY, Hosios AM, Bush LN, Freinkman E, Vander Heiden MG. Supporting Aspartate Biosynthesis Is an Essential Function of Respiration in Proliferating Cells. *Cell.* 2015;162(3):552-563.
41. Williamson JR, Jakob A, Refino C. Control of the removal of reducing equivalents from the cytosol in perfused rat liver. *J Biol Chem.* 1971;246(24):7632-7641.
42. Yang C, Ko B, Hensley CT, et al. Glutamine oxidation maintains the TCA cycle and cell survival during impaired mitochondrial pyruvate transport. *Mol Cell.* 2014;56(3):414-424.
43. Haijes HA, Willemsen M, van der Ham M, et al. Direct Infusion Based Metabolomics Identifies Metabolic Disease in Patients' Dried Blood Spots and Plasma. *Metabolites.* 2019;9(1):12.

44. Prinsen HCMT, Schiebergen-Bronkhorst BGM, Roeleveld MW, et al. Rapid quantification of underivatized amino acids in plasma by hydrophilic interaction liquid chromatography (HILIC) coupled with tandem mass-spectrometry. *J Inherit Metab Dis.* 2016;39(5):651-660.

SUPPLEMENTARY MATERIAL

A



B

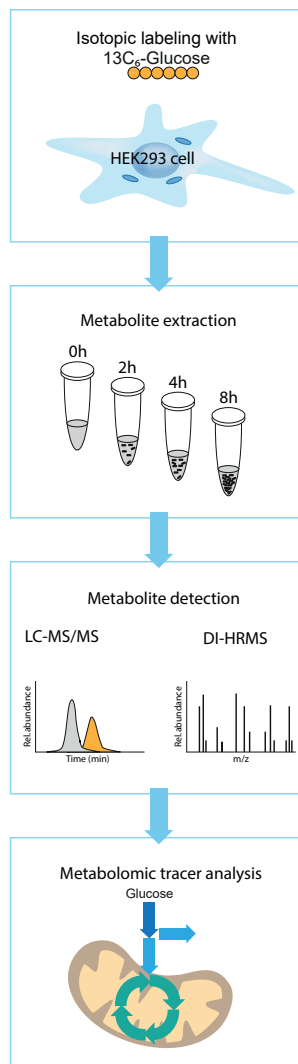


Figure S1. MAS KO cell lines and experimental set-up. Related to methods. **(A)** Western blot of MAS WT and KO cell lines to demonstrate protein absence. The cell line numbers correspond to the number in the key resources table before sgRNA. * indicates the WT HEK293 cell line. **(B)** Schematic of the experimental setup. Each HEK293 cell line was incubated with $[\text{U}-^{13}\text{C}]$ -glucose for 0, 2, 4 and 8 hours. Metabolites were extracted and detected using LC-MS/MS and DI-HRMS (only for $t = 8$ hours), whereafter metabolomic tracer data analysis was performed.

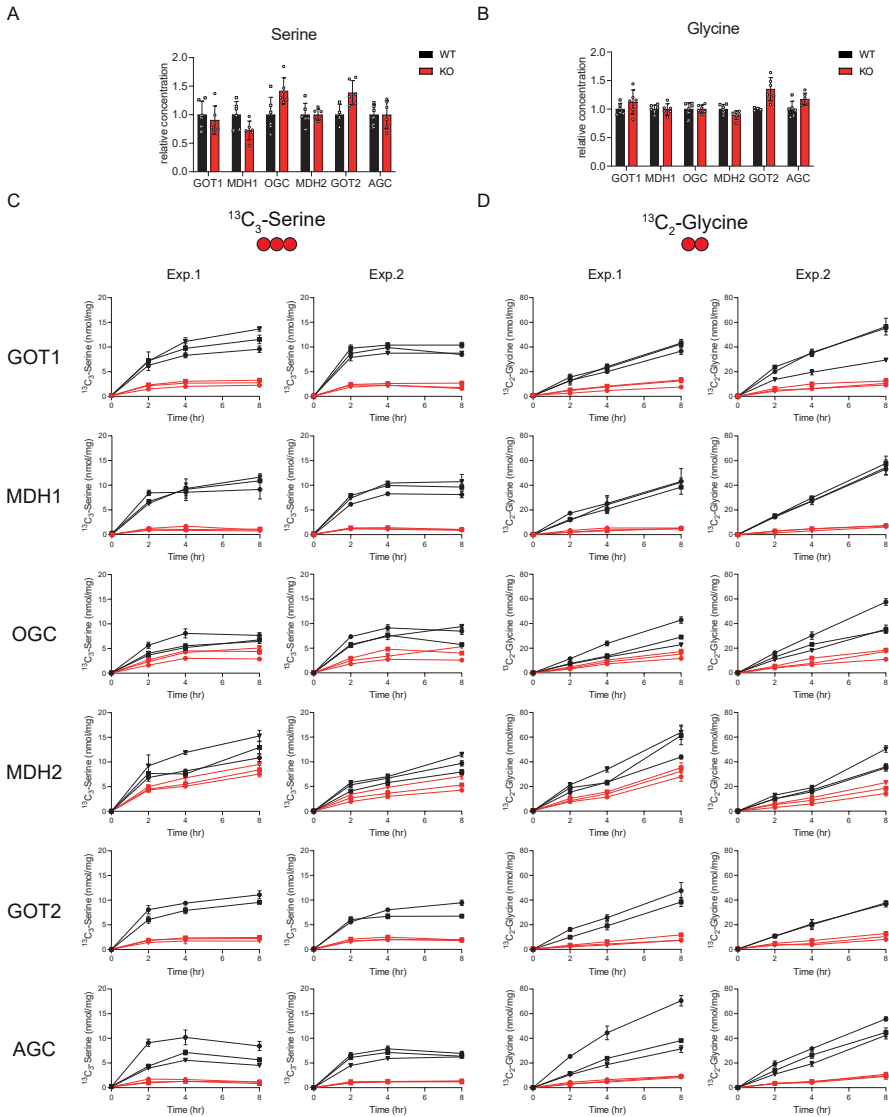


Figure S2. Unlabeled and labeled serine and glycine concentrations in MAS KO cells. Related to Figure 1. Unlabeled (A) serine and (B) glycine concentrations after an 8-hour incubation with [U- ^{13}C]-glucose. Concentrations in KO cells are expressed relative to control. WT ($n = 34$), KO ($n = 6$ for each KO). Data shown are mean \pm SD of three biological replicates from two independent experiments. Parametric unpaired t-tests were followed by Holm-Sidak's multiple comparisons test to compare each KO to its corresponding WT. (C) $^{13}\text{C}_3$ -serine and (D) $^{13}\text{C}_2$ -glycine concentrations in MAS KO HEK293 cells incubated with [U- ^{13}C]-glucose for 2, 4 and 8 hours in two independent experiments. Each connecting line represents a different cell line, which is marked in black (WT) or red (KO). Data shown are mean \pm SD of three technical triplicates.

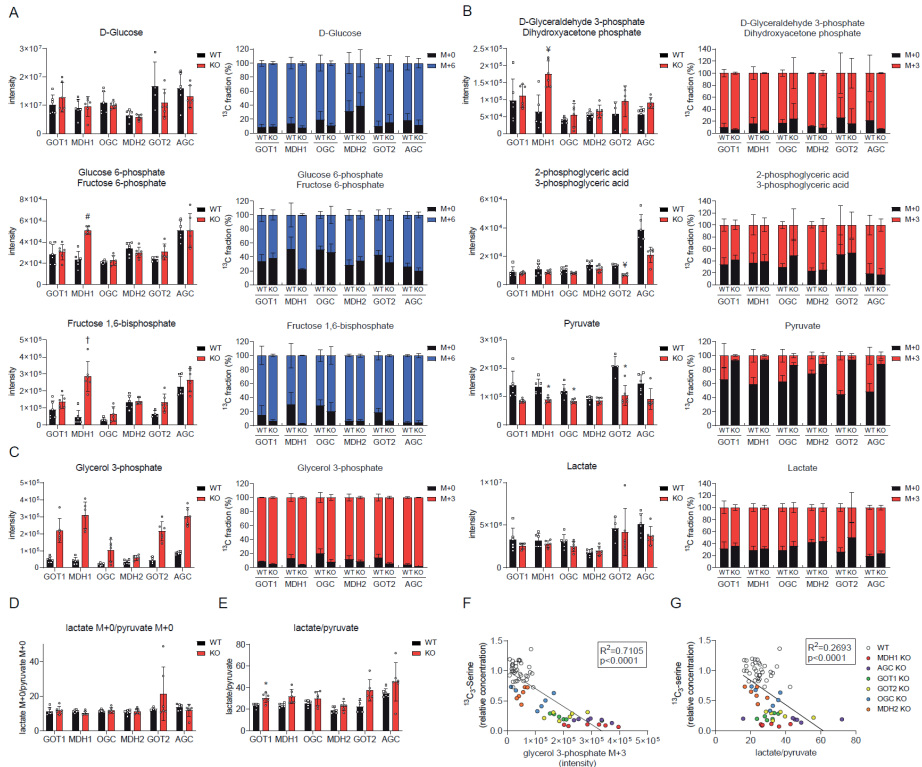


Figure S3. Labeling of glycolytic intermediates in MAS KO cells. Related to figure 2. **(A-C)** Total (unlabeled and labeled) intensity and fractional enrichment of glycolytic intermediates after an 8-hour incubation with [U- ^{13}C]-glucose, resulting in **(A)** six labeled carbons in glycolytic intermediates from the first steps of glycolysis and **(B)** three labeled carbons in glycolytic intermediates in the later steps of glycolysis, as well as in **(C)** glycerol 3-phosphate. Additional isobaric compounds are listed in Table S1. **(D)** Unlabeled lactate M+0/pyruvate M+0 ratio and **(E)** total lactate/pyruvate ratio in MAS WT and KO cells ($n = 4-6$). Data shown are mean \pm SD of three biological replicates from two independent experiments. Parametric unpaired t-tests were followed by Holm-Sidak's multiple comparisons test to compare each KO to its corresponding WT. The adjusted p-values are indicated as * $p < 0.05$, $\dagger p < 0.01$, $\ddagger p < 0.001$, $\# p < 0.0001$. Correlation between the relative $^{13}\text{C}_3$ -serine concentration and **(F)** glycerol 3-phosphate M+3 intensity and **(G)** the total lactate/pyruvate ratio in MAS WT and KO cells displayed with Pearson correlation coefficients.

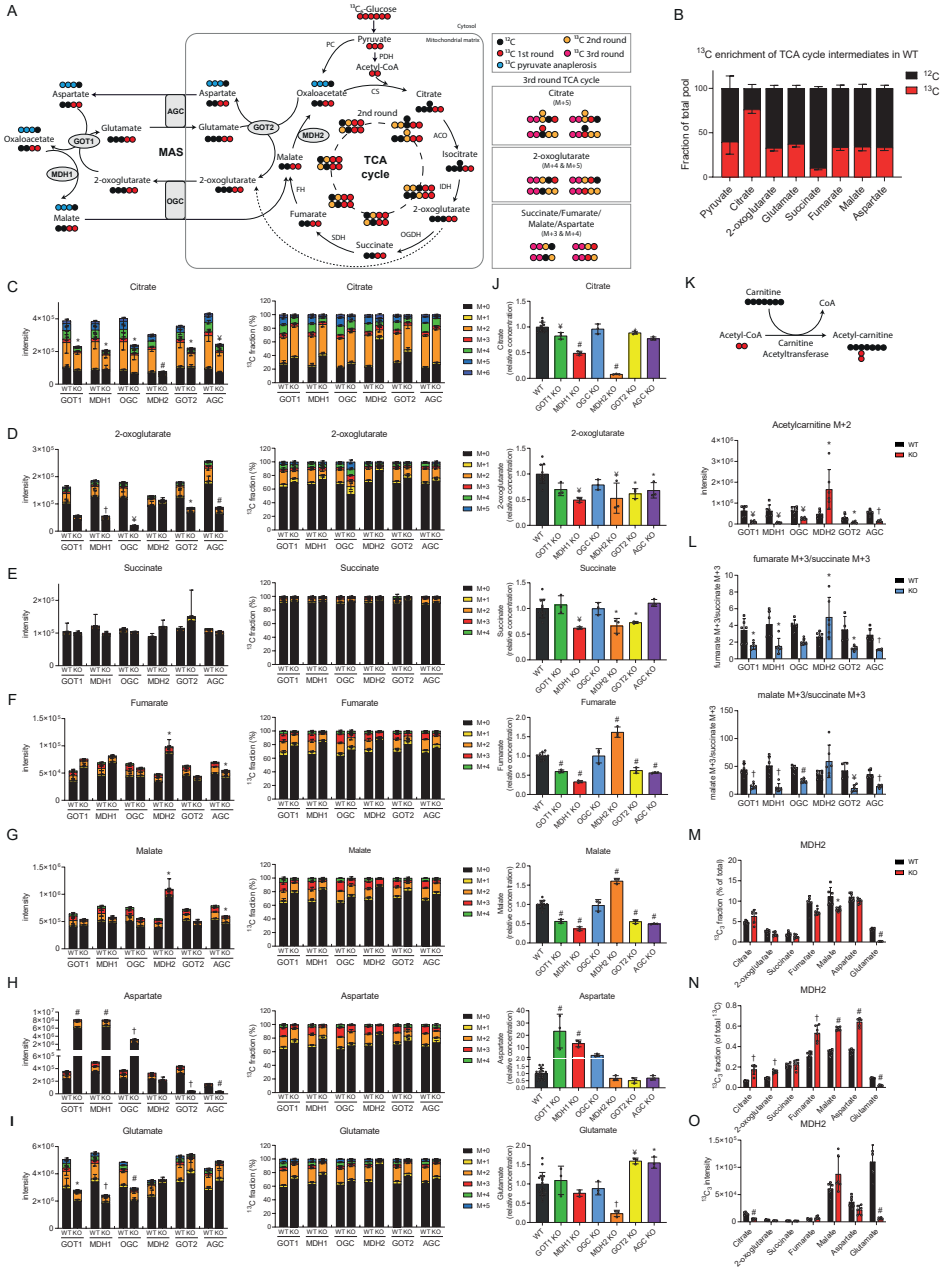


Figure S4. Labeling of TCA cycle intermediates in MAS KO cells. Related to figure 3. **(A)** A schematic of $[\text{U}-^{13}\text{C}]$ -glucose labeling in the first, second and third round of the TCA cycle and MAS, as well as pyruvate anaplerosis. **(B)** ^{13}C enrichment of the TCA cycle and MAS intermediates in WT cells ($n = 17$) after an 8- hour incubation with $[\text{U}-^{13}\text{C}]$ -glucose. **(C-I)** Total intensity and fractional enrichment of TCA cycle and MAS intermediates after an 8-hour incubation with $[\text{U}-^{13}\text{C}]$ -glucose. Additional isobaric compounds are listed in Table S1. **(J)** TCA cycle intermediates and TCA cycle-derived amino acids after

a 24-hour cell culture in presence of serum. Data shown are mean \pm SD and expressed as the relative concentration to corresponding controls (WT; $n = 11$, KO; $n = 3$). A one-way ANOVA was followed by Dunnett's multiple comparisons test. The adjusted p-values are denoted as * $p < 0.05$, ¥ $p < 0.01$, † $p < 0.001$, # $p < 0.0001$. **(K)** Reaction scheme of acetyl-CoA M+2 to acetylcarnitine M+2 conversion and the intensity of acetylcarnitine M+2 after an 8-hour incubation with [U- ^{13}C]-glucose. **(L)** Malate M+3/succinate M+3 and fumarate M+3/succinate M+3 ratios as a readout for pyruvate carboxylation.²² **(M)** $^{13}\text{C}_3$ -fraction of the total intensity, **(N)** the total intensity of the ^{13}C -pool and **(O)** the total intensity of the $^{13}\text{C}_3$ -pool of TCA cycle and MAS intermediates in MDH2 KO cells. Data shown are mean \pm SD of three biological replicates from two independent experiments, except for figure J. Parametric unpaired t-tests were followed by Holm-Sidak's multiple comparisons test to compare each KO to its corresponding WT. The adjusted p-values are denoted as * $p < 0.05$, ¥ $p < 0.01$, † $p < 0.001$, # $p < 0.0001$.

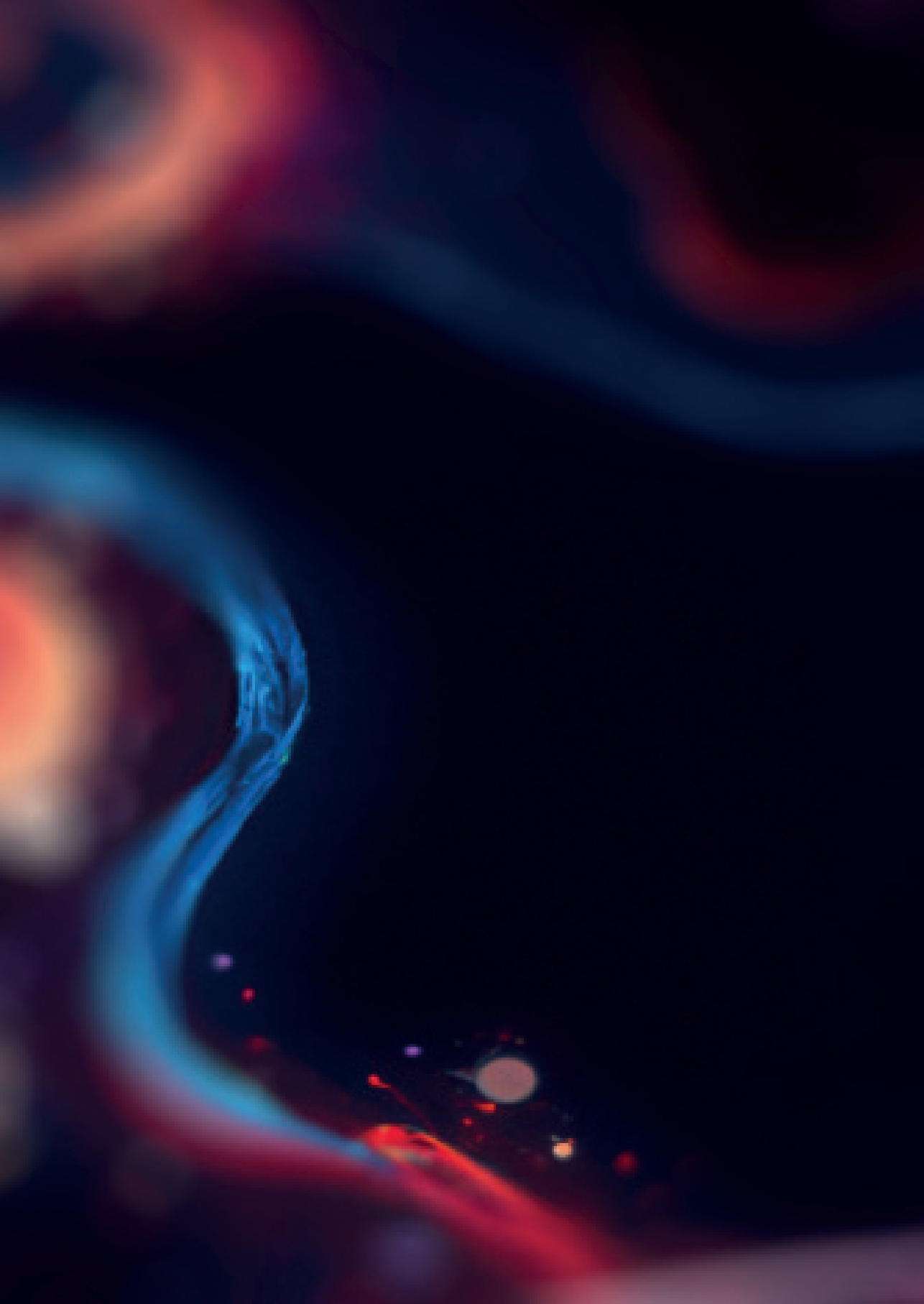
Table S1. Assigned HMDB names to the *m/z* values identified by DI-HRMS in negative and positive ionization modes for isotopologues. Related to Figure 2,3 and Methods.

Assigned HMDB name	[Isotopologue]	<i>m/z</i>
Negative ionization mode		
Glucose		
D-Glucose;D-Galactose;D-Mannose;Myoinositol;3-Deoxyarabinohexonic acid;Beta-D-Glucose;D-Fructose;Allose;L-Sorbose;Alpha-D-Glucose;D-Tagatose;Beta-D-Galactose;Scyllitol;L-Gulose;L-Galactose	[M] ⁻	179.056112
NA	[M+6] ⁻	185.075506
Glucose 6-phosphate/ Fructose 6-phosphate		
Fructose 6-phosphate;Glucose 6-phosphate;Myo-inositol 1-phosphate;Galactose 1-phosphate;Dolichyl phosphate D-mannose; Fructose 1-phosphate;Mannose 6-phosphate;D-Myo-inositol 4-phosphate;Glucose 1-phosphate;Inositol phosphate; Beta-D-Glucose 6-phosphate;Beta-D-Fructose 6-phosphate;D-Tagatose 1-phosphate;D-Mannose 1-phosphate;Sorbitol 1-phosphate;Beta-D-Fructose 2-phosphate;1D-myoinositol 3-phosphate;D-Tagatose 6-phosphate;D-fructose 1-phosphate	[M] ⁻	259.022442
NA	[M+6] ⁻	265.042125
Fructose 1,6-bisphosphate		
"Fructose 1,6-bisphosphate";"1D-Myo-inositol 1,4-bisphosphate";"D-Fructose 2,6-bisphosphate";"Alpha-D-Glucose 1,6-bisphosphate";"1D-Myo-inositol 1,3-bisphosphate";"1D-Myo-inositol 3,4-bisphosphate";"D-Tagatose 1,6-bisphosphate";"D-Mannose 1,6-bisphosphate";"beta-D-Fructose 1,6-bisphosphate"	[M] ⁻	338.988773
NA	[M+6] ⁻	345.009013
Glyceraldehyde 3-phosphate/ Dihydroxyacetone phosphate		
D-Glyceraldehyde 3-phosphate;Dihydroxyacetone phosphate	[M] ⁻	168.990748
NA	[M+3] ⁻	172.001667
2-phosphoglycerate/ 3-phosphoglycerate		
2-Phosphoglyceric acid;3-Phosphoglyceric acid;2-Phospho-D-glyceric acid;(2R)-2-Hydroxy-3-(phosphonatooxy)propanoate	[M] ⁻	184.985663
NA	[M+3] ⁻	187.995349
Pyruvate		
Pyruvic acid; Malonic semialdehyde	[M] ⁻	87.008768
NA	[M+3] ⁻	90.019029
Lactate		
L-Lactic acid; Hydroxypropionic acid; Glyceraldehyde; D-Lactic acid; Dihydroxyacetone; Methoxyacetic acid	[M] ⁻	89.024418
NA	[M+3] ⁻	92.034222

Assigned HMDB name	[Isotopologue]	m/z
Glycerol 3-phosphate		
Glycerol 3-phosphate;Beta-Glycerophosphoric acid	[M] ⁻	171.006398
NA	[M+3] ⁻	174.016079
Citrate		
Citric acid; Isocitric acid; D-threo-Isocitric acid; Diketogulonic acid;"2,3-Diketo-L-gulonate";"(1R,2R)-Isocitric acid";"D-Glucaro-1,4-lactone"	[M] ⁻	191.019726
NA	[M+1] ⁻	192.022957
Succinylacetone [M+Cl] ⁻	[M+2] ⁻	193.027153
NA	[M+3] ⁻	194.029835
NA	[M+4] ⁻	195.034137
NA	[M+5] ⁻	196.036287
NA	[M+6] ⁻	197.040795
2-oxoglutarate		
Oxoglutaric acid; 3-Oxoglutaric acid	[M] ⁻	145.014247
NA	[M+1] ⁻	146.017558
NA	[M+2] ⁻	147.020325
NA	[M+3] ⁻	148.024076
NA	[M+4] ⁻	149.027789
NA	[M+5] ⁻	150.031067
Succinate		
Succinic acid; Methylmalonic acid;"Erythrono-1,4-lactone";Threonolactone	[M] ⁻	117.019332
NA	[M+1] ⁻	118.022797
NA	[M+2] ⁻	119.025778
NA	[M+3] ⁻	120.029097
NA	[M+4] ⁻	121.032874
Fumarate		
Fumaric acid; Maleic acid	[M] ⁻	115.003682
NA	[M+1] ⁻	116.007591
NA	[M+2] ⁻	117.009858
NA	[M+3] ⁻	118.013918
NA	[M+4] ⁻	119.017375
Malate		
L-Malic acid; Malic acid; D-Malic acid	[M] ⁻	133.014247
NA	[M+1] ⁻	134.017430
Senecioic acid [M+Cl] ⁻ ;2-Ethylacrylic acid [M+Cl] ⁻ ;3-Methylbutyrolactone [M+Cl] ⁻	[M+2] ⁻	135.021100

Assigned HMDB name	[Isotopologue]	m/z
NA	[M+3] ⁻	136.024221
NA	[M+4] ⁻	137.027804
Aspartate		
L-Aspartic acid; D-Aspartic acid; Iminodiacetic acid	[M] ⁻	132.030231
NA	[M+1] ⁻	133.033826
NA	[M+2] ⁻	134.037328
NA	[M+3] ⁻	135.039815
NA	[M+4] ⁻	136.043587
Glutamate		
L-Glutamic acid; N-Methyl-D-aspartic acid; N-Acetylserine; D-Glutamic acid; L-4-Hydroxyglutamate semialdehyde; DL-Glutamate	[M] ⁻	146.045881
NA	[M+1] ⁻	147.048524
NA	[M+2] ⁻	148.052978
NA	[M+3] ⁻	149.055207
NA	[M+4] ⁻	150.058626
2H3-Methionine (IS)	[M+5] ⁻	151.062603
Positive ionization mode		
L-Acetylcarnitine	[M] ⁺	204.1230345
NA	[M+2] ⁺	206.1287845

[M]⁻ = [M-H]⁻, [M]⁺ = [M+H]⁺, NA=not assigned, HMDB=human metabolome database.



Chapter 5

Pyruvate reverses the metabolic consequences of malate dehydrogenase 1 deficiency

Melissa H. Broeks¹, Johan Gerrits¹, Hannah M. German¹, Fried J.T. Zwartkruis², Nanda M. Verhoeven-Duif¹ & Judith J.M. Jans¹

¹ Department of Genetics, Section Metabolic Diagnostics, University Medical Center Utrecht, Lundlaan 6, 3584 EA Utrecht, The Netherlands

² Division of Laboratories, Pharmacy and Biomedical Genetics, Center for Molecular Medicine, University Medical Center Utrecht, Universiteitsweg 100, 3584 CG, Utrecht, The Netherlands

ABSTRACT

Malate dehydrogenase 1 (MDH1) is a cytosolic enzyme that catalyzes the reversible reduction of oxaloacetate to malate as part of the malate-aspartate shuttle (MAS). The MAS transports reducing equivalents across the inner mitochondrial membrane to support respiratory chain activity. MDH1 deficiency is a metabolic disorder recently discovered in two patients with global developmental delay, infantile epileptic encephalopathy, and microcephaly. To gain insight into the pathophysiological mechanisms of MDH1 deficiency, we studied the metabolic consequences of MDH1 deficiency in HEK293T cells. We demonstrated that MDH1-deficient cells have impaired glycolysis, which affects glycerol synthesis, serine synthesis, the polyol pathway, and the pentose phosphate pathway. Pyruvate supplementation restores the disturbed pathways while also fueling the TCA cycle. Pyruvate supplementation may be considered as a treatment strategy in MDH1 deficiency.

INTRODUCTION

Malate dehydrogenase 1 (MDH1) is a cytosolic enzyme that catalyzes the reversible reduction of oxaloacetate to malate as part of the malate-aspartate shuttle (MAS). The MAS is an NADH redox shuttle that transports electrons from the cytosol to the mitochondrial matrix, maintaining the cytosolic NAD⁺/NADH balance.^{1,2} MDH1 plays a key role in the MAS, since it transfers the reducing equivalents of cytosolic NADH to oxaloacetate, which results in the formation of malate and NAD⁺. The malate-oxoglutarate carrier then transports malate into the mitochondrial matrix, where MDH2 oxidizes malate to oxaloacetate as part of the tricarboxylic acid (TCA) cycle to regenerate NADH. Finally, the electron transport chain consumes the reducing equivalents from NADH to produce ATP. The recycled cytosolic NAD⁺ is used for the continuation of oxidative pathways in the cytosol, such as glycolysis.³ MDH1 is thus important for electron transfer across the mitochondrial membrane as well as the maintenance of the cytosolic NAD⁺/NADH balance. Due to its central role in energy metabolism, MDH1 is strongly expressed in tissues with high aerobic metabolic demands, such as the heart, skeletal muscle, and brain.

We previously reported an inherited MDH1 defect in two consanguineous patients.⁴ The patients with MDH1 deficiency presented with global developmental delay, infantile epileptic encephalopathy, and microcephaly. Biochemically, we identified high levels of glycerol 3-phosphate in dried blood spots (DBS).⁴ We also demonstrated that MDH1 and other MAS defects result in low NAD⁺/NADH ratios and disturbed glycolysis, which leads to increased glycerol 3-phosphate formation and decreased serine biosynthesis (Broeks *et al.*, accepted). In this study, we aimed to gain more in-depth insight into the metabolic consequences of MDH1 deficiency. We performed untargeted metabolomics and isotope tracer analyses in MDH1 KO HEK293 cells using [U-¹³C]-glucose in the absence and presence of the electron acceptors pyruvate and 2-ketobutyrate. We found that disturbed glycolysis due to MDH1 deficiency increases influx into the pentose phosphate pathway. In addition, we demonstrated accumulation of sorbitol due to an NAD⁺-dependent block in the polyol pathway. Pyruvate supplementation was effective in restoring disturbed cytosolic redox pathways while also fueling the TCA cycle. Low-dose pyruvate supplementation may be considered as a treatment strategy for MDH1 deficiency.

RESULTS

MDH1 deficiency affects multiple glycolysis branching pathways

In order to identify pathophysiological leads in an MDH1 defect, we used direct-infusion high-resolution mass spectrometry (DI-HRMS) to analyze the metabolomes of both MDH1-deficient patients (dried blood spots, DBS) and MDH1 KO cells. The DBS metabolome of MDH1-deficient patients displayed increased responses of masses corresponding to glycerol 3-phosphate, threonic acid and a pentitol (ribitol/arabitol) compared to controls (Figures 1A and S1A). Similarly, MDH1-deficient cells had higher levels of glycerol 3-phosphate, threonic acid and a pentitol (ribitol/arabitol) when compared to controls (Figures 1A and S1B). In addition, both MDH1-deficient patients and cells displayed an elevated lactate/pyruvate ratio, indicative of a disturbed NAD^+/NADH ratio (Figure 1A). MDH1-deficient cells also had higher levels of aspartate, homocysteine, and a hexitol (galactitol/sorbitol) (Figure S1B). Pyruvate, TCA cycle intermediates (citrate, oxoglutarate, malate and fumarate), serine synthesis intermediates (phosphohydroxypyruvate, phosphoserine and serine) and several amino acids (glutamate, threonine and alanine) were decreased in MDH1-deficient cells compared to controls (Figure S1B).

To determine whether these differences result from a disturbed NAD^+/NADH ratio, we supplemented cells with the electron acceptors pyruvate or 2-ketobutyrate, which can regenerate cytosolic NAD^+ from NADH (Figure 1B).^{5,6} Indeed, the total NAD^+/NADH ratio increased in MDH1-deficient cells upon the addition of an electron acceptor (Figure S2A). Although pyruvate supplementation did not significantly increase the intracellular lactate levels, 2-hydroxybutyrate increased upon supplementation with 2-ketobutyrate (Figures 1B and S2B). Several differences between control and KO cells diminished upon the addition of pyruvate or 2-ketobutyrate. Glycerol 3-phosphate, a pentitol (ribitol/arabitol), a hexitol (galactitol/sorbitol), aspartate, threonic acid, homocysteine and orotidine decreased in MDH1-deficient cells upon addition of an electron acceptor (Figures 1C, 1D and S2C). In contrast, intermediates of serine synthesis, the TCA cycle, and several amino acids (threonine and alanine) increased when an electron acceptor was added to MDH1-deficient cells (Figures 1C and 1D). These findings indicate that MDH1 deficiency affects multiple metabolic pathways in central carbon metabolism, such as glycolysis, glycerol synthesis, the polyol pathway and the pentose phosphate pathway. All perturbations are partially or fully normalized when an external electron acceptor is made available.

Pyruvate restores disturbed glycolysis, glycerol synthesis and serine synthesis in MDH1- deficient cells

Since the addition of an electron acceptor mainly affects the branching pathways of glycolysis, we performed stable isotope tracing with [U- ^{13}C]-glucose to gain more insight into the underlying mechanisms. Cells were incubated with [U- ^{13}C]-glucose for 1.5, 6 (with and without pyruvate), and 16 hours, and cell lysates were analyzed using LC-MS/MS and DI-HRMS. Total NAD^+ levels decreased gradually in both WT and KO cells, while NADH levels remained elevated in MDH1-deficient cells, resulting in a lower NAD^+/NADH ratio after 16 hours (Figure S3A).

We previously demonstrated that MDH1- and other MAS-deficient cells affect glycolytic flux at the level of GAPDH, resulting in increased G3P and decreased serine synthesis (Broeks *et al.*, accepted). In line with these findings, we found increased intermediates of the first steps of glycolysis in MDH1-deficient cells, including $^{13}\text{C}_6$ -fructose 1,6-bisphosphate, $^{13}\text{C}_3$ -dihydroxyacetone phosphate (DHAP), and $^{13}\text{C}_3$ -G3P (Figures 2A, 2B, and S4A). Interestingly, $^{13}\text{C}_3$ -GA3P levels were not elevated (Figures 2B and S4A). Glycerol 3-phosphate dehydrogenase (GPD1) catalyzes the conversion of DHAP to G3P while also regenerating NAD^+ , which may be beneficial in MDH1-deficient cells. Indeed, MDH1-deficient cells had an increased $^{13}\text{C}_3$ -G3P/ $^{13}\text{C}_3$ -DHAP ratio after 1.5 hours of incubation with [U- ^{13}C]-glucose, indicating an increased conversion of DHAP to G3P at that time (Figure 2E). However, at 6 and 16 hours, the $^{13}\text{C}_3$ -G3P/ $^{13}\text{C}_3$ -DHAP ratio normalizes and decreases, suggesting that saturation of this pathway results in accumulation of both DHAP and G3P (Figure 2E). Moreover, the decreased conversion of DHAP to G3P may be associated with the decreasing NAD^+/NADH ratio at 6 and 16 hours (Figure S3A). As reflected by the $^{13}\text{C}_3$ -lactate/ $^{13}\text{C}_3$ -pyruvate ratio, the conversion of $^{13}\text{C}_3$ -pyruvate to $^{13}\text{C}_3$ -lactate continues to increase over time in MDH1-deficient cells (Figure 2E). However, although the $^{13}\text{C}_3$ -lactate/ $^{13}\text{C}_3$ -pyruvate ratio increases, the total intracellular lactate/pyruvate ratio remains unaltered, indicating that most glycolysis-derived pyruvate is shunted into lactate to maintain a favorable NAD^+/NADH balance in MDH1-deficient cells over this time course (Figures 2E and S4B). The unchanged intracellular lactate/pyruvate ratio may be due to increased lactate excretion from cells, which was indeed revealed by analysis of the medium fraction of MDH1-deficient cells (Figure S5).

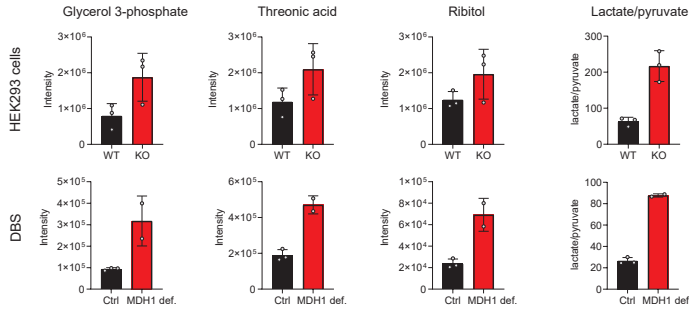
Pyruvate supplementation restored glycolysis in MDH1-deficient cells by decreasing $^{13}\text{C}_3$ -GA3P, $^{13}\text{C}_3$ -DHAP, $^{13}\text{C}_3$ -G3P, and $^{13}\text{C}_3$ -lactate concentrations while increasing the $^{13}\text{C}_3$ -pyruvate concentration (Figures 2B, 2D, S4A and S4B). In addition, pyruvate supplementation increased the NAD^+/NADH ratio while decreasing the $^{13}\text{C}_3$ -G3P/ $^{13}\text{C}_3$ -DHAP and $^{13}\text{C}_3$ -lactate/ $^{13}\text{C}_3$ -pyruvate ratios (Figures 2E and S3B). Since pyruvate

supplementation increased both unlabeled and labeled pyruvate levels, the total lactate/pyruvate ratio decreased in both MDH1-deficient cells and controls upon pyruvate supplementation (Figures 2E and S4B). Overall, these findings demonstrate that pyruvate supplementation recycles NAD^+ and restores glycolysis in MDH1 KO cells.

MDH1-deficient cells had lower levels of glycolytic intermediates downstream from GAPDH, with a modest decrease in $^{13}\text{C}_3$ -3-phosphoglycerate (3-PG) and $^{13}\text{C}_3$ -2-phosphoglycerate and a more severe decrease in $^{13}\text{C}_3$ -phosphoenolpyruvate and $^{13}\text{C}_3$ -pyruvate (Figures 2C, 2D, S4B and S4C). The glycolytic intermediate 3-PG serves as a precursor for the serine synthesis pathway, where NAD^+ -dependent phosphoglycerate dehydrogenase converts it to 3-phosphohydroxypyruvate (3-PHP) (Figure 2A). Subsequently, phosphoserine aminotransferase (PSAT) converts 3-PHP to 3-phosphoserine, which is then converted to serine by phosphoserine phosphatase. We previously hypothesized that a low cytosolic NAD^+/NADH ratio affects the NAD^+ -dependent PHGDH and, subsequently, serine synthesis (Broeks *et al.*, accepted). We found an increase in $^{13}\text{C}_3$ -3-PHP and in the $^{13}\text{C}_3$ -3-PHP/ $^{13}\text{C}_3$ -3-PG ratio, whereas $^{13}\text{C}_3$ -3-PS and the $^{13}\text{C}_3$ -3-PS/ $^{13}\text{C}_3$ -3-PHP ratio were severely decreased in MDH1-deficient cells (Figures 2C and 2F). In contrast to our hypothesis, these findings indicate either an increased conversion of $^{13}\text{C}_3$ -3-PG to $^{13}\text{C}_3$ -3-PHP or the accumulation of $^{13}\text{C}_3$ -3-PHP over time, which is most likely due to a block in serine synthesis at the level of PSAT rather than a block at the level of the NAD^+ -dependent phosphoglycerate dehydrogenase. Pyruvate supplementation normalizes the serine synthesis, implying that this block is linked to metabolic consequences resulting from a low NAD^+/NADH ratio, either directly or indirectly (Figures 2C and S4D).

Figure 1. MDH1 deficiency affects multiple metabolic pathways. (A) Overlapping metabolic > consequences of MDH1 deficiency in DBS ($n = 2$) and MDH1 KO cells ($n = 3$) include increased glycerol 3-phosphate, threonic acid, ribitol/arabitol and lactate/pyruvate ratio (B) Reaction schemes of 2-ketobutyrate to hydroxybutyrate and pyruvate to lactate by lactate dehydrogenase (LDH). (C) Heatmap of the top 60 differentially affected compounds in MDH1 KO cells in Figure S1B cultured in a concentration range of 2-ketobutyrate (2-KB) (left) or pyruvate (pyr) (right). The heatmap (with feature scaling) represents the \log_2 fold change (FC) of KO samples compared to controls, which is calculated by dividing the intensity of the KO by the geometric mean of intensities of experimentally matched WT ($n = 1$). See Table S1 for isobaric compounds. (D) Raw intensities of compounds with masses corresponding to glycerol 3-phosphate, ribitol/arabitol, sorbitol/galactitol, aspartate, serine and oxoglutarate in MDH1 WT and KO cells cultured in the presence of indicated concentrations of 2-ketobutyrate and pyruvate. Data are presented as mean \pm SD for technical triplicates ($n = 1$).

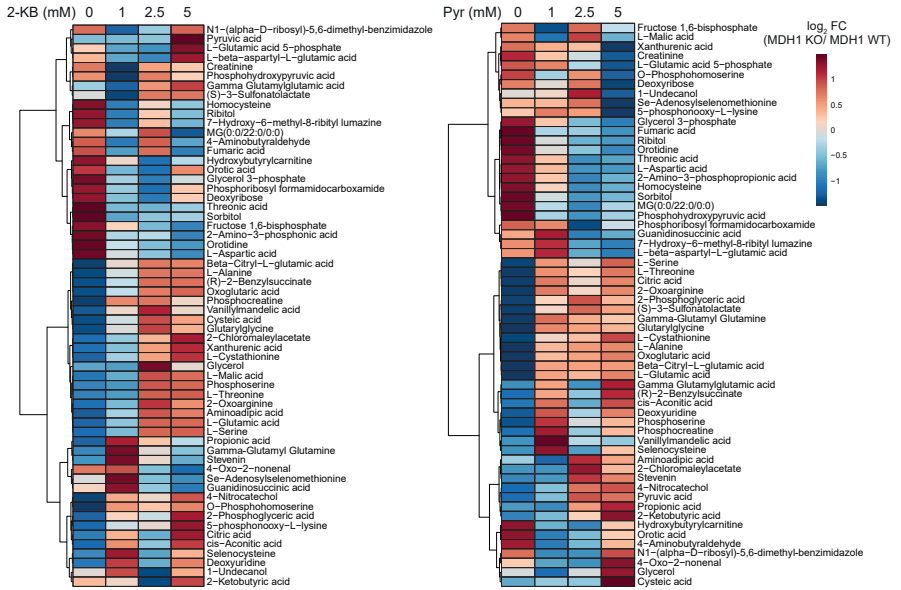
A



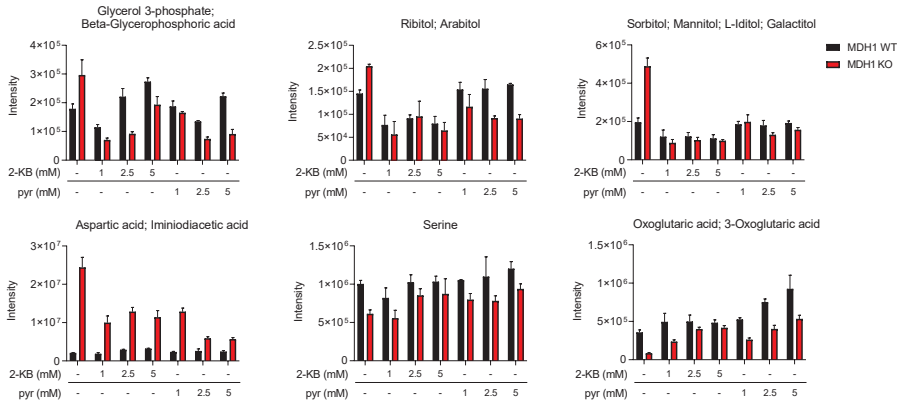
B



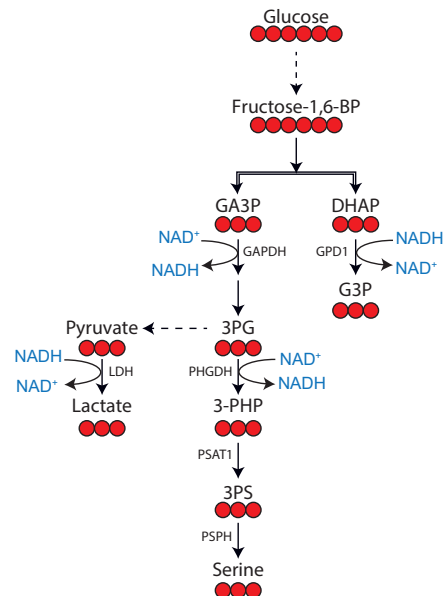
C



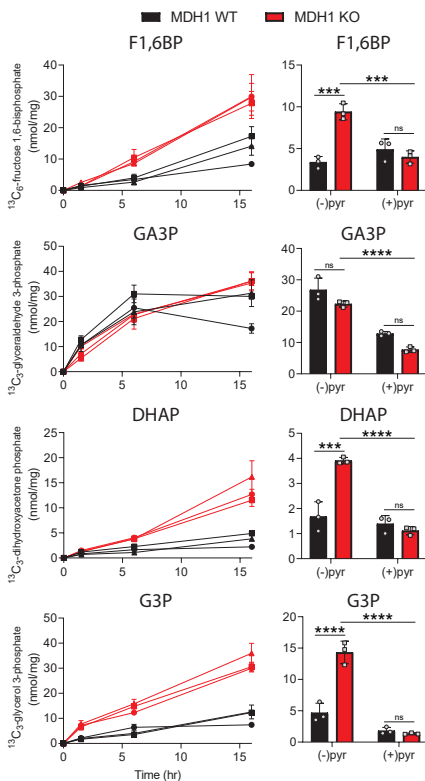
D



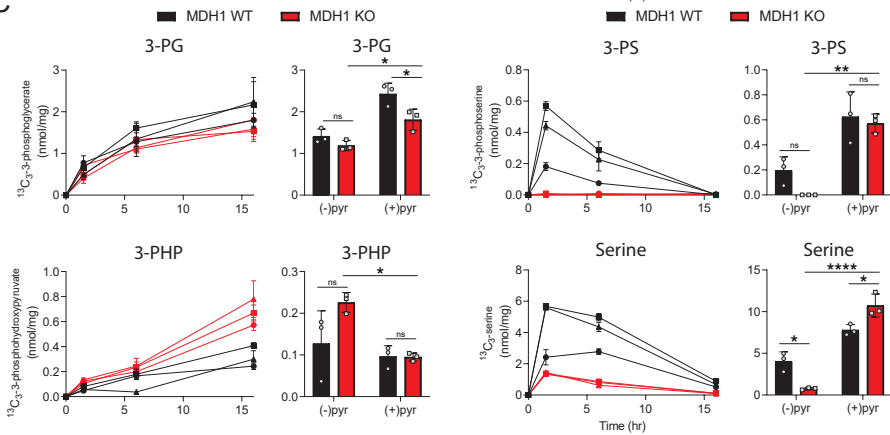
A



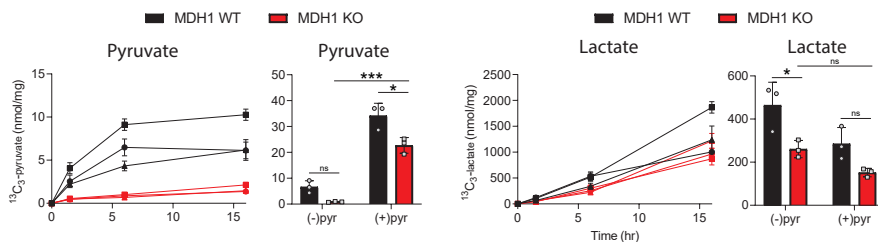
B



C



D



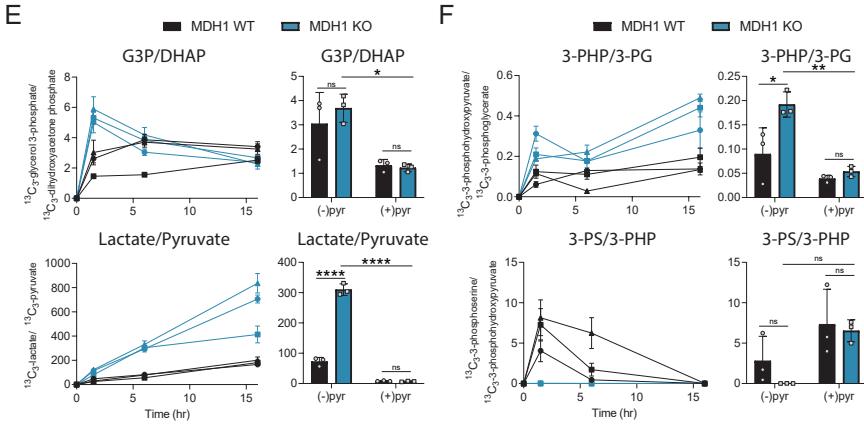


Figure 2. Pyruvate restores disturbed glycolysis, glycerol synthesis and serine synthesis in MDH1 KO cells. (A) Schematic of [U- ^{13}C]-glucose labeling in glycolysis. Concentrations of (B) labeled fructose 1,6-bisphosphate (F1,6BP), glyceraldehyde 3-phosphate (GA3P), dihydroxyacetone phosphate (DHAP), glycerol 3-phosphate (G3P), (C) 3-phosphoglycerate (3-PG), 3-phosphohydroxypyruvate (3-PHP), 3-phosphoserine (3-PS), serine, (D) pyruvate and lactate from [U- ^{13}C]-glucose over time (left) and in absence and presence of 5 mM pyruvate for 6 hours (right). (E) Ratios of labeled intermediates over time (left) and in absence and presence of 5 mM pyruvate for 6 hours (right). Data are presented as mean \pm SD for technical triplicates (left) and biological triplicates (right) in MDH1 WT and KO cells ($n = 3$). A two way ANOVA was followed by Tukey's multiple comparisons test to compare WT and KO cells and the effect of pyruvate supplementation in KO cells. The adjusted p-values are indicated as * $p < 0.05$, ** $p < 0.01$, *** $p < 0.001$, **** $p < 0.0001$, and ns indicates no significance.

Disturbed glycolysis increases influx in the pentose phosphate pathway in MDH1 deficient cells

The glycolytic intermediate glucose 6-phosphate can be metabolized in either glycolysis or in the pentose phosphate pathway (PPP). Since the upper glycolytic intermediates accumulate in MDH1-deficient cells, we further analyzed intermediates of the PPP in cells incubated with [U- ^{13}C]-glucose. The oxidative branch of the PPP generates NADPH, which is the reducing power required for the synthesis of fatty acids, sterols, nucleotides, and non-essential amino acids. In addition, NADPH contributes to the cellular antioxidant defenses by converting oxidized glutathione to reduced glutathione. The end-product of the oxidative branch of the PPP is ribulose 5-phosphate (Ru5P), which is further catalyzed by ribose-5-phosphate isomerase (RPI) into ribose 5-phosphate (R5P), a building block for nucleic acid synthesis (Figure 3A). Alternatively, Ru5P is converted into xylulose 5-phosphate (X5P) by ribulose 5-phosphate epimerase (RPE) (Figure 3A).

In MDH1-deficient cells, both $^{13}\text{C}_5$ -Ru5P and $^{13}\text{C}_5$ -R5P increased similarly over time and decreased upon pyruvate supplementation, whereas the $^{13}\text{C}_5$ -R5P/ $^{13}\text{C}_5$ -Ru5P ratio remained unaltered (Figures 4B, 4C and S5). In the non-oxidative branch of the PPP, both R5P and X5P are converted by transketolase (TKT) to sedoheptulose 7-phosphate (S7P) and glyceraldehyde 3-phosphate (GA3P), respectively (Figure 3A). In line with increases in $^{13}\text{C}_5$ -Ru5P and $^{13}\text{C}_5$ -R5P, $^{13}\text{C}_7$ -S7P increased over time and was normalized upon pyruvate addition in MDH1-deficient cells (Figures 4B and S6). Furthermore, the increase in the $^{13}\text{C}_7$ -S7P/ $^{13}\text{C}_5$ -R5P ratio suggests increased conversion of $^{13}\text{C}_5$ -R5P to $^{13}\text{C}_7$ -S7P by TKT or the accumulation of $^{13}\text{C}_7$ -S7P (Figure 3C). Interestingly, MDH1-deficient cells display a significant contribution of unlabeled S7P to the total pool that remains unaltered upon pyruvate supplementation, indicating that another unknown carbon source feeds in the PPP in MDH1-deficient cells (Figure S6A). However, using [U- ^{13}C]-glucose we were unable to distinguish the carbon flux from PPP and glycolysis to GA3P and F6P and vice versa (Figure S6B). GA3P and F6P produced by the PPP might funnel back into glycolysis, contributing to additional accumulation of glycolytic intermediates in the upper part of glycolysis. Alternatively, the accumulated F6P may contribute to elevated PPP intermediates.

The accumulation of PPP intermediates may explain the increased levels of a pentitol in MDH1-deficient cells. Using GC-FID, we identified the increased pentitol as ribitol (Figure 3D). Although the pathway from the PPP to ribitol is not fully elucidated, ribitol is considered a human metabolic end-product that is most likely derived from the PPP intermediates D-ribulose and D-ribose, which are in turn derived from Ru5P and R5P, respectively.⁷ Ribitol levels were increased in both DBS from MDH1-deficient patients as well as MDH1-deficient cells (Figures 1A and S1), and cellular concentrations normalized upon pyruvate supplementation (Figure 3D). DI-HRMS analysis of cells incubated with [U- ^{13}C]-glucose revealed the accumulation of a mass corresponding to ribitol (m+5) over time in MDH1-deficient cells, which decreased upon pyruvate supplementation (Figure 3E). Overall, these findings indicate that disturbed glycolysis increases flux into the PPP, resulting in the accumulation of PPP intermediates. When glycolysis is normalized by pyruvate supplementation, the PPP intermediates and their metabolic end-product ribitol normalize concurrently in MDH1-deficient cells.

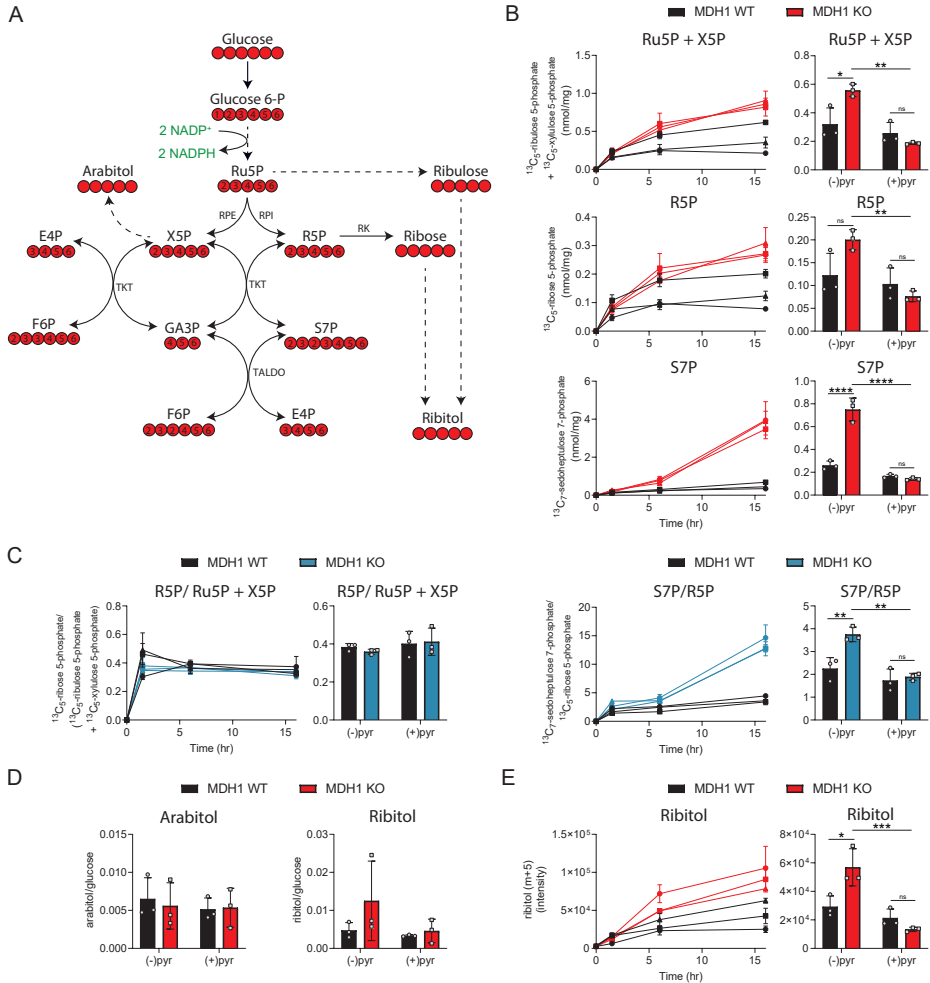


Figure 3. Increased influx in the pentose phosphate pathway in MDH1 KO cells. (A) Schematic of [U-¹³C]-glucose labeling in the pentose phosphate pathway and its presumable metabolic end-products. **(B)** Concentrations of labeled ribulose 5-phosphate (Ru5P) and xylulose 5-phosphate (indistinguishable by LC-MS/MS), ribose 5-phosphate (R5P), sedoheptulose 7-phosphate (S7P) from [U-¹³C]-glucose over time (left) and in absence and presence of 5 mM pyruvate (pyr) for 6 hours (right). **(C)** Ratios of labeled intermediates over time (left) and in absence and presence of 5 mM pyruvate for 6 hours (right). **(D)** Arabitol and ribitol in absence and presence of 5 mM pyruvate for 6 hours measured by GC-FID ($n = 3$). **(E)** Compound with a mass corresponding to ribitol ($m+5$) following [U-¹³C]-glucose incubation over time (left) and in absence and presence of 5 mM pyruvate for 6 hours (right) measured by DI-HRMS. Data are presented as mean \pm SD for technical triplicates (left) and biological triplicates (right) in MDH1 WT and KO cells ($n = 3$). A two way ANOVA was followed by Tukey's multiple comparisons test to compare WT and KO cells and the effect of pyruvate supplementation in KO cells. The adjusted p-values are indicated as * $p < 0.05$, ** $p < 0.01$, *** $p < 0.001$, **** $p < 0.0001$, and ns indicates no significance.

Sorbitol accumulates in MDH1-deficient cells

Using GC-FID, we identified the increased hexitol in MDH1-deficient cells as sorbitol. Sorbitol is an intermediate of the polyol pathway which originates from glucose and consists of two enzymatic steps (Figure 4A). First, aldose reductase (AR) reduces glucose to sorbitol, which is then oxidized to fructose by NAD⁺-dependent sorbitol dehydrogenase (SORDH). MDH1-deficient cells displayed an increase in sorbitol, whereas fructose and the fructose/sorbitol ratio were decreased, indicating a block in SORDH (Figure 4B). In addition, DI-HRMS analysis of cell lysates incubated with [U-¹³C]-glucose revealed that a compound with a mass corresponding to sorbitol (m+6) accumulates in MDH1-deficient cells over time, which was normalized by pyruvate (Figure 4C). These findings indicate that the polyol pathway is disturbed in MDH1-deficient cells due to a disturbed NAD⁺/NADH ratio.

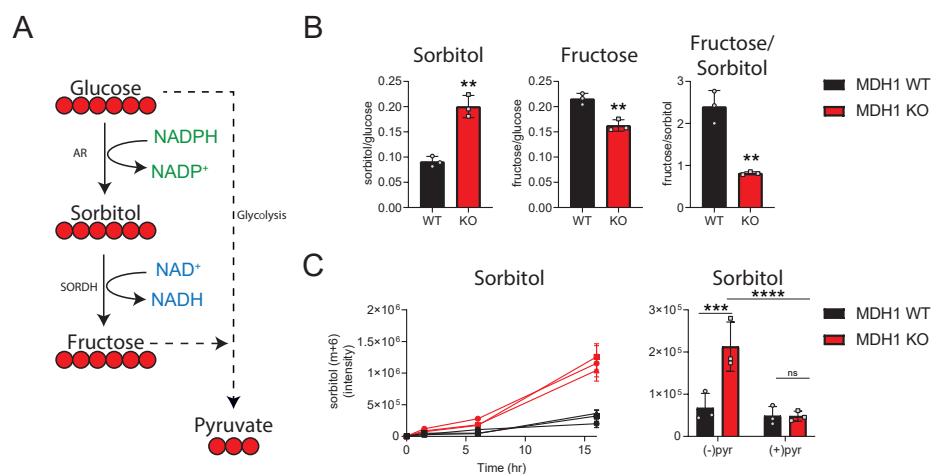


Figure 4. Polyol pathway in MDH1 KO cells. (A) Schematic of [U-¹³C]-glucose labeling in the polyol pathway. (B) Sorbitol, fructose and fructose/sorbitol ratio in HEK293 cells measured by GC-FID. Data are presented as mean ± SD for biological triplicates ($n = 3$). A student's t-test was performed. (C) Compound with a mass corresponding to sorbitol (m+6) following [U-¹³C]-glucose incubation over time (left) and in absence and presence of 5 mM pyruvate (pyr) for 6 hours (right) measured by DI-HRMS. Data are presented as mean ± SD for technical triplicates (left) and biological triplicates (right) in MDH1 WT and KO cells ($n = 3$). A two-way ANOVA was followed by Tukey's multiple comparisons test to compare WT and KO cells and the effect of pyruvate supplementation in KO cells. The adjusted p-values are indicated as * $p < 0.05$, ** $p < 0.01$, *** $p < 0.001$, **** $p < 0.0001$, and ns indicates no significance.

Pyruvate restores TCA cycle activity and limits aspartate accumulation in MDH1-deficient cells

Aspartate accumulation is the most prominent metabolic alteration in MDH1 deficiency^{3,4}(Broeks *et al.*, accepted). Interestingly, pyruvate addition resulted in lower aspartate concentrations (Figure 1C). To identify the underlying mechanisms hereof, we examined the labeling in the TCA cycle and MAS metabolites in cell lysates incubated with [U-¹³C]-glucose in the presence and absence of pyruvate for 6 hours and analyzed using DI-HRMS (Figure 5A). Labeling of TCA cycle intermediates from [U-¹³C]-glucose was lower in MDH1-deficient cells, likely as a consequence of disturbed glycolysis and the increased conversion of glycolysis-derived pyruvate to lactate (Figures 2, 5B and S7). Pyruvate supplementation increased unlabeled citrate and 2-oxoglutarate in both control and MDH1-deficient cells but did not elevate unlabeled glutamate or malate (Figure 5B). Due to the stimulating effect of pyruvate on glycolysis, the labeled carbons from [U-¹³C]-glucose entering the TCA cycle also increased, illustrated by an increase in labeled pyruvate and acetylcarnitine (reflecting acetyl-CoA) in MDH1-deficient cells (Figures 2D, 5C and S4B). Consequently, both control and MDH1-deficient cells had increased labeled TCA cycle intermediates upon pyruvate supplementation, including glutamate and malate (Figure 5B). In contrast, both unlabeled and labeled aspartate decreased when pyruvate was added in MDH1-deficient cells (Figure 5D). Within mitochondria, aspartate is formed from oxaloacetate by mitochondrial glutamate-oxaloacetate transaminase (GOT2) as part of the MAS. Alternatively, oxaloacetate is converted to citrate by citrate synthase to continue the TCA cycle. Since oxaloacetate requires acetyl-CoA to form citrate, decreased acetyl-CoA in MDH1-deficient cells may prevent citrate formation, hence resulting in low citrate levels (Figure 5B). The increased oxaloacetate availability for GOT2 may then result in increased conversion to aspartate in MDH1-deficient cells (Figure 5B). Altogether, our findings indicate that restoring glycolysis and thus acetyl-CoA levels fuels the TCA cycle while preventing aspartate accumulation in MDH1-deficient cells (Figure 5D).

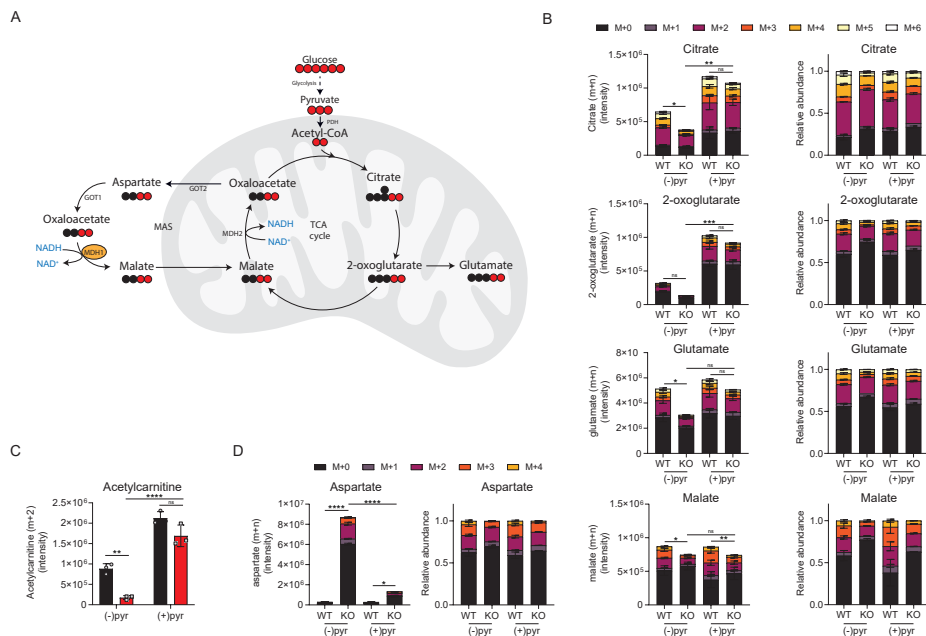


Figure 5. Pyruvate fuels the TCA cycle and lowers aspartate in MDH1 KO cells. (A) Schematic of [U - ^{13}C]-glucose labeling in the tricarboxylic acid (TCA) cycle and malate aspartate shuttle (MAS). (B) Summed intensities of ^{13}C labeled (M+1-6) and unlabeled (M+0) citrate, 2-oxoglutarate, glutamate and malate and their fractional enrichment following 6 hour incubation with [U - ^{13}C]-glucose in absence and presence of 5 mM pyruvate (pyr). (C) Intensity of acetylcarnitine (m+2) following 6 hour incubation with [U - ^{13}C]-glucose in absence and presence of 5 mM pyruvate. (D) Summed intensity of ^{13}C labeled (M+1-6) and unlabeled (M+0) aspartate and their fractional enrichment following 6 hour incubation with [U - ^{13}C]-glucose in absence and presence of 5 mM pyruvate. See Table S2 for isobaric compounds. Data are presented as mean \pm SD for biological triplicates in MDH1 WT and KO cells ($n = 3$). A two-way ANOVA was followed by Tukey's multiple comparisons test to compare the total compound intensity in WT and KO cells and the effect of pyruvate supplementation in KO cells. The adjusted p -values are indicated as * $p < 0.05$, ** $p < 0.01$, *** $p < 0.001$, **** $p < 0.0001$, and ns indicates no significance.

DISCUSSION

Malate dehydrogenase 1 (MDH1) deficiency is an inherited metabolic disorder of the malate-aspartate shuttle (MAS) that results in a cytosolic NAD^+/NADH redox imbalance. Here, we studied the pathophysiology of MDH1 deficiency and revealed that disturbed glycolysis in MDH1 KO cells has broad metabolic consequences for its branching pathways, including glycerol synthesis, serine synthesis, the polyol pathway, and the pentose phosphate pathway. Pyruvate supplementation largely restores the disturbed cytosolic redox pathways while fueling the TCA cycle.

Previously, we demonstrated that all MAS defects result in a low cytosolic NAD^+/NADH ratio, leading to varying degrees of impaired glycolysis (Broeks *et al.*, accepted). In this study, we provide an in-depth analysis of glycolysis and branching pathways in MDH1-deficient cells. Glycolysis and other cytosolic pathways require NAD^+ as an electron acceptor, thereby forming NADH. To enable the continuation of these pathways, NADH needs to be re-oxidized to NAD^+ to maintain the cytosolic redox balance. Several cytosolic dehydrogenases recycle NAD^+ , including glycerol 3-phosphate dehydrogenase (GPD1), lactate dehydrogenase (LDH), and MDH1. GPD1 and MDH1 are part of NADH shuttles that consequently deliver cytosolic electrons to the electron transport chain, whereas LDH drives lactate production for excretion. The loss of MDH1 drastically reduces the NAD^+ -regenerating capacity and leads to an increase in pathway activity of alternative NAD^+ -recycling pathways, as illustrated by increased DHAP to G3P conversion and pyruvate to lactate conversion. Although we observed an initial increase in the conversion of DHAP to G3P in MDH1-deficient cells, the ratio decreased after 1.5 hours in a similar way as the NAD^+/NADH ratio decreases. This may imply that G3P formation in MDH1-deficient cells is beneficial for regenerating NAD^+ and is in line with the high levels of G3P in MDH1-deficient patients.⁴ However, the glycerol phosphate shuttle may rapidly reach its maximum capacity, resulting in the accumulation of its intermediates, while pyruvate oxidation becomes the major mechanism for NAD^+ -recycling.^{8,9}

The *de novo* serine synthesis is severely diminished in MDH1-deficient cells (Broeks *et al.*, accepted). We previously hypothesized that the low cytosolic NAD^+/NADH ratio affects the NAD^+ -dependent PHGDH and, subsequently, serine synthesis. In this study, we further investigated the serine synthesis pathway and identified that 3-PHP, the product of PHGDH, accumulated. This indicates that the low serine synthesis in MDH1 KO cells may only partially be due to affected NAD^+ -dependent PHGDH and in part to an additional block at the level of PSAT1. PSAT1 is a cytosolic transaminase that converts glutamate to oxoglutarate to generate phosphoserine from 3-PHP. Recently, a study demonstrated that PSAT also has affinity for DHAP,

thereby generating serinol phosphate.¹⁰ The accumulation of DHAP in MDH1 KO cells may limit serine synthesis at the level of PSAT1 due to substrate competition that is re-established by restoration of glycolysis upon pyruvate supplementation. These data suggest that the severity of the secondary serine synthesis defect may depend on the accumulation of DHAP in MDH1 KO cells and may provide an additional explanation for the previously reported correlation between G3P and serine synthesis in MDH1 and other MAS defects (Broeks *et al.*, accepted).

In line with the inhibition of glycolysis, glucose carbons are increasingly channeled into the PPP, resulting in accumulation of PPP intermediates in MDH1-deficient cells. The restoration of PPP flux by the addition of an electron acceptor indicates that the increased flux in the PPP is a secondary consequence of disturbed glycolysis since reactions in the PPP do not directly depend on NAD(H). In addition, overflow of PPP intermediates may result in increased conversion to one of its metabolic end-products, ribitol, which is supported by the elevated ribitol levels in the DBS of MDH1-deficient patients. Increased ribitol levels have been previously reported in two metabolic disorders of the PPP, TALDO and RPI deficiency.¹¹⁻¹³ However, whether the accumulation of ribitol plays a role in the pathophysiology is unknown. We further identified that MDH1-deficient cells accumulated sorbitol, likely due to disturbance of NAD⁺-dependent sorbitol dehydrogenase. Sorbitol accumulation is thought to contribute to pathophysiology in galactosemia and diabetes mellitus through intoxication of neurons.¹⁴ In addition, the loss of SORDH activity in SORDH deficient patients results in the accumulation of intracellular sorbitol and leads to neuropathy.¹⁵ These findings imply that the intracellular accumulation of sorbitol might contribute to the neurological phenotype of MDH1 deficiency.

Supplementation of the NAD⁺-recycling electron acceptors 2-ketobutyrate and pyruvate normalized the disturbed fluxes in glycolysis and its branching pathways in MDH1-deficient cells. In addition, pyruvate supplementation restored flux through the TCA cycle by providing pyruvate through glycolysis and uptake, while preventing the accumulation of oxaloacetate and aspartate. Boosting oxidative phosphorylation and energy metabolism via continuation of the TCA cycle may be beneficial for patients with MDH1 deficiency and may be achieved with therapeutic pyruvate supplementation. Previously, sodium pyruvate was used for treatment of the liver-specific MAS disorder AGC2 deficiency.¹⁶ Although pyruvate supplementation in defects affecting multiple organs increases the risk of lactic acidosis, the evaluation of pyruvate therapy was promising in patients with inherited mitochondrial disease, such as Leigh syndrome.¹⁷ Pyruvate supplementation in these patients demonstrated a remarkable decrease in plasma lactate levels and the lactate/pyruvate ratio, as well as improvements in clinical

symptoms.^{18,19} Plasma lactate may be lowered due to prioritizing pyruvate entry in the TCA cycle, as observed in MDH1-deficient cells where pyruvate supplementation increased TCA cycle intermediates but not lactate. Alternatively, a combination of pyruvate and uridine – required for pyrimidine synthesis in the absence of a functional respiratory chain²⁰ – was studied in fibroblasts from patients with OXPHOS dysfunction.²¹ Upon pyruvate and uridine supplementation they observed a similar decrease in the lactate/pyruvate ratio and normalization of TCA cycle intermediates, aspartate (decreased in OXPHOS dysfunctional fibroblasts) and glycerol 3-phosphate (increased in OXPHOS dysfunctional fibroblasts).²¹ The similarities in metabolic disturbances and effects of NAD⁺-recycling in OXPHOS deficient fibroblasts and MDH1-deficient cells imply that the findings of this study provide insights into the metabolic consequences of other disorders with a cytosolic NAD⁺/NADH imbalance.

Our results were mainly obtained from cell culture experiments in high glucose conditions, which revealed many disturbances related to glycolysis. Accumulation of compounds such as sorbitol and glycerol 3-phosphate may be prevented by treatment with a low-glucose diet, such as the ketogenic diet. Indeed, patients with the MAS disorder AGC1 deficiency demonstrate impressive clinical improvement, along with lowering of glycerol/G3P in the brain.²² Moreover, a ketogenic diet with ketone bodies and fatty acids is capable of fueling the TCA cycle via β -oxidation, which is likely beneficial in MDH1 deficiency as well.

In conclusion, using stable isotope-resolved metabolomics we demonstrated that a disturbed NAD⁺/NADH cytosolic redox balance in MDH1 deficiency leads to disturbed glycolysis and branching pathways, including glycerol synthesis, the polyol pathway, and the pentose phosphate pathway. Due to the multifaceted benefits of pyruvate, a low dose of pyruvate may be considered as a treatment for MDH1 deficiency.

Acknowledgements

We thank Ramon Versteeg and Deena van Logchem for their technical assistance. This work was supported by Metakids (2017-075 to J.J.M.J) and Stofwisselkracht (2019 to N.M.V).

Author contributions

J.J.M.J., N.M.V., F.J.T.Z. and M.H.B. were involved in conceptualization and design of the study. M.H.B. and J.G. performed mass spectrometry and data processing. H.M.G. performed cell collection experiment for sugar alcohols. M.H.B. performed metabolic tracing experiments, data processing, statistical analysis and wrote the manuscript. All authors helped with the editing of the manuscript.

Declaration of Interests

The authors declare no competing interests.

MATERIALS AND METHODS

Cell culture

Knockouts (KO) of MDH1 were generated in human embryonic kidney (HEK293T) cells using CRISPR/Cas9, as described in Broeks *et al.*, 2019⁴ and Broeks *et al.*, accepted. A total of three wildtype (WT) and three KO cell lines were used for the experiments. Cells were maintained in DMEM, high glucose, GlutaMAX™, pyruvate with 10% (v/v) heat-inactivated FBS and 1% P/S (v/v) in a humidified, 5% CO₂ atmosphere at 37 °C. Cells were passaged upon reaching confluence. Cell culture experiments were performed with DMEM, no glucose, no pyruvate with 1% P/S (v/v). Dulbecco's Modified Eagle Medium (DMEM), high glucose, GlutaMAX™, pyruvate; DMEM, no glucose; fetal bovine serum (FBS); penicillin-streptomycin (P/S) (10,000 U/ml) and trypsin-ethylenediaminetetraacetic acid (Trypsin-EDTA (0.5%), no phenol red) were purchased from Gibco™ (ThermoFisher Scientific). D-Glucose (U-13C6, 99%) was purchased from Cambridge Isotope Laboratories, Inc.

Cell culture and metabolite extraction experiment with pyruvate and 2-ketobutyrate

WT and KO HEK293 cells were seeded at a density of 300,000 cells per well in six-well dishes in parallel and grown to ~80-90% confluency. The medium was refreshed 24 hours before the start of the experiment. Cells were incubated with concentrations of 1, 2.5 and 5 mM sodium pyruvate (Fluka Chemika, Buchs, Switzerland) or 2-ketobutyrate (Sigma Aldrich) in medium containing 25 mM D-Glucose for 6 hours. Following incubation, cells were washed with 2 ml cold PBS (4 °C). Cells were harvested by scraping them twice in 0.25 ml pre-chilled 100% methanol (-80 °C), whereafter the cell lysate was collected. After centrifuging the 0.5 ml cell lysate/methanol-mixture (16,200 g, 10 min, 4 °C), the supernatant was transferred to a new 1.5 ml Eppendorf tube. The supernatant was stored at -80 °C until further analysis with DI-HRMS and GC-FID (for identification of sorbitol).

Cell culture and metabolite extraction experiment with pyruvate and [U-¹³C]-glucose

WT and KO HEK293 cells were seeded at a density of 300,000 cells per well in six-well dishes in parallel and grown to ~80-90% confluency. The medium was refreshed 24 hours before the start of the experiment. Cells were incubated with 5 mM sodium pyruvate (Fluka Chemika, Buchs, Switzerland) in medium containing 25 mM [U-¹³C]-glucose for 1.5, 6 and 16 hours. Following incubation, cells were washed with 2 ml cold PBS (4 °C). Cells were harvested by scraping them twice in 0.25 ml pre-chilled 100% methanol (-80 °C), whereafter the cell lysate was collected. After centrifuging

the 0.5 ml cell lysate/methanol-mixture (16,200 g, 10 min, 4 °C), the supernatant was transferred to a new 1.5 ml Eppendorf tube. The supernatant was stored at -80 °C until further analysis with DI-HRMS and LC-MS/MS.

Cell culture and metabolite extraction for identification of ribitol/arabitol

WT and KO HEK293 cells were seeded in parallel in 10-cm dishes and grown until ~80-90% confluency. The medium was refreshed 24 hours before start of the experiment. Cells were incubated with 5 mM sodium pyruvate (Fluka Chemika, Buchs, Switzerland) in medium containing 25 mM D-Glucose for 6 hours. Following incubation, cells were washed with 10 ml cold PBS (4 °C). Cells were harvested by scraping them twice in a 2.5 ml pre-chilled methanol/pure H₂O-mixture (80/20%) (-80 °C). After centrifuging the 5 ml cell lysate/methanol-mixture (16,200 g, 10 min, 4 °C), the supernatant was transferred to a new 10-ml tube. The samples were evaporated under a gentle stream of nitrogen at 40 °C until dryness and reconstituted with 600 µl of methanol/pure H₂O-mixture (80/20%). The supernatant was stored at -80 °C until further analysis with GC-FID.

Direct infusion mass spectrometry analysis

Methanol samples collected after 8 hours incubation with [U-¹³C]-glucose were diluted 10 times. 70 µl cell working solution and 60 µl 0.3% formic acid (Emsure, Darmstadt, Germany) were added to 70 µl of diluted cell lysate in methanol. Solutions were filtered using a methanol preconditioned 96 well filter plate (Acro prep, 0.2 µm GHP, NTRL, 1 ml well; Pall Corporation, Ann Arbor, MI, USA) and a vacuum manifold, after which the sample filtrate was collected in a 96 well plate (Advion, Ithaca, NY, USA). Direct-infusion high-resolution mass spectrometry (DI-HRMS) metabolomics was performed as previously described.²³ Samples were analyzed using a TriVersa NanoMate system (Advion, Ithaca, NY, USA) controlled by Chipsoft software (version 8.3.3, Advion), mounted on a Q-Exactive Plus high-resolution mass spectrometer (Thermo Scientific). 13 µl sample was automatically aspirated and injected through nozzles on an ESI-chip (Advion) using nitrogen gas (0.5 psi, voltage = 1.6 kV), and measured in positive and negative ion mode with a total run time of 3.0 min. Parameters were: scan range = 70-600 m/z, resolution = 140,000 at 200 m/z, automatic gain control target = 3e6, capillary temperature = 275 °C, S-lens RF level = 70. Data acquisition was performed using Xcalibur software (version 3.0, Thermo Scientific, Waltham, MA, USA). A peak calling pipeline, developed in R programming language, annotated the raw mass spectrometry data according to the Human Metabolome DataBase (HMDB, version 3.6) with a range of 2 ppm (<https://github.com/UMCUGenetics/DIMS>). Only metabolites that were endogenously relevant

(according to HMDB) and with the following adduct ions were selected: $[M+H]^+$, $[M+Na]^+$, $[M+K]^+$ (positive mode), $[M-H]^-$ and $[M+Cl]^-$ (negative mode). As DI-HRMS is unable to separate isomers, the resulting mass peak intensities consist of summed intensities of these isomers. Isobaric compounds are listed in Table S1.

Isotopologue identification DI-HRMS

In order to extract isotopologues of metabolites from the resulting data, the theoretical m/z value for the annotated metabolite in the negative or ionization mode was used to determine the expected m/z of the ^{13}C labeled metabolite. Potential isobaric compounds are listed in Table S2. All samples were measured in a single run. Different isotopologues, molecules with different isotopic composition, are formed as a result of increasing labeling of metabolites with each round of the TCA cycle. The fractional enrichment of each isotopologue is calculated as a percentage of the sum of all possible isotopologues. Isotopologues range from $M+0$ to $M+n$ (1-6), in which $M+0$ reflects the unlabeled ^{12}C carbons and $M+n$ the labeled ^{13}C carbons.

Liquid chromatography-mass spectrometry analysis for intermediates of glycolysis, serine biosynthesis and the pentose phosphate pathway

The concentration of intermediates from glycolysis, serine biosynthesis and the pentose phosphate pathway were measured using LC-MS/MS. The internal standard solution consisted of 2H_3 -Lactic acid (100 μM), 2H_3 -Pyruvic acid (255 μM), $^{13}C_6$ -Glucose (133 μM) and $^{13}C_3,^{15}N$ -Serine (100 μM) (Sigma-Aldrich, Denmark), and 2H_4 -NAD $^+$ (25 μM) (Toronto Research Chemicals, Canada). Calibration standards were prepared in the concentration range of 0.2-100 μM , the NAD compounds in the concentration range of 0.1-50 μM . 20 μl internal standard solution was added to 0.5 ml methanol cell extract and 50 μl calibration standard. The mixtures are evaporated with nitrogen at a temperature of 40 $^{\circ}C$ and reconstituted in a mixture of 50%/50% v/v Acetonitril (Merck) and Milli-Q purified H_2O (Merck, Darmstadt, Germany).

Samples were analysed using a Q-Exactive HF High resolution mass spectrometer (Thermo Scientific $^{\text{TM}}$, Bremen, Germany). Chromatographic separation was achieved by injecting 3 μl sample on a Atlantis Premier BEH Z-HILIC 1.7 μm , 2.1 x 100 mm (Waters, Milford, USA). The flow rate remained constant at 0.5 ml/min, column temperature was maintained at 40 $^{\circ}C$ and the autosampler at 10 $^{\circ}C$. Solvent A consisted of 20 mM ammonium bicarbonate (Sigma-Aldrich, Denmark), pH 9.00 in Milli-Q purified H_2O and solvent B was 20 mM ammonium bicarbonate in acetonitrile 10%/90% v/v. The mobile phase gradient (%B) was as follows: 0.0-5.0 min linear gradient from 90% to 65% B; 5.0-6.0 min isocratic 65% B; 6.0-6.5 min linear gradient

from 65% to 90%. 6.5-12.5 min isocratic at 90 for column equilibration. Samples were detected in full scan positive ionization mode for the NAD-compounds, the other compounds in negative ionization mode with a scan range of 70-900 m/z and a resolution of 120000 (for both modes). Parameters for negative and positive ESI were as follows: capillary voltage = 4 kV, capillary temperature = 350 °C, automatic gain control target = 1E6, sheath gas = 50, aux gas = 30, spare gas = 0, S-lens RF level = 75. Peak integration was performed with TraceFinder software (Thermo Scientific) version: 4.1 SP4. The concentration of each analyte was calculated using the calibration curve. Technical triplicates of cell lysates were measured and concentrations were normalized to total protein concentrations, obtained by the Pierce BCA protein assay.

Gas-chromatography- flame ionization detection for identification of sugar alcohols

Sorbitol, fructose, ribitol and arabitol were analyzed using gas-chromatography-flame ionization detection (GC-FID). The internal standard solution consisted of β -d-phenylglucoside (Sigma-Aldrich, Denmark). Calibration standards were prepared in the concentration range of 0-100 μ M. 100 μ l internal standard solution (3.9 mM) was added to 500 μ l methanol cell extract and 500 μ l calibration standards, evaporated with nitrogen and reconstituted in 300 μ l Tri-Sil TBT (Trimethylsilyl N-trimethylsilylacetamidate, 1-(Trimethylsilyl)-1 H-imidazole, Chlorotrimethylsilane) (Supelco) dissolved Milli-Q purified H₂O (Merck, Darmstadt, Germany). Samples were then derivatized as follows: samples were incubated for 30 min at 105 °C. After cooling down of the samples, 1 ml Milli-Q purified H₂O and 500 μ l hexane (VWR) was added. The mixture was vortexed for 10 seconds and centrifuged (5 min, 3000 rpm, RT), after which the supernatant was transferred to a new tube. Next, 1 ml 0.1 M HCl was added and vortexed and centrifuged again (5 min, 3000 rpm, RT). Then supernatant was transferred to a new tube, after which Anhydrous Sodium Sulfate (Sigma-Aldrich, Denmark) was added. The mixture was vortexed and transferred to the final vials. Finally, a few drops of N,O-Bis(Trimethylsilyl)Trifluoroacetamide (Sigma Aldrich) were added before analysis. Samples were analyzed using a Trace 1300 GC-FID (Thermo Fisher Scientific, Waltham, USA) equipped with AI/AS 3000 autosampler and iConnect flame ionization detector (FID). Two μ l of the mixture was injected into the GC-FID with a split/splitless injector (split mode set to 1:15) at 280 °C on a HP-1 column (25m x 0.2 mm; 0.11 μ m; Agilent Technologies, J&W Scientific) connected to the FID at 300 °C. Helium was used as a carrier gas at a flow rate of 1 ml/min and the purge flow was 5 ml/min. The GC oven temperature was held at 120 °C for 10 minutes, increased to 265 °C at a rate of 3 °C/min, followed by an additional increase to 295 °C at a rate of 10 °C/min, which was maintained for 5 minutes. Peak integration

was performed using Empower software 3.6.0 (Waters) and Chromeleon software 7.2.10 (Thermo Scientific). Technical triplicates of cell lysates were measured and concentrations were normalized to the glucose concentration of that sample.

Quantification and statistical analysis

Peak intensities were extracted from LC-MS data as described in the corresponding method above. Statistical analyses were performed in GraphPad Prism (V9.3.0) as indicated. Data are presented as mean \pm standard deviation (SD). An adjusted p-value of <0.05 was considered statistically significant.

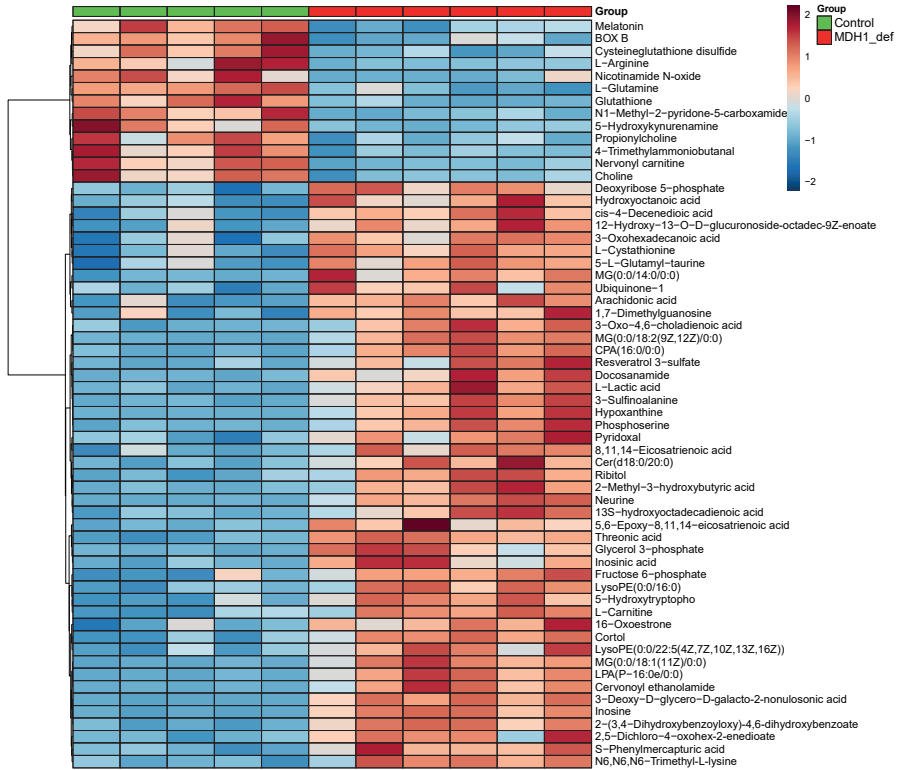
REFERENCES

1. Borst P. Hydrogen transport and transport metabolites. In: *Funktionelle Und Morphologische Organisation Der Zelle*. Springer Berlin Heidelberg; 1963:137-162.
2. Borst P. The malate–aspartate shuttle (Borst cycle): How it started and developed into a major metabolic pathway. *IUBMB Life*. 2020;72(11):2241-2259.
3. Hanse EA, Ruan C, Kachman M, Wang D, Lowman XH, Kelekar A. Cytosolic malate dehydrogenase activity helps support glycolysis in actively proliferating cells and cancer. *Oncogene*. 2017;36(27):3915-3924.
4. Broeks MH, Shamseldin HE, Alhashem A, et al. MDH1 deficiency is a metabolic disorder of the malate–aspartate shuttle associated with early onset severe encephalopathy. *Hum Genet*. 2019;138(11-12):1247-1257.
5. Sullivan LB, Gui DY, Hosios AM, Bush LN, Freinkman E, Vander Heiden MG. Supporting Aspartate Biosynthesis Is an Essential Function of Respiration in Proliferating Cells. *Cell*. 2015;162(3):552-563.
6. Diehl FF, Lewis CA, Fiske BP, Vander Heiden MG. Cellular redox state constrains serine synthesis and nucleotide production to impact cell proliferation. *Nat Metab*. 2019;1(9):861-867.
7. Huck JHJ, Roos B, Jakobs C, Van Der Knaap MS, Verhoeven NM. Evaluation of pentitol metabolism in mammalian tissues provides new insight into disorders of human sugar metabolism. *Mol Genet Metab*. 2004;82(3):231-237.
8. Wang Y, Stancliffe E, Fowle-Grider R, et al. Saturation of the mitochondrial NADH shuttles drives aerobic glycolysis in proliferating cells. *Mol Cell*. 2022;82(17):3270-3283.e9.
9. Yeh JI, Chinte U, Du S. Structure of glycerol-3-phosphate dehydrogenase, an essential monotopic membrane enzyme involved in respiration and metabolism. *Proc Natl Acad Sci U S A*. 2008;105(9):3280-3285.
10. Caligiore F, Zangelmi E, Vetro C, et al. Human cytosolic transaminases: side activities and patterns of discrimination towards physiologically available alternative substrates. *Cell Mol Life Sci*. 2022;79(8).
11. Verhoeven NM, Huck JHJ, Roos B, et al. Transaldolase deficiency: liver cirrhosis associated with a new inborn error in the pentose phosphate pathway. *Am J Hum Genet*. 2001;68(5):1086-1092.
12. Huck JHJ, Verhoeven NM, Struys EA, Salomons GS, Jakobs C, van der Knaap MS. Ribose-5-phosphate isomerase deficiency: new inborn error in the pentose phosphate pathway associated with a slowly progressive leukoencephalopathy. *Am J Hum Genet*. 2004;74(4):745-751.
13. Wamelink MMC, Struys EA, Jakobs C. The biochemistry, metabolism and inherited defects of the pentose phosphate pathway: A review. *J Inherit Metab Dis*. 2008;31(6):703-717.
14. Hao W, Tashiro S, Hasegawa T, et al. Hyperglycemia promotes Schwann cell de-differentiation and de-myelination via sorbitol accumulation and Igf1 protein down-regulation. *J Biol Chem*. 2015;290(28):17106-17115.
15. Cortese A, Zhu Y, Rebelo AP, et al. Biallelic mutations in SORD cause a common and potentially treatable hereditary neuropathy with implications for diabetes. *Nat Genet* 2020 525. 2020;52(5):473-481.
16. Mutoh K, Kurokawa K, Kobayashi K, Saheki T. Treatment of a citrin-deficient patient at the early stage of adult-onset type II citrullinaemia with arginine and sodium pyruvate. *J Inherit Metab Dis*. 2008;31 Suppl 2:S343-S347.
17. Li M, Zhou S, Chen C, et al. Therapeutic potential of pyruvate therapy for patients with mitochondrial diseases: a systematic review. *Ther Adv Endocrinol Metab*. 2020;11.
18. Koga Y, Povalko N, Inoue E, Nashiki K, Tanaka M. Biomarkers and clinical rating scales for sodium pyruvate therapy in patients with mitochondrial disease. *Mitochondrion*. 2019;48:11-15.
19. Komaki H, Nishigaki Y, Fuku N, et al. Pyruvate therapy for Leigh syndrome due to cytochrome c oxidase deficiency. *Biochim Biophys Acta*. 2010;1800(3):313-315.
20. King MP, Attardi G. Human cells lacking mtDNA: repopulation with exogenous mitochondria by complementation. *Science*. 1989;246(4929):500-503.

21. Adant I, Bird M, Decru B, et al. Pyruvate and uridine rescue the metabolic profile of OXPHOS dysfunction. *Mol Metab.* 2022;63.
22. Bölsterli BK, Boltshauser E, Palmieri L, et al. Ketogenic Diet Treatment of Defects in the Mitochondrial Malate Aspartate Shuttle and Pyruvate Carrier. *Nutrients.* 2022;14(17):3605.
23. Haijes HA, Willemsen M, van der Ham M, et al. Direct infusion based metabolomics identifies metabolic disease in patients' dried blood spots and plasma. *Metabolites.* 2019;9(1):12.

SUPPLEMENTARY MATERIAL

A



B

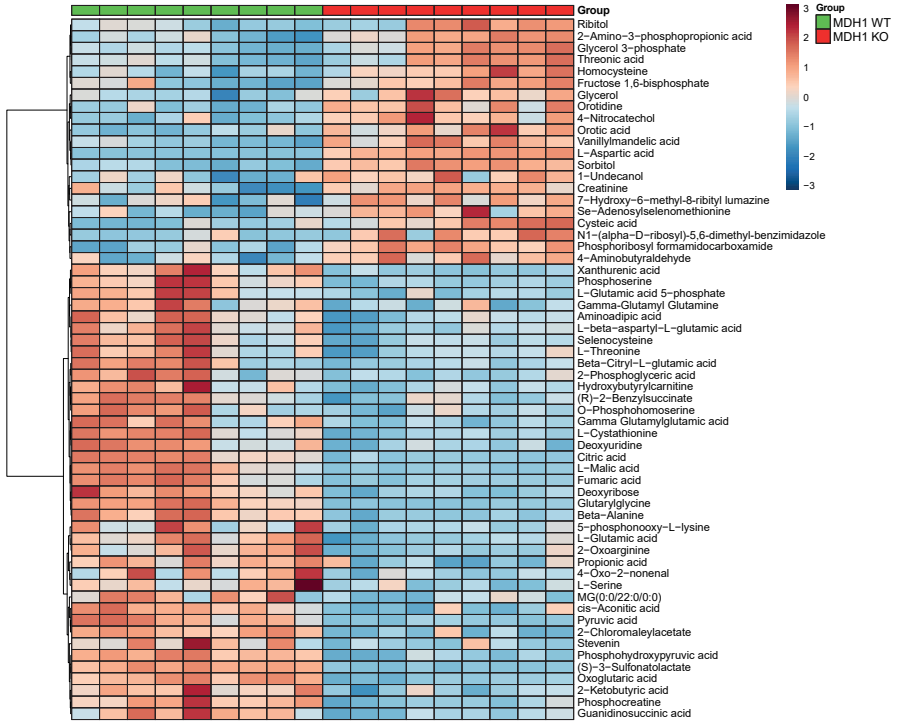


Figure S1. Metabolic profile of MDH1 deficiency and MDH1 KO HEK293 cells. (A) Heatmap of top 60 metabolite features identified by t-test for controls and MDH1-deficient patients as determined in DBS. **(B)** Heatmap of top 60 metabolite features identified by t-test for MDH1 WT and KO HEK293 cells. Heatmaps were created in MetaboAnalyst using Euclidian ward clustering with autoscaling of features. A comprehensive overview of p-values and isomers is displayed in Table S1.

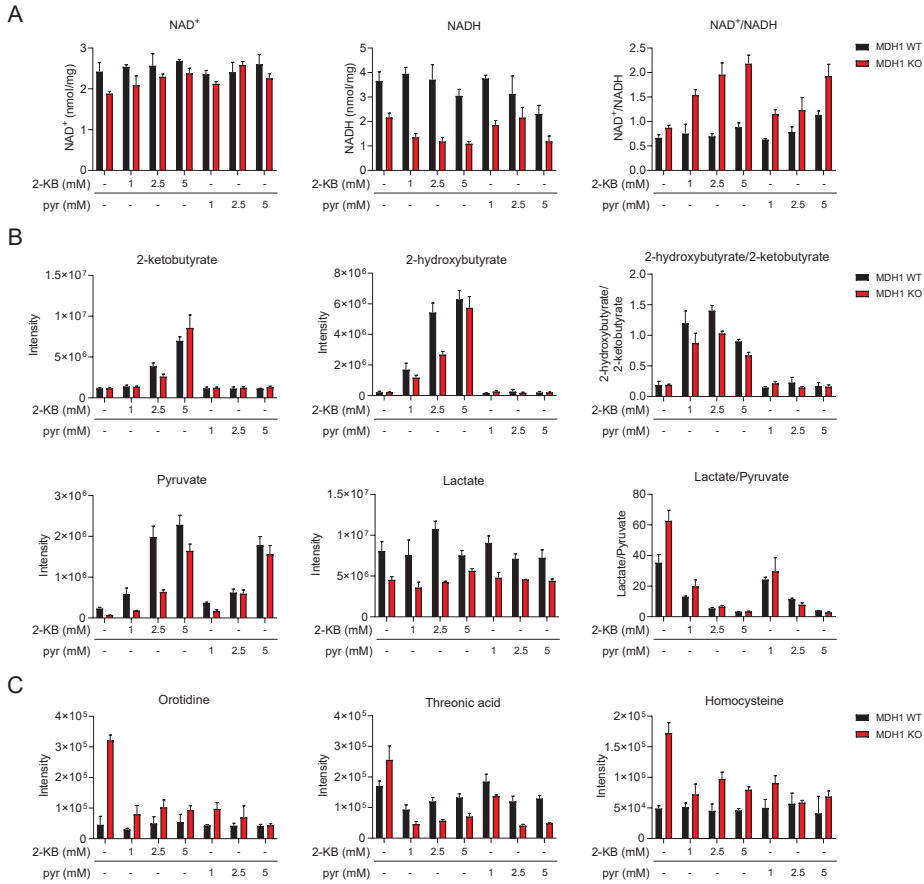
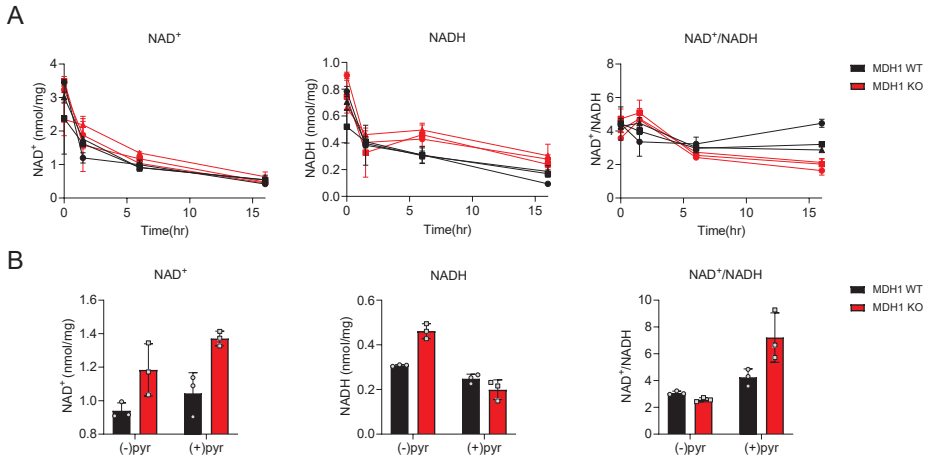
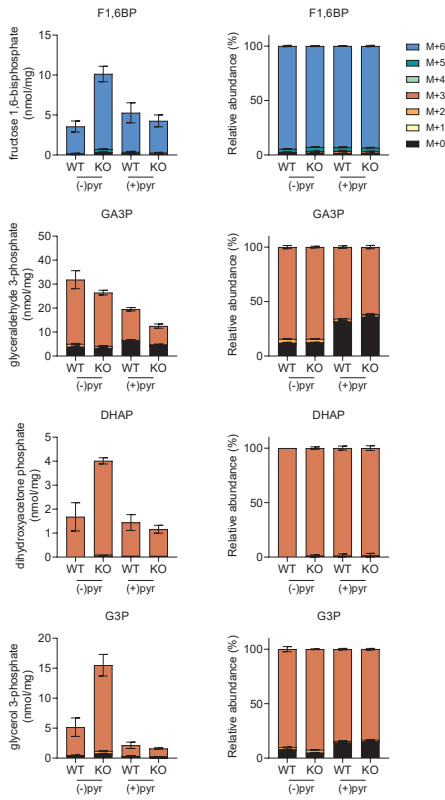


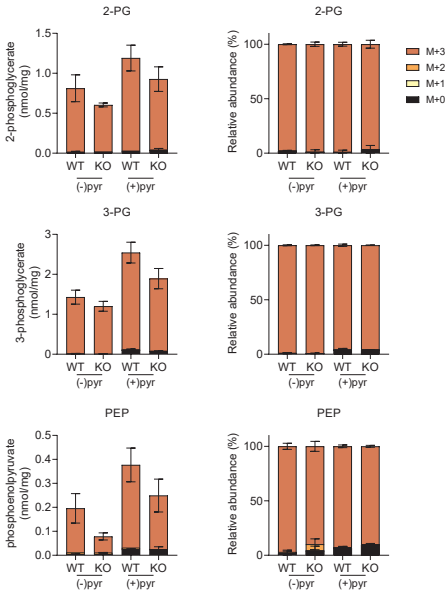
Figure S2. Metabolic consequences of pyruvate and 2-ketobutyrate supplementation in MDH1 WT and KO HEK293 cells. (A) Concentrations of total NAD⁺, NADH and the NAD⁺/NADH ratio in presence of 2-ketobutyrate (2-KB) or pyruvate (pyr) (*n* = 1). **(B)** Intensities of 2-ketobutyrate, 2-hydroxybutyrate, pyruvate, lactate in WT and MDH1 KO HEK293 cells cultured in the presence of indicated concentrations of 2-KB or pyr (*n* = 1). Isobaric compounds for 2-hydroxybutyrate include (R)-3-hydroxybutyric acid; (S)-3-hydroxyisobutyric acid; (R)-3-hydroxyisobutyric acid; 3-hydroxybutyric acid; (S)-3-hydroxybutyric acid; 4-hydroxybutyric acid; 2-methyl-3-hydroxypropanoate. See Table S2 for other isobaric compounds. **(C)** Intensities of Orotidine, Threonine acid, Homocysteine in WT and MDH1 KO HEK293 cells (*n* = 1). Data are presented as mean ± SD for technical triplicates in MDH1 WT and KO cells.



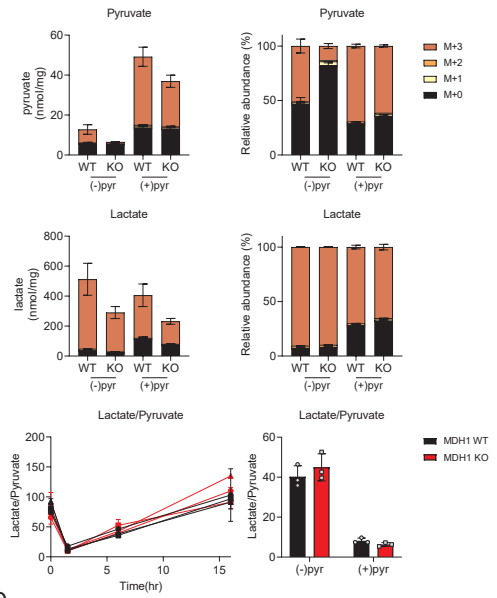
A



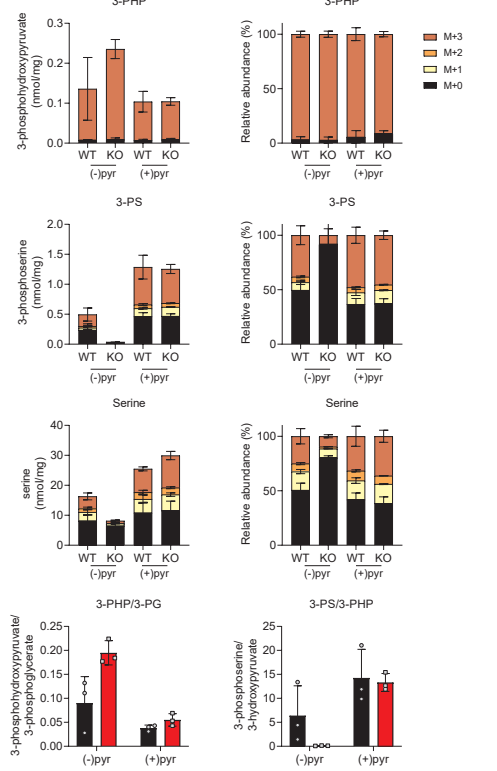
C



B



D



< **Figure S4. Intermediates of glycolysis upon pyruvate supplementation.** Isotopomer concentrations (left) and its relative abundance (right) for **(A)** fructose 1,6-bisphosphate (F1,6BP), glyceraldehyde 3-phosphate (GA3P), dihydroxyacetone phosphate (DHAP) and glycerol 3-phosphate (G3P), **(B)** pyruvate and lactate, **(C)** 2-phosphoglycerate (2-PG), 3-phosphoglycerate (3-PG) and phosphoenolpyruvate (PEP), **(D)** 3-phosphohydroxypyruvate (3-PHP), 3-phosphoserine (3-PS) and serine from [U-¹³C]-glucose labeling in absence and presence of 5 mM pyruvate for 6 hours. In addition, the ratios of total concentrations were displayed for lactate/pyruvate, 3-PHP/3-PG and 3-PS/3-PHP in absence and presence of 5 mM pyruvate for 6 hours. Data are presented as mean ± SD for biological triplicates in MDH1 WT and KO cells (*n* = 3).

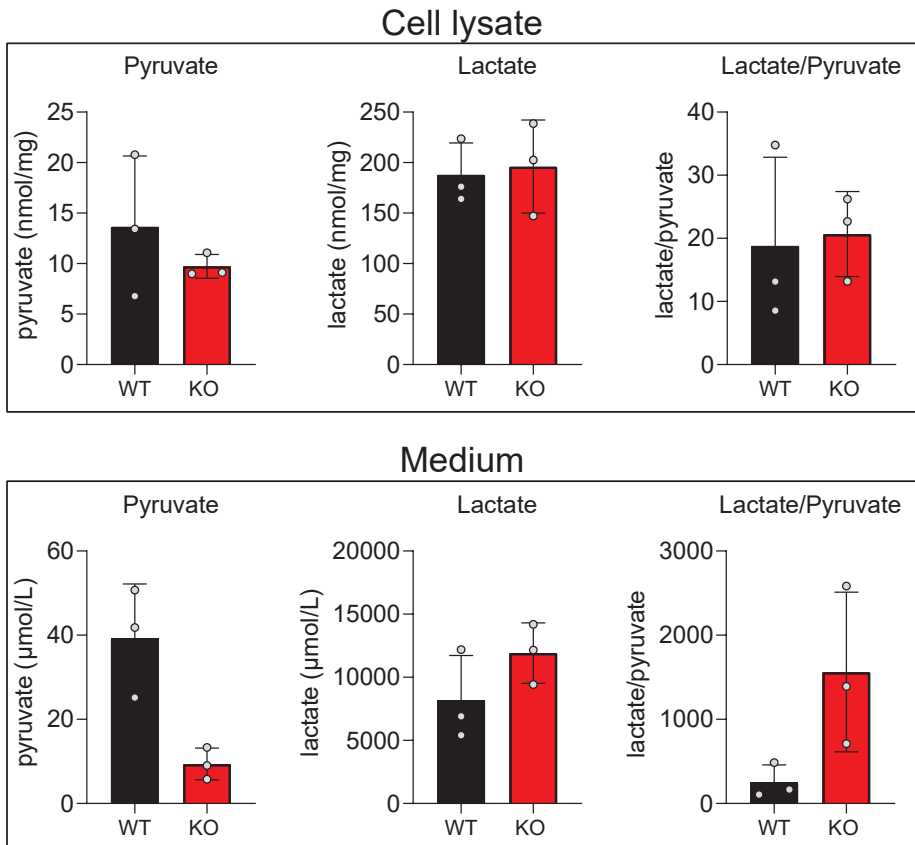


Figure S5. Intra- and extracellular pyruvate and lactate in MDH1 KO cells. Concentrations of pyruvate, lactate and the lactate/pyruvate ratio in cell lysates and in medium after 24 hours of cell culture. Data are presented as mean ± SD for biological triplicates in WT and MDH1 KO cells (*n* = 3).

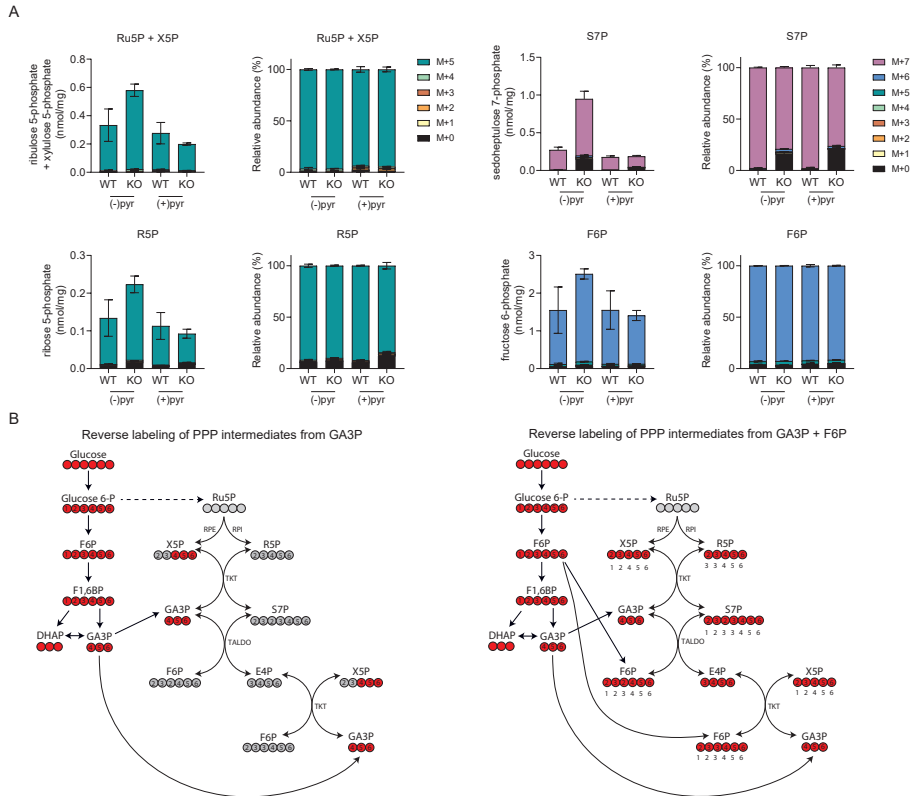


Figure S6. Intermediates of the pentose phosphate pathway (PPP) upon pyruvate supplementation. (A) Isotopomer concentrations (left) and its relative abundance (right) for ribulose 5-phosphate (Ru5P) and xylulose 5-phosphate (indistinguishable by LC-MS/MS), ribose 5-phosphate (R5P), sedoheptulose 7-phosphate (S7P) and fructose 6-phosphate (F6P) from [U-¹³C]-glucose labeling in absence and presence of 5 mM pyruvate for 6 hours. Data are presented as mean \pm SD for biological triplicates in MDH1 WT and KO cells ($n = 3$). **(B)** Schematic of reverse labeling of PPP intermediates from ¹³C-labeled and unlabeled glycolytic intermediates glyceraldehyde 3-phosphate (GA3P) and fructose 6-phosphate. F1,6BP, fructose 1,6-bisphosphate; DHAP, dihydroxy acetone phosphate; E4P, erythrose 4-phosphate

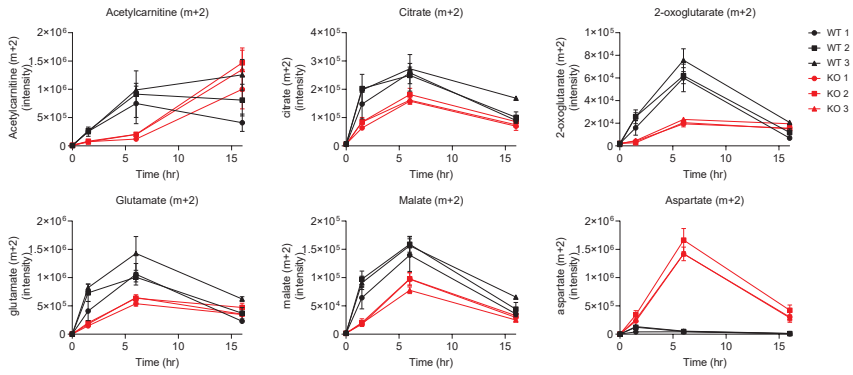


Figure S7. First round labeling in TCA cycle from $[U-^{13}C]$ -glucose. Intensities of acetylcarnitine, citrate, 2-oxoglutarate, glutamate, malate and aspartate labeled by $[U-^{13}C]$ -glucose in the first round of the TCA cycle (m+2) over a time course of 16 hours. See Table S2 for isobaric compounds. Data are presented as mean \pm SD for technical triplicates in MDH1 WT and KO cells ($n = 3$).

Table S1A. Isobaric compounds untargeted DI-HRMS analysis in DBS corresponding to figure S1A.

Feature	T-statistic	p-value	FDR	Isomers
Threonic acid	-11.518	1.09E-06	0.001896	-
3-Deoxy-D-glycero-D-galacto-2-nonulosonic acid	-9.8217	4.16E-06	0.002496	-
Inosine	-9.7792	4.31E-06	0.002496	Allopurinol riboside; Arabinosylhypoxanthine
2-(3,4-Dihydroxybenzoyloxy)-4,6-dihydroxybenzoate	-7.9573	2.31E-05	0.010038	-
L-Glutamine	7.6932	3.02E-05	0.010501	D-Glutamine; Ureidoisobutyric acid; Alanyl-glycine; Alanyl-glycine
Glutathione	7.3718	4.23E-05	0.012247	-
MG(0:0/18:1(11Z)/0:0)	-6.9511	6.68E-05	0.016577	MG(0:0/18:1(9Z)/0:0); MG(18:1(11Z)/0:0/0:0); MG(18:1(9Z)/0:0/0:0)
LPA(P-16:0e/0:0)	-6.7927	7.97E-05	0.017316	-
N1-Methyl-2-pyridone-5-carboxamide	6.6316	9.57E-05	0.018487	N1-Methyl-4-pyridone-3-carboxamide
MG(0:0/14:0/0:0)	-6.3554	0.000132	0.022212	MG(14:0/0:0/0:0)
Cortol	-6.3024	0.000141	0.022212	Beta-Cortol
Neurine	-6.2065	0.000158	0.02283	-
Nervonyl carnitine	6.1105	0.000177	0.023278	-
MG(0:0/18:2(9Z,12Z)/0:0)	-6.0185	0.000198	0.023278	MG(18:2(9Z,12Z)/0:0/0:0)
Arachidonic acid	-6.0065	0.000201	0.023278	-
3-Sulfinolalanine	-5.919	0.000224	0.024305	3-Sulfinato-L-alaninate
L-Cystathionine	-5.8209	0.000253	0.025843	Allocystathionine; CysteinyL-Threonine; Threonyl-Cysteine
Cervonoyl ethanolanamide	-5.7559	0.000274	0.02648	-
Melatonin	5.6685	0.000306	0.026737	-

Table S1A. Continued

Feature	T-statistic	p-value	FDR	Isomers
CPA(16:0/0:0)	-5.665	0.000308	0.026737	-
5-Hydroxytryptophol	-5.5892	0.000339	0.028049	1,2-Dehydrosolinol
Deoxyribose 5-phosphate	-5.5481	0.000357	0.028227	1-Deoxy-D-xy]ulose 5-phosphate; Deoxyribose 1-phosphate; Deoxyribose 5-monophosphate; 5-Deoxyribose-1-phosphate
S-Phenylmercapturic acid	-5.3289	0.000475	0.034737	-
N6,N6-Trimethyl-L-lysine	-5.3221	0.00048	0.034737	-
Cysteineglutathione disulfide	5.2425	0.000533	0.035557	-
Choline	5.1975	0.000566	0.035557	-
BOX B	5.1803	0.000579	0.035557	BOX A
Glycerol 3-phosphate	-5.1752	0.000583	0.035557	Beta-Glycerophosphoric acid
4-Trimethylammoniobutanol	5.1623	0.000593	0.035557	-
Hypoxanthine	-5.0978	0.000647	0.036744	-
Ribitol	-5.0884	0.000655	0.036744	D-Arabitol; L-Arabitol
5-L-Glutamyl-taurine	-5.061	0.00068	0.036939	-
Docosanamide	-5.0121	0.000727	0.038281	-
5-Hydroxykynurenamine	4.983	0.000756	0.038663	3-Hydroxykynurenamine
Propionylcholine	4.9601	0.00078	0.038755	-
cis-4-Decenedioic acid	-4.9036	0.000843	0.040718	cis-5-Decenedioic acid
Phosphoserine	-4.8242	0.000941	0.043027	DL-O-Phosphoserine
L-Lactic acid	-4.8085	0.000962	0.043027	D-Lactic acid; Hydroxypropionic acid; Glyceraldehyde; Dihydroxyacetone; Methoxyacetic acid

Table S1A. Continued

Feature	T-statistic	p-value	FDR	Isomers
LysoPE(0:0/16:0)	-4.7968	0.000978	0.043027	LysoPE(16:0/0:0)
L-Carnitine	-4.7636	0.001025	0.043027	-
Cer(d18:0/20:0)	-4.7375	0.001063	0.043027	-
Inosinic acid	-4.7374	0.001063	0.043027	Inosine 2'-phosphate
Fructose 6-phosphate	-4.7362	0.001065	0.043027	Myo-inositol 1-phosphate; Galactose 1-phosphate; Dolichyl phosphate D-mannose; Fructose 1-phosphate; Mannose 6-phosphate; D-Myo-inositol 4-phosphate; Glucose 6-phosphate; Glucose 1-phosphate; Inositol phosphate; Beta-D-Glucose 6-phosphate; Beta-D-Fructose 6-phosphate; D-Tagatose 1-phosphate; D-Mannose 1-phosphate; Sorbose 1-phosphate; Beta-D-Fructose 2-phosphate; 1D-myo-Inositol 3-phosphate; D-Tagatose 6-phosphate; D-fructose 1-phosphate
16-Oxoestrone	-4.6273	0.001242	0.048684	Estrone-2,3-quinone; Estrone-3,4-quinone
2,5-Dichloro-4-oxohex-2-enedioate	-4.6166	0.001261	0.048684	-
L-Arginine	4.5578	0.001371	0.049654	D-Arginine
3-Oxohexadecanoic acid	-4.5499	0.001386	0.049654	-
1,7-Dimethylguanosine	-4.5482	0.001389	0.049654	N2,N2-Dimethylguanosine
3-Oxo-4,6-choladienoic acid	-4.543	0.0014	0.049654	-
12-Hydroxy-13-O-D-glucuronoside-octadec-9Z-enoate	-4.5264	0.001434	0.049833	12-O-D-Glucuronoside-13-hydroxyoctadec-9Z-enoate; 10-Hydroxy-octadec-12Z-enoate-9-beta-D-glucuronide; 9-Hydroxy-10-O-D-glucuronoside-12Z-octadecenoate
Nicotinamide N-oxide	-4.3988	0.001723	0.05134	Urocanic acid
Hydroxyoctanoic acid	-4.38	0.001771	0.057601	3-Hydroxyoctanoic acid; (R)-2-Hydroxycaprylic acid; (R)-3-Hydroxyoctanoic acid; 7-Hydroxyoctanoic acid

Table S1A. Continued

Feature	T-statistic	p-value	FDR	Isomers
Pyridoxal	-4.3513	0.001847	0.058077	Isopyridoxal; 3-Methoxyanthranilate
2-Methyl-3-hydroxybutyric acid	-4.343	0.001869	0.058982	2-Ethylhydracrylic acid; 2-Hydroxy-3-methylbutyric acid; 3-Hydroxy-2-methyl-[S-(R,R)]-butanoic acid; 3-Hydroxyvaleric acid; Erythronilic acid; 3-Hydroxyisovaleric acid; 2-Hydroxyvaleric acid; 2-Hydroxy-2-methylbutyric acid; 4-Hydroxyisovaleric acid; 3-Hydroxy-2-methyl-[R-(R,S)]-butanoic acid
Ubiquinone-1	-4.3253	0.001918	0.058982	-
5,6-Epoxy-8,11,14-eicosatrienoic acid	-4.3037	0.00198	0.058982	8,9-Epoxyeicosatrienoic acid; 14R,15S-EpETri; 15(S)-HETE; 14,15-Epoxy-5,8,11-eicosatrienoic acid; 11,12-Epoxyeicosatrienoic acid; 8-HETE; 16(R)-HETE; 11(R)-HETE; 20-Hydroxyeicosatetraenoic acid; 12-HETE; 18-Hydroxyarachidonic acid; 9-HETE; 11,12-EpETri; 5-HETE; 19(S)-HETE; 10-HETE; 13-HETE; 17-HETE; 12 Hydroxy arachidonic acid; Arachidonate
8,11,14-Eicosatrienoic acid	-4.3006	0.001989	0.058982	5,8,11-Eicosatrienoic acid; 11,14,17-Eicosatrienoic acid
LysoPE(0:0/22:5(4Z,7Z,10Z,13Z,16Z))	-4.2881	0.002026	0.058982	LysoPE(0:0/22:5(7Z,10Z,13Z,16Z,19Z)); LysoPE(22:5(4Z,7Z,10Z,13Z,16Z)/0:0); LysoPE(22:5(7Z,10Z,13Z,16Z,19Z)/0:0)
13S-hydroxyoctadecadienoic acid	-4.2846	0.002036	0.058982	Alpha-dimorphocolic acid; 9,10-Epoxyoctadecenoic acid; 12,13-EpOME; 9-HODE
Resveratrol 3-sulfate	-4.3988	0.001723	0.058982	trans-Resveratrol 4'-sulfate; cis-Resveratrol 3-sulfate; cis-Resveratrol 4'-sulfate

Table S1B. Isobaric compounds untargeted DI-HRMS analysis in MDH1 HEK293 cells corresponding to figures 1 and S1B.

Feature	T-statistic	p-value	FDR	Isomers
(S)-3-Sulfonatolactate	24.5	4.10E-14	7.06E-11	-
L-Aspartic acid	-22.131	2.00E-13	1.72E-10	D-Aspartic acid; Iminodiacetic acid
Oxoglutaric acid	12.462	1.19E-09	6.82E-07	3-Oxoglutaric acid
Sorbitol	-10.963	7.53E-09	3.24E-06	Mannitol; L-Iditol; Galactitol
Phosphohydroxypyruvic acid	9.9643	2.89E-08	9.94E-06	-
Glutaryl-glycine	9.6744	4.35E-08	1.25E-05	N-Acetylglutamic acid
L-Alanine	7.9105	6.42E-07	0.000158	D-Alanine; Beta-Alanine; Sarcosine
Pyruvic acid	7.7487	8.37E-07	0.00018	Malonic semialdehyde
2-Chloromaleylacetate	7.4824	1.31E-06	0.00025	-
Phosphoribosyl formamidocarboxamide	-7.336	1.67E-06	0.000288	-
Citric acid	7.1697	2.23E-06	0.000349	Isocitric acid; D-threo-Isocitric acid; Diketogulonic acid; 2,3-Diketo-L-gulonate; (1R,2R)-Isocitric acid; D-Glucaro-1,4-lactone
Phosphocreatine	6.968	3.17E-06	0.000455	-
Vanillylmandelic acid	-6.855	3.87E-06	0.000512	3-(3,4-Dihydroxyphenyl) lactic acid; 3-Hydroxy-4-methoxymandelate
L-Malic acid	6.6654	5.43E-06	0.000668	Malic acid; D-Malic acid
Deoxyribose	6.6067	6.03E-06	0.000693	1-Deoxy-D-xylulose; (R)-2,3-Dihydroxy-isovalerate; (R)-glycerol 1-acetate; 2,3-Dihydroxyvaleric acid
Orotidine	-5.7338	3.08E-05	0.003313	-
Xanthurenic acid	5.6481	3.63E-05	0.003679	-
L-Glutamic acid	5.5155	4.70E-05	0.004278	D-Glutamic acid; DL-Glutamate; N-Methyl-D-aspartic acid; N-Acetylserine; L-4-Hydroxyglutamate semialdehyde
Orotic acid	-5.5134	4.72E-05	0.004278	-
Fumaric acid	5.385	6.07E-05	0.005124	Maleic acid
cis-Aconitic acid	5.3705	6.25E-05	0.005124	trans-Aconitic acid; Dehydroascorbic acid
2-Amino-3-phosphonopropionic acid	-5.3255	6.83E-05	0.005346	-

Table S1B. Continued

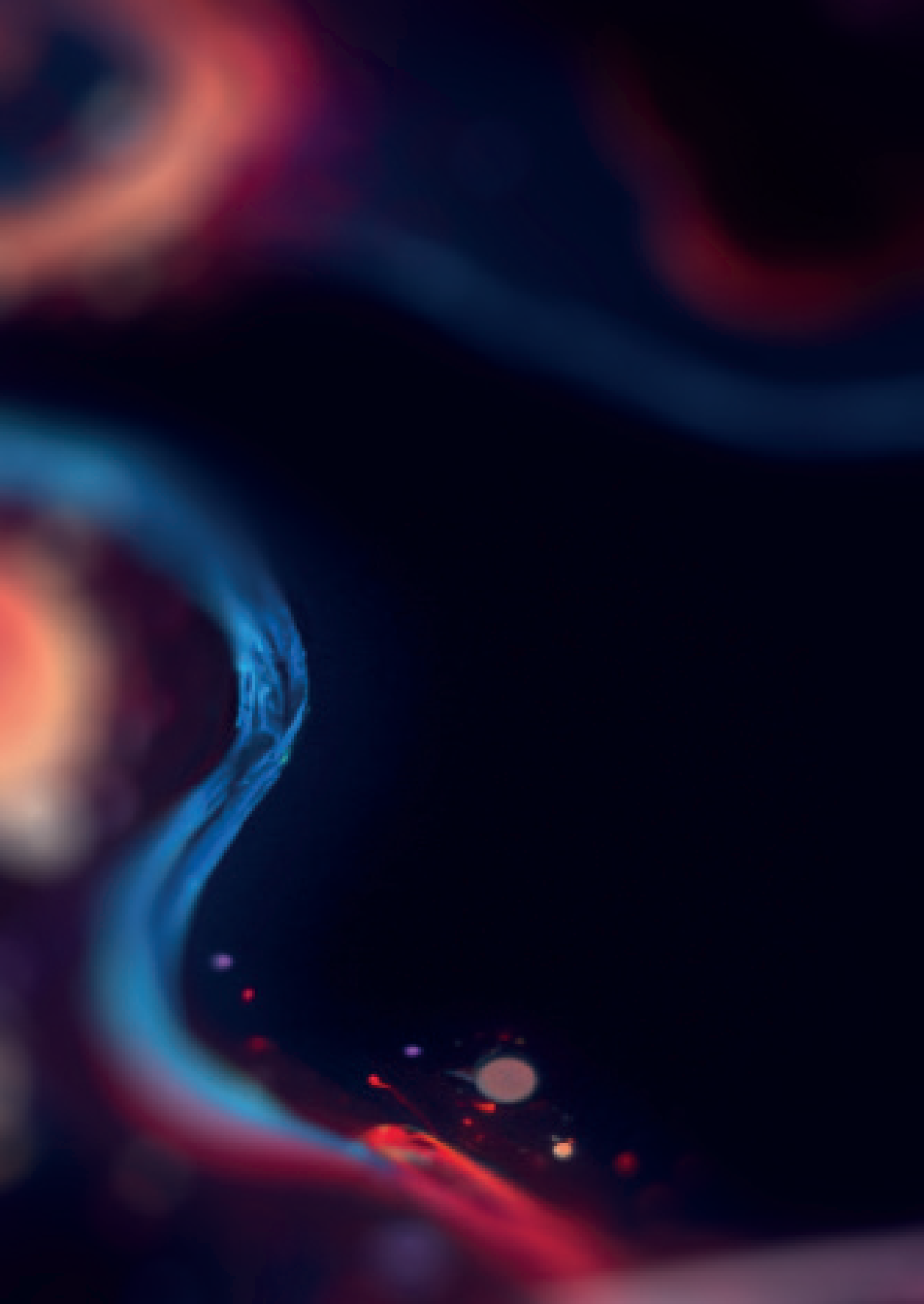
Feature	T-statistic	p-value	FDR	Isomers
L-Cystathionine	5.2951	7.25E-05	0.00543	Allocystathionine; Cysteinyl-Threonine; Threoninyl-Cysteine
Deoxyuridine	5.1423	9.83E-05	0.007055	-
2-Oxoarginine	5.114	0.000104	0.007068	-
4-Nitrocatechol	-5.0979	0.000107	0.007068	-
Phosphoserine	5.0826	0.000111	0.007068	DL-O-Phosphoserine
Guanidinosuccinic acid	5.0233	0.000125	0.007679	-
Propionic acid	4.9611	0.000142	0.008406	Lactaldehyde; D-Lactaldehyde
Gamma Glutamylglutamic acid	4.8727	0.000169	0.009719	-
Glycerol 3-phosphate	-4.7556	0.000215	0.011941	Beta-Glycerophosphoric acid
2-Ketobutyric acid	4.7252	0.000229	0.012309	Acetoacetic acid; 2-Methyl-3-oxopropanoic acid; Succinic acid semialdehyde; (S)-Methylmalonic acid semialdehyde; 4-Hydroxycrotonic acid
Cysteic acid	-4.6848	0.000248	0.012965	-
Homocysteine	-4.6122	0.000288	0.014609	-
Fructose 1,6-bisphosphate	-4.3424	0.000504	0.0248	D-Fructose 2,6-bisphosphate; Alpha-D-Glucose 1,6-bisphosphate; 1D-Myo-inositol 1,4-bisphosphate; 1D-Myo-inositol 1,3-bisphosphate; 1D-Myo-inositol 3,4-bisphosphate; D-Tagatose 1,6-bisphosphate; D-Mannose 1,6-bisphosphate; beta-D-Fructose 1,6-bisphosphate; beta-D-Fructose 1,6-bisphosphate
L-beta-aspartyl-L-glutamic acid	4.2241	0.000645	0.030859	-
4-Aminobutyraldehyde	-4.1155	0.00081	0.037687	-
Selenocysteine	4.0926	0.00085	0.038498	-
Glycerol	-3.9689	0.001102	0.048646	-
Aminoadipic acid	3.9378	0.001176	0.049649	-
L-Glutamic acid 5-phosphate	3.9355	0.001182	0.049649	-
Hydroxybutyrylcarnitine	3.8967	0.001283	0.05259	-
(R)-2-Benzylsuccinate	3.8666	0.001367	0.054733	5-(3',5'-Dihydroxyphenyl)-gamma-valerolactone
Creatinine	-3.8373	0.001454	0.056891	-

Table S1B. Continued

Feature	T-statistic	p-value	FDR	Isomers
Se-Adenosylselenomethionine	-3.7862	0.001619	0.061965	-
Threonic acid	-3.6819	0.002018	0.075542	-
N1-(alpha-D-ribose)-5,6-dimethyl-benzimidazole	-3.5646	0.002585	0.09472	L-phenylalanyl-L-hydroxyproline; Phenylalanyl-Hydroxyproline; Prolyl-Tyrosine; Tyrosyl-Proline
7-Hydroxy-6-methyl-8-ribityl lumazine	-3.5455	0.002692	0.096567	-
Beta-Citryl-L-glutamic acid	3.5079	0.002914	0.10011	-
MG(0:0/22:0/0:0)	3.501	0.002957	0.10011	MG(22:0/0:0/0:0)
1-Undecanol	-3.4998	0.002965	0.10011	-
4-Oxo-2-nonenal	3.4852	0.003058	0.10127	-
L-Threonine	3.3537	0.004035	0.1272	L-Homoserine; L-Allothreonine
2-Phosphoglyceric acid	3.3517	0.004053	0.1272	3-Phosphoglyceric acid; 2-Phospho-D-glyceric acid; (2R)-2-Hydroxy-3-(phosphonatooxy) propanoate
Gamma-Glutamyl Glutamine	3.3506	0.004063	0.1272	Norophthalmic acid
O-Phosphohomoserine	3.3248	0.004289	0.13189	O-Phosphothreonine; Iminoerythrose 4-phosphate
Stevenin	3.3038	0.004483	0.13544	-
L-Serine	3.2872	0.004643	0.13785	D-Serine
Ribitol	-3.2272	0.005268	0.15372	D-Arabitol; L-Arabitol
5-phosphonoxy-L-lysine	3.2193	0.005356	0.15372	-

Table S2. Isobaric compounds untargeted DI-HRMS analysis of [U-13C]-glucose labeling in MDH1 HEK293 cells corresponding to figures 3,4 and 5.

[Isotopologue]	Assigned HMDB name
Sorbitol	[M+Cl] ⁻ Galactitol [M+Cl] ⁻ ;Sorbitol [M+Cl] ⁻ ;Mannitol [M+Cl] ⁻ ;L-Iditol [M+Cl] ⁻
	[M+6+Cl] ⁻ NA
Ribitol	[M+Cl] ⁻ Ribitol [M+Cl] ⁻ ;D-Arabitol [M+Cl] ⁻ ;L-Arabitol [M+Cl] ⁻
	[M+5+Cl] ⁻ NA
Citrate	[M] ⁻ Citric acid; Isocitric acid; D-threo-Isocitric acid; Diketogulonic acid; 2,3-Diketo-L-gulonate; (1R,2R)-Isocitric acid; D-Glucaro-1,4-lactone
	[M+1] ⁻ NA
	[M+2] ⁻ Succinylacetone [M+Cl] ⁻
	[M+3] ⁻ NA
	[M+4] ⁻ NA
	[M+5] ⁻ NA
	[M+6] ⁻ NA
2-oxoglutarate	[M] ⁻ Oxoglutaric acid; 3-Oxoglutaric acid
	[M+1] ⁻ NA
	[M+2] ⁻ NA
	[M+3] ⁻ NA
	[M+4] ⁻ NA
	[M+5] ⁻ NA
Glutamate	[M] ⁻ L-Glutamic acid; N-Methyl-D-aspartic acid; N-Acetylserine; D-Glutamic acid;L-4-Hydroxyglutamate semialdehyde; DL-Glutamate
	[M+1] ⁻ NA
	[M+2] ⁻ NA
	[M+3] ⁻ NA
	[M+4] ⁻ NA
	[M+5] ⁻ 2H3-Methionine (IS)
Malate	[M] ⁻ L-Malic acid; Malic acid; D-Malic acid
	[M+1] ⁻ NA
	[M+2] ⁻ Senecioic acid [M+Cl] ⁻ ;2-Ethylacrylic acid [M+Cl] ⁻ ;3-Methylbutyrolactone [M+Cl] ⁻
	[M+3] ⁻ NA
	[M+4] ⁻ NA
Aspartate	[M] ⁻ L-Aspartic acid; D-Aspartic acid; Iminodiacetic acid
	[M+1] ⁻ NA
	[M+2] ⁻ NA
	[M+3] ⁻ NA
	[M+4] ⁻ NA
Acetylcarnitine	[M] ⁺ L-Acetylcarnitine
	[M+2] ⁺ NA



Chapter 6

Untargeted metabolic profiling in dried blood spots identifies disease fingerprint for pyruvate kinase deficiency

Birgit van Dooijeweert^{1,2*}, Melissa H. Broeks^{3*}, Nanda M. Verhoeven-Duif³, Eduard J. van Beers⁴, Edward E.S. Nieuwenhuis², Wouter W. van Solinge¹, Marije Bartels^{2,4}, Judith J.M. Jans³ & Richard van Wijk¹

¹ Central Diagnostic Laboratory-Research, University Medical Center Utrecht, Utrecht, The Netherlands.

² Department of Pediatric Hematology, University Medical Center Utrecht, Utrecht, The Netherlands.

³ Section Metabolic Diagnostics, Department of Genetics, University Medical Center Utrecht, Utrecht, The Netherlands.

⁴ Van Creveldkliniek, University Medical Center Utrecht, Utrecht, The Netherlands.

*These authors contributed equally to this work

ABSTRACT

The diagnostic evaluation and clinical characterization of rare hereditary anemia (RHA) is to date still challenging. In particular, there is little knowledge on the broad metabolic impact of many of the molecular defects underlying RHA. In this study we explored the potential of untargeted metabolomics to diagnose a relatively common type of RHA: Pyruvate Kinase Deficiency (PKD). In total, 1903 unique metabolite features were identified in dried blood spot samples from 16 PKD patients and 32 healthy controls. A metabolic fingerprint was identified using a machine learning algorithm, and subsequently a binary classification model was designed. The model showed high performance characteristics (AUC: 0.990, 95% CI: 0.981-0.999) and an accurate class assignment was achieved for all newly added control ($n = 13$) and patient samples ($n = 6$), with the exception of one patient (accuracy 94%). Important metabolites in the metabolic fingerprint included glycolytic intermediates, polyamines and several acyl carnitines. In general, the application of untargeted metabolomics in dried blood spots is a novel functional tool that holds promise for diagnostic stratification and studies on disease pathophysiology in RHA.

Key points:

- We identified a metabolic fingerprint for patients with Pyruvate Kinase Deficiency using untargeted metabolomics in dried blood spots.
- This approach opens up a novel area of diagnosis and research in the field of red blood cell disorders.

INTRODUCTION

The group of rare hereditary anemias (RHA) includes a large variety of intrinsic defects of red blood cells and erythropoiesis. Our knowledge of the pathophysiology of RHA has recently vastly improved, powered by genetic testing and subsequent increased knowledge of underlying molecular defects.¹⁻⁴ However, in a substantial number of patients, the clinical phenotype does not fit classical disease criteria, the response to therapy is unexpectedly poor, or a molecular defect cannot be identified.⁵⁻⁷ In addition, in patients with well-described genetic defects, there is often no clear genotype-phenotype correlation.⁷⁻⁹

Pyruvate kinase deficiency (PKD, OMIM #266200), the most common red cell glycolytic enzyme defect, is no exception in this respect. The clinical phenotype of PKD varies widely, from well-compensated hemolytic anemia to severe hemolysis and neonatal mortality. Currently, the diagnosis of PKD relies on the measurement of PK activity and/or the identification of homozygous or compound heterozygous mutations in the *PKLR* gene.^{10,11} However, in a significant number of patients only one mutation is identified. In addition, the exact mechanisms leading to reduced lifespan of PK-deficient erythrocytes are still largely unknown. Thus, in order to improve the diagnostic evaluation as well as our understanding of PKD pathophysiology and the genotype-to-phenotype correlation, novel functional tests are needed. In this study we demonstrate the potential of untargeted metabolomics in dried blood spots (DBS) in the diagnostic evaluation of PKD and report for the first time a metabolic fingerprint for PKD.

METHODS

Samples

Sixteen patients diagnosed with PKD based on clinical phenotype, enzyme activity assays and molecular defect were included. Healthy controls (HC, from an institutional blood donor service) served as controls. All patients or their legal guardians approved the use of remnant samples for method development and validation, in agreement with institutional and national regulations. All procedures followed were in accordance with the ethical standards of the University Medical Center Utrecht and with the Helsinki Declaration of 1976, as revised in 2000. For DBS, 50 μ L aliquots were spotted onto Guthrie card filter paper (Whatman™ 903 Protein Saver Cards). All papers were left to dry for at least four hours at room temperature, and subsequently stored at -80°C in a foil bag with a desiccant package pending further analysis.

Metabolic profiling

Sample preparation, direct infusion high resolution mass spectrometry (DI-HRMS) and data processing was performed as previously reported.^{12,13} Mass peak intensities for metabolite annotation were averaged over technical triplicates. In addition, as DI-HRMS is unable to separate isomers, mass peak intensities consisted of summed intensities of these isomers. Metabolite annotation was performed using a peak calling bioinformatics pipeline developed in R programming software, based on the human metabolome database (version 3.6) (<https://github.com/UMCUGenetics/DIMS>).¹⁴ This resulted in 3835 metabolite annotations corresponding to 1903 unique metabolite features.

To compare the metabolic profiles between HC and PKD, mass peak intensities for each identified feature were converted to Z-scores. These scores, based on metabolic control samples that were added to each DI-HRMS run, were calculated by the following formula:

$$Z - score = \frac{(\text{Mass peak intensity of Pt or HC sample} - \text{Mean mass peak intensities of metabolic control samples})}{\text{Standard deviation mass peak intensities of metabolic control samples} \ddagger}$$

* Metabolic controls exist of a batch of banked DBS samples from individuals in whom an inborn error of metabolism (IEM) was excluded after an extensive diagnostic workup.

Data analysis

T-test and multivariate analysis were conducted in MetaboAnalyst.¹⁵ Classification of data was performed in R-software (Version 3.6.1) using the *caret* package, which contains a set of data processing functions that facilitate the generation of predictive models. Support vector machine (SVM) with linear kernel was used for the classification of HC and PKD samples. SVM algorithms use a set of mathematical functions that are defined as the kernel. The function of kernel is to take data as input and transform it into the required form, for example a linear or polynomial kernel. We applied SVM with a linear kernel, the simplest kernel function, to perform the classification of HC and PKD. SVM with linear kernel is a supervised machine learning model that uses a classification method, which is based on mapping the data into a high dimensional space. This allows the separation of two groups of samples into distinctive regions by the identification of a small fraction of samples that separates the groups, also referred to as ‘support vectors’. Separation can be achieved by identifying a separating hyperplane, or decision boundary, between the support vectors.¹⁶ Classification of the test set was determined by projecting each of the new samples into this space. Data and R code are available upon request.

RESULTS

Explorative untargeted metabolomics analysis

A total of 1903 unique metabolite features (and their respective isomers) were analyzed for 16 PKD patients and 32 HC samples. Clinical and laboratory characteristics, and baseline comparison are summarized in Table 1. The most significant differences between groups, identified by a t-test, included glycolytic intermediates like phosphoenolpyruvic acid and 2-/3-phosphoglyceric acid, polyamines (spermidine and spermine) and several acyl carnitines (methylmalonylcarnitine and propionylcarnitine) (Figure 1A). Broad data exploration to assess the variation between samples and separation between groups was performed by unsupervised principal component analysis (PCA) and supervised partial least square discriminant analysis (PLS-DA), the latter taking group label into account as a response variable. Both analyses revealed close clustering of control samples and a more heterogeneous delineation for PKD patients (Figure S1).

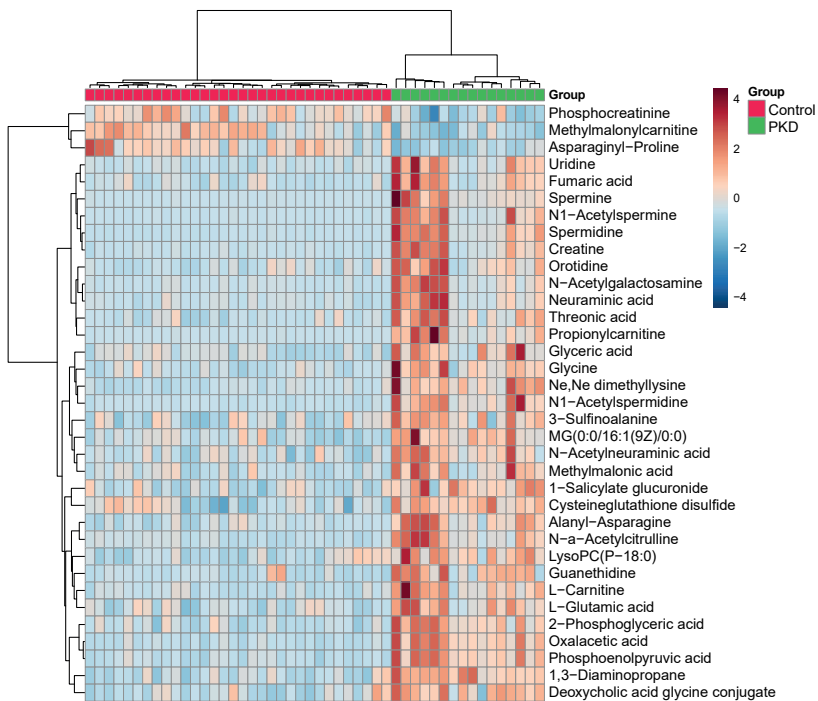
A machine-learning algorithm identifies metabolic profile for PKD

In order to explore the potential of this extensive metabolic fingerprint in predicting PKD a binary classification model was constructed using a support vector machine (SVM) with linear kernel. SVM has advantages over PLS-DA with regard to robustness to outliers, resistance to overfitting and predictive power.¹⁶ An optimal hyperplane to separate classes based on all metabolomics data was determined by cross validation (4-fold, five repeats). The final model had high performance characteristics with an average accuracy of 96%. In addition, receiver operator characteristic curves with area under the curve (AUC) were used as performance indicator (Figure S2A). Important features for classification in this model include the polyamines spermidine and spermine, as well as phosphoenolpyruvic acid, 2-/3-phosphoglyceric acid and glutathione (Figure 1B). Most of these features were increased in PKD, with the exception of glutathione and asparaginy-proline/prolyl-asparagine (Figure 1C).

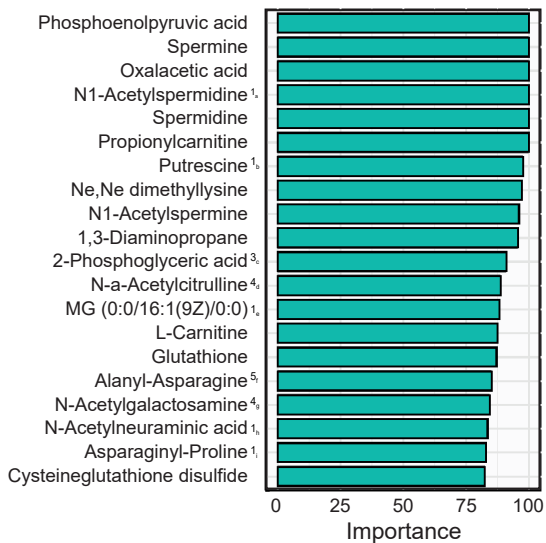
Metabolic profile predicts new samples with high accuracy

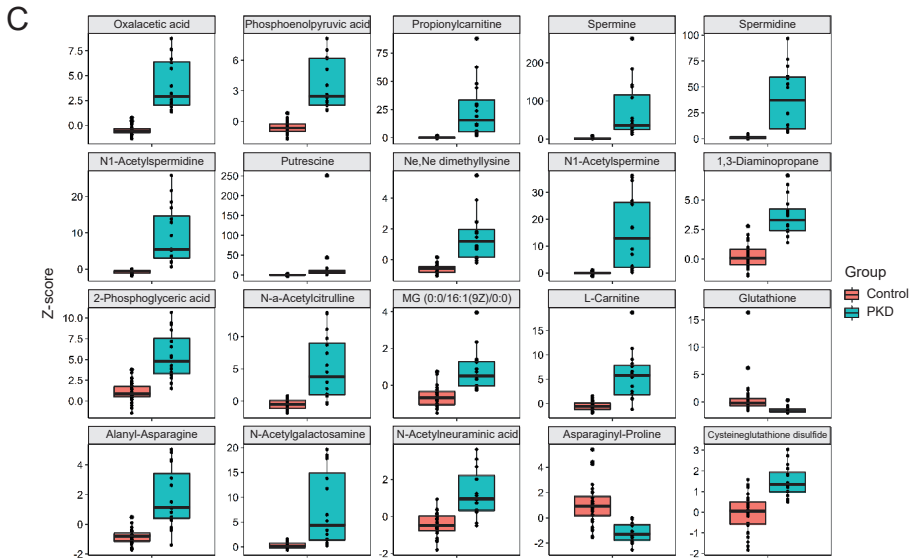
External model validation was performed by predicting new control ($n = 13$) and PKD samples ($n = 6$). This resulted in accurate prediction for all controls, and all but one patient (accuracy = 94%) (Figure 1D). In order to assess uncertainty of the model and its predictive ability, bootstrap resampling was applied to the complete dataset. By randomly generating training and validation (test) data from the original data, a similarly high prediction performance was achieved, supporting the validity of the presented model (Figure S2B).

A



B





D

		Predicted	
		HC	PKD
Reference	n=19 HC	13	0
	PKD	1	5

Figure 1. Univariate and multivariate analysis of untargeted metabolomics data from pyruvate kinase deficiency patients and healthy controls. **A.** Heatmap of top 35 significant features identified by t-test (p -value cutoff = 0.05). The heatmap was created using Euclidean ward clustering with autoscaling of features. **B.** Top 20 important features represented as percentage identified by support vector machine classification. As isomers could not be distinguished using direct infusion high resolution mass spectrometry, the annotated numbers near the important features indicate the amount of isomers. In addition, letters in the footnote correspond to the following isomers: a) N8-acetylspermidine, b) 1,4-butanediammonium, c) 3-phosphoglyceric acid; 2-phospho-D-glyceric acid; (2R)-2-hydroxy-3-(phosphonatoxy)propanoate, d) alanyl-glutamine; alanyl-gamma-glutamate; glutaminy-alanine; gamma-glutamyl-alanine, e) MG(16:1(9Z)/0:0/0:0), f) asparaginy-alanine; glutaminy-glycine; glycy-glutamine; glycy-gamma-glutamate; gamma-glutamyl-glycine, g) N-acetyl-D-glucosamine; Beta-N-acetylglucosamine; N-acetyl-b-D-galactosamine; N-acetylmannosamine, h) N-acetyl-a-neuraminic acid, i) prolyl-asparagine. **C.** Boxplots of each feature showing Z-scores for control and pyruvate kinase deficiency (PKD) groups, respectively. **D.** Confusion matrix for the prediction of additional samples by the SVM model.

Table 1. Clinical characteristics of pyruvate kinase deficiency patients and baseline comparison to healthy controls. A. Clinical characteristics of pyruvate kinase deficiency (PKD) patients regarding age, gender, hemoglobin (Hb), red blood cell count (RBC), reticulocyte count (Retics), white blood cell count (WBC), platelets (Plts), treatment and genetic diagnostics. Regular transfusions are defined as ≥ 6 per 12 months. ND: not determined. **B.** Comparison of age, Hb, Retics and time between blood withdrawal and spotting (time to dried blood spots (DBS)) between healthy controls (HC) and PKD patients. Data are presented as mean \pm standard deviation, except for time to DBS which is presented as the median.

Age (yrs)	Gender	Hb (mmol/L)	RBC ($\times 10^{12}/L$)	Retics ($\times 10^9/L$)	WBC ($\times 10^9/L$)	Plts ($\times 10^9/L$)
65	female	6.4	2.84	1014	7.3	576
2	female	4.8	2.59	343	13.4	345
6	female	6.6	3.79	431	10.6	645
51	female	9.1	5.26	37.8	4.97	188
28	male	5.0	2.27	1011	21.1	ND
29	female	6.3	2.99	180	7.1	239
23	female	6.3	2.52	ND	10.0	696
35	male	6.2	3.45	198	5.5	179
48	female	4.1	1.79	694	9.8	657
25	male	8.4	3.76	627	12.4	732
48	male	5.4	2.18	945	13.1	876
21	male	7.2	3.60	181	5.5	245
51	female	5.6	2.86	950	12.3	719
24	male	ND	ND	ND	ND	ND
20	female	7.2	3.60	112	6.4	186
46	male	7.6	3.74	204	6.0	327
Normal range*		7.4-10.7	3.6-5.5	25-120	4.0-13.5	150-450

*Age- and gender-dependent; **A third and rare mutation (c. 1639C>T; p(Arg547Cys)) with uncertain pathogenicity was identified in this patient.

B. Baseline comparison	PKD	HC
Age (years)	32.6 \pm 17.4	38.9 \pm 12.8
Hb (mmol/L)	6.41 \pm 1.35	9.12 \pm 0.7
Retics ($\times 10^9/L$)	494.8 \pm 367.5	58.6 \pm 22.4
Median time to DBS (hours)	2.33	2.21

Treatment	Allele 1	Allele 2
splenectomy; no current treatment	c.1178A>G; p.(Asn393Ser)	not identified
regular transfusions	c.331G>A; p.(Gly111Arg)	c.331G>A; p.(Gly111Arg)
splenectomy; sporadic transfusion	c.331G>A; p.(Gly111Arg)	c.331G>A; p.(Gly111Arg)
no current treatment	c.1456C>T; p.(Arg486Trp)	c.1529G>A; p.(Arg510Gln)
splenectomy; sporadic transfusion	c.1073G>A; p.(Gly358Glu)	c.1073G>A; p.(Gly358Glu)
no current treatment	c.142_159del; p.(Thr48_Thr53 del)	c.1269G>A; p.(?)
splenectomy; no current treatment	c.1269G>A; p.([Met373_ Ala423del;0])	c.1654G>A; p.(Val553Met)
no current treatment	c.194T>C; p.(Met65Thr)	c.721G>T; p.(Glu241*)
splenectomy; no current treatment	c.1462C>T; p.(Arg488*)	c.1529G>A; p.(Arg510Gln)
splenectomy; no current treatment	c.142_159del; p.(Thr48_Thr53 del)	c.494G>T(p.Gly165Val)
splenectomy; no current treatment	c.376-2A>C; p.(?)	c.1529G>A; p.(Arg510Gln)
no current treatment	c.390_392het_delCAT; p.(Ile131del)	c.1456C>T; p.(Arg486Trp)
splenectomy; regular transfusions	c.507+1G>A; p.[=;0]	c.1436G>A; p.(Arg479His)
splenectomy; no current treatment	c.694G>T; p.(Gly232Cys)	c.1529G>A; p.(Arg510Gln)
regular transfusions	c.1529G>A; p.(Arg510Gln)	c.1705C>T; p.(Arg569Trp)**
no current treatment	c.1121T>C; p.(Leu374Pro)	c.1706G>A; p.(Arg569Glu)

Metabolic profiles reflect PKD disease severity

In order to explore the heterogeneity of PKD metabolic profiles in relation to clinical phenotype, PCA and PLS-DA were performed for the entire group of patients and controls. Based on presence of spleen and transfusion frequency phenotypes were distinguished as mild, moderate and severe. Most resemblance to controls in metabolic profile was clear for mild phenotypes, followed by severely affected patients (Figure S3).

DISCUSSION

In this study we performed untargeted metabolomics on DBS and report for the first time a metabolic disease fingerprint for PKD. By establishing a predictive machine learning model, the diagnostic potential of this approach was demonstrated. This metabolic fingerprint has potential to mature into a powerful clinical tool, capable of confirming or ruling out the diagnosis of PKD. However, the limitations of machine learning models were also demonstrated by the incorrect classification of one PKD patient who was homozygous for the common p.(Arg510Gln) mutation.¹⁷ Clinically, this patient exhibited very mild phenotypic features. As confirmed by the clinical severity PLS-DA, patients with a mild phenotype and controls overlap most in their DBS metabolome (Figure S3). Since approximately 30% of the initial cohort consists of such mildly affected patients, this could further explain why PCA and PLS-DA were unable to achieve separation between groups.

Interestingly, severely affected patients who are heavily transfused (>6 erythrocyte transfusions in the past 12 months) despite having undergone a splenectomy, still showed a clearly distinctive metabolic profile compared to HC and two of them were furthermore correctly assigned as patients (Figure 1D, Table S1). Although numbers are modest and further studies are needed, this indicates that this approach is reliable even in the setting of transfusions.

Our approach using untargeted metabolomics provides novel insights regarding the broad metabolic impact of PKD that could be relevant to better understand the etiology of PKD-related symptoms. While glycolytic metabolites and their disturbance have been characterized to some extent, little is known regarding the broad scale impact of PKD on metabolism. In this respect, the identification of novel distinctive metabolites, such as polyamines, which have been found to stabilize the red blood cell (RBC) plasma membrane,¹⁸ and acyl carnitines, which are involved in turnover and repair of the RBC membrane,¹⁹ are promising starting points for further studies of the PKD pathophysiology.

We here report for the first time a metabolic profile for PKD obtained from dried whole blood spots. This profile resembles the integrated disease specific metabolome to a greater extent compared to the exclusive investigation of the RBC metabolome.^{20,21} In addition, this analysis requires only 50 μ L of whole blood and can be obtained in a minimally invasive manner by sampling a single blood drop, making it very attractive for (international) sample exchange. Further advantages of DI-HRMS include relatively uncomplicated sample extraction steps and a short run-time of 3 minutes per sample.

The rise of 'omic' approaches in the recent past has provided new opportunities for understanding and classifying a wide range of disorders. In contrast to conventional medical biology approaches, which focus on individual genes, proteins or metabolites, modern biology regards diseases as a complex, dynamic and especially integrated network.²² Our study, demonstrates the potential diagnostic application of untargeted metabolomics for PKD. However, the current model was constructed for the binary classification of healthy controls and PKD patients. Future applications, including more samples from various types of RHA could enable development of an algorithm which is suited for the broader differential diagnosis of RHA in patients.

In conclusion, we demonstrate by proof of principle for PKD, that untargeted metabolomics in DBS is a novel functional tool to identify disease fingerprints and study pathophysiology in RHA. This approach opens up a novel area of diagnosis and research in the field of RBC disorders and has the potential to improve diagnostic evaluation and clinical management of patients.

Disclosures

EvB receives research funding from Agios Pharmaceuticals, Novartis, Bayer, Pfizer and RR Mechatronics, does consultancy for Agios Pharmaceuticals, Novartis and is on the data safety monitoring board for Imara; RvW receives research funding from RR Mechatronics and Agios Pharmaceuticals. The other authors report no relevant conflicts of interest

Contributions

BvD and MBr contributed to collection, analysis and interpretation of the data, and wrote the first draft of the manuscript; EvB was actively involved in collecting patient samples and carefully revised the manuscript; WvS, EN and NV were all involved in the study design and carefully revised the manuscript; MBa, JJ and RvW were principal investigators and were involved in all aspects of the study, including design, collection, and interpretation of data, as well as revising and co-writing the manuscript.

Acknowledgements

The authors thank Nienke van Unen for her technical support in Bio-informatics.

Funding

This study was supported in part by research funding from Metakids (Grant No. 2017-075) to JJ.

REFERENCES

1. Da Costa L, Narla A, Mohandas N. An update on the pathogenesis and diagnosis of diamond-blackfan anemia. *F1000Research*. 2018;7(F1000 Faculty Rev):1350.
2. Grace RF, Zanella A, Neufeld EJ, et al. Erythrocyte pyruvate kinase deficiency: 2015 status report. *Am J Hematol*. 2015;90(9):825-830.
3. Albuissou J, Murthy SE, Bandell M, et al. Dehydrated hereditary stomatocytosis linked to gain-of-function mutations in mechanically activated PIEZO1 ion channels. *Nat Commun*. 2013;4:1884.
4. Roy NBA, Babbs C. The pathogenesis, diagnosis and management of congenital dyserythropoietic anaemia type I. *Br J Haematol*. 2019;185(3):436-449.
5. Vercellati C, Marcello AP, Fermo E, Barcellini W, Zanella A, Bianchi P. A case of hereditary spherocytosis misdiagnosed as pyruvate kinase deficient hemolytic anemia. *Clin Lab*. 2013;59(3-4):421-424.
6. Steinberg-Shemer O, Keel S, Dgany O, et al. Diamond Blackfan Anemia: A Nonclassical Patient With Diagnosis Assisted by Genomic Analysis. *J Pediatr Hematol Oncol*. 2016;38(7):e260-e262.
7. Russo R, Andolfo I, Manna F, et al. Multi-gene panel testing improves diagnosis and management of patients with hereditary anemias. *Am J Hematol*. 2018;93(5):672-682.
8. van Dooijeweert B, van Ommen CH, Smiers FJ, et al. Pediatric Diamond-Blackfan anemia in the Netherlands: An overview of clinical characteristics and underlying molecular defects. *Eur J Haematol*. 2018;100(2):163-170.
9. Zanella A, Fermo E, Bianchi P, Chiarelli LR, Valentini G. Pyruvate kinase deficiency: the genotype-phenotype association. *Blood Rev*. 2007;21(4):217-231.
10. Grace RF, Bianchi P, van Beers EJ, et al. Clinical spectrum of pyruvate kinase deficiency: data from the Pyruvate Kinase Deficiency Natural History Study. *Blood*. 2018;131(20):2183-2192.
11. Bianchi P, Fermo E, Glader B, et al. Addressing the diagnostic gaps in pyruvate kinase deficiency: Consensus recommendations on the diagnosis of pyruvate kinase deficiency. *Am J Hematol*. 2019;94(1):149-161.
12. Haijes HA, Willemsen M, van der Ham M, et al. Direct infusion based metabolomics identifies metabolic disease in patients' dried blood spots and plasma. *Metabolites*. 2019;9(1):12.
13. de Sain-van der Velden MGM, van der Ham M, Gerrits J, et al. Quantification of metabolites in dried blood spots by direct infusion high resolution mass spectrometry. *Anal Chim Acta*. 2017;979:45-50.
14. Wishart DS, Jewison T, Guo AC, et al. HMDB 3.0-The Human Metabolome Database in 2013. *Nucleic Acids Res*. 2013;41(D1):D801-D807.
15. Chong J, Wishart DS, Xia J. Using MetaboAnalyst 4.0 for Comprehensive and Integrative Metabolomics Data Analysis. *Curr Protoc Bioinforma*. 2019;68(1):e86.
16. Gromski PS, Muhamadali H, Ellis DI, et al. A tutorial review: Metabolomics and partial least squares-discriminant analysis - a marriage of convenience or a shotgun wedding. *Anal Chim Acta*. 2015;879:10-23.
17. Bianchi P, Fermo E, Lezon-Geyda K, et al. Genotype-phenotype correlation and molecular heterogeneity in pyruvate kinase deficiency. *Am J Hematol*. 2020;95(5):472-482.
18. Ballas SK, Mohandas N, Marton LJ, Shohet SB. Stabilization of erythrocyte membranes by polyamines. *Proc Natl Acad Sci U S A*. 1983;80(7):1942-1946.
19. Arduini A, Mancinelli G, Radatti GL, Dottori S, Molajoni F, Ramsay RR. Role of carnitine and carnitine palmitoyltransferase as integral components of the pathway for membrane phospholipid fatty acid turnover in intact human erythrocytes. *J Biol Chem*. 1992;267(18):12673-12681.
20. Darghouth D, Koehl B, Madalinski G, et al. Pathophysiology of sickle cell disease is mirrored by the red blood cell metabolome. *Blood*. 2011;117(6):e57-66.

21. Darghouth D, Koehl B, Heilier JF, et al. Alterations of red blood cell metabolome in overhydrated hereditary stomatocytosis. *Haematologica*. 2011;96(12):1861-1865.
22. Tebani A, Afonso C, Marret S, Bekri S. Omics-based strategies in precision medicine: Toward a paradigm shift in inborn errors of metabolism investigations. *Int J Mol Sci*. 2016;17(9):1555.

SUPPLEMENTARY MATERIAL

Table S1. Clinical characteristics of additional pyruvate kinase deficiency patients in test-cohort. Clinical characteristics of pyruvate kinase deficiency (PKD) patients regarding age, gender, hemoglobin (Hb), red blood cell count (RBC), reticulocyte count (Retics), white blood cell count (WBC), platelets (Plts), treatment and genetic diagnostics. Regular transfusions are defined as ≥ 6 per 12 months. The patient who was classified incorrectly as control in the machine-learning model (Figure 1D) is shown in italics.

Age (yrs)	Gender	Hb (mmol/l)	RBC ($\times 10^{12}/L$)	Retics ($\times 10^9/L$)	WBC ($\times 10^9/L$)	Plts ($\times 10^9/L$)	Treatment	Allele 1	Allele 2
43	female	5.5	2.20	1045	11.6	714	splenectomy; no current treatment	c.401T>A; p.(Val134Asp)	c.1529G>A; p.(Arg510Gln)
44	female	5.7	2.75	756	9.3	841	splenectomy; regular transfusions	c.283G>A; p.(Gly95Arg)	c.401T>A; p.(Val134Asp)
32	female	6.5	3.49	338	9	464	splenectomy; regular transfusions	c.283G>A; p.(Gly95Arg)	c.401T>A; p.(Val134Asp)
26	male	5.0	2.33	930	15.7	780	splenectomy; sporadic transfusion	c.721C>T; p.(Glu241*)	c.1529G>A; p.(Arg510Gln)
4	<i>female</i>	7.6	4.00	194	7.8	275	<i>no current treatment</i>	<i>c.1529G>A; p.(Arg510Gln)</i>	<i>c.1529G>A; p.(Arg510Gln)</i>
54	male	6.2	3.08	166	5.3	150	no current treatment	c.142_159del; p.(Thr48_Thr53 del)	c.376-2A>C; p.(?)
Normal range*		7.4-10.7	3.6-5.5	25-120	4.0-13.5	150-450			

*Age- and gender-dependent

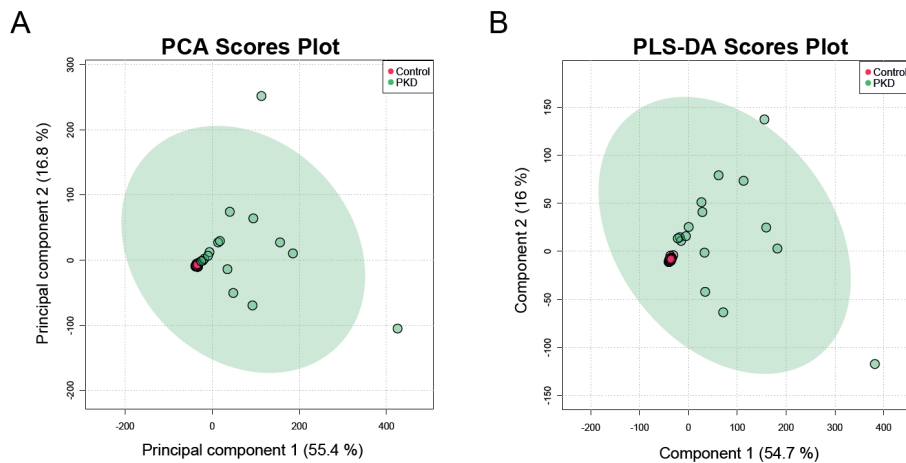


Figure S1. Score plots for principal component analysis and partial least square discriminant analysis of metabolic profiles from pyruvate kinase deficiency and control groups. **A.** Principal component analysis (PCA) of the metabolic profiles from pyruvate kinase deficiency (PKD) patients and control groups. **B.** Partial least square discriminant analysis (PLS-DA) of the metabolic profiles from PKD patients and control groups.

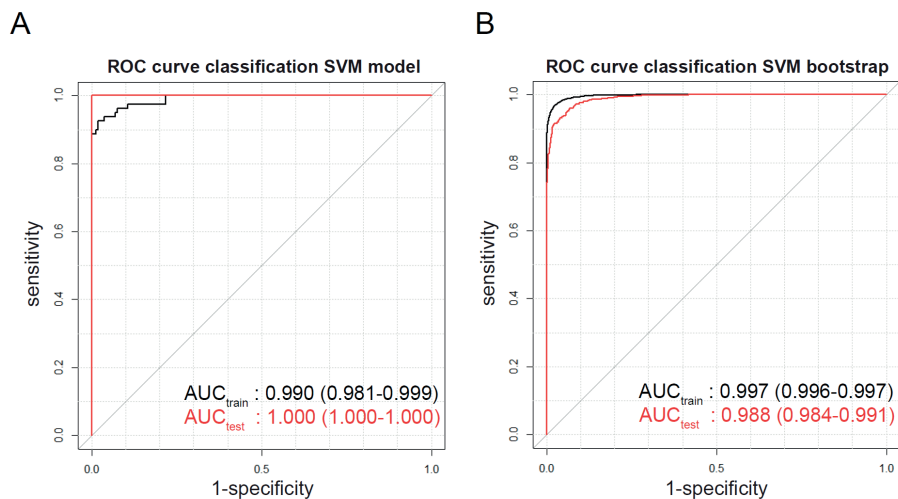


Figure S2. Receiver Operator Characteristic curves (ROC) for classification of training and test sets by support vector machine models. **A.** Classification performance of samples in training and test set according to AUC. Note that AUC is a measure of the ability to rank samples according to the probability of class membership, meaning that even falsely classified samples can have a higher rank towards the correct class compared to other samples. **B.** Classification performance of samples in bootstrap models ($n=100$) based on the complete data set.

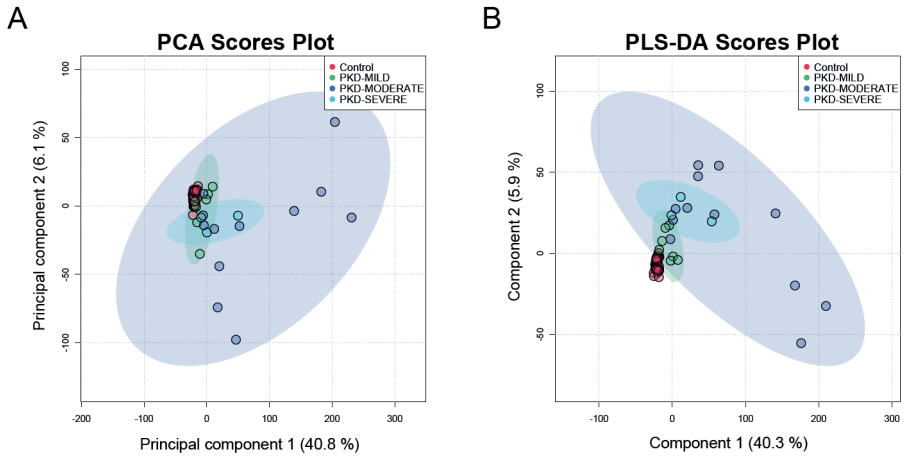
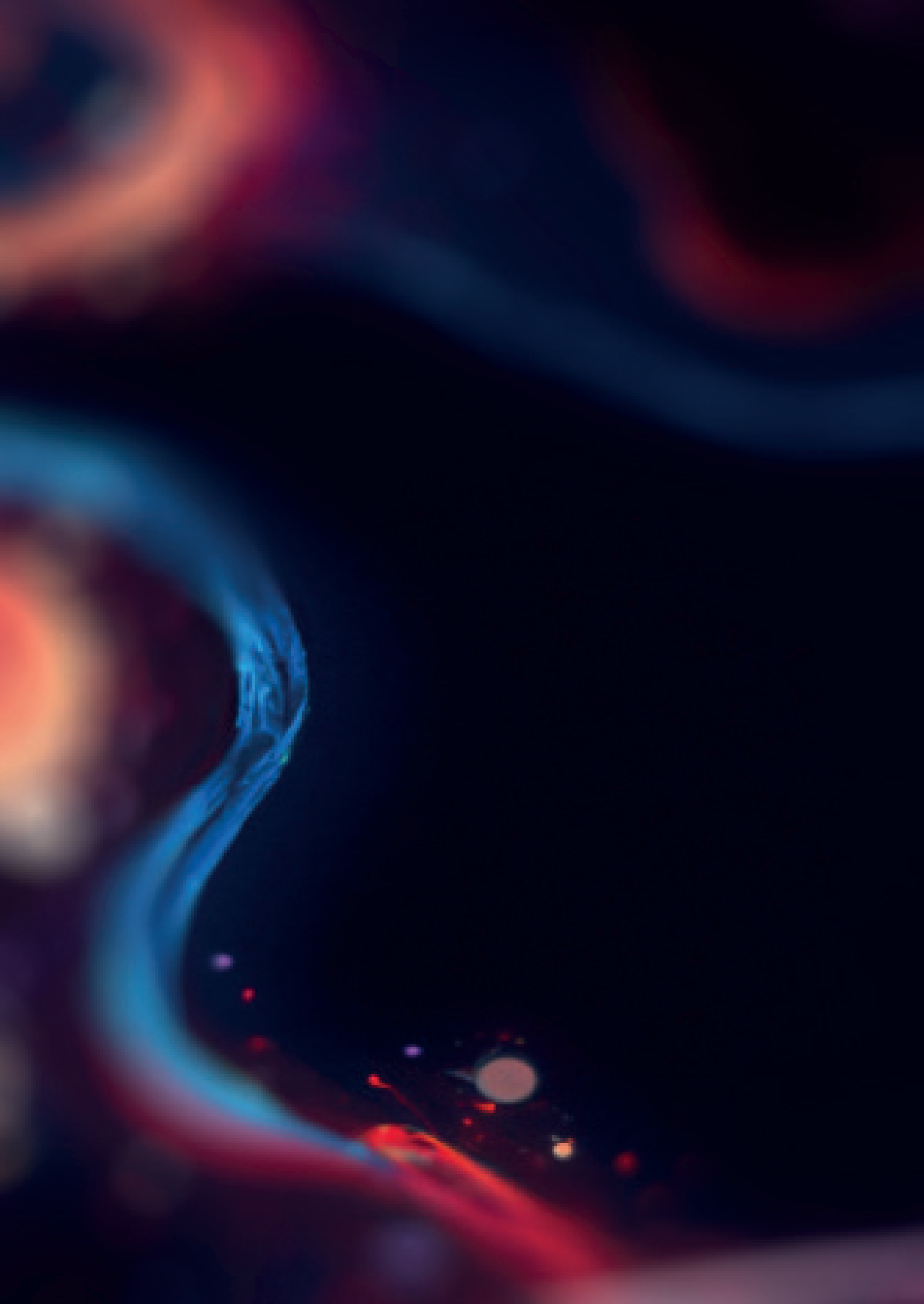


Figure S3. Multivariate analysis with distinction of phenotype severity. **A.** Principal component analysis (PCA) plot, and **B.** partial least squares discriminant analysis (PLS-DA) plot of metabolic profiles distinguishing between disease phenotypes based on transfusion dependence and splenectomy. The resemblance in metabolic profile to controls is most clear for mild phenotypes, followed by severely affected phenotypes from pyruvate kinase deficiency (PKD) patients (possibly related to interference of frequent transfusions).



Chapter 7

Dried blood spot metabolomics reveals a metabolic fingerprint with diagnostic potential for Diamond Blackfan anaemia

Birgit van Dooijeweert^{1,2*}, Melissa H. Broeks^{3*}, Eduard J. van Beers⁴,
Nanda M. Verhoeven-Duif³, Wouter W. van Solinge¹, Edward E.S. Nieuwenhuis²,
Judith J. Jans³, Richard van Wijk¹ & Marije Bartels^{2,4}

¹ Central Diagnostic Laboratory-Research, University Medical Center Utrecht, Utrecht, The Netherlands.

² Department of Pediatric Hematology, University Medical Center Utrecht, Utrecht, The Netherlands.

³ Section Metabolic Diagnostics, Department of Genetics, University Medical Center Utrecht, Utrecht, The Netherlands.

⁴ Van Creveldkliniek, University Medical Center Utrecht, Utrecht, The Netherlands.

*These authors contributed equally to this work

ABSTRACT

The diagnostic evaluation of Diamond Blackfan anaemia (DBA), an inherited bone marrow failure syndrome characterized by erythroid hypoplasia, is challenging because of a broad phenotypic variability and the lack of functional screening tests. In this study we explored the potential of untargeted metabolomics to diagnose DBA. In dried blood spot samples from 18 DBA patients and 40 healthy controls, a total of 1752 unique metabolite features were identified. This metabolic fingerprint was incorporated into a machine learning algorithm, and a binary classification model was constructed using a training set. The model showed high performance characteristics (average accuracy 91.9%) and correct prediction of class was observed for all controls ($n = 12$) and all but one patient ($n = 4/5$) from the validation or 'test' set (accuracy 94%). Importantly, in patients with congenital dyserythropoietic anaemia (CDA) - an erythroid disorder with overlapping features - we observed a distinct metabolic profile, indicating the disease specificity of the DBA fingerprint and underlining its diagnostic potential. Furthermore, when exploring phenotypic heterogeneity, DBA treatment subgroups yielded discrete differences in metabolic profiles, which could hold future potential in understanding therapy responses. Our data demonstrate that untargeted metabolomics in dried blood spots is a promising new diagnostic tool for DBA.

Keywords: untargeted metabolomics, Diamond Blackfan Anaemia, disease fingerprint, dried blood Spots, machine-learning algorithm

INTRODUCTION

Diamond Blackfan Anaemia (DBA, OMIM #105650) is a rare inherited bone marrow failure syndrome (IBMFS) characterized by erythroid hypoplasia, congenital malformations (~50%), growth defects and an increased risk of developing malignancies.¹⁻³ From a clinical and genetic perspective the disorder is highly heterogeneous, and clear genotype-phenotype correlations are absent. Since the majority of molecular defects have been found in ribosomal protein (RP) genes, resulting in impaired ribosome biogenesis, DBA is regarded a 'ribosomopathy'.^{4,5} While its genetic basis has been studied intensively, the pathophysiology of DBA is still not fully understood. One of the major unresolved issues is how RP gene mutations result in the specific erythroid defect that characterizes DBA.⁶

Establishing the diagnosis of DBA can be particularly difficult since, in contrast to other IBMFS, no validated functional screening tests exists. Furthermore, the clinical presentation is highly heterogeneous, even within families who share a molecular defect.^{7,8} Currently, the diagnosis relies on consensus criteria and exclusion of other IBMFs and causes of anaemia. The consensus criteria include age (i.e. presentation in the first year of life), macrocytic anaemia, reticulocytopenia and normal marrow cellularity with a paucity of erythroid precursors. Alternative criteria that confirm or support the diagnosis include the identification of a known molecular defect, elevated erythrocyte adenosine deaminase activity and elevated levels of foetal haemoglobin.⁹ In order to improve the diagnostic evaluation of DBA as well as our understanding of phenotypic heterogeneity and clinical severity, novel functional approaches are needed. One such tool might be metabolomics - the large scale, unbiased study of metabolites which directly reflects the biochemical activity and state of a sample - and thereby represents the cellular phenotype.¹⁰ Here we identify and report for the first time on a metabolic fingerprint for DBA using untargeted metabolomics in dried blood spots, and demonstrate the potential of this approach in the diagnostic evaluation of DBA.

METHODS

Patients and samples

Eighteen patients diagnosed with DBA were included. Diagnosis in all patients was based on a combination of the widely used consensus and supporting criteria and/or confirmed defects in DBA-associated genes.^{5,9} In addition, six patients diagnosed with the related disorder congenital dyserythropoietic anaemia (CDA) were included for subgroup analysis. Healthy volunteers (from an institutional blood donor service) served as controls (HC). All patients or their legal guardians approved the use of their remnant samples for method development and validation, in agreement with institutional and national regulations. All procedures followed were in accordance with the ethical standards of the University Medical Center Utrecht and with the Helsinki Declaration of 1976, as revised in 2000. Sampling was performed at least three weeks after the last transfusion in transfused patients. For dried blood spots (DBS), 50 µL aliquots were spotted onto Guthrie card filter paper (Whatman™ 903 Protein Saver Cards). All papers were left to dry for at least four hours at room temperature, and were subsequently stored at -80 °C in a foil bag with a desiccant package pending further analysis.

Metabolic phenotyping

Sample preparation, direct infusion high resolution mass spectrometry (DI-HRMS) and data processing were performed as previously reported.^{11–13} Mass peak intensities for metabolite annotations were averaged over technical triplicates. In addition, as DI-HRMS is unable to separate isomers, mass peak intensities consisted of summed intensities of these isomers. Metabolite annotation was performed using a peak-calling bioinformatics pipeline developed in R-programming software, based on the human metabolome database (version 3.6) (<https://github.com/UMCUGenetics/DIMS>).

DBS samples were distributed over several DI-HRMS runs. In each run, an extra set of control samples was included. To compare the metabolic profiles between DBA, CDA and HC, mass peak intensities for each identified feature were converted to Z-scores. These scores, based on the extra control samples, were calculated by the following formula:

$$Z - score = \frac{(\text{Mass peak intensity of Pt or HC sample} - \text{Mean mass peak intensities of metabolic control samples})}{\text{Standard deviation mass peak intensities of metabolic control samples} \ddagger}$$

‡ Metabolic controls exist of a batch of banked DBS samples from individuals in whom an inborn error of metabolism (IEM) was excluded after an extensive diagnostic workup.

Data analysis

Z-scores calculated from multiple DI-HRMS runs were combined in a final dataset. Data analyses were conducted in MetaboAnalyst without further data filtering or normalisation.¹⁴ Outlying metabolite features were identified using the PCA loadings plot. In total, 15 outlying features were removed, culminating in a final dataset of 1765 unique features corresponding to 3541 metabolite annotations.

Classification of data was performed in R-software (Version 3.6.1) using the *'caret'* package. This package contains a set of data-processing functions that facilitate the generation of classification and regression models. In this study, a support vector machine (SVM) with linear kernel[‡] - the simplest kernel function without further data transformation - was used for classifying DBA and HC samples. SVM is a supervised machine-learning model that classifies samples based on the mapping of all data into a high dimensional space, allowing for the separation of two groups of samples into distinct regions by the identification of 'support vectors'. Classification is then achieved by identifying a separating hyperplane - or decision boundary - between support vectors, and projecting new/unclassified samples into this space. For this analysis, additional features with missing values were removed, resulting in 1737 unique features for modelling. Data and R-code are available upon request.

‡ The function of kernel is to take data as input and transform it into the required form, for example a linear or polynomial kernel

RESULTS

Explorative untargeted metabolomics identifies metabolic fingerprint

In total, 1752 unique metabolite features were analysed from DBS samples of 18 patients and 40 controls. Baseline characteristics of patients are summarised in Table 1. The DBA patient cohort was characterised by a female predominance (72%) and a lower median age than the controls (9.19 versus 33.8 years). To determine the variation and distinction between samples and groups (DBA and HC), initial data exploration was performed by principal component analysis (PCA), an unsupervised technique which does not take the group label into account. This demonstrated equally distributed variance in metabolic profiles, with a certain degree of overlap between DBA and HC (Figure 1A).

Furthermore, using univariate t-test analysis, we observed significant differences between groups, including decreased metabolites corresponding in mass to methylmalonylcarnitine (an acyl carnitine), homo-L-arginine, hippuric acid (an acyl

glycine), and lipoic acid (an essential cofactor for mitochondrial enzyme complexes). In addition, we found significantly increased glutamic acid, threonic acid (possibly a metabolite of ascorbic acid (vitamin C)), dodecanedioic acid (a medium-chain fatty acid) and inosine (one of the purine nucleosides) (Figure 1B). We next performed partial least squares discriminant analysis (PLS-DA), a supervised analysis that takes into account the group label. This resulted in clear separation between DBA and HC, thereby confirming distinct metabolic signatures (Figure 1C). Metabolites contributing most to the separation are shown in Figure 1D.

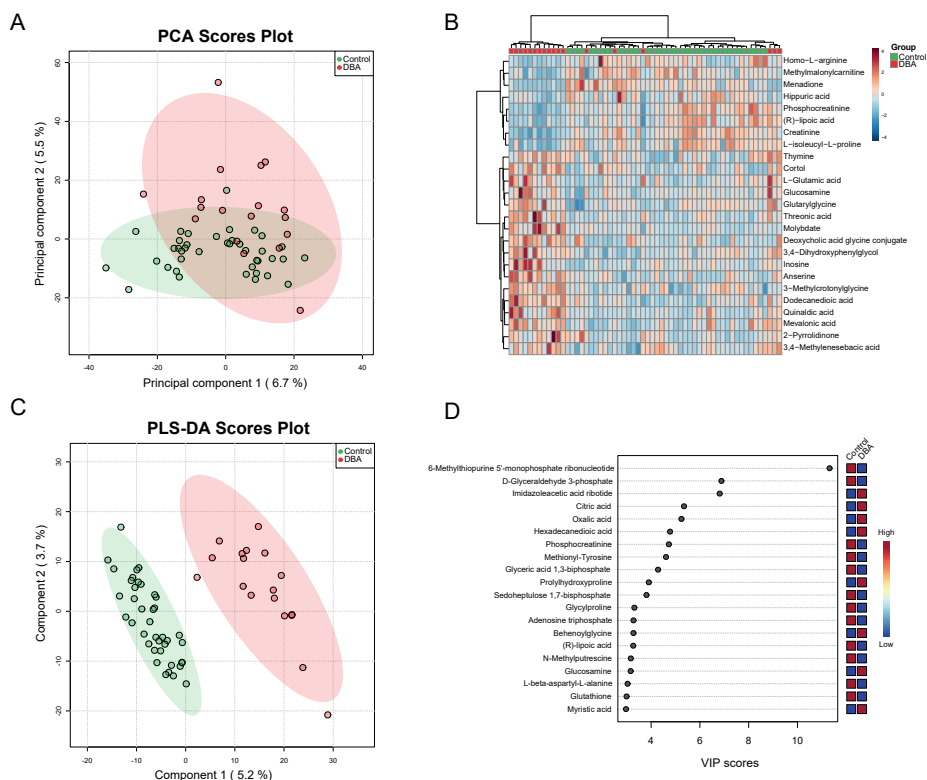


Figure 1. Metabolic fingerprint in DBS of DBA patients. **A.** Principal component analysis (PCA) of Diamond Blackfan Anaemia (DBA) and healthy controls (HC) displayed with 95% confidence regions. **B.** Heatmap of 25 most significant features identified by t-test (raw p-value <0.0001). The heatmap was created using Euclidian ward-clustering with autoscaling of features. A comprehensive overview of p-values and isomers is displayed in supplementary Table S2. **C.** Partial least squares discriminant analysis (PLS-DA) of DBA and HC displayed with 95% confidence regions. **D.** Variable importance in projection (VIP)-scores demonstrating the 25 features contributing the most to separation of patients and controls in the PLS-DA. An overview of VIP-scores and isomers is displayed in supplementary Table S3.

Table 1. A. Clinical characteristics of Diamond Blackfan Anaemia (DBA) patients: age, gender, haemoglobin (Hb), red blood cell count (RBC), reticulocyte count (Retics), mean corpuscular volume (MCV), white blood cell count (WBC), platelets (Plts), treatment and molecular defect. ND: not determined. The patient who was classified incorrectly as control in the machine-learning model (Figure 2A) is shown in italics. **B.** Comparison of age, Hb, Retics and time between blood withdrawal and spotting (time to DBS) between healthy controls (HC) and DBA patients. Data are presented as mean \pm standard deviation, except for time to DBS which is presented as the median.

Age (years)	Gender	Hb (mmol/L)	RBC ($\times 10^{12}/L$)	Retics ($\times 10^9/L$)	MCV (fL)	WBC ($\times 10^9/L$)	Plts ($\times 10^9/L$)	Treatment	Molecular defect
0.7	female	5.4	2.72	50.8	93.1	9.5	508	Transfusions	RPL11; c.396+1G>T; p.(?)
16	female	4.1	1.98	61.7	100	3.8	260	Prednisone (0.17 mg/kg/day)	RPL5; c.493G>T; p.(Gly165*)
4	female	6.2	2.87	15.7	105	14.0	633	Transfusions	RPS26; c.-362_*del
10	male	5.0	2.53	69.4	100	7.1	323	Prednisone (0.18 mg/kg/day)	GATA1; c.220+2T>C; p.(?)
14	female	8.0	3.49	86.3	109	7.3	272	Prednisone (0.06 mg/kg/day)	RPS26; c.95_98dup; p.(Asp333Gluufs*6)
5	male	4.1	1.90	29.5	92	5.0	192	Prednisone (0.5 mg/kg/day)	none identified
18	female	5.4	2.91	17.3	86	4.4	294	Transfusions	RPS26; c.2T>C; p.(Met11Thr)
17	female	6.7	3.16	33.0	102	3.7	183	Prednisone (0.04 mg/kg/day)	none identified
11	female	7.6	3.83	48.3	97	5.9	337	Prednisone (0.07 mg/kg/day)	RPS24; c.*20-2A>G
5	female	7.3	3.61	56.8	93	6.7	379	none	RPS26; c.344T>C; p.(Met115Thr)
2	female	4.3	2.31	5.9	86	8.6	262	Transfusions	RPL5; c.353C>T; p.(Arg179X)
6	male	7.0	3.84	52.3	86	19.0	465	none	RPL9; c.-2+1G>C; p.(?)
4	female	ND	ND	ND	ND	ND	ND	Prednisone (0.5 mg/kg/day)	RPS26; c.3+1G>C; p.(?)
5	male	ND	ND	ND	ND	ND	ND	Transfusions	none identified
1	female	6.5	3.77	70.8	86	11.9	438	none	1p22.1 deletion (incl. RPL5)
0.8	female	4.5	2.43	50.1	89	8.7	240	Transfusions	none identified
21	male	9.6	4.63	58.8	102	3.9	167	none	15q25.2 deletion (incl. RPS17)
25	female	6.9	3.32	81.5	101	4.6	248	none	RPS19; c.167G>C; p.(Arg56Pro)
Normal range*		7.4-10.7	3.6-5.5	25-120	70-97	4.0-13.5	150-450		

*Age- and gender-dependent

Table 1. Continued

	DBA	HC
Age (years)	9.19 ± 7.59	33.8 ± 8.64
Hb (mmol/L)	6.16 ± 1.58	9.07 ± 0.80
Retics (x10 ⁹ /L)	49.3 ± 23.5	60.0 ± 18.4
Time to DBS (hours)	4.56 ± 6.59	4.42 ± 7.45

A machine-learning algorithm enables prediction of DBA with high accuracy

To generate a model that can predict the diagnosis of DBA based on the metabolic profile, the dataset was incorporated into a machine-learning algorithm. Using a support vector machine with a linear kernel, a binary classification model was constructed by randomly dividing patients and controls into a 'training' set (28 HC, 13 DBA) or 'test' set (12 HC, 5 DBA), followed by repeated (internal) cross validation (3-fold, three repeats) to identify the optimal hyperplane separating patients from controls. The final model had high performance characteristics with an average accuracy of 91.9%. In addition, receiver operator characteristic curves with the area under the curve were used as performance indicator (Figure 2A, AUC train: 0.903 (0.827-0.980)). External model validation was performed by predicting the 'new' control and patient samples from the 'test' set (12 HC, 5 DBA) (Figure 2A, AUC test: 0.933 (0.791-1.000)). For the selected final model, this resulted in the accurate prediction of class for 4/5 patients and all controls (accuracy 94.1%, 95% CI: 71.3-0.99.9) (Figure 2B). To assess the uncertainty of the final model and its predictive ability, bootstrap resampling (100 repeats) was applied to the entire dataset, resulting in a similarly high prediction performance (AUC test: 0.930 (0.914-0.946)), and supporting the validity of the presented model (Figure 2C). Important features for classification in this model again included methylmalonylcarnitine, dodecanedioic acid, hippuric acid and glutamic acid (Figure 2D).

DBA and CDA patients show a distinct metabolic profile

To assess disease specificity of the metabolic fingerprint, the DBS-metabolome of six patients with congenital dyserythropoietic anaemia (CDA) - a clinically overlapping disorder of erythropoiesis in which proliferation and differentiation of erythroid precursors is affected - was studied (patient characteristics are shown in Table S1). Although the CDA group was relatively small, a distinct metabolic profile was observed for CDA patients compared to both DBA patients and healthy controls, by natural clustering in the PCA plot (Figure 3A) and evident separation of both patient groups in PLS-DA (Figure 3B). The most significant differences between DBA and CDA,

identified by t-test, are shown in a heatmap in Figure 3C, including an increase in acyl carnitines (stearoylcarnitine, oleoylcarnitine and L-palmitoylcarnitine), riboflavin (a vitamin B2 precursor) and polyamines (spermine, spermic acid 2, spermidine and N1-acetylspermidine) in the CDA patients.

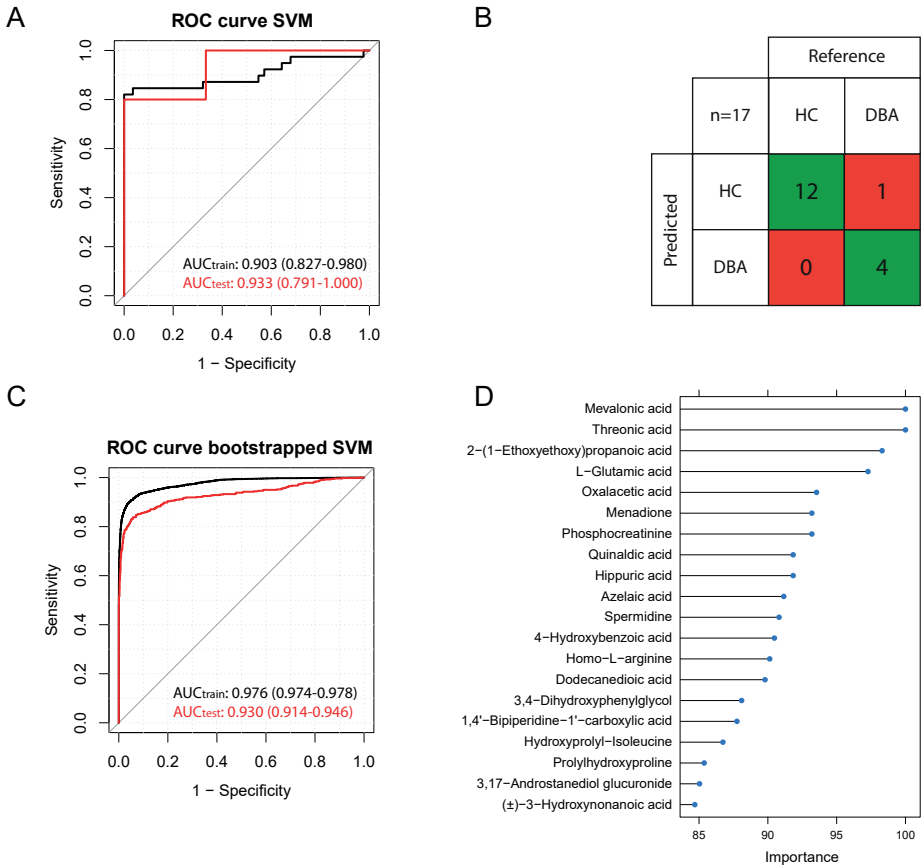


Figure 2. Machine-learning algorithm predicts DBA based on metabolic profile. **A.** Classification performance of samples in training (cross validation SVM model, $n = 84$ control, 39 DBA) and test set ($n = 12$ control, 5 DBA). Note that AUC is a measure of the ability to rank samples according to the probability of class membership, meaning that even falsely classified samples can have a higher rank towards the correct class compared to other samples. **B.** Confusion matrix for the prediction of samples from the test set by the SVM model. **C.** Classification performance of samples in 100 bootstrapped SVM models (training: $n = 11901$ control, 5499 DBA; test: $n = 1381$ control, 519 DBA). **D.** Top 20 important features with importance score identified by support vector machine. An overview of importance scores and isomers is displayed in Table S4.

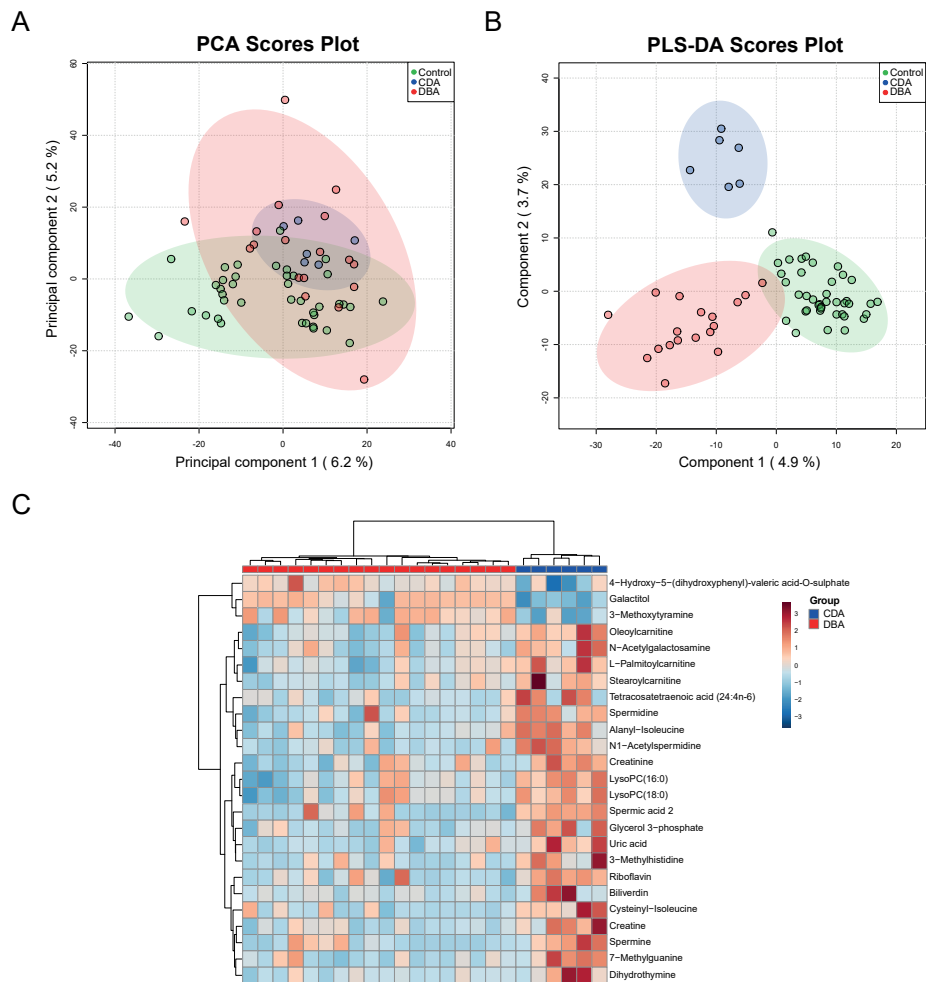


Figure 3. Metabolic profile of DBA compared to CDA. **A.** Principal component analysis (PCA) plot, and **B.** partial least squares discriminant analysis (PLS-DA) plot of the metabolic profiles from DBA patients compared to CDA patients and healthy controls, displayed with 95% confidence regions. **C.** Heatmap of 25 most significant features identified by t-test (raw p-value < 0.002) for DBA vs. CDA. The heatmap was created using Euclidian ward-clustering with autoscaling of features. A comprehensive overview of p-values and isomers is displayed in Table S5.

DBS metabolome are instrumental to study differences in therapeutic subgroups

To investigate the heterogeneity of DBA metabolic profiles in relation to treatment modalities, PCA (data not shown) and PLS-DA were performed for the entire group of patients and controls. Based on treatment (Table 1), patients were divided in non-treated (DBA-N), glucocorticoid-treated (DBA-G) and transfused groups

(DBA-T). In terms of metabolic profile, untreated DBA patients and patients treated with glucocorticoids overlapped and profiles differed the least from controls. Transfused DBA patients were metabolically most distinct from controls (Figure 4A). When controls were removed from the respective analyses, the most significant differences between DBA treatment subgroups, included increased alpha-tocopherol (active vitamin E) in non-treated patients, increased pantothenic acid (vitamin B5) in transfused patients and decreased 3-hydroxy-cis-5-tetradecenoylcarnitine in glucocorticoid treated patients (Figure 4B).

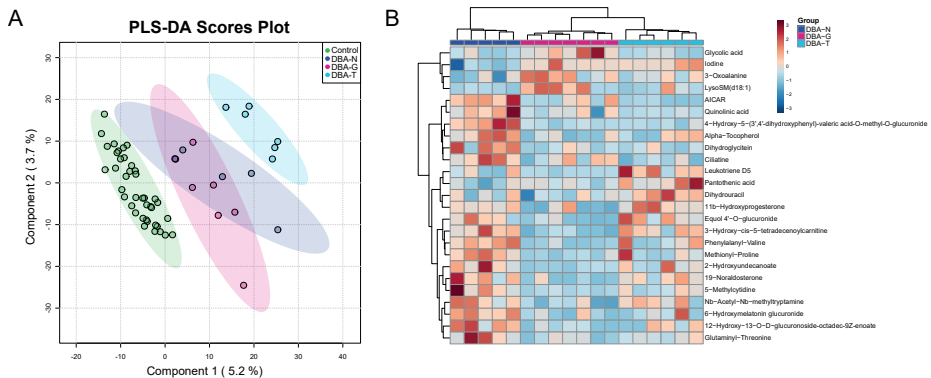


Figure 4. Metabolic profile in relation to treatment modality. **A.** Partial least squares discriminant analysis (PLS-DA) of non-treated (DBA-N), steroid (DBA-G) and transfused DBA patients (DBA-T) displayed with 95% confidence regions. **B.** Heatmap of 25 most significant features identified by t-test (raw p-value <0.02). The heatmap was created using Euclidian ward-clustering with autoscaling of features. A comprehensive overview of p-values and isomers is displayed in Table S6.

DISCUSSION

In this study, we performed untargeted metabolomics in dried blood spots in a relatively large cohort of DBA patients with diverse genotypes and clinical phenotypes. We report here for the first time a specific metabolic fingerprint for DBA.

By incorporating the metabolic fingerprint of DBA in a machine learning algorithm, we demonstrate promising performance characteristics for predicting DBA. This highlights the diagnostic potential of our approach. This is further strengthened by the distinct metabolic profile of DBA and CDA patients, the latter being a disorder with clinical and diagnostic features similar to DBA. Due to the rare nature of CDA and, consequently, the relatively small sample size in this study, it is currently not possible to design a machine learning algorithm that integrates both CDA and

DBA patients. The distinct profile in our cohort of CDA patients, however, supports the hypothesis that the metabolic fingerprint of DBA is disease specific. Further study of a larger number of CDA-samples could enable the construction of a multi-diagnosis model.

Generally, the validity of machine-learning-based algorithms is strongly dependent on the input that is used in its construction. Considering that DBA is a rare disease, the current cohort of patients on which our model is based is substantial, yet relatively small and too heterogeneous to generate a powerful prediction model. This is demonstrated by the incorrect classification of one DBA patient with a pathogenic RPS19 mutation yet only mild clinical features. While distinct profiles were identified, and the algorithm performed robustly despite group heterogeneity, increasing sample size (including better age-matched controls) will allow for better stratification of patients. For example, the specific profiles seen for different treatment modalities, illustrate that this approach of DBS metabolomics can be instrumental in investigating subgroups and heterogeneity in DBA. In line with this, the current approach could offer a platform for investigating treatment responses. This is supported by the finding that non-treated patients (those in haematological remission) and glucocorticoid-treated patients cluster most closely to controls, while transfused patients show the most deviant profile. Studying the DBS metabolome in glucocorticoid-treated patients in particular could identify determinants of steroid response, and help predict steroid response in patients. To this end, future investigations should include sampling patients before start of - and during treatment with - glucocorticoids.

Targeting cellular metabolism is increasingly and successfully being explored as a therapeutic option for various forms of hereditary anaemias, and metabolic insights have proven vital in these developments.¹⁵⁻¹⁸ In particular, the amino acid leucine is currently being explored as a potential modulator of protein synthesis in DBA patients.¹⁹ Recently results of the first clinical trial have been published, showing a partial or complete haematological response in 7/43 patients (16.3%), and more strikingly, positive effects on growth in 9/25 (height) and 11/25 (weight) patients, respectively.²⁰ How leucine exerts its effect on both erythropoiesis and growth remains to be defined, but it has been assumed that it involves upregulating of ribosome biosynthesis via the mTOR pathway as well as improved translational efficiency through activation of translation-initiation factors.²¹ While leucine levels in our analyses did not differ significantly between DBA patients and healthy controls (data not shown), increasing insights into the metabolic disturbances that occur in DBA could lead to the identification of new therapeutic targets.

Interestingly, inosine - a purine nucleoside - emerged in the DBA fingerprint among the top metabolites significantly differing between patients and controls. Although the long-recognized increased activity of erythrocyte adenosine deaminase - an enzyme of the purine salvage pathway - has remained elusive to date in the majority of DBA patients, our findings suggest that purine metabolism might be more broadly involved in DBA disease biology. In addition, the finding of increased alpha-tocopherol in the non-treated patients (i.e. patients who are recognised as being in 'haematological remission') is interesting, as vitamin E facilitates intracellular scavenging of ROS, and its levels in blood are known to reflect redox status.^{22,23} Hence, a better anti-oxidant status may be associated with the haematological remission phenotype in these patients. Future studies are required to determine and validate these metabolic disturbances at a (red) cellular level as opposed to the whole blood metabolome that we study here.

In conclusion, we report on a new application of untargeted metabolomics in dried blood spots, a minimally invasive approach with diagnostic potential in Diamond Blackfan Anaemia, which could be instrumental in investigating clinical phenotypes and treatment response.

Acknowledgements

The authors thank Fini de Gruyter for her technical support in Bio-informatics. This study was supported in part by research funding from Metakids (Grant No. 2017-075) to Judith Jans.

Author contributions statement

BD and MBr contributed to collection, analysis and interpretation of the data, and wrote the first manuscript. WS, EN and NV were all involved in the study design and carefully revised the manuscript. EB was actively involved in collecting patient samples and carefully revised the manuscript. MBa, JJ and RW were principal investigators and were involved in all aspects of the study, including design, collection and interpretation of the data, as well as revising and co-writing the manuscript.

REFERENCES

1. Diamond L, Blackfan K. Hypoplastic anemia. *Am J Dis Child*. 1938;(56):464-467.
2. Dianzani I, Garelli E, Ramenghi U. Diamond-Blackfan anemia: a congenital defect in erythropoiesis. *Haematologica*. 1996;81(6):560-572.
3. Bartels M, Bierings M. How I manage children with Diamond-Blackfan anaemia. *Br J Haematol*. 2019;184(2):123-133.
4. Narla A, Ebert BL. Ribosomopathies: human disorders of ribosome dysfunction. *Blood*. 2010;115(16):3196-3205.
5. Ulirsch JC, Verboon JM, Kazerounian S, et al. The Genetic Landscape of Diamond-Blackfan Anemia. *Am J Hum Genet*. 2018;103(6):930-947.
6. Glader BE, Backer K, Diamond LK. Elevated erythrocyte adenosine deaminase activity in congenital hypoplastic anemia. *N Engl J Med*. 1983;309(24):1486-1490.
7. Smetanina NS, Mersyanova I V., Kurnikova MA, et al. Clinical and genomic heterogeneity of Diamond Blackfan anemia in the Russian Federation. *Pediatr Blood Cancer*. 2015;62(9):1597-1600.
8. van Dooijeweert B, van Ommen CH, Smiers FJ, et al. Pediatric Diamond-Blackfan anemia in the Netherlands: An overview of clinical characteristics and underlying molecular defects. *Eur J Haematol*. 2018;100(2):163-170.
9. Vlachos A, Ball S, Dahl N, et al. Diagnosing and treating Diamond Blackfan anaemia: results of an international clinical consensus conference. *Br J Haematol*. 2008;142(6):859-876.
10. Patti GJ, Yanes O, Siuzdak G. Innovation: Metabolomics: the apogee of the omics trilogy. *Nat Rev Mol Cell Biol*. 2012;13(4):263-269.
11. de Sain-van der Velden MGM, van der Ham M, Gerrits J, et al. Quantification of metabolites in dried blood spots by direct infusion high resolution mass spectrometry. *Anal Chim Acta*. 2017;979:45-50.
12. Haijes HA, Willemsen M, van der Ham M, et al. Direct infusion based metabolomics identifies metabolic disease in patients' dried blood spots and plasma. *Metabolites*. 2019;9(1):12.
13. Van Dooijeweert B, Broeks MH, Verhoeven-Duif NM, et al. Untargeted metabolic profiling in dried blood spots identifies disease fingerprint for pyruvate kinase deficiency. *Haematologica*. 2021;106(10):2720-2725.
14. Chong J, Wishart DS, Xia J. Using MetaboAnalyst 4.0 for Comprehensive and Integrative Metabolomics Data Analysis. *Curr Protoc Bioinforma*. 2019;68(1):e86.
15. Cox SE, Ellins EA, Marealle AI, et al. Ready-to-use food supplement, with or without arginine and citrulline, with daily chloroquine in Tanzanian children with sickle-cell disease: a double-blind, random order crossover trial. *Lancet Haematol*. 2018;5(4):e147-e160.
16. Darghouth D, Koehl B, Madalinski G, et al. Pathophysiology of sickle cell disease is mirrored by the red blood cell metabolome. *Blood*. 2011;117(6):e57-e66.
17. Morris CR, Kuypers FA, Lavrisha L, et al. A randomized, placebo-controlled trial of arginine therapy for the treatment of children with sickle cell disease hospitalized with vaso-occlusive pain episodes. *Haematologica*. 2013;98(9):1375-1382.
18. Grace RF, Rose C, Layton DM, et al. Safety and Efficacy of Mitapivat in Pyruvate Kinase Deficiency. *N Engl J Med*. 2019;381(10):933-944.
19. Pospisilova D, Cmejlova J, Hak J, Adam T, Cmejla R. Successful treatment of a Diamond-Blackfan anemia patient with amino acid leucine. *Haematologica*. 2007;92(5):e66-e67.
20. Vlachos A, Atsidaftos E, Lababidi ML, et al. L-leucine improves anemia and growth in patients with transfusion-dependent Diamond-Blackfan anemia: Results from a multicenter pilot phase I/II study from the Diamond-Blackfan Anemia Registry. *Pediatr Blood Cancer*. 2020;67(12):e28748.
21. Xu B, Gogol M, Gaudenz K, Gerton JL. Improved transcription and translation with L-leucine stimulation of mTORC1 in Roberts syndrome. *BMC Genomics*. 2016;17:25.

22. Margaritelis NV, Veskoukis AS, Paschalis V, et al. Blood reflects tissue oxidative stress: A systematic review. *Biomarkers*. 2015;20(2):97-108.
23. Niki E. Role of vitamin E as a lipid-soluble peroxy radical scavenger: in vitro and in vivo evidence. *Free Radic Biol Med*. 2014;66:3-12.

SUPPLEMENTARY MATERIAL

Table S1. Patient characteristics of congenital dyserythropoietic anaemia (CDA) patients: age, gender, haemoglobin (Hb), red blood cell count (RBC), reticulocyte count (Retics), white blood cell count (WBC), platelets (Plts), treatment, molecular defect and CDA type.

Age (years)	Gender	Hb (mmol/L)	RBC ($\times 10^{12}/L$)	Retics ($\times 10^9/L$)	WBC ($\times 10^9/L$)	Plts ($\times 10^9/L$)	Treatment	Molecular defect	CDA Type
11	female	6.2	3.12	140	5.0	278	none	homozygous CDAN1 c.3389C>T (p.Pro1130Leu)	Type Ia
58	male	6.5	2.95	87.4	12.4	276	chelation	SEC23B (Glu109Lys; del Leu245)	Type II
55	male	5.7	2.69	50.4	10.2	678	chelation	SEC23B (Glu109Lys; del Leu245)	Type II
35	female	6.5	3.09	82.6	6.8	240	none	homozygous CDAN1 c.3389C>T (p.Pro1130Leu)	Type Ia
44	male	7.3	3.9	111	6.5	150	phlebotomy	SEC23B (His3Asp heterozygous)	Type II
55	female	7.5	4.24	145	13.3	597	splenectomy; phlebotomy	SEC23B (Arg17Trp + Arg217Stop)	Type II
Normal range*		7.4-10.7	3.6-5.5	25-120	4.0-13.5	150-450			

*Age- and gender-dependent

Table S2. Overview of p-values and isomers corresponding to the features in the heatmap of DBA vs. controls in Figure 1B.

Feature	T-statistic	p-value	FDR	Isomers
Homo-L-arginine	4.1896	1.0006E-4	0.0088304	-
Methylmalonylcarnitine	5.0878	4.3705E-6	0.0012856	-
Menadione	4.906	8.3778E-6	0.0018484	-
Hippuric acid	4.4922	3.5754E-5	0.0042245	-
Phosphocreatinine	5.7171	4.3648E-7	2.568E-4	-
(R)-Lipoic acid	4.196	9.7915E-5	0.0088304	(S)-lipoic acid
Creatinine	5.84	2.7664E-7	2.568E-4	-
L-isoleucyl-L-proline	4.6524	2.05E-5	0.0035459	L-leucyl-L-proline; Isoleucyl-Proline; Leucyl-Proline
Thymine	-4.5285	3.1543E-5	0.0042245	Imidazoleacetic acid; Imidazol-4-ylacetate
Cortol	-4.8174	1.1477E-5	0.0022507	Beta-cortol
L-Glutamic acid	-5.527	8,8165E-7	3.8903E-4	N-Methyl-D-aspartic acid; N-acetylserine; D-Glutamic acid; L-4-Hydroxyglutamate semialdehyde; DL-Glutamate
Glucosamine	-4.6309	2.2099E-5	0.0035459	Fructosamine; beta-D-Glucosamine
Gutarylglucine	-4.1139	1.2878E-4	0.010823	N-Acetylglutamic acid
Threonic acid	-5.7393	4.0197E-7	2.568E-4	-
Molybdate	-4.2819	7.332E-5	0.0080881	-
Deoxycholic acid glycine conjugate	-3.907	2.5419E-4	0.017946	Glycoursodeoxycholic acid; Chenodeoxyglycocholic acid
3,4-Dihydroxyphenylglycol	-4.4995	3.4861E-5	0.0042245	3,4-Methyleneadipic acid
Inosine	-4.491	3.5902E-5	0.0042245	Allopurinol riboside; Arabinosylhypoxanthine
Anserine	-4.2183	9.0856E-5	0.0088304	Homocarnosine; Balenine
3-Methylcrotonylglycine	-4.0118	1.8051E-4	0.013275	Tiglylglycine
Dodecanedioic acid	-5.2805	2.1746E-6	7.6765E-4	-
Quinaldic acid	-4.9707	6.6529E-6	0.0016775	-
Mevalonic acid	-4.2627	7.8235E-5	0.0081227	(R) 2,3-Dihydroxy-3-methylvalerate; (R)-mevalonate; (2-Methoxyethoxy) propanoic acid
2-Pyrrolidinone	-4.0826	1.429E-4	0.011465	-
3,4-Methylenesebacic acid	-4.0449	1.6185E-4	0.01242	-

Table S3. Overview of variables important in projection (VIP)-scores and isomers corresponding to the features in the PLS-DA of DBA vs controls in Figure 1D.

Feature	PLS-DA VIP (1)	PLS-DA VIP (2)	Isomers
6-Methylthiopurine 5'-monophosphate ribonucleotide	11.319	11.923	-
D-Glyceraldehyde 3-phosphate	6.8841	6.4275	Dihydroxyacetone phosphate
Imidazoleacetic acid ribotide	6.8118	6.3539	-
Citric acid	5.3514	4.9771	Isocitric acid; D-threo-Isocitric acid; Diketogulonic acid; 2,3-Diketo-L-gulonate; (1R,2R)-Isocitric acid; D-Glucaro-1,4-lactone
Oxalic acid	5.2433	4.8822	-
Hexadecanedioic acid	4.7787	4.4478	-
Phosphocreatinine	4.729	4.3996	-
Methionyl-Tyrosine	4.6122	4.3979	Tyrosyl-Methionine
Glyceric acid 1,3-biphosphate	4.2866	4.0979	2,3-Diphosphoglyceric acid
Prolylhydroxyproline	3.9068	3.9834	Hydroxyprolyl-Proline; Prolyl- Hydroxyproline
Sedoheptulose 1,7-bisphosphate	3.8101	3.821	-
Glycylproline	3.3158	3.0856	L-prolyl-L-glycine
Adenosine triphosphate	3.2784	3.1263	dGTP; 2-hydroxy-dATP
Behenoylglycine	3.2766	3.0535	-
(R)-Lipoic acid	3.2678	3.0473	(S)-lipoic acid
N-Methylputrescine	3.1696	2.9486	N-Methylputrescinium
Glucosamine	3.1628	2.9582	Fructosamine; beta-D-Glucosamine
L-beta-aspartyl-L-alanine	3.0369	3.0527	5-L-Glutamylglycine; Alanyl-Aspartate; Aspartyl-Alanine
Glutathione	2.9944	2.6621	-
Myristic acid	2.9714	2.7639	2,6,10-Trimethylundecanoic acid

Table S4. Overview of important features in the support vector machine (SVM) model and isomers corresponding to the features in Figure 2D.

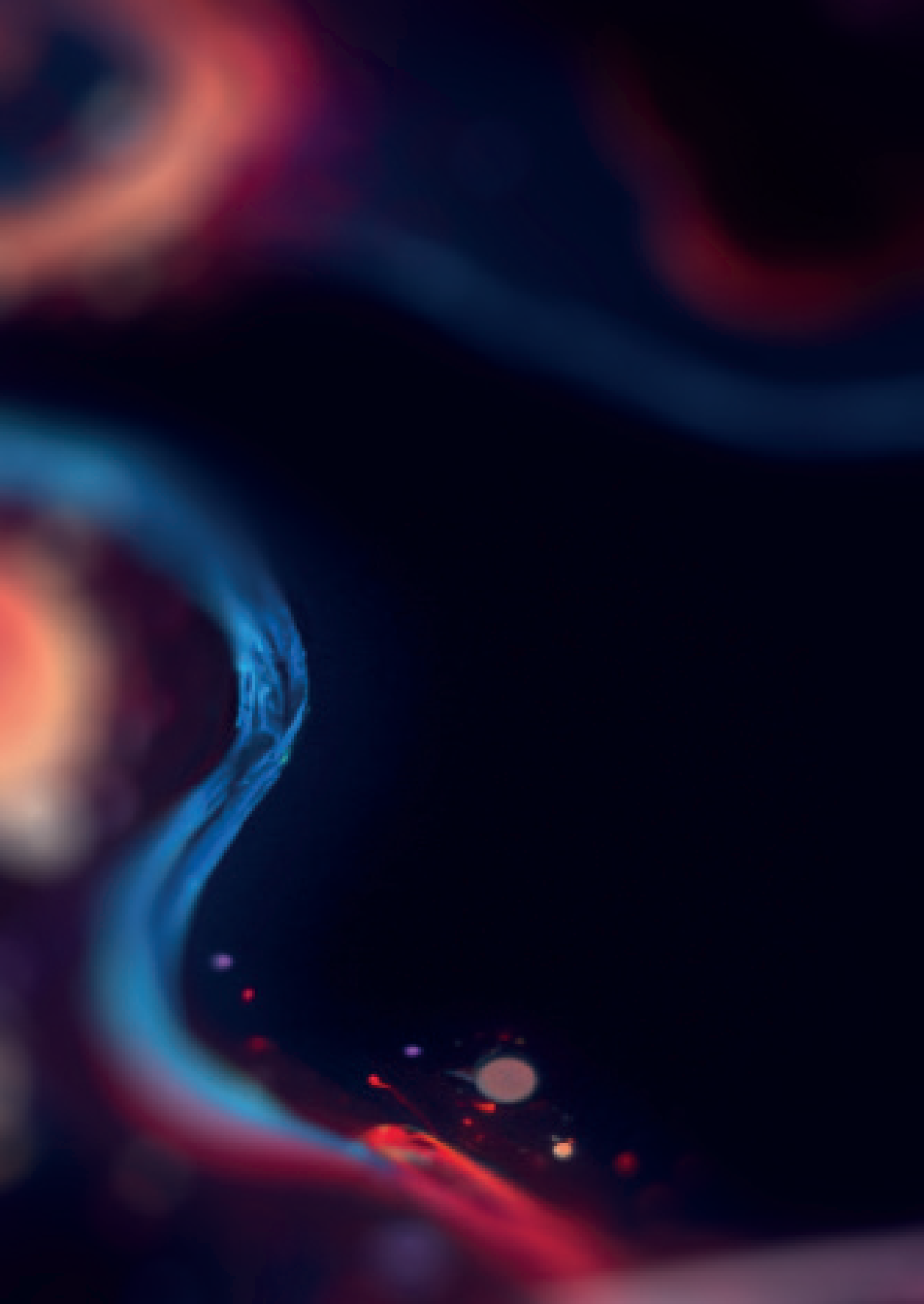
Feature	SVM importance score	Isomers
Threonic acid	100	
Mevalonic acid	100	(R) 2,3-Dihydroxy-3-methylvalerate; (R)-mevalonate; (2-Methoxyethoxy) propanoic acid
2-(1-Ethoxy)propanoic acid	98.3	
L-Glutamic acid	97.28	N-Methyl-D-aspartic acid; N-acetylserine; D-Glutamic acid; L-4-Hydroxyglutamate semialdehyde; DL-Glutamate
Oxalacetic acid	93.54	
Phosphocreatinine	93.2	
Menadione	93.2	
Hippuric acid	91.84	
Quinaldic acid	91.84	
Azelaic acid	91.16	Nonate; 2,4-Dimethylpimelic acid; 3-Methylsuberic acid; Diethyl methylsuccinate; Diethyl glutarate
Spermidine	90.82	
4-Hydroxybenzoic acid	90.48	Gentisate aldehyde
Homo-L-arginine	90.14	
Dodecanedioic acid	89.8	
3,4-Dihydroxyphenylglycol	88.1	3,4-Methyleneadipic acid
1,4'-Bipiperidine-1'-carboxylic acid	87.76	
Hydroxyprolyl-Isoleucine	86.73	Hydroxyprolyl-Leucine; Isoleucyl-Hydroxyproline; Leucyl-Hydroxyproline
Prolylhydroxyproline	85.37	Hydroxyprolyl-Proline; Prolyl-Hydroxyproline
3,17-Androstanediol glucuronide	85.03	3- α -Androstanediol glucuronide; 17-Hydroxyandrostane-3-glucuronide
(\pm)3-Hydroxynonanoic acid	84.69	

Table S5. Overview of p-values and isomers corresponding to the features in the heatmap of DBA vs. CDA in Figure 3C.

Feature	T-statistic	p-value	FDR	Isomers
4-Hydroxy-5-(dihydroxyphenyl)-valeric acid-O-sulphate	-3.989	6.1953E-4	0.072074	4-Hydroxy-5-(dihydroxyphenyl)-valeric acid-O-sulphate III
Galactitol	-6.3344	2.2492E-6	0.0039699	Sorbitol; Mannitol; L-Iditol
3-Methoxytyramine	-3.6715	0.0013393	0.098496	p-Syneprine; 4-Methoxytyramine; Epinine; 4-Hydroxynorephedrine; a-Methyldopamine
Oleoylcarnitine	4.2583	3.2108E-4	0.069832	Vaccenyl carnitine; Elaidic carnitine; 11Z-Octadecenylcarnitine
N-acetylgalactosamine	3.9672	6.5336E-4	0.072074	N-Acetyl-D-glucosamine; Beta-N-Acetylglucosamine; N-Acetyl-b-D-galactosamine; N-Acetylmannosamine
L-Palmitoylcarnitine	4.2111	3.6027E-4	0.069382	-
Stearoylcarnitine	3.9825	6.2949E-4	0.072074	-
Tetracosatetraenoic acid (24:4n-6)	3.8876	7.9297E-4	0.082329	-
Spermidine	3.8059	9.6717E-4	0.089845	-
Alanyl-isoleucine	5.6065	1.2298E-5	0.010853	Alanyl-Leucine; Isoleucyl-Alanine; Leucyl-Alanine
N1-Acetylspermidine	5.4224	1.9066E-5	0.011217	N8-Acetylspermidine
Creatinine	3.6746	0.0013292	0.098496	-
LysoPC(16:0)	4.2335	2.7446E-4	0.069832	-
LysoPC(18:0)	3.7155	0.001204	0.096598	LysoPC(0:0/18:0)
Spermic acid 2	3.8572	8.5383E-4	0.083723	Isoleucyl-Threonine; Leucyl-Threonine; Threoninyl-Isoleucine; Threoninyl-Leucine
Glycerol 3-phosphate	3.7538	0.0010974	0.092233	Beta-Glycerophosphoric acid
Uric acid	4.1728	3.9565E-4	0.069832	-
3-Methylhistidine	4.017	5.7864E-4	0.072074	-
Riboflavin	3.7753	0.0010417	0.091928	-
Cysteinyl-Isoleucine	4.2441	3.3238E-4	0.069832	Cysteinyl-Leucine; Isoleucyl-Cysteine; Leucyl-Cysteine
Creatine	4.9804	5.5243E-5	0.024376	Beta-Guanidinopropionic acid
Spermine	3.9964	6.085E-4	0.072074	-
7-Methylguanine	4.488	1.8318E-4	0.064662	3-Methylguanine; 1-Methylguanine; N2-Methylguanine
Dihydrothymine	4.0208	5.7332E-4	0.072074	-

Table S6. Overview of p-values and isomers corresponding to the features in the heatmap of DBA treatment modalities in Figure 4B.

Feature	f-value	p-value	FDR	Isomers
Glycolic acid	6.4902	0.0093172	0.98225	-
Iodine	9.2976	0.0023637	0.91568	-
3-Oxoalanine	5.7528	0.013985	0.98225	-
LysoSM(d18:1)	5.1625	0.019682	0.98225	-
AlCAR	13.362	4.6531E-4	0.41063	-
Quinolinic acid	5.594	0.015308	0.98225	-
4-Hydroxy-5-(3,4'-dihydroxyphenyl)-valeric acid-O-methyl-O-glucuronide	26.575	1.1741E-5	0.020723	-
Alpha-Tocopherol	6.6789	0.0084262	0.98225	4alpha-Hydroxymethyl-4beta-methyl-5alpha-cholesta-8-en-3beta-ol; 4-beta-Hydroxymethyl-4-alpha-methyl-5-alpha-cholest-7-en-3-beta-ol
Dihydroglycitein	8.3888	0.0035874	0.91568	-
Ciliatine	5.8392	0.013319	0.98225	-
Leukotriene D5	6.797	0.0079182	0.98225	-
Pantothenic acid	6.4853	0.00934117	0.98225	-
Dihydrouracil	5.7494	0.014011	0.98225	N-Methylhydantoin
11b-Hydroxyprogesterone	5.3133	0.01801	0.98225	7'-Carboxy-gamma-tocotrienol
Equol 4'-O-glucuronide	6.8418	0.0077345	0.98225	Equol 7-O-glucuronide
3-Hydroxy-cis-5-tetradecenoylcarnitine	11.648	8.850E-4	0.52072	-
Phenylalanyl-Valine	8.0829	0.0041504	0.91568	Valyl-Phenylalanine
Methionyl-Proline	5.232	0.01889	0.98225	Prolyl-Methionine
2-Hydroxyundecanoate	5.1679	0.019619	0.98226	-
19-Noraldosterone	8.1293	0.0040589	0.91568	-
5-Methylcytidine	6.1175	0.011408	0.98225	-
Nb-Acetyl-Nb-methyltryptamine	7.398	0.0058144	0.98225	-
6-Hydroxymelatonin glucuronide	5.4177	0.016947	0.98225	-
12-Hydroxy-13-O-D-glucuronoside-octadec-9Z-enoate	8.9675	0.0027431	0.91568	12-O-D-Glucuronoside-13-hydroxyoctadec-9Z-enoate; 10-Hydroxy-octadec-12Z-enoate-9-beta-D-glucuronide; 9-Hydroxy-10-O-D-glucuronoside-12Z-octadecenoate
Glutaminy-Threonine	5.5984	0.015269	0.98225	Threoninyl-Glutamine; Threoninyl-Gamma-glutamate; Gamma-glutamyl-Threonine



Chapter 8

Metabolic fingerprint in hereditary spherocytosis correlates with red blood cell characteristics and clinical severity

Birgit van Dooijeweert^{1,2*}, Melissa H. Broeks^{3*}, Nanda M. Verhoeven-Duif³,
Wouter W. van Solinge¹, Eduard J. van Beers⁴, Minke A.E. Rab^{1,4}, Edward E.S. Nieuwenhuis²,
Judith J.M. Jans³, Marije Bartels^{2,4} & Richard van Wijk¹

¹ Central Diagnostic Laboratory-Research, University Medical Center Utrecht, Utrecht, The Netherlands.

² Department of Pediatric Hematology, University Medical Center Utrecht, Utrecht, The Netherlands.

³ Section Metabolic Diagnostics, Department of Genetics, University Medical Center Utrecht, Utrecht, The Netherlands.

⁴ Van Creveldkliniek, University Medical Center Utrecht, Utrecht, The Netherlands.

* These authors contributed equally to this work

Adapted version in HemaSphere. 2021;125(7):e591

ABSTRACT

Hereditary spherocytosis (HS) is a clinically and molecularly heterogeneous disorder in which genotype-phenotype correlations are largely unclear. Although the mechanistic basis of decreased red blood cell (RBC) deformability in HS is well established, little is known about the metabolic consequences of reduced membrane-cytoskeleton integrity in HS. This question is especially relevant given the role of RBC membrane proteins in cellular metabolism. In this study, we used untargeted metabolomics to investigate broad metabolic changes in the dried blood spots (DBS) from a substantial cohort of HS patients. In DBS samples from 35 HS patients and 50 healthy controls, the 1770 uniquely identified metabolite features revealed distinct metabolic profiles between groups using principal component analysis and partial least square discriminant analysis. Distinctively increased metabolites in the HS metabolic fingerprint include polyamines and (acyl)carnitines, whereas vitamin B6 intermediates, 2,3-diphosphoglyceric acid and glyceraldehyde 3-phosphate were significantly decreased in HS ($p < 0.0001$). Interestingly, the HS metabolic profiles related to clinical subgroups of mildly, moderately and severely affected patients, and they correlated with full blood count parameters and red cell characteristics, such as deformability. Here, we demonstrate that untargeted metabolomics in DBS is instrumental in investigating phenotypic heterogeneity and provides promising leads for studying pathophysiological mechanisms in HS.

Keywords: untargeted metabolomics, hereditary spherocytosis, disease fingerprint, dried blood spots, polyamines.

INTRODUCTION

Hereditary spherocytosis (HS) is the most common cause of hereditary chronic hemolytic anemia in people of northern European descent (1:2000-3000).¹ Characterized by impaired red blood cell (RBC) membrane integrity due to disruption of the (vertical) association between the cytoskeleton and the plasma membrane, RBCs from HS patients show enhanced membrane loss and thereby surface area. As a result, RBCs become spheroidal with decreased deformability, leading to premature splenic sequestration.^{2,3}

HS is highly heterogeneous both molecularly and phenotypically. Mutations have been identified in many of the major proteins of the cytoskeleton or RBC membrane (i.e. Band 3, ankyrin, α -spectrin, β -spectrin, protein 4.2). Clinically, a broad phenotypic spectrum is recognized, ranging from asymptomatic or well-compensated anemia to severe forms requiring regular blood transfusions and splenectomy. Moreover, genotype-phenotype correlations are incompletely understood.⁴

In light of the reported association between membrane proteins (especially band 3) and regulation of RBC metabolism,^{5,6} we investigated the metabolic impact of membrane defects using untargeted metabolomics in dried blood spots (DBS). Here we report a metabolic fingerprint for HS that provides promising leads for understanding clinical heterogeneity in patients as well as leads for further study into pathophysiological mechanisms associated with decreased membrane and cytoskeleton integrity.

METHODS

Patients and samples

Thirty-five patients diagnosed with HS were included. Diagnosis was based on full blood count, general markers of hemolysis, family history and functional testing (osmotic gradient ektacytometry, eosin-5'-maleimide binding and the osmotic fragility test). Diagnosis was confirmed in the majority of cases by next generation sequencing gene panel analysis. Healthy volunteers (from an institutional blood donor service) served as controls (HC). All patients or their legal guardians approved the use of left-over material for method development and validation, in agreement with institutional and national legislation. All procedures followed were in accordance with the Helsinki Declaration of 1976, as revised in 2000, and the ethical standards of the University Medical Center Utrecht (University Medical Center Utrecht Biobank Regulations;

version June 19th 2013). For DBS, 50 μ L aliquots of whole blood (EDTA) were spotted onto Guthrie card filter paper (Whatman™ 903 Protein Saver Cards). All spots were left to dry for at least four hours at room temperature, and were subsequently stored at -80 °C in a foil bag with a desiccant package pending further analysis.

Untargeted metabolic phenotyping

Sample preparation, direct infusion high resolution mass spectrometry (DI-HRMS) and data processing were performed as previously reported.⁷⁻⁹ Mass peak intensities for metabolite annotation were averaged over technical triplicates. As DI-HRMS is unable to separate isomers, mass peak intensities consisted of summed intensities of isomers. Metabolite annotation was performed using a peak-calling bioinformatics pipeline developed in R-programming software, based on the human metabolome database (version 3.6) (<http://github.com/UMCUGenetics/DIMS>).¹⁰

DBS samples were distributed over several DI-HRMS runs. To each DI-HRMS run, an extra set of control samples was added (spotted from heparin blood). To compare the metabolic profiles of HS and HC between runs, mass peak intensities for each identified feature were converted to Z-scores. These scores, based on the extra control samples, were calculated by the following formula:

$$Z - score = \frac{(\text{Mass peak intensity of Pt or HC sample} - \text{Mean mass peak intensities of extra control samples})}{\text{Standard deviation mass peak intensities of extra control samples} \ddagger}$$

‡ Extra controls exist of a batch of banked DBS samples from individuals in whom an inborn error of metabolism (IEM) was excluded after an extensive diagnostic workup.

Data analysis

Z-scores calculated from several DI-HRMS runs were combined to create a final metabolomics dataset. Data analyses were conducted in MetaboAnalyst.¹¹ No further data filtering or normalization was applied. Outlying metabolite features were identified using the principal component analysis (PCA) loadings plot. In total, 10 outlying features were removed, resulting in a final dataset of 1770 unique features corresponding to 3565 metabolite annotations. Multivariate PCA and partial least squares discriminant analysis (PLS-DA) were conducted, as well as a two-sample t-test with equal group variance. Additional analyses were performed in GraphPad Prism (Version 8.3.0.538). Individual Z-scores of features were compared using the Mann-Whitney test. Correlations between Z-scores and blood characteristics were analyzed using Spearman's Rank. A Bonferroni correction for multiple testing was applied, considering p-values statistically significant when $p < 0.001$.

Ektacytometry

Osmotic gradient ektacytometry data were available for 30 of 35 HS patients. This functional test of RBC deformability is performed using the Laser optical rotational red cell analyzer (Lorrca, RR Mechatronics, Zwaag, The Netherlands). Deformability is expressed as the elongation index (EI), which is calculated by the height and width of the diffraction pattern that reflects elongation of RBCs within the sample solution during increasing osmolality (50-600 mOsm/kg) at a constant shear stress of 30 Pa. Measurements were carried out according to the manufacturer's guidelines, as described elsewhere.^{12,13} Briefly, 250 μL of whole blood was standardized to a fixed RBC count of $1000 \cdot 10^6$ and injected into a viscous solution (Iso-elon, RR Mechatronics) and subsequently exposed to an osmolality gradient and shear of 30 Pa. The main outcome parameters are: 1) Omin, which reflects the surface area-to-volume ratio; 2) Elmax, which is the maximum deformability during changing osmolality; 3) Ohyper, which reflects RBC dehydration status; and 4) Area under the curve (AUC) (Figure S4A).

For the cell membrane stability test (CMST), whole blood standardized for a fixed RBC count of $200 \cdot 10^6$ is mixed with 5 mL of the Iso-Elon and sheared at 100 Pa during 1 hour. During this test, EI is constantly measured and the main outcome parameter ΔEI is derived from the difference in EI between the first 100 seconds and the last 100 seconds of the CMST. The ΔEI is indicative of the ability of the RBC to shed membrane when exposed to shear stress, reflecting membrane health (Figure S4B).

Data sharing statement

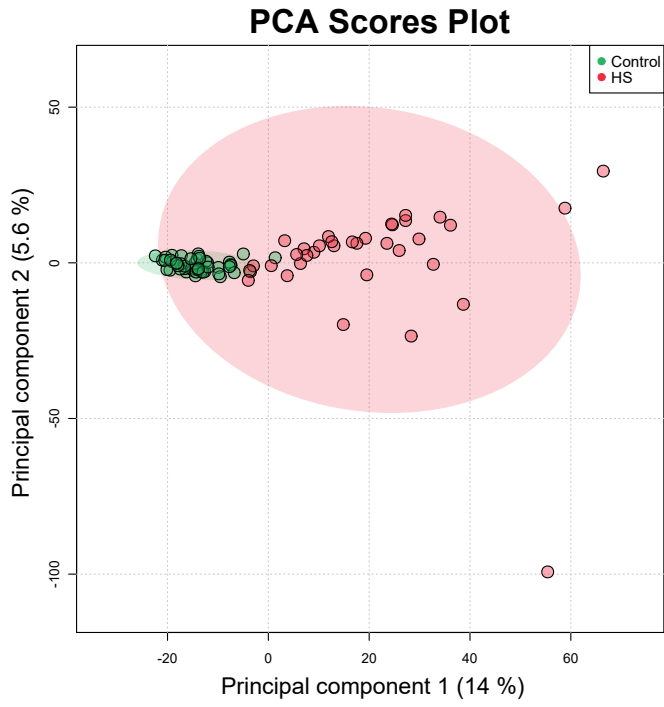
Further details of analysis and raw data are available upon request.

RESULTS

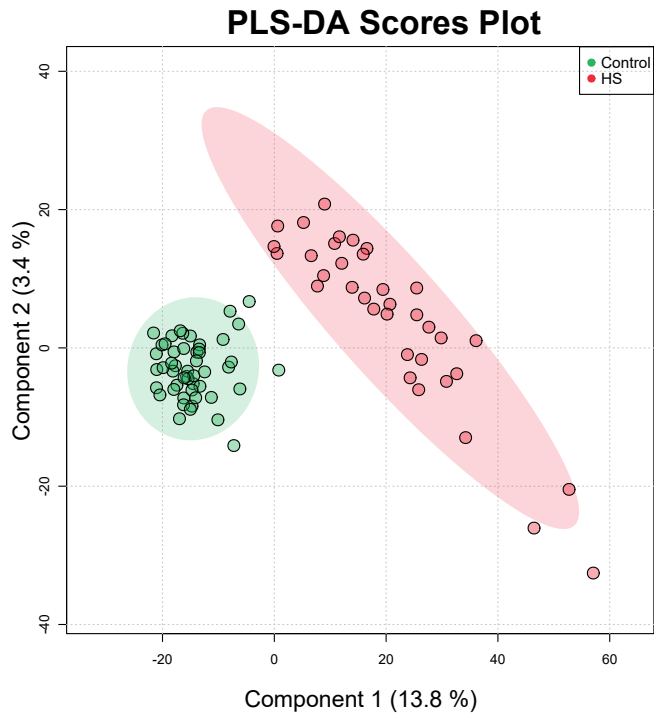
Explorative untargeted metabolomics analysis

In total, 1770 unique features (and their respective metabolite annotations) were analyzed for 35 HS patients and 50 HC samples. Clinical and laboratory characteristics and baseline comparisons are summarized in Table 1. The variation in metabolic fingerprints between both groups was analyzed using PCA and PLS-DA, in which the number of features is reduced by combining them into fewer explanatory variables. PLS-DA takes group label into account (HS or HC) to maximize the variance between groups, whereas PCA does not. The PCA revealed an evident separation between patients and controls (Figure 1A). As expected, the separation was more pronounced in PLS-DA (Figure 1B). Both PCA and PLS-DA indicated a distinct metabolic profile for the investigated groups, with close clustering for controls and a higher level of heterogeneity in HS patients (Figures 1A and 1B). Metabolites contributing most to the separation of groups in PLS-DA are reflected by high Variable Importance in Projection scores. These metabolites include multiple polyamines (spermidine, spermine, N1-acetylspermidine, putrescine), (acyl)carnitines (propionylcarnitine, oleoylcarnitine, stearoylcarnitine, L-acetylcarnitine, L-palmitoylcarnitine, linoelaidylcarnitine, L-carnitine) and the glycolytic intermediates 2,3-diphosphoglycerid acid (2,3-DPG) and glyceraldehyde 3-phosphate (GA3P) (Figure 1C and Table S1). Furthermore, t-test analysis identified corresponding metabolites as significantly different between patients and controls, as well as metabolites involved in vitamin B6 metabolism (4-pyridoxolactone and pyridoxal) (Figure 1D and Table S2).

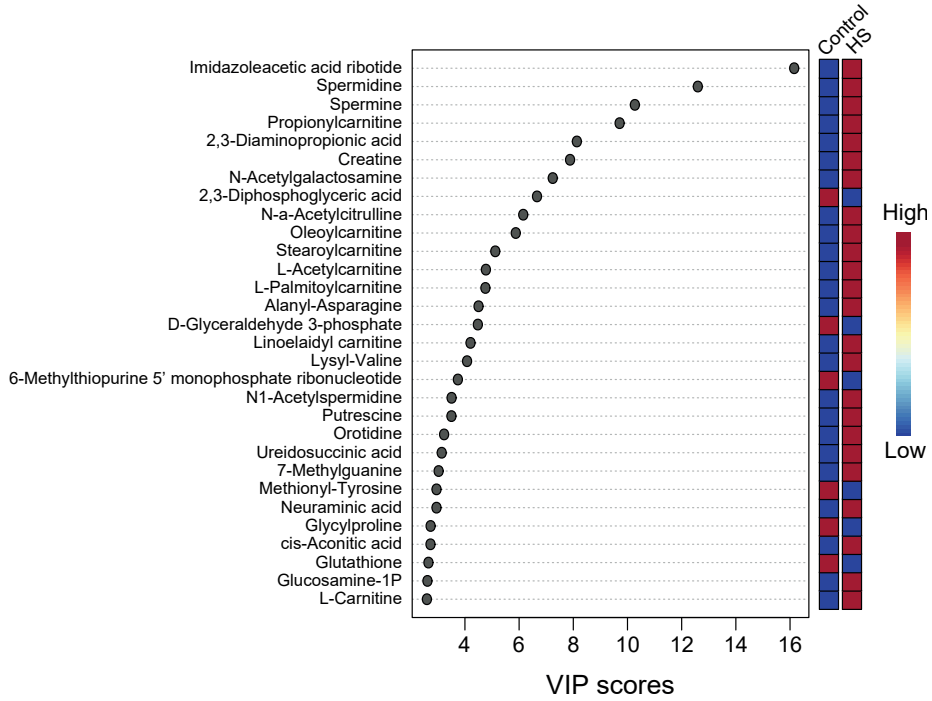
A



B



C



D

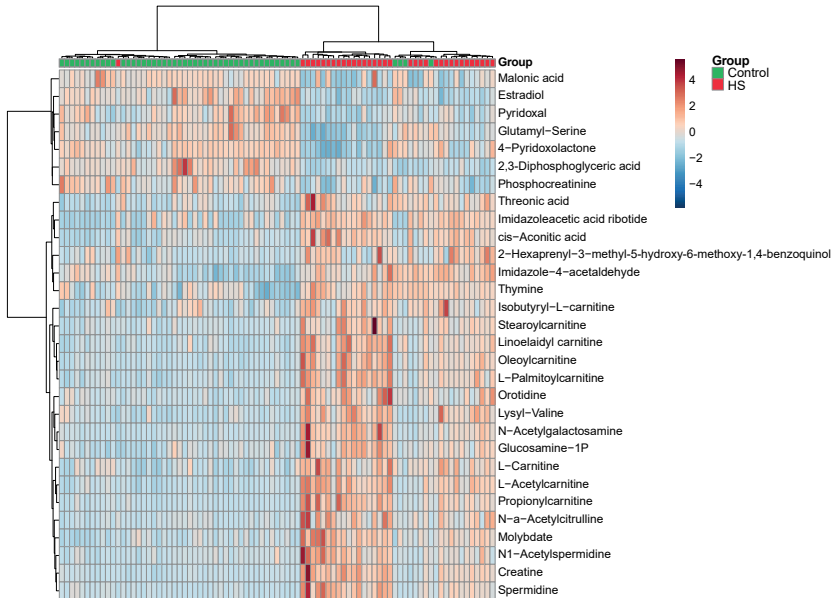


Figure 1. Metabolic profile in dried blood spots of hereditary spherocytosis patients. **A.** Principal component analysis (PCA) plot and **B.** Partial least square discriminant analysis (PLS-DA) plot of the metabolic profile from hereditary spherocytosis (HS) patients and healthy controls are displayed with 95% confidence regions. Both analyses reduce dimensionality to identify the overall variation by combining all metabolite features (weighted) into new variables called principal components. The first two principal components capture most of the variation in the dataset, expressed as a percentage of total variation within a dataset, and are displayed on the x- and y-axes. Each dot represents a patient or control sample and is colored by group label. The position of these dots is based on the metabolite profile of 1770 unique Z-scores. Samples that have a similar metabolic profile cluster more closely. **C.** Variable importance in projection (VIP) scores of PLS-DA demonstrating the 30 features that contribute the most to the separation of patients and HC. An overview of VIP scores and isomers is displayed in Table S1. **D.** Heatmap of the 30 most significant features identified by t-test (p -value < 0.000003). Each colored cell in the heatmap corresponds to the autoscaled Z-score per metabolite feature (rows). The columns of the heatmap are colored by group label. The heatmap was created with hierarchical Ward's linkage clustering using Euclidean distances. The dendrogram represents the clustering of samples and metabolite features. Figures were created using MetaboAnalyst. A comprehensive overview of p -values and isomers is displayed in Table S2.

Table 1. Clinical characteristics of hereditary spherocytosis patients and baseline comparison to healthy controls. A. Clinical characteristics of hereditary spherocytosis (HS) patients regarding age, gender, hemoglobin (Hb), red blood cell count (RBC), reticulocyte count (Retics), white blood cell count (WBC), platelets (Plts), treatment, genetics diagnostics and severity category. Sporadic transfusions are defined as ≤ 6 per 12 months. ND: not determined. X: no additional defect was identified. **B.** Comparison of age, Hb, Retics and time between blood withdrawal and spotting (time to DBS) between healthy controls (HC) and HS patients. Data are presented as mean \pm standard deviation (SD)

Age (years)	Gender	Hb (mmol/L)	RBC ($\times 10^{12}/L$)	Retics ($\times 10^9/L$)	WBC ($\times 10^9/L$)	Plts ($\times 10^9/L$)
8	female	5.7	3.01	485	8.9	225
8	male	5.6	3.21	434	5.1	268
1.5	male	3.9	2.50	484	15.7	280
0.2	female	4.2	2.33	350	14.7	742
12	male	7.3	4.04	433	6.5	340
58	male	7.6	3.55	441	5.9	148
43	female	7.1	3.45	350	4.6	169
14	male	8.6	4.58	624	6.1	274
64	male	5.9	3.00	212	6.0	276
4	male	6.4	3.55	348	21.1	232
0.7	male	5.8	3.53	341	9.6	331
2	male	7.5	3.87	386	11.4	367
39	female	9.0	4.94	313	8.4	365
6	female	7.2	3.86	369	7.7	488
30	female	5.7	2.83	201	3.6	138
4	female	6.8	3.64	389	10.7	301
0.3	male	5.0	3.21	298	12.9	505
3	male	5.4	3.02	553	8.0	376
2	male	7.1	4.53	150	10.5	428
73	male	7.4	3.49	143	4.6	158
0.8	male	6.9	4.15	158	10.5	558
9	male	8.8	5.49	162	8.7	615
4	male	7.5	4.24	298	9.6	360

Treatment	Allele 1	Allele 2	Severity category
splenic embolization (50% residu)	ND	ND	Severe
sporadic transfusions	SPTA1: c.4339-99C>T; p.(?)	SPTA1: c.6769G>T; p.(Glu2257*)	Severe
no current treatment	SPTA1: c.1850dup; p.(Ser618fs)	SPTA1: c.4339-99C>T; p.(?)	Severe
sporadic transfusions/ no current	ANK1: c.2390_2393del; p.(Leu797fs)	SPTA1: c.6889; p.(Arg2297Trp)	Severe
no current treatment	ANK1: c.462C>T; p.(Arg1488*)	SPTA1: c.6531-12C>T; p.(?)	Severe
splenectomy; no current treatment	SLC4A1: c.1225G>T; p.(Val409Phe)	x	Severe
splenectomy; no current treatment	SLC4A1: c.2494C>T; p.(Arg832Cys)	x	Severe
no current treatment	ND	ND	Severe
no current treatment	SPTA1: c.4339-99C>T; p.(?)	SPTA1: c.6989G>A; p.(Arg2330Lys)	Moderate
sporadic transfusions	ND	ND	Moderate
no current treatment	ND	ND	Moderate
no current treatment	ND	ND	Moderate
splenectomy; no current treatment	SPTB: c.4978C>T; p.(Gln1660*)	x	Moderate
no current treatment	ANK1: c.3123del; p.(Ser1042fs)	x	Moderate
splenectomy; no current treatment	SPTA1: c.3527dup; p.(Leu1086fs)	SPTA1: c.6531-12C>T; p.(?)	Moderate
no current treatment	SPTB: c.1714_1723del; p.(Met573fs)	x	Moderate
sporadic transfusions	ND	ND	Moderate
regular transfusions	SPTB: c.2889C>A; p.(Cys963*)	x	Moderate
no current treatment	SPTA1: c.134G>C; p.(Arg45Thr)	SPTA1: c.6531-12C>T; p.(?)	Mild
no current treatment	SPTA1: c.5805G>A; p.(Tryp1935*)	SPTA1: c.6531-12C>T; p.(?)	Mild
no current treatment	ANK1: c.4391-2@>G; p.(?)	SPTA1: c.4339-99C>T; p.(?)	Mild
splenic embolization/ coiling	ANK1 c.2563_2586delinsCCAG p.(Glu855fs)	x	Mild
no current treatment	SPTB: c.4978C>T; p.(Gln1660*)	x	Mild

Table 1. Continued

Age (years)	Gender	Hb (mmol/L)	RBC ($\times 10^{12}/L$)	Retics ($\times 10^9/L$)	WBC ($\times 10^9/L$)	Plts ($\times 10^9/L$)
27	male	9.4	5.42	137	9.4	307
9	male	8.1	4.56	188	7.6	314
7	male	7.5	4.15	128	6.9	290
6	male	7.5	4.32	560	8.1	436
13	male	8.7	4.94	87.4	17.1	620
65	female	8.0	4.06	275	5.6	252
5	female	7.6	5.70	162	14.1	812
7	male	8.0	6.03	124	14.8	911
21	female	8.1	4.02	444	6.8	244
9	male	8.0	4.33	245	4.0	181
2	male	7.1	4.16	245	9.0	443
70	female	ND	ND	ND	ND	ND
Normal range*		7.4-10.7	3.6-5.5	25-120	4.0-13.5	150-450

*Age- and gender-dependent

	HS (mean \pm SD)	HC (mean \pm SD)
Age (years)	17.9 \pm 22.5	38.4 \pm 11.7
Hb (mmol/L)	7.07 \pm 1.33	9.07 \pm 0.75
Retics ($\times 10^9/L$)	309.3 \pm 143.7	58.1 \pm 17.7
Time to DBS (hours)	3.92 \pm 1.9	3.97 \pm 6.7

Treatment	Allele 1	Allele 2	Severity category
splenectomy; no current treatment	ANK1: c.23dup; p.(Glu9fs)	x	Mild
no current treatment	ANK1: c.4559del; p.(Glu1520fs*)	x	Mild
no current treatment	SPTA1: c.6788+1G>A; p.(?)	SPTA1: c.6531-12C>T; p(?)	Mild
sporadic transfusions	SPTB: c.5128G>T; p.(Glu1710*)	x	Mild
splenectomy; no current treatment	SPTB: c.5898C>T; p.(=)	x	Mild
no current treatment	SPTA1: c.6788+1G>A ; p.(?)	SPTA1: c.6531-12C>T; p(?)	Mild
splenectomy; no current treatment	SPTA1: c.83G>A; p.(Arg28His)	SPTA1: c.6531-12C>T; p(?)	Mild
splenectomy; no current treatment	SPTA1: c.83G>A; p.(Arg28His)	SPTA1: c.6531-12C>T; p(?)	Mild
no current treatment	SLC4A1: c.616_620delG	x	Mild
no current treatment	SLC4A1: c.2608C>T; p.(Arg870Trp)	x	Mild
no current treatment	SPTB: c.4117C>T; p.(Gln1373*)	x	Mild
no current treatment	ANK1: c.4638_4639del; p.(Leu1547fs)	x	ND

Focused erythrocyte pathway analysis

Based on the observation of significantly decreased 2,3-DPG and GA3P in both PLS-DA and t-test, the glycolytic pathway was explored in detail. Apart from a decrease in 2,3-DPG and GA3P, none of the glycolytic intermediates were significantly altered, and no substantial differences were observed in pyruvate and lactate, or glucose 6-phosphate as the respective end- and starting points of glycolysis (Figure 2). Importantly, the decrease of 2,3-DPG, but not GA3P, remained statistically significant when adjusted for hemoglobin level and reticulocyte count ($p < 0.0001$).

Further exploration of red cell metabolism revealed decreased glutathione, but no other metabolites of glutathione metabolism were altered (data not shown). In addition, the pentose phosphate pathway and its respective metabolites appeared unaffected (data not shown). Furthermore, investigation of amino acids and carnitines revealed a significant decrease in aspartate and significant increases in glycine, L-valine, L-carnitine and L-acetylcarnitine (Figure S1 and Tables S2 and S3). Putrescine, spermidine and spermine, players in arginine and polyamine metabolism, were significantly elevated in HS patients compared to controls (Figure S2 and Tables S2 and S3).

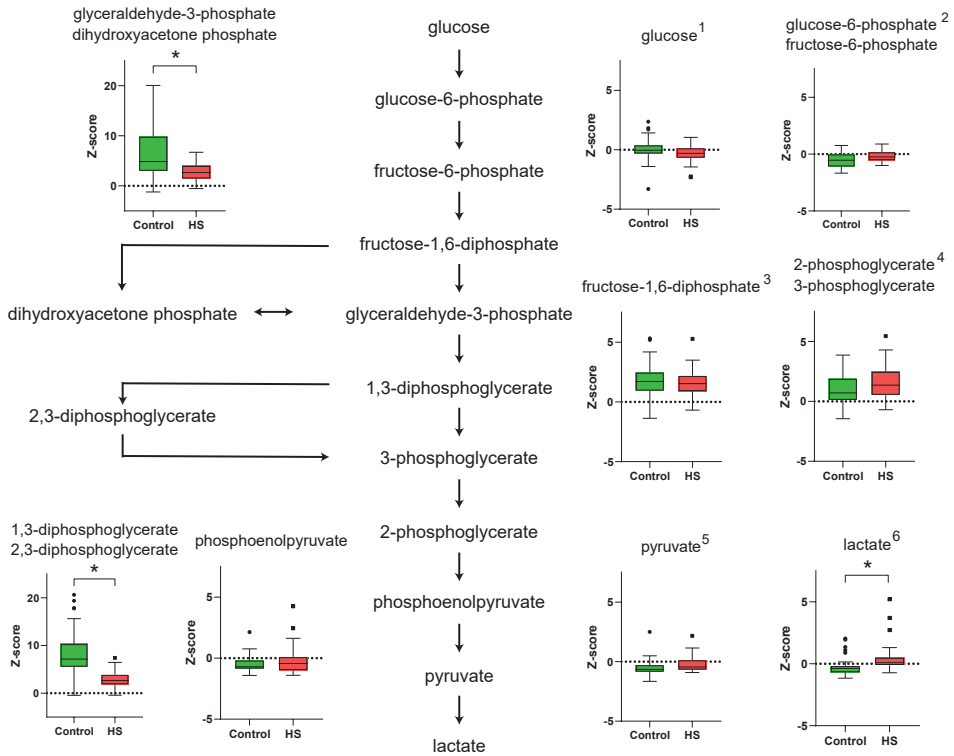


Figure 2. Glycolytic intermediates in dried blood spots of hereditary spherocytosis patients vs. controls. Schematic representation of glycolysis in red blood cells. Z-scores of glycolytic intermediates (and glycolytic isomers) are plotted for healthy controls ($n = 50$) and HS-samples ($n = 35$) in a boxplot with Tukey whiskers. Additional isomers of glycolytic intermediates include: 1) D-Galactose, D-Mannose, Myoinositol, 3-Deoxyarabinohehexonic acid, Beta-D-Glucose, D-Fructose, Allose, L-Sorbose, Alpha-D-Glucose, D-Tagatose, Beta-D-Galactose, Scyllitol, L-Gulose, L-Galactose; 2) Myo-inositol 1-phosphate, Galactose 1-phosphate, Dolichyl phosphate D-mannose, Fructose 1-phosphate, Mannose 6-phosphate, D-Myo-inositol 4-phosphate, Glucose 1-phosphate, Inositol phosphate, Beta-D-Glucose 6-phosphate, Beta-D-Fructose 6-phosphate, D-Tagatose 1-phosphate, D-Mannose 1-phosphate, Sorbose 1-phosphate, Beta-D-Fructose 2-phosphate, 1D-myo-Inositol 3-phosphate, D-Tagatose 6-phosphate, D-fructose 1-phosphate; 3) 1D-Myo-inositol 1,4-bisphosphate, D-fructose 2,6-bisphosphate, Alpha-D-Glucose 1,6-bisphosphate, 1D-Myo-inositol 1,3-bisphosphate, 1D-Myo-inositol 3,4-bisphosphate, D-Tagatose 1,6-bisphosphate, D-Mannose 1,6-bisphosphate, beta-D-Fructose 1,6-bisphosphate; 4) 2-Phospho-D-glyceric acid, (2R)-2-Hydroxy-3-(phosphonatoxy)propanoate; 5) Malonic semialdehyde; 6) Hydroxypropionic acid, Glyceraldehyde, D-Lactic acid, Dihydroxyacetone, Methoxyacetic acid. * indicates a significance of $p < 0.0001$.

Metabolic profiles relate to clinical disease severity

To explore whether the heterogeneity in the HS metabolic profiles related to the clinical phenotype, additional PCA and PLS-DA were performed. Clinical phenotypes were classified as mild, moderate or severe based on the severity of anemia and degree of compensation for hemolysis, according to the modified criteria originally proposed by Eber *et al.*¹⁴ The PLS-DA plot showed that mildly affected HS patients clustered most closely with controls, followed by moderately affected patients, whereas the metabolic profile of severely affected patients differed most from controls (Figures 3A and 3B).

Distinctive metabolites associate with disease severity, red cell characteristics and RBC deformability

Metabolites that contributed the most to the distinction between HC and the clinical severity of HS included polyamines, (acyl)carnitines, 2,3-DPG and creatine (Figure 3C). Increased clinical severity was associated with increased Z-scores of spermidine, N1-acetylspermidine, L-acetylcarnitine and propionylcarnitine (Figure 3D). In addition, analysis of these metabolites in relation to full blood count parameters revealed significant correlations for spermidine, N1-acetylspermidine and L-acetylcarnitine and propionylcarnitine with RBC and reticulocyte counts (Figure 4). Although clinical severity was associated with a decreasing level of 2,3-DPG, no significant correlations were identified for 2,3-DPG and GA3P with full blood count parameters (Figure S3).

Lastly, we explored the correlation of the top 20 features of PLS-DA with functional features of RBC deformability as established with osmotic gradient ektacytometry (Figure S4). For the maximum deformability of RBCs, reflected by the maximum elongation index (EI max), an inverse correlation with Z-scores of spermidine ($r = -0.37$, $p = 0.04$), N1-acetylspermidine ($r = -0.47$, $p = 0.008$), L-acetylcarnitine ($r = -0.42$, $p = 0.02$), and propionylcarnitine ($r = -0.36$, $p = 0.05$) was observed (Figure 4). Further correlations with functional features of RBC deformability were observed between propionylcarnitine and the total area under the curve ($r = -0.37$; $p = 0.04$) and between L-carnitine and Ohyper ($r = 0.37$; $p = 0.04$, plots not shown), suggesting that increases in distinctive metabolites were associated with decreased RBC hydration and deformability. These findings were supported by the relation between the top metabolites and change in deformability (ΔEI) as measured with the cell membrane stability test in a subset of HS patients ($n = 8$), where we observed a strong correlation for propionylcarnitine and ΔEI ($r = 0.74$, $p = 0.05$, Figure S5).

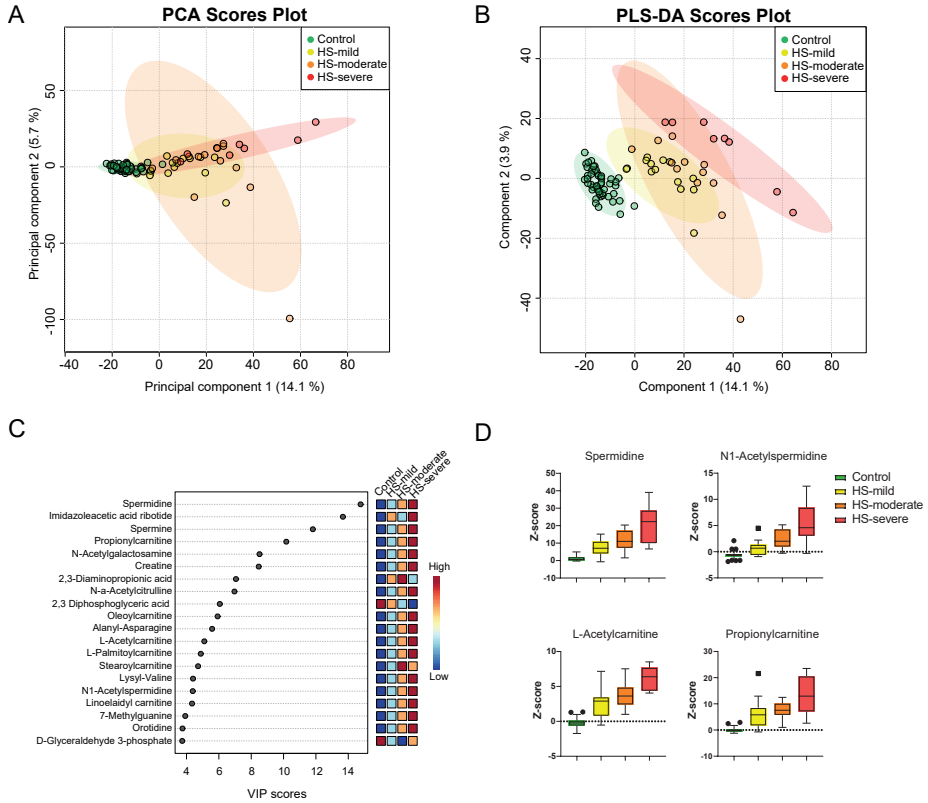


Figure 3. Metabolic profile of hereditary spherocytosis in relation to clinical severity phenotypes.

A. PCA plot and **B.** PLS-DA plot distinguishing between clinical severity phenotypes **C.** The top 20 metabolite features contributing to the separation of hereditary spherocytosis (HS) patients and controls in PLS-DA, reflected by VIP-scores (variable importance in projection). For almost all metabolites a correlation with clinical severity is observed, reflected by an increasing or decreasing color gradient. An overview of VIP scores and isomers is displayed in Table S4. **D.** Z-scores of spermidine, N1-acetylspermidine, L-acetylcarnitine and propionylcarnitine based on clinical severity for control ($n = 50$), HS-mild ($n = 15$), HS-moderate ($n = 12$) and HS-severe ($n = 8$) in a boxplot with Tukey whiskers.

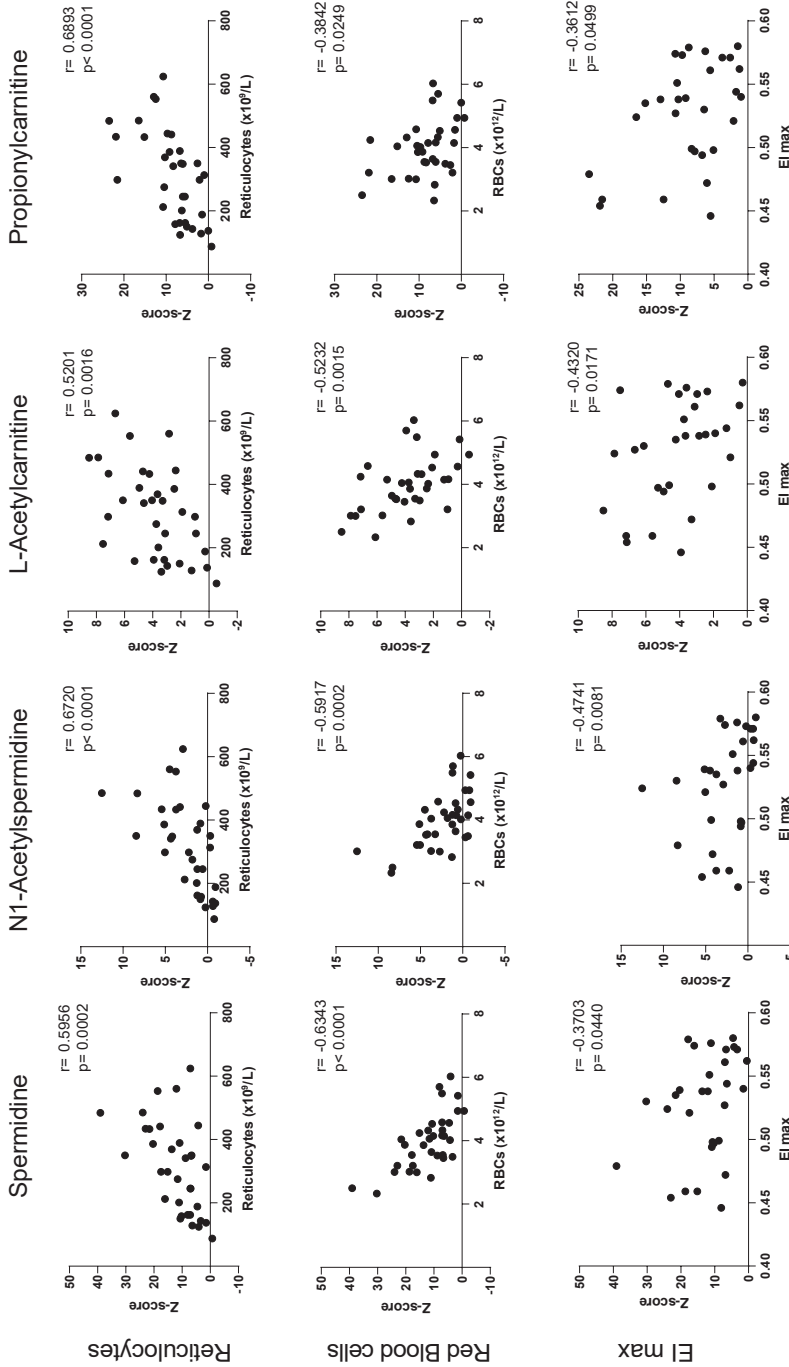


Figure 4. Correlations between metabolites distinguishing clinical severity groups and red cell characteristics in hereditary spherocytosis patients. Correlations between number of reticulocytes ($n = 34$), red blood cells ($n = 34$), EI max ($n = 30$) and Z-scores of spermidine, N1-acetylspermidine, L-acetylcarnitine and propionylcarnitine in hereditary spherocytosis patients.

DISCUSSION

In this study, we have performed untargeted metabolomics in dried blood spots from a substantial cohort of HS patients. We report on a metabolic fingerprint that offers for the first time a comprehensive overview of metabolic disturbances in HS and includes altered levels of polyamines and (acyl)carnitines. These metabolic disturbances correlate with red blood cell (RBC) characteristics (in particular deformability) and, in addition, with clinical severity. We also identified significant decreases in the glycolytic intermediates 2,3-diphosphoglyceric acid (2,3-DPG) and glyceraldehyde-3-phosphate (GA3P). Also, these metabolic disturbances show a gradient with clinical severity and thus relate to the HS clinical phenotype.

Previous studies have shown that glycolytic enzymes associate with the RBC membrane^{5,6,15} and others have reported specifically on decreased pyruvate kinase (PK) activity in HS patients as a consequence of loss of membrane-bound PK.^{16,17} Here, we only found 2,3-DPG and GA3P (and/or features with the same respective mass-to-charge ratio, Table S1) to be significantly decreased in HS patients. This suggests that although glycolytic enzymes might be affected to some extent by decreased RBC membrane integrity, glycolysis in general appears not to be strongly affected. While the metabolic profile was obtained from whole blood, it is highly likely that the observed glycolytic disturbances mainly reflect RBCs, since 2,3-DPG is specific to the RBC.¹⁸ In addition, no correlation was observed for 2,3-DPG and GA3P with any of the full blood count parameters. While the mechanism underlying the decrease in 2,3-DPG in HS remains to be determined, it is intriguing, as 2,3-DPG is an important regulator of hemoglobin oxygen affinity. It binds with greater affinity to deoxygenated hemoglobin than to oxygenated hemoglobin and decreases the p50, thereby promoting the release of oxygen to tissues. While the reported increase of 2,3-DPG in hereditary anemias like pyruvate kinase deficiency (PKD)¹⁹ or beta-thalassemia minor²⁰ is assumed to be clinically beneficial for patients, the robust decrease that we observe in HS patients could also be of clinical importance. In this respect, the reported fatigue-related impairment of quality of life, and 'complaints of fatigue' being reported as critically factored into the decision for splenectomy in a substantial number of HS patients despite relatively mild to moderate hemolysis, might be well worth further exploring.^{21,22}

In the present study, we found significantly increased polyamines in HS patients compared to healthy controls. Previously, the polyamines spermidine, spermine and putrescine have been reported to decrease erythrocyte membrane deformability and stabilize the membrane skeleton of resealed ghosts loaded with polyamines.²³ The

inverse correlation between spermidine and N1-acetylspermidine with the maximal deformability (Elmax) of RBCs in HS patients, although not very strong, as well as the relation with clinical phenotypes, provide supporting evidence for the hypothesis that apart from an *in vitro*-effect in ghosts, the concentration of polyamines is associated with *in vivo* red cell deformability in patients. Whether this contributes to the decreased deformability seen in HS or is a compensatory mechanism remains to be determined.

The observed correlations between polyamines and reticulocyte count, and inverse correlations with hemoglobin and erythrocyte count, but not with leukocytes and platelets, suggest that these alterations are RBC-specific. Interestingly, previous studies demonstrated significant correlations between younger and older red blood cells, with lower levels of polyamines in the older red cells, suggesting the possibility of using red cell polyamines as an indicator of the activity of the bone marrow in anemic states.^{24,25} The increase of polyamines we observed previously in PKD⁹ another hemolytic anemia with a hyper-regenerative bone marrow, further supports these findings. In addition, it has been shown for a number of conditions (hepatectomy, cancer, transplantation), that the RBC concentration of spermidine is a reliable marker of cell proliferation.²⁶ As concentrations of polyamines have also been reported to be increased in RBCs and dried blood spots in sickle cell disease (SCD) and pyruvate kinase deficiency (PKD)^{9,27,28} we anticipate that unraveling the underlying mechanisms and consequences of altered polyamine metabolism may contribute not only to a better understanding of HS pathophysiology but for rare hereditary hemolytic anemia in general.

As the clinical phenotype in HS is highly heterogeneous and severity categories are determined by only four parameters (hemoglobin, reticulocyte count, bilirubin and splenectomy),⁴ the distinction is arbitrary and subject to fluctuation over time. This is likely reflected by the heterogeneity in the 'moderately affected' HS-group (Table 1). Nevertheless, there is a clear distinction between mildly or even moderately affected HS patients and severely affected HS patients. Together with the gradient that is seen for distinctive metabolites that contribute the most, these data indicate that clinical phenotypes do correlate with the metabolic profiles of these patients. These findings need to be validated in a larger cohort of patients, but this approach offers new perspectives for a better understanding of the complex genotype-phenotype associations that are seen in HS.

Previously, we have shown that this non-invasive and minimally laborious approach of untargeted metabolomics in dried blood spots, holds diagnostic potential in the

context of PKD, by incorporating the metabolic fingerprint into a machine learning model. The diagnostic workflow for HS is rather well established²⁹ and the added value of such a machine learning model would probably be arguable. Here, we demonstrate that untargeted metabolomics can be instrumental in investigating the phenotypic heterogeneity in patients and our results provide promising leads for further study into the pathophysiological mechanisms that determine the phenotypic expression of HS. The comprehensive characterization of metabolic disturbances in HS might serve as a starting point for the development of new therapeutic strategies.

Disclosures

EJvB and RvW perform consultancy and receive research funding from Agios Pharmaceuticals. All the other authors have no conflicts of interest to disclose.

Contributions

BvD and MHB contributed to collection, analysis and interpretation of the data, and wrote the first manuscript. WWvS, EESN and NMV were all involved in the study design and carefully revised the manuscript. EJvB and MAER were actively involved in collecting patient samples and carefully revised the manuscript. MB, JJMJ and RvW were principal investigators and were involved in all aspects of the study, including design, collection, and interpretation of the data, as well as revising and co-writing the manuscript.

Acknowledgements

We thank Nienke van Unen and Fini de Gruyter for their technical support in Bio-informatics.

Funding

This study was supported in part by research funding from Metakids (Grant No. 2017-075) to JJMJ.

REFERENCES

1. Mohandas N, Gallagher PG. Red cell membrane: past, present, and future. *Blood*. 2008;112(10):3939-3948.
2. Narla J, Mohandas N. Red cell membrane disorders. *Int J Lab Hematol*. 2017;39 Suppl 1:47-52.
3. Perrotta S, Gallagher PG, Mohandas N. Hereditary spherocytosis. *Lancet (London, England)*. 2008;372(9647):1411-1426.
4. Van Vuren A, Van Der Zwaag B, Huisjes R, et al. The Complexity of Genotype-Phenotype Correlations in Hereditary Spherocytosis: A Cohort of 95 Patients: Genotype-Phenotype Correlation in Hereditary Spherocytosis. *HemaSphere*. 2019;3(4):e276.
5. Chu H, Low PS. Mapping of glycolytic enzyme-binding sites on human erythrocyte band 3. *Biochem J*. 2006;400(1):143-151.
6. Rogers SC, Ross JGC, D'Avignon A, et al. Sickle hemoglobin disturbs normal coupling among erythrocyte O₂ content, glycolysis, and antioxidant capacity. *Blood*. 2013;121(9):1651-1662.
7. Haijes HA, Willemssen M, van der Ham M, et al. Direct infusion based metabolomics identifies metabolic disease in patients' dried blood spots and plasma. *Metabolites*. 2019;9(1):12.
8. de Sain-van der Velden MGM, van der Ham M, Gerrits J, et al. Quantification of metabolites in dried blood spots by direct infusion high resolution mass spectrometry. *Anal Chim Acta*. 2017;979:45-50.
9. Van Dooijeweert B, Broeks MH, Verhoeven-Duif NM, et al. Untargeted metabolic profiling in dried blood spots identifies disease fingerprint for pyruvate kinase deficiency. *Haematologica*. 2021;106(10):2720-2725.
10. Wishart DS, Jewison T, Guo AC, et al. HMDB 3.0-The Human Metabolome Database in 2013. *Nucleic Acids Res*. 2013;41(D1):D801-D807.
11. Chong J, Wishart DS, Xia J. Using MetaboAnalyst 4.0 for Comprehensive and Integrative Metabolomics Data Analysis. *Curr Protoc Bioinforma*. 2019;68(1):e86.
12. Da Costa L, Suner L, Galimand J, et al. Diagnostic tool for red blood cell membrane disorders: Assessment of a new generation ektacytometer. *Blood Cells Mol Dis*. 2016;56(1):9-22.
13. Lazarova E, Gulbis B, Oirschot B Van, Van Wijk R. Next-generation osmotic gradient ektacytometry for the diagnosis of hereditary spherocytosis: interlaboratory method validation and experience. *Clin Chem Lab Med*. 2017;55(3):394-402.
14. Eber SW, Armbrust R, Schröter W. Variable clinical severity of hereditary spherocytosis: relation to erythrocytic spectrin concentration, osmotic fragility, and autohemolysis. *J Pediatr*. 1990;117(3):409-416.
15. Puchulu-Campanella E, Chu H, Anstee DJ, Galan JA, Tao WA, Low PS. Identification of the components of a glycolytic enzyme metabolon on the human red blood cell membrane. *J Biol Chem*. 2013;288(2):848-858.
16. Andres O, Loewecke F, Morbach H, et al. Hereditary spherocytosis is associated with decreased pyruvate kinase activity due to impaired structural integrity of the red blood cell membrane. *Br J Haematol*. 2019;187(3):386-395.
17. Bruce LJ, Beckmann R, Ribeiro ML, et al. A band 3-based macrocomplex of integral and peripheral proteins in the RBC membrane. *Blood*. 2003;101(10):4180-4188.
18. Huehns ER. The physiological consequences of changes in oxygen affinity in the red cell enzyme defects. *J Clin Pathol*. 1974;27(Suppl 8):142-144.
19. Al-Samkari H, van Beers EJ, Kuo KHM, et al. The variable manifestations of disease in pyruvate kinase deficiency and their management. *Haematologica*. 2020;105(9):2229-2239.
20. Pearson HA, Motoyama E, Genel M, Kramer M, Zigas CJ. Intraerythrocytic adaptation (2,3 DPG,P50) in thalassemia minor. *Blood*. 1977;49(3):463-465.

21. Teunissen M, Hijmans CT, Cnossen MH, Bronner MB, Grootenhuis MA, Peters M. Quality of life and behavioral functioning in Dutch pediatric patients with hereditary spherocytosis. *Eur J Pediatr.* 2014;173(9):1217-1223.
22. Roy SM, Buchanan GR, Crary SE. Splenectomy in children with "mild" hereditary spherocytosis. *J Pediatr Hematol Oncol.* 2013;35(6):430-433.
23. Ballas SK, Mohandas N, Marton LJ, Shohet SB. Stabilization of erythrocyte membranes by polyamines. *Proc Natl Acad Sci U S A.* 1983;80(7):1942-1946.
24. Natta CL, Kremzner LT. Erythrocyte polyamines of normal individuals and patients with Sickle Cell Anemia (SCA). *Age (Omaha).* 1988;11(1):11-14.
25. Cooper KD, Shukla JB, Rennert OM. Polyamine distribution in cellular compartments of blood and in aging erythrocytes. *Clin Chim Acta.* 1976;73(1):71-88.
26. Jeevanandam M, Petersen SR. Clinical role of polyamine analysis: problem and promise. *Curr Opin Clin Nutr Metab Care.* 2001;4(5):385-390.
27. Natta CL, Motyczka AA, Kremzner LT. Polyamines in sickle cell disease. *Biochem Med.* 1980;23(2):144-149.
28. Darghouth D, Koehl B, Madalinski G, et al. Pathophysiology of sickle cell disease is mirrored by the red blood cell metabolome. *Blood.* 2011;117(6):e57-66.
29. King MJ, Garçon L, Hoyer JD, et al. ICSH guidelines for the laboratory diagnosis of nonimmune hereditary red cell membrane disorders. *Int J Lab Hematol.* 2015;37(3):304-325.

SUPPLEMENTARY MATERIAL

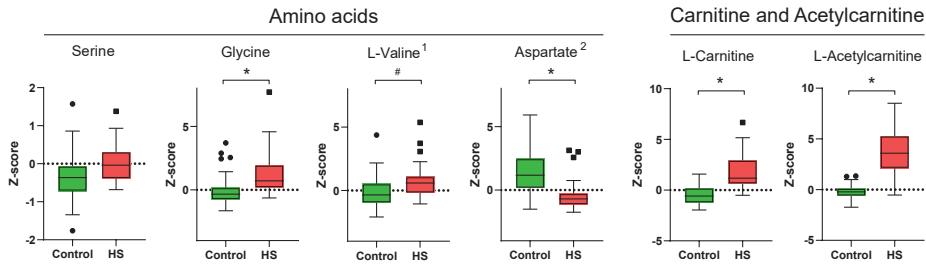


Figure S1. Amino acids and RBC membrane turnover metabolites. Z-scores for amino acids, carnitine and acetylcarnitine plotted for healthy control ($n = 50$) and hereditary spherocytosis (HS) samples ($n = 35$) in a boxplot with Tukey whiskers. Serine ($p=0.0013$), Glycine ($p<0.0001$), Aspartate ($p<0.0001$), Valine ($p=0.0002$), L-carnitine ($p<0.0001$), L-Acetylcarnitine ($p<0.0001$). Isomers include 1) Betaine, N-methyl-a-aminoisobutyric acid, 5-Aminopentanoic acid, Norvaline. 2) Iminodiacetic acid. * $p<0.0001$, # $p<0.001$.

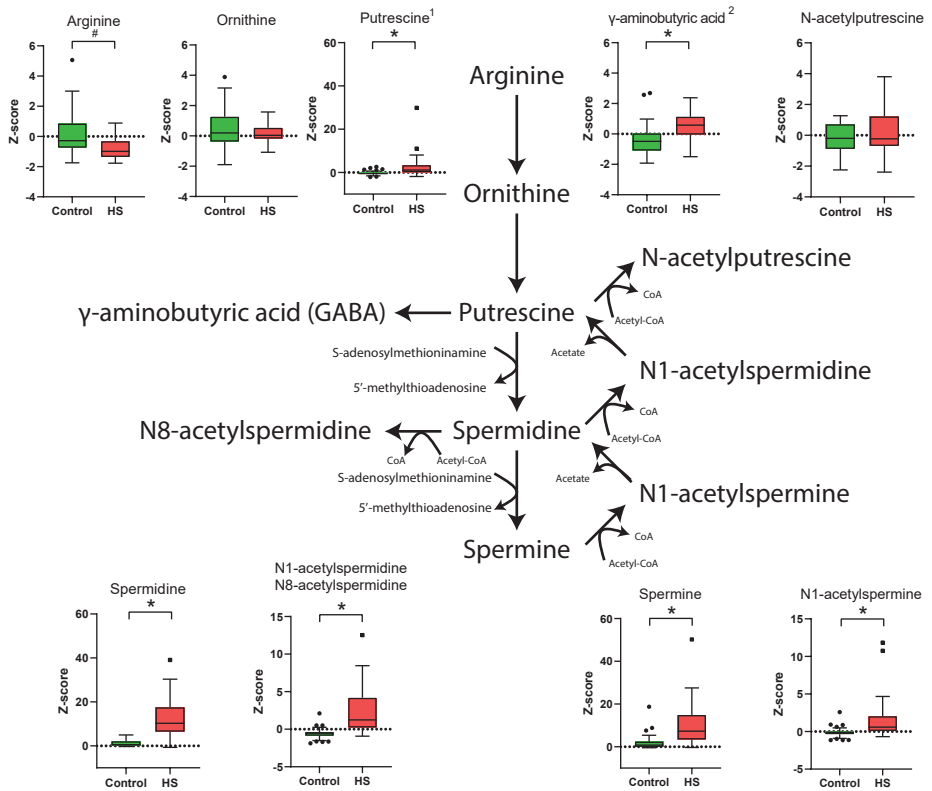


Figure S2. Arginine and polyamine metabolism. Schematic view of arginine and polyamine metabolism. Z-scores for metabolites in polyamine metabolism are plotted for healthy control ($n = 50$) and hereditary spherocytosis (HS) samples ($n = 35$) in a boxplot with Tukey whiskers. Arginine ($p=0.0002$), Ornithine ($p=0.3702$), Putrescine ($p<0.0001$), γ -aminobutyric acid ($p<0.0001$), N-acetylputrescine ($p=0.5531$), Spermidine ($p<0.0001$), N1/N8-acetylspermidine ($p<0.0001$), Spermine ($p<0.0001$), N1-acetylspermine ($p<0.0001$). Isomers include 1) 1,4-Butanediammonium. 2) Dimethylglycine, L/D-Alpha-aminobutyric acid, 2-Aminoisobutyric acid, (S)-b-aminoisobutyric acid, (R)-b-aminoisobutyric acid, 3-Aminoisobutanoic acid, 3-Aminobutanoic acid, N-Ethylglycine. * $p<0.0001$, # $p<0.001$.

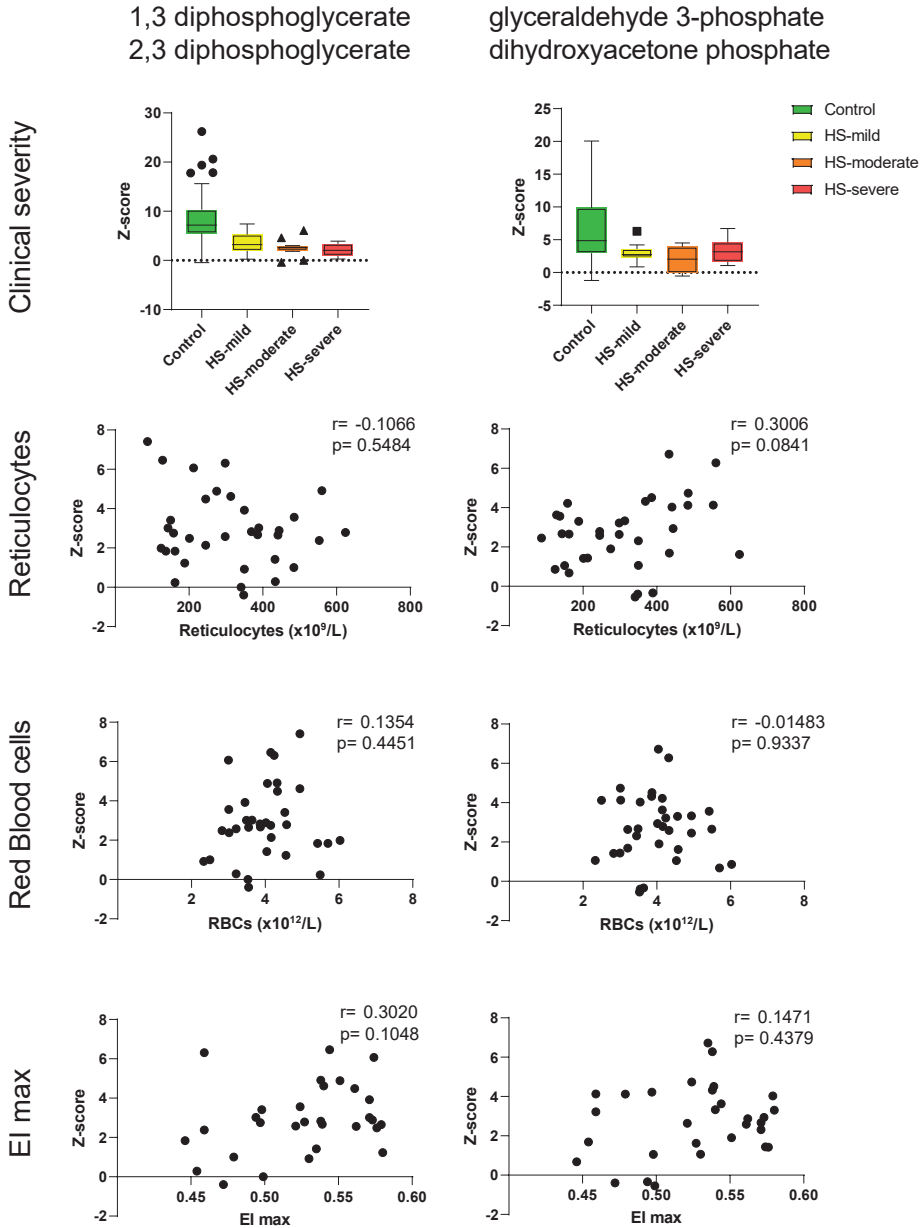


Figure S3. Association and correlation of 2,3-DPG and GA3P with disease severity and red cell characteristics in hereditary spherocytosis patients. Association and correlation of clinical severity (control ($n = 50$); HS-mild ($n = 15$); HS-moderate ($n = 12$); HS-severe ($n = 8$)) and reticulocytes ($n = 34$), red blood cells ($n = 34$) and EI max ($n = 30$), with Z-scores of 2,3 diphosphoglyceric acid and glyceraldehyde 3-phosphate in hereditary spherocytosis (HS) patients.

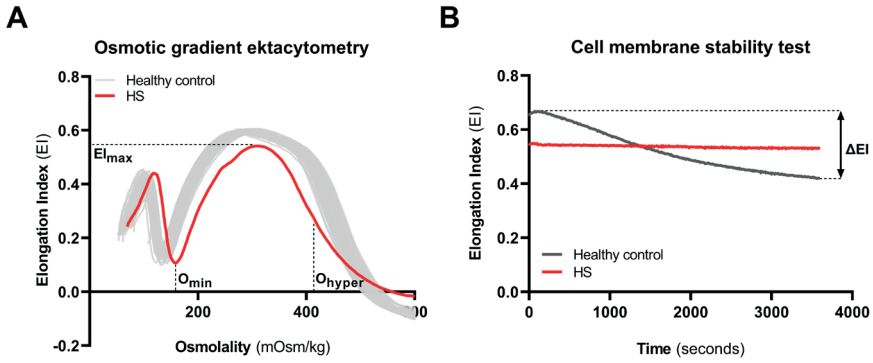


Figure S4. Ektactometry parameters. **A.** Osmotic gradient ektactometry showing representative curves of the elongation index for controls (grey) and hereditary spherocytosis (HS) patients (red). **B.** Representative curves for controls (grey) and HS patients (red) of the elongation index during the cell membrane stability test.

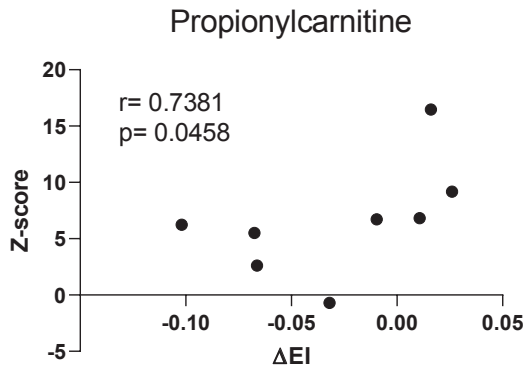


Figure S5. Correlation between propionylcarnitine and ΔEI . Correlation between Z-scores of propionylcarnitine and ΔEI (delta elongation index), as determined by the cell membrane stability test, in a subset of 8 hereditary spherocytosis patients

Table S1. Overview of variables important in projection (VIP)-scores and isomers corresponding to features in PLS-DA HS vs. controls in Figures 1C.

Feature	PLS-DA VIP (1)	PLS-DA VIP (2)	Isomers
Imidazoleacetic acid ribotide	16.153	15.398	-
Spermidine	12.596	11.933	-
Spermine	10.273	10.54	-
Propionylcarnitine	9.7093	8.9405	-
2,3-Diaminopropionic acid	8.1319	8.6139	-
Creatine	7.8802	7.3045	Beta-Guanidinopropionic acid
N-Acetylgalactosamine	7.2417	6.7968	-
2,3-Diphosphoglyceric acid	6.6605	6.2612	Glyceric acid 1,3-biphosphate
N-a-Acetylcitrulline	6.1522	5.7562	Alanyl-Glutamine; Alanyl-Gamma-glutamate; Glutaminy-Alanine; Gamma-glutamyl-Alanine
Oleoylcarnitine	5.8766	5.3717	Vaccenyl carnitine; Elaidic carnitine; Octadecenylcarnitine
Stearoylcarnitine	5.1206	4.6816	-
L-Acetylcarnitine	4.7738	4.3622	-
L-Palmitoylcarnitine	4.756	4.3483	-
Alanyl-Asparagine	4.5023	4.6997	Asparaginy-Alanine; Glutaminy-Glycine; Glycyl-Glutamine; Glycyl-Gamma-glutamate; Gamma-glutamyl-Glycine
D-Glyceraldehyde 3-phosphate	4.4768	4.285	Dihydroxyacetone phosphate
Linoelaidyl carnitine	4.2061	3.8438	Linoleyl carnitine
Lysyl-Valine	4.0785	3.7283	Valyl-Lysine
6-Methylthiopurine 5'-monophosphate ribonucleotide	3.7393	4.4437	-
N1-Acetylspermidine	3.5074	3.4406	N8-Acetylspermidine
Putrescine	3.5019	3.562	1,4-Butanediammonium
Orotidine	3.2311	2.9686	-
Ureidosuccinic acid	3.1428	3.0682	-
7-Methylguanane	3.0294	3.021	3-Methylguanane; 1-Methylguanane; N2-Methylguanane
Methionyl-Tyrosine	2.9513	2.8	Tyrosyl-Methionine
Neuraminic acid	2.9509	2.7679	-
Glycylproline	2.7333	3.0383	L-prolyl-L-glycine
cis-Aconitic acid	2.7288	2.6058	trans-Aconitic acid; Dehydroascorbic acid
Glutathione	2.6537	2.4294	-
Glucosamine-1P	2.6164	2.4412	Glucosamine 6-phosphate; Aminofructose 6-phosphate
L-Carnitine	2.5964	2.3736	-

Table S2. Overview of p-values and isomers corresponding to features in heatmap HS vs. controls in Figure 1D.

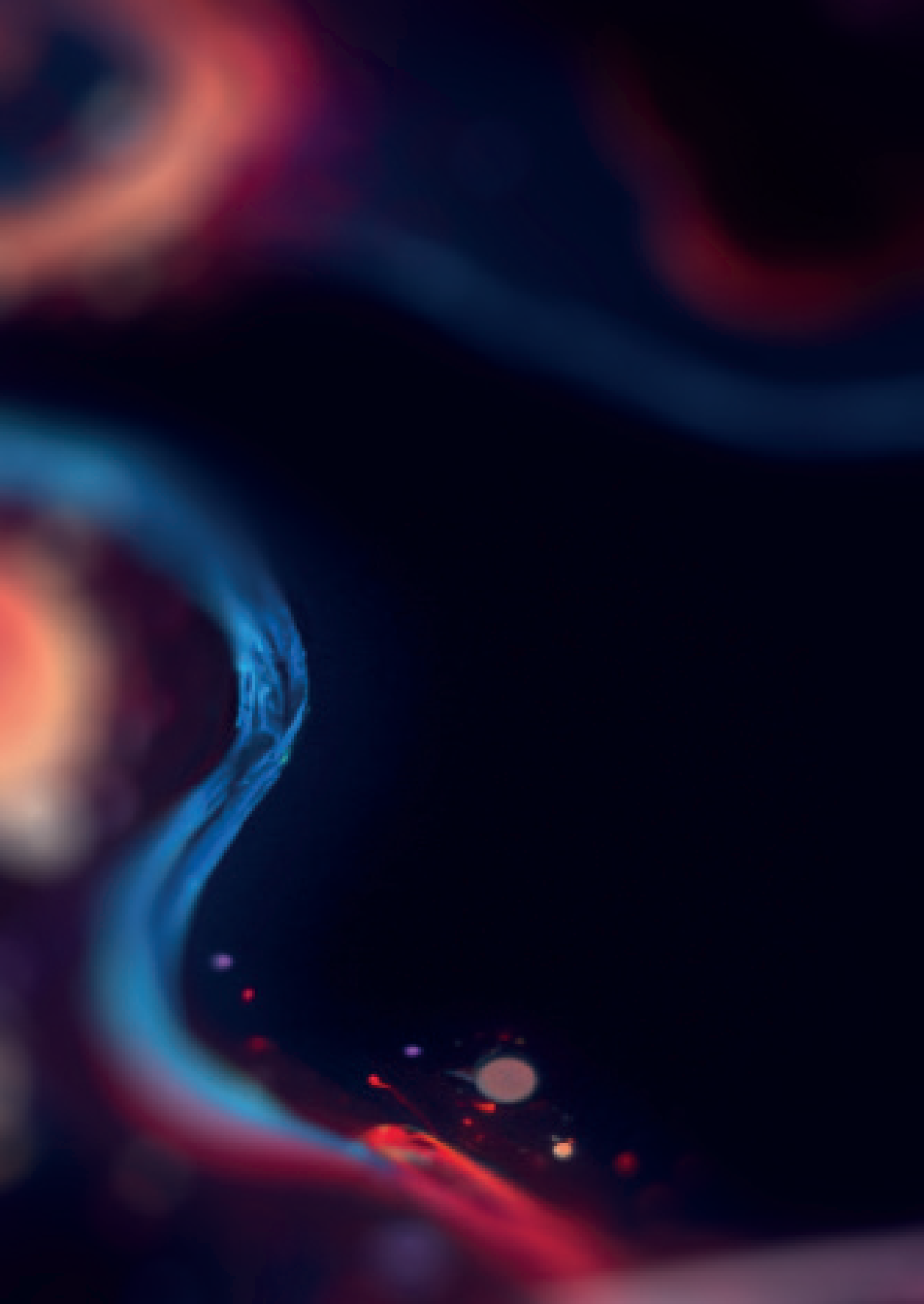
Feature	T-statistic	p-value	FDR	Isomers
L-Acetylcarnitine	-11.391	1.20E-18	2.12E-15	-
Imidazoleacetic acid ribotide	-10.757	2.09E-17	1.85E-14	-
cis-Aconitic acid	-10.399	1.06E-16	6.27E-14	trans-Aconitic acid; Dehydroascorbic acid
Propionylcarnitine	-9.3669	1.21E-14	5.33E-12	-
Molybdate	-9.1663	3.03E-14	1.07E-11	-
Estradiol	9.1087	3.96E-14	1.17E-11	17a-Estradiol
Oleoylcarnitine	-9.0075	6.31E-14	1.46E-11	Vaccenyl carnitine; Elaidic carnitine; 11Z-Octadecenylcarnitine
Creatine	-8.9981	6.59E-14	1.46E-11	Beta-Guanidinopropionic acid
L-Palmitoylcarnitine	-8.9282	9.09E-14	1.79E-11	-
Lysyl-Valine	-8.4544	8.06E-13	1.43E-10	Valyl-Lysine
Spermidine	-8.4091	9.93E-13	1.48E-10	-
Linoelaidyl carnitine	-8.4068	1.00E-12	1.48E-10	Linoleyl carnitine
L-Carnitine	-7.8443	1.33E-11	1.81E-09	-
N-Acetylgalactosamine	-7.7965	1.65E-11	2.09E-09	-
Imidazole-4-acetaldehyde	-7.4558	7.80E-11	9.21E-09	-
N-a-Acetylcitrulline	-7.3869	1.07E-10	1.18E-08	Alanyl-Glutamine; Alanyl-Gamma-glutamate; Glutamyl-Alanine; Gamma-glutamyl-Alanine
Glutamyl-Serine	7.1869	2.64E-10	2.74E-08	Seriny-Glutamate
Glucosamine-1P	-6.8325	1.29E-09	1.27E-07	Glucosamine 6-phosphate; Aminofructose 6-phosphate
Thymine	-6.7978	1.51E-09	1.41E-07	Imidazoleacetic acid; Imidazol-4-ylacetate
Stearoylcarnitine	-6.7648	1.75E-09	1.55E-07	-
N1-Acetylspermidine	-6.6223	3.29E-09	2.77E-07	N8-Acetylspermidine
Pyridoxal	6.2199	1.92E-08	1.55E-06	Isopyridoxal; 3-Methoxyanthranilate
2-Hexaprenyl-3-methyl-5-hydroxy-6-methoxy-1,4-benzoquinol	-6.1225	2.93E-08	2.16E-06	-
2,3-Diphosphoglyceric acid	6.1117	3.07E-08	2.16E-06	Glyceric acid 1,3-biphosphate
Phosphocreatinine	6.1063	3.14E-08	2.16E-06	-
4-Pyridoxolactone	6.1041	3.17E-08	2.16E-06	Formylanthranilic acid; 5-Pyridoxolactone; Noradrenochrome
Isobutyryl-L-carnitine	-6.0783	3.55E-08	2.32E-06	Butyrylcarnitine
Threonic acid	-6.0566	3.90E-08	2.42E-06	-
Malonic acid	6.0518	3.98E-08	2.42E-06	Hydroxypyruvic acid; Tatronate semialdehyde
Orotidine	-6.0446	4.10E-08	2.42E-06	-

Table S3. P-values and isomers of additional significant metabolites by t-test.

Feature	T-statistic	p-value	FDR	Isomers
4-Hydroxyproline	-5.9966	5.04E-08	2.87E-06	N-Acetyl-L-alanine; Propionylglycine; 5-Aminolevulinic acid; L-Glutamic gamma-semialdehyde; 4-Hydroxy-L-proline; 5-Amino-2-oxopentanoic acid; 4-Hydroxy-2-pyrrolidinecarboxylic acid; Trans-3-hydroxy-L-proline; cis-4-Hydroxy-D-proline
Vanilloylglycine	5.9896	5.19E-08	2.87E-06	-
Menadione	5.9479	6.21E-08	3.33E-06	-
MG(0:0/18:1(11Z)/0:0)	-5.8593	9.06E-08	4.72E-06	MG(0:0/18:1(9Z)/0:0); MG(18:1(11Z)/0:0/0:0); MG(18:1(9Z)/0:0/0:0)
Spermine	-5.7634	1.36E-07	6.87E-06	-
Neuraminic acid	-5.7516	1.43E-07	6.87E-06	-
Hydroxyphenylacetyl glycine	5.7508	1.44E-07	6.87E-06	-
Asparaginy-Proline	5.7324	1.55E-07	7.21E-06	Prolyl-Asparagine
3, 5-Tetradecadiencarnitine	-5.7268	1.59E-07	7.21E-06	-
Cytidine	-5.6782	1.95E-07	8.63E-06	Cytarabine
2-Keto-glutaramic acid	-5.6389	2.30E-07	9.94E-06	-
4-Hydroxy-2-oxoglutaric acid	-5.6286	2.40E-07	1.01E-05	D-4-Hydroxy-2-oxoglutarate
Ureidosuccinic acid	-5.6019	2.69E-07	1.11E-05	-
Alanyl-Asparagine	-5.5615	3.18E-07	1.28E-05	Asparaginy-Alanine; Glutaminyl-Glycine; Glycyl-Glutamine; Glycyl-Gamma-glutamate; Gamma-glutamyl-Glycine
Vinylacetyl glycine	-5.5471	3.38E-07	1.33E-05	-
Thiomorpholine 3-carboxylate	5.5048	4.03E-07	1.55E-05	-
Hexadecanedioic acid	5.496	4.18E-07	1.57E-05	-
Dodecanoylcarnitine	-5.42	5.73E-07	2.10E-05	-
3-Methyldioxyindole	5.4158	5.82E-07	2.10E-05	-
7-Methylguanine	-5.3847	6.62E-07	2.34E-05	3-Methylguanine; 1-Methylguanine; N2-Methylguanine
3,4-Dihydroxybenzylamine	5.3609	7.30E-07	2.50E-05	-
L-Aspartic acid	5.3582	7.38E-07	2.50E-05	D-Aspartic acid; Iminodiacetic acid
Citric acid	5.3547	7.49E-07	2.50E-05	Isocitric acid; D-threo-Isocitric acid; Diketogulonic acid; 2,3-Diketo-L-gulonate; (1R,2R)-Isocitric acid; D-Glucaro-1,4-lactone
L-Cystine	-5.3476	7.71E-07	2.53E-05	-

Table S4. Overview of variables important in projection (VIP)-scores and isomers corresponding to features in PLS-DA clinical severity HS vs controls in Figures 3C.

Feature	PLS-DA VIP (1)	PLS-DA VIP (2)	Isomers
Spermidine	14.763	13.888	-
Imidazoleacetic acid ribotide	13.668	12.906	-
Spermine	11.81	11.404	-
Propionylcarnitine	10.169	9.5686	-
N-Acetylgalactosamine	8.5139	8.0319	-
Creatine	8.4635	7.9687	Beta-Guanidinopropionic acid
2,3-Diaminopropionic acid	7.055	8.7283	-
N-a-Acetylcitrulline	6.9647	6.5514	Alanyl-Glutamine; Alanyl-Gamma-glutamate; Glutaminyl-Alanine; Gamma-glutamyl-Alanine
2,3-Diphosphoglyceric acid	6.0569	5.7429	Glyceric acid 1,3-biphosphate
Oleoylcarnitine	5.9224	5.5769	Vaccenyl carnitine; Elaidic carnitine; Octadecenylcarnitine
Alanyl-Asparagine	5.5823	5.277	Asparaginyl-Alanine; Glutaminyl-Glycine; Glycyl-Glutamine; Glycyl-Gamma-glutamate; Gamma-glutamyl-Glycine
L-Acetylcarnitine	5.1	4.8538	-
L-Palmitoylcarnitine	4.8819	4.5914	-
Stearoylcarnitine	4.7144	4.482	-
Lysyl-Valine	4.4029	4.2066	Valyl-Lysine
N1-Acetylspermidine	4.3864	4.1303	N8-Acetylspermidine
Linoelaidyl carnitine	4.3415	4.0896	Linoleyl carnitine
7-Methylguanine	3.9213	3.6971	3-Methylguanine; 1-Methylguanine; N2-Methylguanine
Orotidine	3.7519	3.5833	-
D-Glyceraldehyde 3-phosphate	3.7352	3.5269	Dihydroxyacetone phosphate



Chapter 9

Summary and general discussion

Summary

The main objective of this thesis was to contribute to a better understanding of the pathophysiology of several genetic diseases using untargeted metabolomics. We investigated the underlying mechanisms of disorders in the malate-aspartate shuttle (part 1) and introduced untargeted metabolomics as a novel investigative tool in rare hereditary anemias (part 2). Overall, we demonstrated that metabolomics aided in biomarker discovery (**chapter 2**) and identified novel pathophysiological leads (**chapter 5-8**). In addition, the combination of isotope tracing and untargeted metabolomics in cell models proved to be a powerful tool for unraveling pathophysiology and finding therapeutic targets (**chapter 4 and 5**). Furthermore, we demonstrated potential applications of untargeted metabolomics for diagnostic evaluation (**chapters 6 and 7**), response to treatment (**chapter 7**) and the assessment of clinical severity (**chapter 8**).

PART 1 – Pathophysiological insights into disorders of the malate-aspartate shuttle

In the first part of this thesis, we aimed to elucidate the pathophysiological mechanisms of inherited disorders of the malate-aspartate shuttle (MAS). The MAS is an important metabolic pathway for intracellular NADH oxidation and plays an important role in energy metabolism. Malate dehydrogenase 1 (MDH1) is a cytosolic enzyme that converts oxaloacetate to malate by oxidizing NADH to NAD⁺ and thus regenerates NAD⁺ in the cytosol. We reported a deficiency in MDH1 for the first time in two patients from a consanguineous family (**chapter 2**). Using untargeted metabolomics, we found significantly elevated levels of glycerol 3-phosphate in dried blood spots (DBS) of the patients. In the future, elevated glycerol 3-phosphate may be used as a biomarker for MDH1 deficiency.

Clinically, both MDH1-deficient patients presented with an early neurological phenotype of global developmental delay, epilepsy and progressive microcephaly. In a literature review, we compared our clinical and biochemical findings to the phenotypes of other MAS disorders (**chapter 3**). Currently, other MAS disorders that have been reported include MDH2, GOT2, AGC1 and AGC2 deficiency (which include the brain- and liver-specific isoforms for the aspartate glutamate carrier (AGC), respectively). Epilepsy, hypotonia and global developmental delay are common clinical features in MAS disorders with a neurological phenotype (excluding AGC2 deficiency). In addition, patients with MDH1, GOT2 and AGC1 deficiencies presented

with microcephaly. We concluded that there are currently no specific markers to support clinical diagnosis and that the disturbed redox homeostasis in MAS deficiencies affects multiple NAD⁺-dependent pathways with complex consequences due to compartmental and tissue-specific expression of the components. Some biochemical clues for these disorders include elevated lactate (MDH2, GOT2, AGC1), elevated glycerol 3-phosphate (MDH1), abnormalities of TCA cycle intermediates (MDH2), elevated ammonia (AGC2, GOT2), and low serine (GOT2).

To better understand MAS disorders and identify therapeutic targets, we investigated the metabolic consequences of MAS deficiencies. Due to limited availability of patient material, we used CRISPR/Cas9 to genetically disrupt each MAS component in cell lines. We identified a shared pathophysiological mechanism in all MAS-defective cells, including a low cytosolic NAD⁺/NADH ratio that disrupts both glycolysis and serine biosynthesis (**chapter 4**). Previously, it has been reported that GOT2-deficient patients had low serine synthesis, in whom serine supplementation proved clinically effective. Our findings imply that patients with other MAS deficiencies may benefit from serine supplementation as well.

A more systemic approach to restore the disturbed cytosolic NAD⁺/NADH ratio in MAS defects is to add electron acceptors that recycle NAD⁺, such as pyruvate and 2-ketobutyrate. We demonstrated that the addition of these electron acceptors restores the flux through glycolysis and serine biosynthesis in MDH1-deficient cells (**chapter 5**). Furthermore, we found an NAD⁺-dependent accumulation of ribitol and sorbitol. Ribitol, a metabolic end-product of the pentose phosphate pathway, was also found in high concentrations in DBS of patients with MDH1-deficient patients. This is likely due to the increased flux into the pentose phosphate pathway as a result of disrupted glycolysis. The conversion of sorbitol to fructose in the polyol pathway is also NAD⁺-dependent, and a block in this pathway may also contribute to the pathomechanism in MDH1-deficiency.

PART 2 – Metabolic phenotyping in rare hereditary anemias

In the second part of this thesis, we introduced metabolomics as a novel investigative tool for rare hereditary anemias (RHA). RHA are a group of heterogeneous disorders caused by either intrinsic red blood cell (RBC) defects or defects in erythropoiesis, resulting in increased decay or impaired synthesis of RBCs, respectively. RBCs are metabolically limited to glycolysis for ATP production, which is generated

by the conversion of phosphoenolpyruvate to pyruvate by pyruvate kinase (PK). PK deficiency (PKD) causes anemia by diminishing ATP production in RBCs, while glycolytic intermediates accumulate. Indeed, the metabolic profile in DBS from 22 PKD patients revealed increased levels of the glycolytic intermediates phosphoenolpyruvate and 2-/3-phosphoglycerate (**chapter 6**). In addition, we identified a disease fingerprint for PKD that includes increased polyamines, (acyl) carnitines, and decreased glutathione, providing leads for future pathophysiological investigations in PKD. Moreover, we demonstrated that we could confirm or rule out the diagnosis of PKD based on a metabolic fingerprint using a predictive machine learning model. This illustrates how untargeted metabolomics in DBS can be used to identify disease-specific fingerprints and aid in the diagnosis of an anemic disease.

Within the spectrum of RHAs, Diamond Blackfan Anemia (DBA) is a ribosome biogenesis disorder resulting in anemia. To investigate the diagnostic potential of untargeted metabolomics in an even more clinically and genetically heterogeneous disorder without established screening tests, we studied the DBS of DBA patients (**chapter 7**). Again, we used machine-learning to predict the diagnosis of DBA patients based on their metabolic fingerprints. The metabolic fingerprints of DBA patients revealed increased inosine levels and decreased glutathione, 2,3-DPG and glyceraldehyde 3-phosphate levels compared to controls. In addition, a clinically and diagnostically similar disease, congenital dyserythropoietic anemia (CDA), revealed a different metabolic fingerprint compared to DBA, implying that delineating a diagnosis based on metabolic fingerprint is feasible in these disorders. In addition, we found that different treatment modalities resulted in a different metabolic signature in DBA patients, suggesting that untargeted metabolomics could be a useful tool for investigating and monitoring treatment response.

Finally, we used untargeted metabolomics to investigate the clinical phenotypic heterogeneity in patients with hereditary spherocytosis (HS), an RBC membrane integrity disorder (**chapter 8**). We found that HS patients with severe clinical phenotypes had the most distinct metabolic fingerprint compared to controls and HS patients with milder phenotypes. In addition, several metabolites correlated with underlying RBC characteristics of anemia in HS patients, such as the number of reticulocytes and RBCs. Furthermore, discovered pathophysiological leads for HS included a decrease in glycolytic intermediates (glyceraldehyde 3-phosphate and 2,3-DPG) and glutathione, as well as an increase in polyamines, acetylcarnitine and propionylcarnitine. These findings demonstrate that untargeted metabolomics can be used to provide insight into the clinical heterogeneity of a highly heterogeneous disorder.

General discussion

Rare hereditary diseases encompass a broad spectrum of diseases, and their diagnosis and treatment present a unique challenge. Identifying the causal variant in a gene is often essential for diagnosis and prognosis. However, the genetic and phenotypic heterogeneity of many rare hereditary diseases complicates the recognition of individual disorders. Many disorders present with a non-specific and widely divergent clinical phenotype, affecting many tissues, organ systems, or specific biological functions. As a result, untargeted metabolomics applications can play a complementary role in improving the diagnostics and treatment of rare hereditary diseases. The metabolome, as a functional readout of the interactions between the genome and the environment, can provide crucial insights into disease and disease progression. In this thesis, we applied untargeted metabolomics to increase our pathophysiological knowledge of several rare inherited diseases to ultimately improve their diagnosis and treatment.

PART 1 – Pathophysiological insights into disorders of the malate-aspartate shuttle

Diagnosing MAS defects

Observations on the surface: the phenotypic spectrum

Twenty years after the first report of a malate-aspartate shuttle (MAS) disorder, citrin deficiency,¹ the discovery of two novel MAS disorders (GOT2 and MDH1 deficiency) renewed interest in studying the metabolic consequences of MAS disorders. The most recently discovered disorder, MDH1 deficiency, is described in this thesis in two patients from a consanguineous Saudi family (**chapter 2**). Clinically, the patients presented with global developmental delay, microcephaly and seizures, which are clinical phenotypes shared by other neurological MAS disorders (AGC1, MDH2 and GOT2) (**chapter 3**). Understanding which genetic mutations cause specific phenotypic traits can aid in the diagnosis of future patients with a clinically similar phenotype. One way to compare clinical phenotypes is to use a standardized vocabulary for describing phenotypic abnormalities in human disease: the Human Phenotype Ontology (HPO) database.² Using the HPO database, we identified a uniform neurological MAS phenotype with early onset epilepsy, severe global developmental delay and muscle hypotonia (**chapter 3**). Clinical phenotypic differences may depend on the genetic variant, but they also partly depend on the number of reported cases and the patient's age at the time of reporting.

The phenotypic spectrum will probably expand when the number of diagnosed patients and follow-up reports increases, as illustrated by the recent descriptions of additional patients with AGC1 and MDH2 deficiency.³⁻⁶ As a result, the reported clinical phenotype of MDH1 deficiency may not be representative of the disease's overall clinical phenotype (**chapter 2**).

Recognizing a disease solely based on clinical phenotypes is challenging, since phenotypic traits are often not unique to a disorder. Disorders of the MAS present with relatively common phenotypic features, including developmental delay (Citrin, MDH1), seizures (GOT2, MDH2, AGC1), and hypotonia (AGC1, MDH2) (**chapter 3**). These clinical characteristics are among the top 15 HPO terms associated with rare diseases,⁷ illustrating that MAS disorders clinically overlap with a wide range of other disorders. For example, metabolic epilepsies cover a broad group of IMDs, including energy metabolism defects, neurotransmitter disorders, and disorders of amino acid metabolism, such as urea cycle defects, organic acidurias, and disorders of glycine and serine metabolism.^{8,9} Developmental delay, seizures and hypotonia are shared by 314, 407 and 478 genetic disorders in the IEMbase, respectively (accessed 8-11-2022).¹⁰ Genetic metabolic disorders that also present with developmental delay, seizures and hypotonia include defects related to cobalamin metabolism, vitamin and cofactor metabolism, and pyruvate metabolism and TCA cycle (Figure 1). This exemplifies how different genetic causes can result in similar clinical phenotypes on the surface, but also how a broad and unspecific clinical phenotype complicates the recognition of individual cases. Ultimately, the integration of both phenotypic data and biomedical knowledge can greatly advance the recognition of rare diseases.¹¹ Hence, both phenotypic and molecular data are important in the diagnosis of rare inherited diseases.

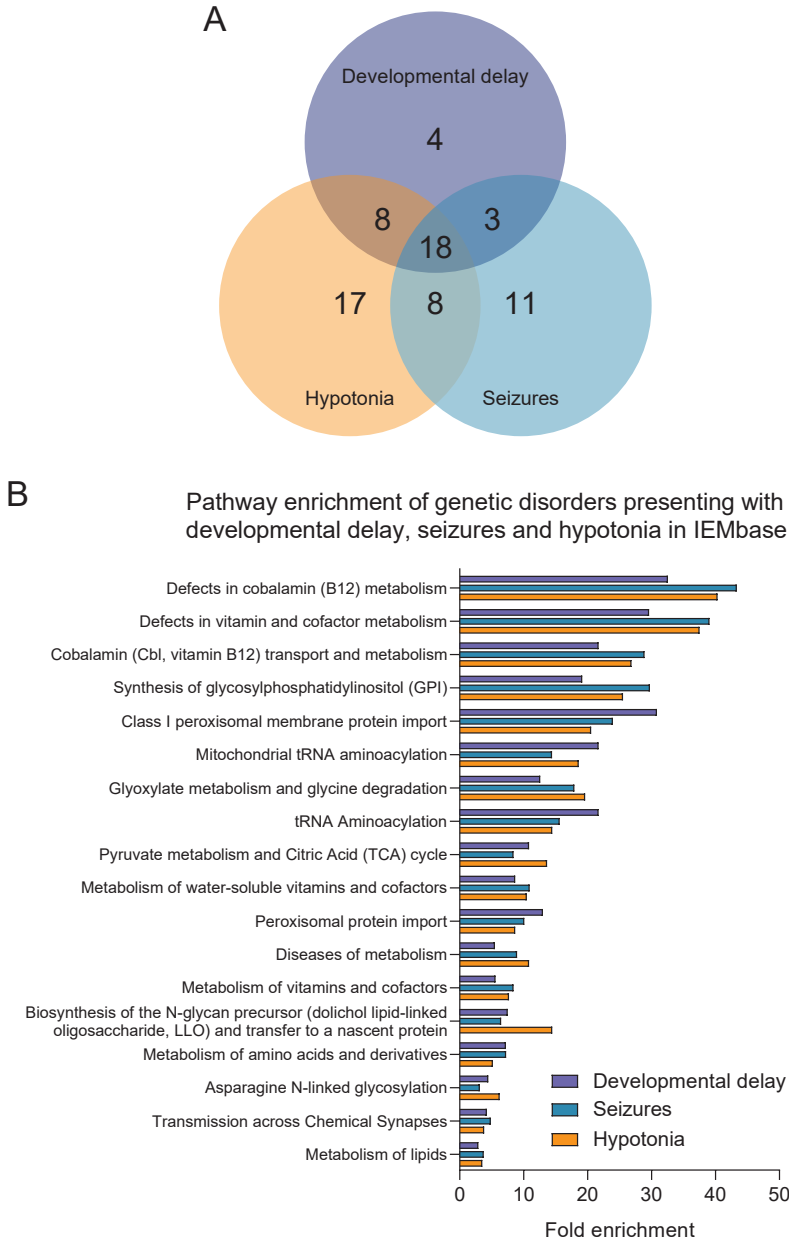


Figure 1. Pathway enrichment analysis of genes associated with common clinical neurological phenotypes. A. Venn diagram depicting the number of IEMbase genes associated with developmental delay, hypotonia and seizures. **B.** The Reactome Pathway Database was used to perform an enrichment analysis of genes associated with developmental delay, seizures and hypotonia in the IEMbase (excluding MAS disorders), where the fold enrichment is calculated from the ratio of expected genes to observed genes in the human genome.

Beneath the surface: the molecular spectrum

Biochemical analysis provides molecular insights that help to narrow down diagnostic indications based on clinical phenotypes. Examining the biochemical similarities and differences in neurologic MAS disorders identified elevated plasma lactate as a shared biochemical biomarker, although its plasma level is reported normal in some cases (**chapter 3**). Since lactate is elevated in many neurological disorders, this does not provide a specific biochemical indication for a MAS disorder. An elevated lactate/pyruvate ratio, on the other hand, is a more specific biochemical parameter that is only shared with a few mitochondrial disorders, such as complex I deficiency or TCA cycle disorders (Figure 2). Individual markers identified through routine diagnostic screening include elevated plasma citrulline in GOT2 and citrin deficiency. Since both components are linked to the urea cycle via the provision of aspartate, hyperammonemia is a biochemical trait that these MAS disorders share with urea cycle disorders but also with many other disorders (Figure 2).¹² Further individual markers of these disorders include elevated arginine in AGC2 deficiency and low serine levels in CSF in GOT2 deficiency, the latter reflecting a biochemical trait shared by disorders of serine biosynthesis (Figure 2).¹³ AGC1 deficiency is mainly characterized by decreased N-acetylaspartate levels in the brain. MDH2 deficiency is associated with elevated urinary malate, fumarate, and, in some cases, succinate.^{4-6,14} Elevated fumarate is associated with several mitochondrial disorders, but increased malate appears to be a relatively unique biochemical aberration among the reported disorders in the IEMbase.¹⁰ In addition, elevated concentrations of urinary 3-methylglutaconic acid and methylmalonic acid, which are commonly reported in mitochondrial disorders, organic acidurias, and cobalamin metabolism, have been reported in some patients with MDH2 deficiency (Figure 2).⁴ Interestingly, routine diagnostic screening revealed no abnormalities in the plasma of MDH1-deficient patients. However, we identified increased levels of glycerol 3-phosphate (G3P) and glutamate in dried blood spots (DBS) of patients with MDH1 deficiency using untargeted metabolomics (**chapter 2**). Many MAS biochemical disturbances overlap with groups of disorders with metabolic epilepsies (e.g., disorders in energy and amino acid metabolism),⁸ indicating that these particular underlying biochemical consequences lead to similar clinical phenotypes. Investigating the molecular consequences of MAS disorders provides insights into whether these metabolic disturbances play a role in the pathophysiology. Ultimately, understanding the molecular consequences of a pathogenic mutation can aid in better disease management.

Pathophysiological insights and therapeutic strategies for MAS defects

MAS in the central nervous system

The MAS components are highly expressed in the brain and central nervous system. Neurons and astrocytes are the two main cell types in nervous tissue, with the latter accounting for roughly half of all brain cells. Since neural signaling regulation and membrane potential stabilization require large amounts of energy, a deficiency in energy metabolism may result in seizures due to the destabilization of ion gradients and membrane potentials.^{15,16} Since the MAS plays an important role in energy metabolism, this is also reflected in MAS disorders that present with a clinical neurological and epileptic phenotype (**chapter 3**). Interestingly, accumulating evidence suggests that neurons and astrocytes use different redox shuttles.^{17–21} Since these cells do not fully express both shuttles, cell type-specific MAS and glycerol phosphate shuttle (GPS) component expression *in vivo* is likely to play an important role in the neuropathophysiological consequences of MAS disorders. All MAS components are highly expressed in neurons, but AGC1 is only weakly expressed in astrocytes.^{22,23} The GPS components are expressed in both cell types,^{24,25} but the overall GPS activity in the brain appears to be low.²⁵ Since astrocytes have high glycolysis and lactate production while mitochondria have low oxygen consumption,^{20,21,26,27} GPS appears to be the primary NADH shuttle in transferring reducing equivalents to mitochondria in astrocytes. Furthermore, neurons are thought to take up lactate in order to use it as a direct NADH source, which is consistent with neurons having lower glycolytic activity than astrocytes,²⁸ though the proposed use of lactate as the preferred substrate in neurons leads to controversy in literature.^{29,30} In order to facilitate the conversion of lactate to pyruvate and NADH, the MAS is required to sustain NAD⁺-regeneration and the transport of reducing equivalents into neuronal mitochondria.²⁸ In addition, when neurons are stimulated in the presence of glucose, Ca²⁺-dependent activation of the MAS drives glycolysis and oxidative phosphorylation.³¹ The exact mechanisms, preferred substrates, and role of the MAS in neuronal energy metabolism may be dependent on the cellular location in the brain and availability of substrates, but this is yet unresolved. Furthermore, energy metabolism is intimately linked to multiple cellular processes, including the glutamine-glutamate cycle, which is involved in regulating neurotransmission. Astrocytes supply glutamine to neurons, which is used to replenish neuronal glutamate and GABA pools. Only astrocytes are capable of *de novo* glutamate synthesis, since neurons lack the enzyme pyruvate carboxylase, which is required for this anaplerotic process.^{32,33} The astrocyte-specific glutamine synthetase converts glutamate and ammonia into glutamine.^{34,35} Glutamine can then be transported to neurons, where it is converted to glutamate before being excreted

for neurotransmission. Similar to MAS disorders, glutamate homeostasis disorders can cause severe neonatal encephalopathies.^{36,37}

Glycerol 3-phosphate: a convenient consequence?

Cytosolic glycerol phosphate dehydrogenase (cGPD) converts dihydroxyacetone phosphate (DHAP) to G3P, which is paired with cytosolic NAD⁺-regeneration and thus may play a role in maintaining NAD⁺/NADH balance in MAS disorders. Indeed, elevated G3P levels have been reported in DBS of MDH1-deficient patients (**chapter 2**), and elevated glycerol/G3P levels have been demonstrated in the brain MRS of an AGC1-deficient patient.³ Furthermore, all MAS-deficient cells had increased G3P due to increased flux from glycolysis, which was associated with the extent of the NAD⁺/NADH imbalance (**chapters 4 and 5**). Due to low cytosolic NAD⁺/NADH and disturbed glycolysis, mice and cells with respiratory chain dysfunction display elevated G3P in a similar fashion.^{25,38} Overexpression of cGPD increased the NAD⁺-regenerating capacity in mice with complex I dysfunction, alleviating the cytosolic NAD⁺/NADH redox imbalance and, consequently, the neurological phenotype.²⁵ These findings imply that increased GPS activity may serve as a convenient mechanism in the case of an NAD⁺/NADH imbalance. Indeed, recent evidence has shown that when MAS activity and calcium signaling are impaired, the GPS provides some metabolic flexibility to maintain ATP production in hippocampal neurons.^{39,40} Although we observed an initial increase in the conversion of DHAP to G3P in MDH1-deficient cells, this decreased over time (**chapter 5**). When the enzymatic capacity of cGPD is insufficient, the GPS may rapidly reach its maximum capacity, resulting in the accumulation of its intermediates.⁴¹ DHAP accumulation may lead to additional product inhibition of the irreversible mitochondrial GPD.⁴² Furthermore, mGPD competes for available coenzyme Q with dihydroorotate dehydrogenase (DHODH), which catalyzes the conversion of dihydroorotate to orotate in the pyrimidine synthesis from aspartate and glutamine.⁴³ Since aspartate levels are increased in MDH1-deficient cells, this mechanism may play a role as well. Overall, this suggests that a dysfunctional MAS disrupts glycolysis resulting in increased metabolic flux to G3P and, as a result, the ability to compensate energetically for a dysfunctional MAS. However, this mechanism is likely to be temporary in parts of the brain and may not be adequate in the long term.

Fueling the TCA cycle: supplying energy sources

The TCA cycle, which generates NADH to facilitate ATP production in the electron transport chain, plays an essential role in mitochondrial energy metabolism. TCA cycle activity requires fueling with energy-rich substrates, such as pyruvate, glutamate and malate.⁴⁴ MAS dysfunction disturbs glycolysis and decreases the flux from glucose to pyruvate and thus the TCA cycle (**chapter 4**). The flux from

pyruvate in the TCA cycle is further constrained by a low cytosolic NAD^+/NADH balance that suppresses pyruvate dehydrogenase (PDH) activity to generate lactate and NAD^+ from pyruvate.⁴⁵ Interestingly, it has been shown that upon inhibition of pyruvate entry into the mitochondria, neurons rewire their metabolism and can use glutamate as a major source that fuels the TCA cycle at the expense of glutamergic neurotransmission.⁴⁶ This is in line with the fall of glutamine and glutamate in AGC1-deficient mice, which points to a gradual impairment of glutamergic transmission and may also occur in other MAS disorders. In addition to neuronal tissue, the TCA cycle is essential for all other tissues in the body. Thus, therapeutic strategies to fuel the TCA cycle intermediates are of great interest in MAS disorders.

Pyruvate

Pyruvate supplementation in those MAS disorders in which intracellular pyruvate is decreased has two potentially beneficial effects since it may support cytosolic NAD^+ -recycling by its conversion to lactate and also fuels the TCA cycle by providing a direct source for acetyl-CoA. In MDH1-deficient cells, pyruvate supplementation restored glycolysis and increased citrate while decreasing aspartate accumulation (**chapter 5**). Here, pyruvate allows oxaloacetate to be metabolized with acetyl-CoA via citrate synthase to form citrate rather than being converted to aspartate by GOT2. Since high oxaloacetate levels inhibit SDH/complex II, lowering oxaloacetate levels has an additional beneficial effect on TCA cycle activity.⁴⁷ Pyruvate supplementation may also be effective in other MAS disorders, as illustrated in AGC1-deficient neurons, where pyruvate was able to fully recover the limited respiration.²⁸ In addition, while aspartate synthesis is low in GOT2-deficient cells, pyruvate supplementation has been shown to restore it, most likely in a GOT1-dependent manner.⁴⁸ Low-dose pyruvate supplementation may be considered as a therapeutic option in several MAS disorders due to the low initial concentrations and the multifaceted role of pyruvate in the TCA cycle and NAD^+/NADH redox imbalance, which is further discussed in the section NAD^+ -recycling.

Triheptanoin

Triheptanoin is another anaplerotic compound that fuels the TCA cycle and has recently regained interest in the field. Triheptanoin is a triglyceride composed of glycerol with three heptanoates (seven carbons) that is metabolized to multiple TCA cycle anaplerotic substrates, including acetyl-CoA and propionyl-CoA. It was originally developed for the treatment of long-chain fatty acid oxidation disorders.^{49–51} In the brains of healthy mice, triheptanoin contributes to TCA cycle anaplerosis, primarily in astrocytes, resulting in glutamine production.⁵² In a case of MDH2 deficiency, triheptanoin improved neurological development and the patient's

overall health.⁶ Furthermore, plasma lactate levels decreased significantly. MDH2 deficiency impairs oxaloacetate formation and results in acetyl-CoA accumulation. Abundant acetyl-CoA inhibits PDH and activates pyruvate carboxylase to shunt pyruvate to oxaloacetate, balancing the entry of oxaloacetate with acetyl-CoA in the TCA cycle. Since acetyl-CoA accumulates in MDH2-deficient cells, triheptanoin's beneficial properties are most likely due to propionyl-CoA entering the TCA cycle at the level of succinate. In addition, since acetyl-CoA entry into the TCA cycle is low, MDH2-deficient cells may become more reliant on glutaminolysis to fuel the TCA cycle. The elevated plasma glutamine in the MDH2-deficient patient treated with triheptanoin could be attributed to triheptanoin performing a similar function in fueling the TCA cycle or to an anaplerotic overflow stimulating glutamine production.^{6,52} Other MAS-deficient cells may benefit from triheptanoin in an acetyl-CoA-dependent manner, which may have similar effects on TCA cycle continuation as pyruvate supplementation. The potential multifaceted roles of triheptanoin in MAS disorders warrant further investigation.

Ketogenic diet and beta-hydroxybutyrate

A ketogenic diet (KD) is a low-carbohydrate, high-fat diet that has been proven to be a safe and effective treatment for epilepsy.⁵³ A KD causes metabolism to shift from glycolysis to β -oxidation, thereby lowering the cytosolic NADH/NAD⁺ ratio. In addition, a KD provides ketone bodies and fatty acids that serve as alternative substrates for the TCA cycle, which provides both NADH and FADH₂ to the elements of the electron transport chain. Enzymes in β -oxidation transfer electrons to Coenzyme Q via electron transfer flavoprotein, which is an important regulatory hub that controls electron flow to the respiratory chain via flavoenzyme-linked dehydrogenation reactions. Indeed, KD therapy is effective in improving seizures and overall development in patients with the MAS disorders MDH2 and AGC1 deficiency.^{3,14,54,55} In addition, muscle tone, head control and development improve in some patients. In the case of AGC1 deficiency, a KD resulted in significant clinical improvement as well as normalization of accumulated glycerol/G3P in the brain.³ Since the KD with low carbohydrates is highly unpalatable and has low compliance, the administration of β -hydroxybutyrate, the main metabolic product in a ketogenic diet, was investigated in AGC1-deficient mice in glucose-unrestricted conditions. Administration was shown to be beneficial for myelination and dopamine homeostasis, likely via enhancing mitochondrial NADH production, respiration, and ATP synthesis due to the provision of an acetyl-CoA source.⁵⁶ In addition, AGC1-deficient neurons display increased aspartate and N-acetylaspartate synthesis upon administration of β -hydroxybutyrate. However, by bypassing glycolysis and thus preventing the potentially harmful accumulation of several glycolytic intermediates

and derivatives (e.g., G3P, DHAP and sorbitol), while simultaneously providing alternative sources for ATP generation, we currently support the KD as a dual-effective pathomechanism-based dietary treatment approach for MAS disorders.

Serine biosynthesis, one carbon and folate metabolism

In the brain, serine is an important neuromodulator that is primarily synthesized *de novo* in astrocytes which exclusively express the NAD⁺-dependent phosphoglycerate dehydrogenase (PHGDH).⁵⁷ L-serine serves as a precursor for D-serine synthesis in both glutamatergic and GABAergic neurons, where it regulates glutamatergic neurotransmission by binding to an N-methyl-D-aspartate receptor (NMDAR) subunit.⁵⁸⁻⁶⁰ In addition, L-serine serves as a precursor for the neurotransmitter glycine and the synthesis of neuronal membrane lipids.^{61,62} The importance of serine synthesis in neurodevelopment is demonstrated by disorders in the enzymes of the serine synthesis pathway that present with microcephaly, seizures and psychomotor retardation.^{13,63} As serine was low in GOT2-deficient patients, we hypothesized that the disturbed NAD⁺/NADH ratio in MAS disorders leads to a secondary serine biosynthesis defect.⁶⁴ Indeed, all MAS-deficient cells have diminished *de novo* serine biosynthesis on a cellular level (**chapter 4**). Interestingly, since cells require a constant high cytosolic NAD⁺/NADH ratio for cellular processes, pyruvate to lactate oxidation becomes the primary source of cytosolic NAD⁺-regeneration in MAS deficient cells.^{41,65} The regeneration of cytosolic NAD⁺ by pyruvate to lactate is expected to be sufficient for the continuation of PHGDH-mediated serine biosynthesis, at least to some extent. In MDH1-deficient cells, the PHGDH-dependent conversion of 3-PG to 3-PHP occurred continuously; however, the conversion of 3-PHP to 3-phosphoserine by phosphoserine aminotransferase (PSAT) did not (**chapter 5**). According to a recent study, PSAT also has affinity for DHAP.⁶⁶ The strong correlation between serine and G3P synthesis from glucose may support the hypothesis that G3P and DHAP accumulation contributes to the severity of the secondary serine biosynthesis defect (**chapter 4**). Therefore, the association between G3P, DHAP, PSAT and serine synthesis requires further investigation. In addition, since serine is mainly synthesized in astrocytes and MAS activity occurs primarily in neurons, the *in vivo* serine biosynthesis defect in the brain is challenged. Investigating whether astrocytic G3P levels are elevated, as well as whether elevated systemic G3P levels interfere with *de novo* serine biosynthesis in the brain can provide additional insight into the pathophysiological mechanisms that contribute to the clinical neurological phenotype observed in MAS disorders.

Patients with disorders in the serine biosynthesis clearly benefit from timely serine supplementation; thus, the shared pathophysiological mechanism in MAS disorders

may provide the basis for timely serine supplementation in patients as well. In two patients with GOT2 deficiency, therapeutic serine supplementation partly alleviated the clinical neurological symptoms.⁶⁴ However, a case description of a patient with AGC1 deficiency demonstrated no clear clinical benefit from serine and glycine supplementation.³ Although serine supplementation may not be sufficient to prevent worsening of the disease, it could be a supportive treatment since serine is also an important one-carbon donor in folate metabolism. The conversion of serine to glycine donates a one-carbon unit to tetrahydrofolate (THF) to generate 5,10-methylene-THF.⁶⁷ Cytosolic 5,10-methylene-THF contributes to the continuation of the methionine cycle or can be further oxidized to 10-formyl-THF for purine synthesis. Since disorders of serine biosynthesis can lead to mild to moderate cerebral folate deficiency, folate metabolism may be affected in MAS disorders as well.⁶⁸ Moreover, MAS disorders share phenotypic and biochemical traits with cobalamin metabolism, where the ability to regenerate THF from 5,10-methylene-THF is affected (Figures 1 and 2).⁶⁹ The methylation of homocysteine to methionine requires cobalamin and a methyl-group donor derived from folate metabolism or from betaine, which is derived from choline in the liver and kidney.^{70,71} As such, dietary folate can moderate the dietary requirement for choline (and betaine) and vice versa.⁷¹⁻⁷³ Interestingly, decreased choline in patients with MDH1 deficiency suggests a disturbance in choline metabolism and may indicate increased use of choline as the main donor for methyl-groups (**chapter 5**). Further investigations into one-carbon and folate metabolism in MAS disorders could identify whether folate and choline supplementation serve as additional therapeutic strategies.

MAS disorders share a disturbed cytosolic NAD⁺/NADH ratio and several clinical features with disorders of the respiratory chain,⁷⁴⁻⁷⁶ implying that these patients may benefit from serine supplementation as well. Indeed, dysfunction of the respiratory chain results in impaired *de novo* serine biosynthesis.⁷⁷ In addition, mitochondrial respiratory chain dysfunction disturbs mitochondrial folate metabolism, as demonstrated by impaired serine catabolism to formate.⁷⁸ Furthermore, mitochondrial catabolism of serine has been shown to contribute to the mitochondrial NADH pool upon respiratory chain inhibition.⁷⁹ Although persistent serine catabolism may contribute to toxic NADH accumulation in mitochondrial disorders,⁷⁹ this may provide an additional benefit for MAS disorders with impaired NADH transfer to the mitochondrial matrix.

NAD⁺-recycling and boosting

MAS disorders are characterized by a deficiency in the cytosolic recycling of NAD⁺ from NADH. In addition to the effects on central carbon metabolism, the effects

of a disturbed NAD^+/NADH ratio on metabolism are extensive, as supported by the observed disturbances in purine and serotonin metabolism in untargeted metabolomics data (**chapters 2 and 5**). Hence, a systematic approach to improve NAD^+ -recycling could be more effective in treating MAS disorders. From literature, it is well known that the addition of excess pyruvate to cells can restore the intracellular NAD^+/NADH imbalance. Indeed, alleviating the cytosolic NAD^+/NADH imbalance by pyruvate supplementation in MDH1-deficient cells restored glycolysis, lowered G3P and DHAP and increased serine biosynthesis, in line with previous work in GOT2 KO cells (**chapter 5**).⁶⁴ In addition, 2-ketobutyrate can recycle NAD^+ by its conversion to 2-hydroxybutyrate and also restore the flux through glycolysis and the pathways branching therefrom in MDH1-deficient cells.⁸⁰ 2-ketobutyrate is generated from cysteine or threonine degradation and also feeds the TCA cycle via conversion to propionyl-CoA.⁸¹ Similar to elevated lactate, high levels of 2-hydroxybutyrate have been associated with diabetes and mitochondrial disease, reflecting the redox imbalance in these disorders.^{76,82,83} Although pyruvate supplementation effectively restores the NAD^+/NADH balance, it is also clear that administering pyruvate to patients with a disturbed NAD^+/NADH balance can be problematic due to the risk of lactic acidosis. However, promising results with pyruvate supplementation have been reported in several clinical reports, including in citrin (AGC2) deficiency and mitochondrial disorders.^{84,85} Whether 2-ketobutyrate is suitable for treating patients is unknown. Interestingly, an engineered fusion enzyme between bacterial lactate oxidase and catalase (LOXCAT), which irreversibly converts lactate and oxygen to pyruvate and water, has been found to reduce the NADH/NAD^+ ratio *in vitro* and *in vivo*.⁸⁶ In the future, this type of invention may offer a promising therapeutic option to correct the disturbed cytosolic NAD^+/NADH ratio in MAS defects.⁸⁷

Deficiency in NAD^+ -recycling may also lead to the depletion of total NAD^+ -pools. The total NAD^+ -pools are important for NAD^+ -consuming enzymes, including sirtuins, CD38 and poly (ADP-ribose) polymerases.^{88,89} In these reactions, NAD^+ is irreversibly catabolized by cleavage to nicotinamide. Overall, NAD^+ is a mediator of key cellular functions and adaptation to metabolic needs, including metabolic pathways, redox homeostasis and maintenance and repair of DNA. Continuous NAD^+ -synthesis is required to avoid depletion of intracellular NAD^+ -pools, which can be synthesized *de novo* from tryptophan, through the Preiss-Handler pathway from nicotinic acid, or via the salvage pathway from NAD^+ -precursors (e.g., nicotinamide mononucleotide or nicotinamide riboside).⁸⁹ Whether the total levels of NAD^+ and NAD^+ -related signaling are also disturbed in MAS disorders is unknown; however, untargeted metabolomics data from MDH1-deficient patients point out disturbances in NAD^+ -synthesis by decreased NAD^+ -degradation products (N1-methyl-2-pyridone-5-carboxamide

and nicotinamide N-oxide), as well as a decrease in a side product of tryptophan degradation (5-hydroxykynurenamine) (**chapter 5**). NAD⁺-enhancers are interesting therapeutic options for patients with impaired NAD⁺ metabolism. Supplementation of NAD⁺ has already been shown to improve systemic NAD⁺-deficiency in several disorders, such as mitochondrial myopathy or pathogenic variants that affect the NAD⁺ *de novo* synthesis pathways. Interestingly, a study in GOT2 knockdown cells demonstrated that the NAD⁺-precursor nicotinamide mononucleotide failed to rescue proliferation, in contrast to the cytosolic NAD⁺-recycling mechanisms.⁴⁸ Thus, although boosting NAD⁺ would likely not rescue the metabolic consequences due to the disturbed NAD⁺/NADH balance, it may support NAD⁺-related signaling processes by preventing depletion of the NAD⁺-pool.

A spectrum of therapeutic strategies

The MAS is directly or indirectly involved in many metabolic pathways, including glutamate and aspartate synthesis, ATP synthesis, and hundreds of metabolic reactions via the maintenance of the cytosolic NAD⁺/NADH ratio. Given this, MAS dysfunction results in multifaceted consequences that can be addressed through therapeutic strategies at multiple levels. Overall, MAS disorders primarily cause energy deficiency, which mainly affects the highly energy-demanding central nervous system. We discussed the ketogenic diet, triheptanoin, serine supplementation, pyruvate supplementation and increasing NAD⁺ levels as potential therapeutic strategies. Currently, the ketogenic diet is the most established and safe therapeutic strategy to address energy deficiency while avoiding potentially toxic cytosolic metabolite accumulation, and it may be most effective in the prevention of neurodegeneration.³ Other therapeutic strategies require additional investigation to provide evidence-based medicine. The extent of the serine biosynthesis defect in the central nervous system and the effectiveness of serine supplementation need to be delineated,⁶⁴ since it may support myelination processes and one-carbon metabolism but may also play a role in mitochondrial energy metabolism.⁷⁹ Furthermore, the extent to which NAD⁺-pools are depleted and regulatory mechanisms are altered requires further investigation in order to investigate the therapeutic option of NAD⁺-precursor supplementation. Moreover, it is important to keep in mind that the pathophysiology of each MAS disorder is unique and requires a different therapeutic approach. Our findings indicate that the pathophysiology of GOT1, MDH1, AGC and GOT2 defects is most similar on a cellular level, in contrast to that of MDH2. MDH2 is also classified as a disorder of the TCA cycle and thus may require a different approach focused on restoring mitochondrial energy metabolism, whereas in other disorders cytosolic NAD⁺-recycling can be a major target. There are currently no completely safe therapeutic strategies for recycling cytosolic NAD⁺, but promising

developments are being made, such as LOXCAT, which may eventually be available as enzyme therapy.⁸⁶ Other advances in mRNA therapy that have been studied in a mouse model of citrin deficiency also provide a promising therapeutic strategy.⁹⁰ Ultimately, genetic therapies, such as gene therapy or gene editing, are expected to revolutionize the treatment of rare inherited diseases.^{91,92}

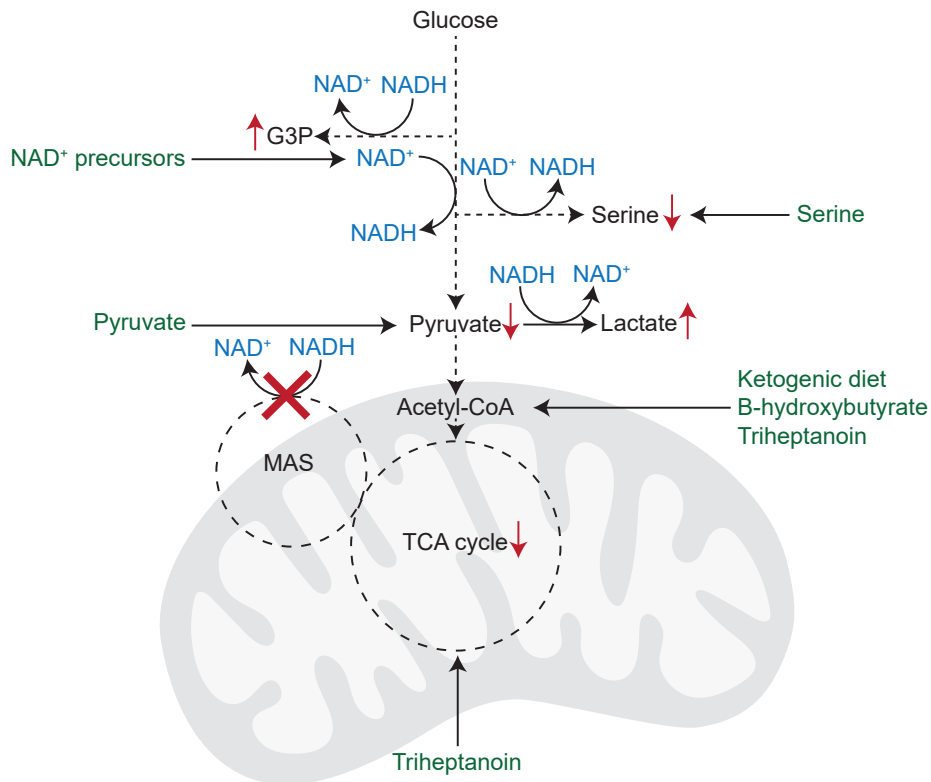


Figure 3. Pathophysiological consequences and therapeutic strategies for MAS disorders.

PART 2 – Metabolic phenotyping in rare hereditary anemias

Metabolomics in hereditary anemias

A functional layer between genotype and phenotype

Diagnostics of rare hereditary anemia (RHA) is challenging due to clinical and genetic heterogeneity, as well as poorly understood relations between the underlying mutations and the clinical severity. To unravel genotype-phenotype relations in RHAs, more functional approaches are required. A metabolic phenotype, representing the functional readout of the genotype leading to a clinical phenotype, may contain important insights that facilitate both the understanding and delineation of disease phenotypes. In addition, these metabolic insights can provide a basis for the development of therapeutic options in RHA.^{93,94} Untargeted metabolomics studies using dried blood spots have been performed in many different diseases, but not yet in RHA. Here, we applied metabolomics to elucidate the disease metabolome of several RHAs as well as to explore its diagnostic potential.

Clinical metabolic phenotyping in RHA

Opportunities for diagnostics

Broad metabolic screening using untargeted metabolomics yields a large amount of data. In the field of medicine and healthcare, machine learning is increasingly used to analyze large datasets to identify patterns and make predictions about patient outcomes in order to improve accuracy and speed of diagnosis.⁹⁵ We initially demonstrated the feasibility of metabolomics in RHA for the metabolic defect pyruvate kinase deficiency (PKD) (**chapter 6**). As a proof-of-principle, patients could be discriminated from healthy controls by a predictive machine-learning model that exclusively used the metabolic fingerprint. From a clinical perspective, the diagnostic potential of a metabolic fingerprint provides opportunities. Hence, we extended this approach to Diamond-Blackfan anemia (DBA), a disorder for which currently no functional diagnostic tests are established (**chapter 7**). While we proved that binary classification models can be a powerful tool in discriminating PKD or DBA from healthy controls, integration in a clinical setting requires a different approach.⁹⁶ A clinical diagnostic algorithm has added value when it processes multiple diagnostic outcomes of clinically similar diseases. This requires disease-specific metabolic fingerprints that discriminate between multiple diseases or recognize healthy individuals. We illustrated that the clinically similar disorders DBA and CDA had disease-specific metabolic phenotypes, therefore holding promise

for the development of such a clinical diagnostic model (**chapter 7**). Although not further explored in this thesis, incorporation of additional data could provide more discriminative power, such as diagnostic metabolite ratios, hemoglobin values, or blood cell counts. The development of an effective algorithm comes down to the statistical power of the sample size, which is often an issue in studying rare diseases. Here, we used repetitive classification to estimate the accuracy of our selected models; however, a larger sample size is preferred.⁹⁷ These algorithms provide a first step toward future diagnostic models that will require the integration of more patient data in their development. On that account, to advance diagnostics in the field of rare diseases, a collaborative effort is required. Overall, the use of metabolomics in predicting diagnostic outcomes is an exciting and rapidly advancing field of research that has the potential to greatly improve the accuracy and speed of diagnosis, ultimately leading to improved outcomes for patients.

Opportunities for clinical management

A functional tool that aids in clinical-decision making could be a valuable asset for the clinical management of patients with RHA. Metabolomics provides opportunities for investigating or eventually predicting treatment response, as illustrated by the different metabolic profiles of DBA patients under different treatment modalities (**chapter 7**). In addition, metabolomics provides the possibility to assess the severity of the disease, as we identified a specific metabolite pattern that is associated with clinical severity in patients with hereditary spherocytosis (HS) (**chapter 8**). Hence, metabolomics in RHA may aid in the discovery of predictors of treatment response or prognostic markers of clinical severity. Ideally, metabolomics aids in the prediction of whether therapeutic interventions such as splenectomy should be performed or not. In prospect, metabolomics may play a role in the development of personalized medicine that improves the effectiveness of treatments and reduces the likelihood of adverse side effects.

Metabolic insights and pathophysiological leads in RHA

Polyamines and carnitines: markers of proliferation or hemolysis?

The large amounts of data yielded by untargeted metabolomics provide the opportunity to generate hypotheses for future investigations. Both HS and PKD, as well as forms of CDA, are hemolytic anemias, which are characterized by the rupture of red blood cells (RBCs) and the release of their contents into the blood. Interestingly, their metabolic profiles revealed elevated polyamines (e.g., spermidine, N1-acetylspermidine), as well as a remarkable number of acylcarnitines (e.g., carnitine, acetylcarnitine, propionylcarnitine) (**chapters 6-8**). Previous metabolomic studies also identified increased polyamines

(spermidine and spermine), carnitine and acetylcarnitine in the RBCs of patients with sickle cell anemia (hemoglobinopathy)⁹⁸ and overhydrated stomatocytosis (RBC membrane disorder).⁹⁹ In addition, elevated polyamines and fatty acids have been observed in the RBCs of PKD patients.¹⁰⁰ This suggests a pathophysiological role for polyamines and carnitines in hemolytic anemia in general. Furthermore, we demonstrated that several polyamines (spermidine and N1-acetylspermidine), acetylcarnitine and propionylcarnitine correlated positively with reticulocytes and negatively with the number of red blood cells and red cell membrane deformability in HS (**chapter 8**). Both polyamines and acetylcarnitine have been associated with stabilization of the RBC membrane.¹⁰¹⁻¹⁰⁴ Polyamines can bind DNA and regulate the activity of genes, thereby controlling the production of proteins to support normal growth and function, which is particularly important during periods of rapid cell growth, such as fetal development and in certain cancer cells.¹⁰⁵ Indeed, increased levels of polyamines have been associated with younger RBCs,¹⁰⁶ suggesting that polyamines may be required for membrane stabilization during the extensive membrane remodeling reticulocytes undergo during RBC maturation remodeling.¹⁰⁷ Interestingly, in overhydrated stomatocytosis but not in sickle cell anemia, spermine was identified as an RBC age-related metabolic signature.^{98,99} Previous work also demonstrated that carnitine, acetylcarnitine and propionylcarnitine correlated positively with the reticulocyte production index in patients with sickle cell/beta-thalassemia disease.¹⁰⁸ Whether polyamines and carnitines are indicators of RBC proliferation, related to RBC characteristics, indirect markers of disease severity, or involved in the pathophysiology of different types of RHA remains to be investigated. Since RBC membrane loss and decreased RBC deformability are strong markers of clinical severity in HS,¹⁰⁹ the increased polyamines may also reflect red cell membrane damage on a metabolic level in clinically severe cases (**chapter 8**). This is supported by the recent finding of an association between polyamines and hemolytic activity in autoimmune hemolytic anemia.¹¹⁰ In addition to a metabolic fingerprint, metabolomics and isotope tracer analysis in isolated red blood cells can provide additional functional in-depth pathophysiological insights.¹¹¹

Dried blood spots metabolomics in RHA

Dried blood spots (DBS) have been used for newborn screening since the 1960s,¹¹² but are increasingly used in various other fields, such as therapeutic drug monitoring and pharmacokinetics.^{113,114} Clinical use of DBS for metabolic profiling has great advantages since it is a non-invasive and quick method that provides many advantages in storage and transport if implemented in a diagnostic workflow. In addition, only a small sample volume is required, enabling at-home sampling and longitudinal analysis. These benefits are of particular interest for comparative metabolomics studies conducted in remote locations or with large cohorts from multiple collaborating centers.

Blood composition and the DBS metabolome in RHA

Since anemia is characterized by altered blood composition, several aspects regarding the use of DBS in RHA need to be addressed. One major concern with the use of DBS-based metabolomics in general is their volumetric accuracy. When a fixed blood spot punch is taken, the spread of blood on DBS is of importance. The blood viscosity is affected by the fraction of red blood cells, also known as the hematocrit level. Hematocrit (Ht) levels vary per age, ranging from 28-64%,^{115,116} but are also intrinsically affected by anemia. A high Ht sample may contain more blood cells than a low Ht sample, introducing metabolite variation. This may be of particular concern for RHA patients, as we demonstrated that some metabolites were strongly correlated with RBC counts (**chapter 8**); however, it is unknown whether normalization for hematocrit levels also improves data interpretation in RHA patients. Recently, it was shown that varying Hts ranging from 31-50% did not play a significant role in the variation of metabolomics results.¹¹⁷ Moreover, the normalization for hemoglobin levels may provide an even better standardization method for DBS metabolomics.¹¹⁸ The extent and need for normalization of DBS metabolomics in RHA require further investigation focused on improving the understanding between Ht, Hb and the metabolic profile. In addition, it is worthwhile to delineate relations between the DBS and RBC metabolome. Finally, the effects of therapeutic interventions, such as blood transfusions and splenectomy, on the blood composition and DBS metabolome require further investigation.

Translation of metabolic insights in rare diseases

Since patient material is often scarce, elucidating rare disorders often requires working with cellular or model organisms. In this thesis, we studied metabolic profiles from both cells and patient material with the aim to increase our pathophysiological knowledge of inherited diseases and ultimately improve their diagnosis and treatment. So how can these metabolic insights eventually contribute to improved patient care? We first demonstrated that by using a broad-metabolic screening platform we were able to establish a detailed biomarker profile in MDH1 deficiency, which would otherwise remain undetected using routine diagnostic biochemical analysis (G3P). This and many other examples illustrate that the implementation of untargeted metabolomics screening platforms in diagnostics has the potential to significantly advance diagnostic biomarker identification and, ultimately, disease recognition.¹¹⁹ In addition, we identified several leads to study pathophysiology in several RHAs. Important to note is that the use of direct-infusion mass spectrometry often requires follow-up targeted mass spectrometry to confirm correct interpretation of the results. Furthermore, the metabolic profile of patients allowed us to compare findings in our *in vitro* cellular models, keeping our findings close to clinical relevance.

Although cell lines serve as a good model for studying cellular consequences, for translational insights, tissue-specific expression of the inherited defects must be considered to obtain clinical translational results that can aid in disease management. In MAS disorders, for instance, serine biosynthesis may be primarily affected in cell types that also express GPD1. Thus, providing a relevant metabolic context for the disorder of interest is an important aspect to take into consideration. Since MAS disorders are primarily neurological disorders, future research can focus on the more specific role of MAS components in different neurological cell types, as demonstrated by studies of the AGC transporter.^{21,28,31,56} In addition, although the use of a single cellular model is a first step toward understanding key mechanistic insights, it is also a significant limitation in this study. More in-depth translational insights could be gained from patient cells containing the pathogenic mutation, e.g. fibroblasts or induced pluripotent stem cells that differentiate in the tissues of interest (e.g. neurons). Although these cellular systems more closely reflect patient pathophysiology, cellular systems do not recapitulate tissues with multiple cell types and three-dimensional organizations. Hence, findings from *in vitro* experiments are still difficult to extrapolate to patients. Here, recent advances, such as three-dimensional organoids or organs-on-a-chip (capable of simulating blood flow), allow for more tissue-specific and dynamic insights. In particular brain organoids may be an interesting model to further study MAS disorders. Ultimately, animal models provide insights into inter-organ effects of disrupted metabolism and can also reflect patient pathophysiology more closely.

In perspective: Applications of metabolomics in rare diseases

Untargeted metabolomics provides many opportunities and openings for future metabolic investigations through its hypothesis-regenerating nature. Metabolomics, as a relatively new -omics field, still faces many technical and data-related challenges, including interpretation. Integration of metabolomics with knowledge from the metabolic network or other omics can further enhance the potential of metabolomics and its meaningful interpretation for diagnostics as well as for research. In this thesis, we demonstrated that metabolomics aids in biomarker discovery, identification of pathophysiological leads, design of therapeutic interventions, assessment of clinical severity and response to treatment. We showed that tracing metabolic pathways can lead to important pathophysiological insights that can ultimately be used to improve clinical patient care. Through its multifaceted aspects in both clinical and diagnostic applications, untargeted metabolomics holds the potential to revolutionize the field of rare inherited diseases.

REFERENCES

1. Kobayashi K, Sinasac DS, Iijima M, et al. The gene mutated in adult-onset type II citrullinaemia encodes a putative mitochondrial carrier protein. *Nat Genet.* 1999;22(2):159-163.
2. Köhler S, Gargano M, Matentzoglou N, et al. The Human Phenotype Ontology in 2021. *Nucleic Acids Res.* 2021;49(D1):D1207-D1217.
3. Bölsterli BK, Boltshauser E, Palmieri L, et al. Ketogenic Diet Treatment of Defects in the Mitochondrial Malate Aspartate Shuttle and Pyruvate Carrier. *Nutrients.* 2022;14(17):3605.
4. Priestley JRC, Pace LM, Sen K, et al. Malate dehydrogenase 2 deficiency is an emerging cause of pediatric epileptic encephalopathy with a recognizable biochemical signature. *Mol Genet Metab Reports.* 2022;33:100931.
5. Ticci C, Nesti C, Rubegni A, et al. Bi-allelic variants in MDH2: Expanding the clinical phenotype. *Clin Genet.* 2022;101(2):260-264.
6. Laemmle A, Steck AL, Schaller A, et al. Triheptanoin – Novel therapeutic approach for the ultra-rare disease mitochondrial malate dehydrogenase deficiency. *Mol Genet Metab Reports.* 2021;29:100814.
7. Frederiksen SD, Avramović V, Maroille T, Lehman A, Arbour L, Tarailo-Graovac M. Rare disorders have many faces: in silico characterization of rare disorder spectrum. *Orphanet J Rare Dis.* 2022;17(1):1-18.
8. Tumiene B, Ferreira CR, van Karnebeek CDM. 2022 Overview of Metabolic Epilepsies. *Genes (Basel).* 2022;13(3):508.
9. Almannai M, El-Hattab AW. Inborn Errors of Metabolism with Seizures: Defects of Glycine and Serine Metabolism and Cofactor-Related Disorders. *Pediatr Clin North Am.* 2018;65(2):279-299.
10. Lee JY, Wasserman WW, Hoffmann GF, Van Karnebeek CDM, Blau N. Knowledge base and mini-expert platform for the diagnosis of inborn errors of metabolism. *Genet Med.* 2018;20(1):151-158.
11. Zhao J, Feng QP, Wei WQ. Integration of Omics and Phenotypic Data for Precision Medicine. *Methods Mol Biol.* 2022;2486:19-35.
12. Matsumoto S, Häberle J, Kido J, Mitsubuchi H, Endo F, Nakamura K. Urea cycle disorders-update. *J Hum Genet.* 2019;64(9):833-847.
13. Van Der Crabben SN, Verhoeven-Duif NM, Brilstra EH, et al. An update on serine deficiency disorders. *J Inherit Metab Dis.* 2013;36(4):613-619.
14. Ait-El-Mkadem S, Dayem-Quere M, Gusic M, et al. Mutations in MDH2, Encoding a Krebs Cycle Enzyme, Cause Early-Onset Severe Encephalopathy. *Am J Hum Genet.* 2017;100(1):151-159.
15. Samokhina E, Popova I, Malkov A, et al. Chronic inhibition of brain glycolysis initiates epileptogenesis. *J Neurosci Res.* 2017;95(11):2195-2206.
16. McDonald T, Puchowicz M, Borges K. Impairments in oxidative glucose metabolism in epilepsy and metabolic treatments thereof. *Front Cell Neurosci.* 2018;12:274.
17. Cahoy JD, Emery B, Kaushal A, et al. A transcriptome database for astrocytes, neurons, and oligodendrocytes: a new resource for understanding brain development and function. *J Neurosci.* 2008;28(1):264-278.
18. Pardo B, Rodrigues TB, Contreras L, et al. Brain glutamine synthesis requires neuronal-born aspartate as amino donor for glial glutamate formation. *J Cereb Blood Flow Metab.* 2011;31(1):90-101.
19. Sharma K, Schmitt S, Bergner CG, et al. Cell type- and brain region-resolved mouse brain proteome. *Nat Neurosci.* 2015;18(12):1819-1831.
20. Lopez-Fabuel I, Le Douce J, Logan A, et al. Complex I assembly into supercomplexes determines differential mitochondrial ROS production in neurons and astrocytes. *Proc Natl Acad Sci U S A.* 2016;113(46):13063-13068.
21. Juaristi I, García-Martín ML, Rodrigues TB, Satrústegui J, Llorente-Folch I, Pardo B. ARALAR/AGC1 deficiency, a neurodevelopmental disorder with severe impairment of neuronal mitochondrial respiration, does not produce a primary increase in brain lactate. *J Neurochem.* 2017;142(1):132-139.

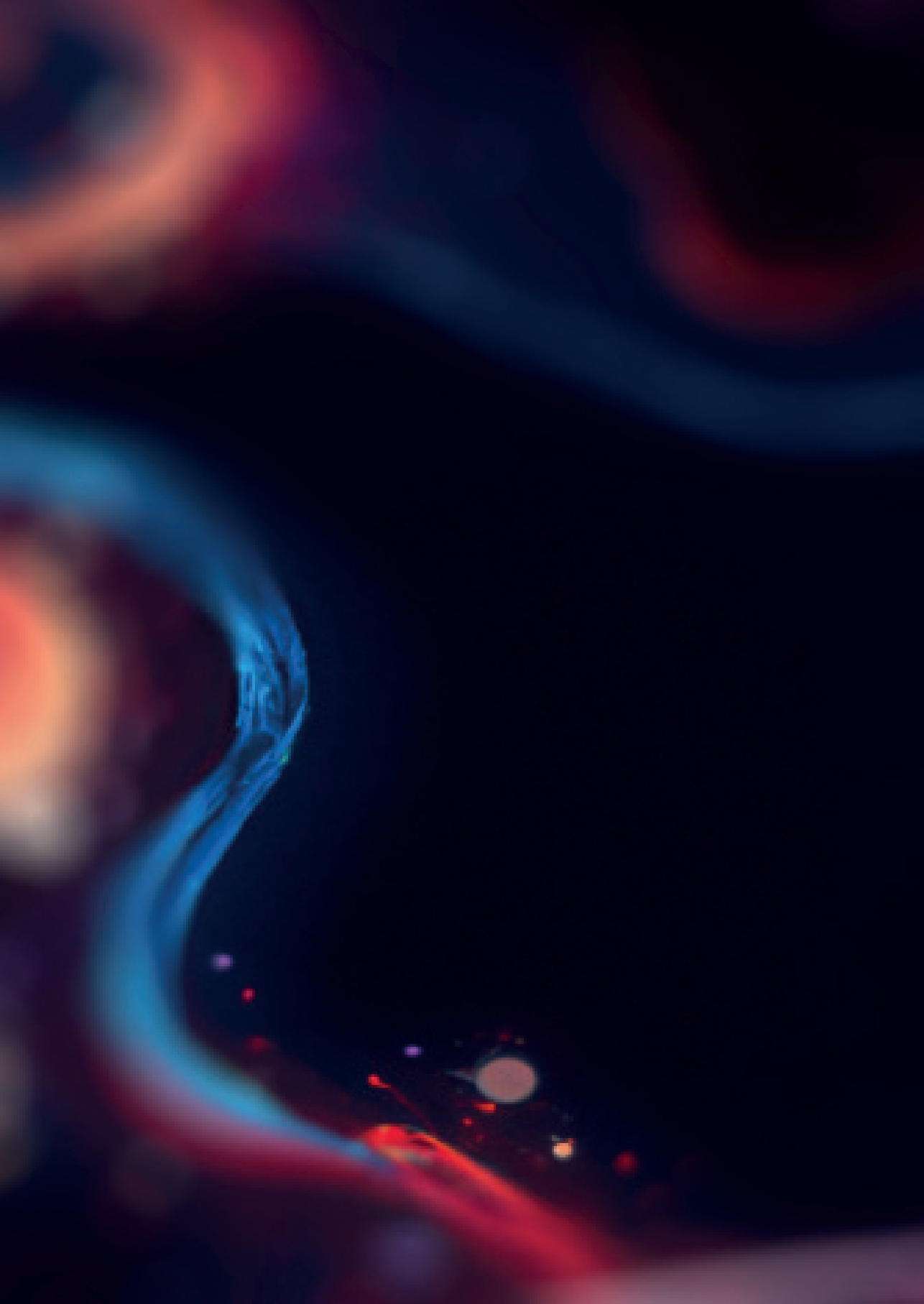
22. Pardo B, Contreras L. Redox Shuttles in the Brain. In: *Neural Metabolism In Vivo. Advances in Neurobiology, Vol 4.*; 2012:841-883.
23. Pardo B, Herrada-Soler E, Satrústegui J, Contreras L, Del Arco A. AGC1 Deficiency: Pathology and Molecular and Cellular Mechanisms of the Disease. *Int J Mol Sci.* 2022;23(1):528.
24. Lovatt D, Sonnewald U, Waagepetersen HS, et al. The transcriptome and metabolic gene signature of protoplasmic astrocytes in the adult murine cortex. *J Neurosci.* 2007;27(45):12255-12266.
25. Liu S, Fu S, Wang G, et al. Glycerol-3-phosphate biosynthesis regenerates cytosolic NAD⁺ to alleviate mitochondrial disease. *Cell Metab.* 2021;33(10):1974-1987.e9.
26. Juaristi I, Llorente-Folch I, Satrústegui J, del Arco A. Extracellular ATP and glutamate drive pyruvate production and energy demand to regulate mitochondrial respiration in astrocytes. *Glia.* 2019;67(4):759-774.
27. Juaristi I, Contreras L, González-Sánchez P, et al. The Response to Stimulation in Neurons and Astrocytes. *Neurochem Res.* 2019;44(10):2385-2391.
28. Llorente-Folch I, Rueda CB, Pérez-Liébana I, Satrústegui J, Pardo B. L-lactate-mediated neuroprotection against glutamate-induced excitotoxicity requires ARALAR/AGC1. *J Neurosci.* 2016;36(16):4443-4456.
29. Bak LK, Walls AB, Schousboe A, Ring A, Sonnewald U, Waagepetersen HS. Neuronal glucose but not lactate utilization is positively correlated with NMDA-induced neurotransmission and fluctuations in cytosolic Ca²⁺ levels. *J Neurochem.* 2009;109 Suppl:87-93.
30. Bak LK, Schousboe A. Misconceptions regarding basic thermodynamics and enzyme kinetics have led to erroneous conclusions regarding the metabolic importance of lactate dehydrogenase isoenzyme expression. *J Neurosci Res.* 2017;95(11):2098-2102.
31. Pérez-Liébana I, Juaristi I, González-Sánchez P, et al. A Ca²⁺-Dependent Mechanism Boosting Glycolysis and OXPHOS by Activating Aralar-Malate-Aspartate Shuttle, upon Neuronal Stimulation. *J Neurosci.* 2022;42(19):3879-3895.
32. Yu ACH, Drejer J, Hertz L, Schousboe A. Pyruvate carboxylase activity in primary cultures of astrocytes and neurons. *J Neurochem.* 1983;41(5):1484-1487.
33. Shank RP, Bennett GS, Freytag SO, Campbell GLM. Pyruvate carboxylase: an astrocyte-specific enzyme implicated in the replenishment of amino acid neurotransmitter pools. *Brain Res.* 1985;329(1-2):364-367.
34. Norenberg MD, Martinez-Hernandez A. Fine structural localization of glutamine synthetase in astrocytes of rat brain. *Brain Res.* 1979;161(2):303-310.
35. Anlauf E, Derouiche A. Glutamine Synthetase as an Astrocytic Marker: Its Cell Type and Vesicle Localization. *Front Endocrinol (Lausanne).* 2013;4:144.
36. Häberle J, Görg B, Rutsch F, et al. Congenital glutamine deficiency with glutamine synthetase mutations. *N Engl J Med.* 2005;353(18):1926-1933.
37. Rumping L, Büttner B, Maier O, et al. Identification of a Loss-of-Function Mutation in the Context of Glutaminase Deficiency and Neonatal Epileptic Encephalopathy. *JAMA Neurol.* 2019;76(3):342-350.
38. Adant I, Bird M, Decru B, et al. Pyruvate and uridine rescue the metabolic profile of OXPHOS dysfunction. *Mol Metab.* 2022;63:101537.
39. Martano G, Murru L, Moretto E, et al. Biosynthesis of glycerol phosphate is associated with long-term potentiation in hippocampal neurons. *Metabolomics.* 2016;12(8):133.
40. Dhoundiyal A, Goeschl V, Boehm S, Kubista H, Hotka M. Glycerol-3-Phosphate Shuttle Is a Backup System Securing Metabolic Flexibility in Neurons. *J Neurosci.* 2022;42(39):7339-7354.
41. Wang Y, Stancliffe E, Fowle-Grider R, et al. Saturation of the mitochondrial NADH shuttles drives aerobic glycolysis in proliferating cells. *Mol Cell.* 2022;82(17):3270-3283.e9.

42. Yeh JI, Chinte U, Du S. Structure of glycerol-3-phosphate dehydrogenase, an essential monotopic membrane enzyme involved in respiration and metabolism. *Proc Natl Acad Sci U S A*. 2008;105(9):3280-3285.
43. Boukalova S, Hubackova S, Milosevic M, Ezrova Z, Neuzil J, Rohlena J. Dihydroorotate dehydrogenase in oxidative phosphorylation and cancer. *Biochim Biophys Acta - Mol Basis Dis*. 2020;1866(6):165759.
44. Gnaiger E. Mitochondrial Pathways and Respiratory Control An Introduction to OXPHOS Analysis 19.12. In: *Mitochondrial Physiology Network*. 4th ed. ; 2014:1-80.
45. Pettit FH, Pelley JW, Reed LJ. Regulation of pyruvate dehydrogenase kinase and phosphatase by acetyl-CoA/CoA and NADH/NAD ratios. *Biochem Biophys Res Commun*. 1975;65(2):575-582.
46. Divakaruni AS, Wallace M, Buren C, et al. Inhibition of the mitochondrial pyruvate carrier protects from excitotoxic neuronal death. *J Cell Biol*. 2017;216(4):1091-1105.
47. Molinié T, Cougouilles E, David C, Cahoreau E, Portais JC, Mourier A. MDH2 produced OAA is a metabolic switch rewiring the fuelling of respiratory chain and TCA cycle. *Biochim Biophys Acta - Bioenerg*. 2022;1863(3):148532.
48. Kerk SA, Lin L, Myers AL, et al. Metabolic Requirement for GOT2 in Pancreatic Cancer Depends on Environmental Context. *Elife*. 2022;11:e73245.
49. Roe CR, Sweetman L, Roe DS, David F, Brunengraber H. Treatment of cardiomyopathy and rhabdomyolysis in long-chain fat oxidation disorders using an anaplerotic odd-chain triglyceride. *J Clin Invest*. 2002;110(2):259-269.
50. Shirley M. Triheptanoin: First Approval. *Drugs*. 2020;80(15):1595-1600.
51. Vockley J, Marsden D, McCracken E, et al. Long-term major clinical outcomes in patients with long chain fatty acid oxidation disorders before and after transition to triheptanoin treatment—A retrospective chart review. *Mol Genet Metab*. 2015;116(1-2):53-60.
52. Marin-Valencia I, Good LB, Ma Q, Malloy CR, Pascual JM. Heptanoate as a neural fuel: energetic and neurotransmitter precursors in normal and glucose transporter I-deficient (G1D) brain. *J Cereb Blood Flow Metab*. 2013;33(2):175-182.
53. Martin K, Jackson CF, Levy RG, Cooper PN. Ketogenic diet and other dietary treatments for epilepsy. *Cochrane Database Syst Rev*. 2016;2:CD001903.
54. Pfeiffer B, Sen K, Kaur S, Pappas K. Expanding Phenotypic Spectrum of Cerebral Aspartate-Glutamate Carrier Isoform 1 (AGC1) Deficiency. *Neuropediatrics*. 2020;51(2):160-163.
55. Dahlin M, Martin DA, Hedlund Z, Jonsson M, Von Döbeln U, Wedell A. The ketogenic diet compensates for AGC1 deficiency and improves myelination. *Epilepsia*. 2015;56(11):e176-e181.
56. Pérez-Liévana I, Casarejos MJ, Alcaide A, et al. bOHB protective pathways in Aralar-Ko neurons and brain: An alternative to ketogenic diet. *J Neurosci*. 2020;40(48):9293-9305.
57. Yamasaki M, Yamada K, Furuya S, Mitoma J, Hirabayashi Y, Watanabe M. 3-Phosphoglycerate dehydrogenase, a key enzyme for L-serine biosynthesis, is preferentially expressed in the radial glia/astrocyte lineage and olfactory ensheathing glia in the mouse brain. *J Neurosci*. 2001;21(19):7691-7704.
58. Basu AC, Tsai GE, Ma CL, et al. Targeted disruption of serine racemase affects glutamatergic neurotransmission and behavior. *Mol Psychiatry*. 2009;14(7):719-727.
59. Balu DT, Takagi S, Puhl MD, Benneyworth MA, Coyle JT. D-serine and serine racemase are localized to neurons in the adult mouse and human forebrain. *Cell Mol Neurobiol*. 2014;34(3):419-435.
60. Coyle JT, Balu D, Wolosker H. D-Serine, the Shape-Shifting NMDA Receptor Co-agonist. *Neurochem Res*. 2020;45(6):1344-1353.
61. Mitoma J, Kasama T, Furuya S, Hirabayashi Y. Occurrence of an unusual phospholipid, phosphatidyl-L-threonine, in cultured hippocampal neurons. Exogenous L-serine is required for the synthesis of neuronal phosphatidyl-L-serine and sphingolipids. *J Biol Chem*. 1998;273(31):19363-19366.
62. Hirabayashi Y, Furuya S. Roles of L-serine and sphingolipid synthesis in brain development and neuronal survival. *Prog Lipid Res*. 2008;47(3):188-203.

63. Tabatabaie L, Klomp LW, Berger R, de Koning TJ. L-Serine synthesis in the central nervous system: A review on serine deficiency disorders. *Mol Genet Metab.* 2010;99(3):256-262.
64. van Karnebeek CDM, Ramos RJ, Wen XY, et al. Bi-allelic GOT2 Mutations Cause a Treatable Malate-Aspartate Shuttle-Related Encephalopathy. *Am J Hum Genet.* 2019;105(3):534-548.
65. Luengo A, Li Z, Gui DY, et al. Increased demand for NAD⁺ relative to ATP drives aerobic glycolysis. *Mol Cell.* 2021;81(4):691-707.e6.
66. Caligiore F, Zangelmi E, Vetro C, et al. Human cytosolic transaminases: side activities and patterns of discrimination towards physiologically available alternative substrates. *Cell Mol Life Sci.* 2022;79(8):421.
67. Ducker GS, Rabinowitz JD. One-Carbon Metabolism in Health and Disease. *Cell Metab.* 2017;25(1):27-42.
68. Van Der Crabben SN, Verhoeven-Duif NM, Brilstra EH, et al. An update on serine deficiency disorders. *J Inherit Metab Dis.* 2013;36(4):613-619.
69. Froese DS, Fowler B, Baumgartner MR. Vitamin B12, folate, and the methionine remethylation cycle—biochemistry, pathways, and regulation. *J Inherit Metab Dis.* 2019;42(4):673-685.
70. Craciunescu CN, Johnson AR, Zeisel SH. Dietary choline reverses some, but not all, effects of folate deficiency on neurogenesis and apoptosis in fetal mouse brain. *J Nutr.* 2010;140(6):1162-1166.
71. Zeisel SH. Metabolic crosstalk between choline/1-carbon metabolism and energy homeostasis. *Clin Chem Lab Med.* 2013;51(3):467-475.
72. Shin W, Yan J, Abratte CM, Vermeylen F, Caudill MA. Choline intake exceeding current dietary recommendations preserves markers of cellular methylation in a genetic subgroup of folate-compromised men. *J Nutr.* 2010;140(5):975-980.
73. Abratte CM, Wang W, Li R, Moriarty DJ, Caudill MA. Folate intake and the MTHFR C677T genotype influence choline status in young Mexican American women. *J Nutr Biochem.* 2008;19(3):158-165.
74. Debray FG, Mitchell GA, Allard P, Robinson BH, Hanley JA, Lambert M. Diagnostic accuracy of blood lactate-to-pyruvate molar ratio in the differential diagnosis of congenital lactic acidosis. *Clin Chem.* 2007;53(5):916-921.
75. Thompson Legault J, Strittmatter L, Tardif J, et al. A Metabolic Signature of Mitochondrial Dysfunction Revealed through a Monogenic Form of Leigh Syndrome. *Cell Rep.* 2015;13(5):981-989.
76. Sharma R, Reinstadler B, Engelstad K, et al. Circulating markers of NADH-reductive stress correlate with mitochondrial disease severity. *J Clin Invest.* 2021;131(2):e136055.
77. Diehl FF, Lewis CA, Fiske BP, Vander Heiden MG. Cellular redox state constrains serine synthesis and nucleotide production to impact cell proliferation. *Nat Metab.* 2019;1(9):861-867.
78. Bao XR, Ong SE, Goldberger O, et al. Mitochondrial dysfunction remodels one-carbon metabolism in human cells. *Elife.* 2016;5:e10575.
79. Yang L, Garcia Canaveras JC, Chen Z, et al. Serine Catabolism Feeds NADH when Respiration Is Impaired. *Cell Metab.* 2020;31(4):809-821.e6.
80. Sullivan LB, Gui DY, Hosios AM, Bush LN, Freinkman E, Vander Heiden MG. Supporting Aspartate Biosynthesis Is an Essential Function of Respiration in Proliferating Cells. *Cell.* 2015;162(3):552-563.
81. Bui D, Ravasz D, Chinopoulos C. The Effect of 2-Ketobutyrate on Mitochondrial Substrate-Level Phosphorylation. *Neurochem Res.* 2019;44(10):2301-2306.
82. Sousa AP, Cunha DM, Franco C, et al. Which role plays 2-hydroxybutyric acid on insulin resistance? *Metabolites.* 2021;11(12):835.
83. Goodman RP, Markhard AL, Shah H, et al. Hepatic NADH reductive stress underlies common variation in metabolic traits. *Nature.* 2020;583(7814):122-126.
84. Mutoh K, Kurokawa K, Kobayashi K, Saheki T. Treatment of a citrin-deficient patient at the early stage of adult-onset type II citrullinaemia with arginine and sodium pyruvate. *J Inherit Metab Dis.* 2008;31 Suppl 2:S343-S347.

85. Moriyama M, Li MX, Kobayashi K, et al. Pyruvate ameliorates the defect in ureogenesis from ammonia in citrin-deficient mice. *J Hepatol.* 2006;44(5):930-938.
86. Patgiri A, Skinner OS, Miyazaki Y, et al. An engineered enzyme that targets circulating lactate to alleviate intracellular NADH:NAD⁺ imbalance. *Nat Biotechnol.* 2020;38(3):309-313.
87. Wanders RJA, Karnebeek CDM, Jans JJM, Verhoeven NM, Houten SM. News and views. *J Inherit Metab Dis.* 2020;43(4):647-650.
88. Covarrubias AJ, Perrone R, Grozio A, Verdin E. NAD⁺ metabolism and its roles in cellular processes during ageing. *Nat Rev Mol Cell Biol.* 2021;22(2):119-141.
89. Zapata-Perez R, Wanders RJA, Van Karnebeek CDM, Houtkooper RH. NAD⁺ homeostasis in human health and disease. *EMBO Mol Med.* 2021;13(7):e13943.
90. Cao J, An D, Galduroz M, et al. mRNA Therapy Improves Metabolic and Behavioral Abnormalities in a Murine Model of Citrin Deficiency. *Mol Ther.* 2019;27(7):1242-1251.
91. Yilmaz BS, Gurung S, Perocheau D, Counsell J, Baruteau J. Gene therapy for inherited metabolic diseases. *J Mother Child.* 2020;24(2):53-64.
92. Schene IF, Joore IP, Oka R, et al. Prime editing for functional repair in patient-derived disease models. *Nat Commun.* 2020;11(1):5352.
93. Grace RF, Rose C, Layton DM, et al. Safety and Efficacy of Mitapivat in Pyruvate Kinase Deficiency. *N Engl J Med.* 2019;381(10):933-944.
94. Al-Samkari H, van Beers EJ. Mitapivat, a novel pyruvate kinase activator, for the treatment of hereditary hemolytic anemias. *Ther Adv Hematol.* 2021;12:1-11.
95. Handelman GS, Kok HK, Chandra RV., Razavi AH, Lee MJ, Asadi H. eDoctor: machine learning and the future of medicine. *J Intern Med.* 2018;284(6):603-619.
96. Mendez KM, Reinke SN, Broadhurst DI. A comparative evaluation of the generalised predictive ability of eight machine learning algorithms across ten clinical metabolomics data sets for binary classification. *Metabolomics.* 2019;15(12):150.
97. Efron B. The Bootstrap and Modern Statistics. *J Am Stat Assoc.* 2000;95(452):1293-1296.
98. Darghouth D, Koehl B, Madalinski G, et al. Pathophysiology of sickle cell disease is mirrored by the red blood cell metabolome. *Blood.* 2011;117(6):e57-e66.
99. Darghouth D, Koehl B, Heilier JF, et al. Alterations of red blood cell metabolome in overhydrated hereditary stomatocytosis. *Haematologica.* 2011;96(12):1861-1865.
100. Roy MK, Cendali F, Ooyama G, Gamboni F, Morton H, D'Alessandro A. Red Blood Cell Metabolism in Pyruvate Kinase Deficient Patients. *Front Physiol.* 2021;12:735543.
101. Ballas SK, Mohandas N, Marton LJ, Shohet SB. Stabilization of erythrocyte membranes by polyamines. *Proc Natl Acad Sci U S A.* 1983;80(7):1942-1946.
102. Arduini A, Rossi M, Mancinelli G, et al. Effect of L-carnitine and acetyl-L-carnitine on the human erythrocyte membrane stability and deformability. *Life Sci.* 1990;47(26):2395-2400.
103. Arduini A, Mancinelli G, Radatti GL, Dottori S, Molajoni F, Ramsay RR. Role of carnitine and carnitine palmitoyltransferase as integral components of the pathway for membrane phospholipid fatty acid turnover in intact human erythrocytes. *J Biol Chem.* 1992;267(18):12673-12681.
104. Ramsay RR, Mancinelli G, Arduini A. Carnitine palmitoyltransferase in human erythrocyte membrane. Properties and malonyl-CoA sensitivity. *Biochem J.* 1991;275(3):685-688.
105. Igarashi K, Kashiwagi K. The functional role of polyamines in eukaryotic cells. *Int J Biochem Cell Biol.* 2019;107:104-115.
106. Cooper KD, Shukla JB, Rennert OM. Polyamine distribution in cellular compartments of blood and in aging erythrocytes. *Clin Chim Acta.* 1976;73(1):71-88.
107. Waugh RE, Mantalaris A, Bauserman RG, Hwang WC, Wu JHD. Membrane instability in late-stage erythropoiesis. *Blood.* 2001;97(6):1869-1875.

108. Papassotiropou I, Panetsos F, Livadara T, Dimopoulou M, Tzivaras A, Voskaridou E. Targeted Metabolomic Profiles Are Strongly Correlated With Metabolic Alterations In Patients With Sickle Cell/Beta Thalassemia Disease. *Blood*. 2013;122(21):4675.
109. Huisjes R, Makhro A, Llaudet-Planas E, et al. Density, heterogeneity and deformability of red cells as markers of clinical severity in hereditary spherocytosis. *Haematologica*. 2020;105(2):338-347.
110. Rabelo IB, Chiba AK, Moritz E, et al. Metabolomic profile in patients with primary warm autoimmune haemolytic anaemia. *Br J Haematol*. 2023;201(1):140-149.
111. Lewis IA, Campanella ME, Markley JL, Low PS. Role of band 3 in regulating metabolic flux of red blood cells. *Proc Natl Acad Sci U S A*. 2009;106(44):18515-18520.
112. Guthrie R, Susi A. A simple phenylalanine method for detecting phenylketonuria in large populations of newborn infants. *Pediatrics*. 1963;32:338-343.
113. Martial LC, Aarnoutse RE, Schreuder MF, Henriët SS, Brüggemann RJM, Joor MA. Cost evaluation of dried blood spot home sampling as compared to conventional sampling for therapeutic drug monitoring in children. *PLoS One*. 2016;11(12):e0167433.
114. Martial LC, Kerkhoff J, Martinez N, et al. Evaluation of dried blood spot sampling for pharmacokinetic research and therapeutic drug monitoring of anti-tuberculosis drugs in children. *Int J Antimicrob Agents*. 2018;52(1):109-113.
115. Newman MS, Brandon TR, Groves MN, Gregory WL, Kapur S, Zava DT. A liquid chromatography/tandem mass spectrometry method for determination of 25-hydroxy vitamin D2 and 25-hydroxy vitamin D3 in dried blood spots: a potential adjunct to diabetes and cardiometabolic risk screening. *J Diabetes Sci Technol*. 2009;3(1):156-162.
116. De Vries R, Barfield M, Van De Merbel N, et al. The effect of hematocrit on bioanalysis of DBS: results from the EBF DBS-microsampling consortium. <http://dx.doi.org/104155/bio13170>. 2013;5(17):2147-2160.
117. Li K, Naviaux JC, Monk JM, Wang L, Naviaux RK. Improved dried blood spot-based metabolomics: A targeted, broad-spectrum, single-injection method. *Metabolites*. 2020;10(3):82.
118. Jain A, Morris M, Lin EZ, et al. Hemoglobin normalization outperforms other methods for standardizing dried blood spot metabolomics: A comparative study. *Sci Total Environ*. 2023;854:158716.
119. Jans JJ, Broeks MH, Verhoeven-Duif NM. Metabolomics in diagnostics of inborn metabolic disorders. *Curr Opin Syst Biol*. 2022;29:100409.



Appendices

Nederlandse Samenvatting

List of abbreviations

List of publications

Dankwoord

Curriculum Vitae

NEDERLANDSE SAMENVATTING

De onderstaande Nederlandse samenvatting is gebaseerd op de inleiding, samenvatting en discussie van dit proefschrift, te vinden in hoofdstuk 1 en 9.

Metabolomics: Een blik op het metabolisme

Het metabolisme is een complex geheel van biochemische reacties die essentieel zijn voor het leven. Metabole processen zetten voedingsstoffen om in zowel moleculaire bouwstenen als energie, en tegelijkertijd ontdoet het ons lichaam van afvalstoffen. Fouten in deze metabole processen kunnen leiden tot diverse ziekten, en het begrijpen ervan biedt mogelijkheden voor preventie en de behandeling van aandoeningen. Een methode om het metabolisme nader te doorgronden is het onderzoeken van het metaboloom – het geheel van alle stoffen in een biologisch monster. De brede studie van het metaboloom, ook wel bekend als metabolomics, onthult als het ware een metabole vingerafdruk, wat diepere inzichten verschaft in de complexe biochemische processen die zich afspelen in cellen en weefsels. Hierdoor kunnen we op moleculair niveau een momentopname maken van een organisme.

Binnen het metabolomics-veld zijn er twee mogelijke benaderingen: gerichte (*targeted*) en niet-gerichte (*untargeted*) metabolomics. Targeted metabolomics focust op een vooraf bepaalde set van metaboliëten, terwijl untargeted metabolomics juist alle meetbare metaboliëten analyseert. De brede 'untargeted' benadering is uiterst waardevol voor het ontdekken van nieuwe biomarkers en het verkrijgen van een diepgaander begrip van verschillende ziekten, juist omdat het vaak onverwachte inzichten oplevert. Gezien het dynamische karakter van het metabolisme, is ook het gebruik van stabiele isotopen van grote toegevoegde waarde om metabolische omzettingen en verstoringen daarin te volgen. Door bijvoorbeeld glucose te voorzien van verzwaarde koolstofatomen (zoals koolstof-13 (^{13}C) in plaats van koolstof-12 (^{12}C)), kunnen we de route van deze gelabelde koolstofatomen door het metabolisme traceren. Door de gegevens uit metabolomics te combineren met inzichten in metabole routes, ontstaat een aanzienlijk dieper begrip van het metabolisme in zowel gezondheid als ziekte. Met name bij zeldzame erfelijke aandoeningen, waarbij de onderliggende pathofysiologie vaak nog grotendeels onbekend is, kan metabolomics van onschatbare waarde zijn bij het identificeren van verstoorde metabole routes en mogelijke aangrijpingspunten voor behandeling.

Erfelijke metabole ziekten: Een uitdaging in diagnose en behandeling

Erfelijke ziekten ontstaan door veranderingen in DNA-sequenties en kunnen een uiteenlopend scala aan klinische symptomen veroorzaken, variërend van

mild tot levensbedreigend. Het is van cruciaal belang om deze ziekten snel te diagnosticeren en te behandelen om de overlevingskansen te vergroten. Binnen dit spectrum vallen erfelijke metabole ziekten, een groep van meer dan 1000 verschillende zeldzame aandoeningen die het stofwisselingsproces verstoren. Het opsporen van deze aandoeningen is vaak mogelijk door specifieke metabolieten in lichaamsvloeistoffen te meten. Een voorbeeld van een erfelijke metabole ziekte is fenylketonurie (PKU), waarbij de omzetting van het aminozuur fenylalanine niet correct verloopt. Dit resulteert in verhoogde fenylalaninewaarden in het bloed, wat vervolgens neurologische symptomen veroorzaakt. De behandeling van PKU omvat onder andere het vermijden van voedsel met fenylalanine, wat de symptomen kan verlichten.

Andere erfelijke metabole ziekten kunnen eveneens een breed scala aan symptomen veroorzaken, zoals spierzwakte, epileptische aanvallen en diverse neurologische stoornissen. Veel van deze ziekten hebben momenteel een weinig begrepen pathofysiologie, wat betekent dat behandeling zich vaak richt op het verlichten van symptomen in plaats van de onderliggende oorzaak. Het begrijpen van de pathofysiologie van deze ziekten is echter cruciaal bij het opstellen van een effectieve behandeling.

Het traceren van metabole paden in een spectrum van erfelijke ziekten: aandoeningen van de malaat-aspartaat shuttle en zeldzame erfelijke anemie

Untargeted metabolomics kan een waardevol hulpmiddel zijn bij het identificeren en karakteriseren van zeldzame erfelijke ziekten. Door het analyseren van een bescheiden biologisch monster, kunnen duizenden metabolieten worden gedetecteerd, wat zowel diagnostische als therapeutische mogelijkheden biedt. In dit proefschrift ligt de focus op het begrijpen van de pathofysiologie van verschillende zeldzame erfelijke ziekten, met behulp van untargeted metabolomics en het traceren van stabiele isotopen in cel modellen. Specifiek richt het onderzoek zich op aandoeningen in de malaat-aspartaat shuttle en zeldzame erfelijke anemie, waarbij fenotypische herkenning, moleculaire diagnostiek en pathofysiologische inzichten centraal staan.

Deel 1 – Pathofysiologische inzichten in aandoeningen van de malaat-aspartaat shuttle

De malaat-aspartaat shuttle

De malaat-aspartaat shuttle (MAS) is een cyclus met een belangrijke rol in de energiestofwisseling van cellen, vooral in weefsels met een hoge energiebehoefte, zoals het centrale zenuwstelsel. Voor een efficiënte energiestofwisseling zijn zowel voedingsstoffen, zoals koolhydraten, eiwitten en vetzuren, als zuurstof (O_2) benodigd. Tijdens de afbraak van voedingsstoffen komen geleidelijk elektronen vrij, die op een gecoördineerde wijze worden uitgewisseld tussen moleculen. Een belangrijke speler in dit proces is de cofactor nicotinamide-adenine-dinucleotide (NAD^+), dat essentieel is voor het verplaatsen van elektronen door ze op te nemen (reductie) en weer af te geven (oxidatie). De elektronen van metabolieten worden overgedragen aan NAD^+ , waardoor NADH wordt gevormd. Onder andere via de MAS, vinden deze elektronen uiteindelijk hun weg naar de mitochondriën, de energiefabrieken van de cel. De MAS transporteert deze elektronen van NADH van het cytosol naar de mitochondriën. Het enzym malaat dehydrogenase 1 (MDH1) speelt hierbij een cruciale rol door de elektronen van NADH over te dragen naar een oxaloacetaat molecuul, waardoor malaat en NAD^+ worden gevormd. Het resulterende malaat wordt vervolgens in de mitochondriën getransporteerd, waar het mitochondriële enzym MDH2 het elektron van malaat afstaat aan een beschikbaar NAD^+ -molecuul. Hierbij wordt NADH opnieuw gevormd in de mitochondriën. De NADH-elektronen worden vervolgens overgedragen aan de mitochondriële elektronentransportketen, waar ze bijdragen aan de vorming van energierijke ATP-moleculen en waarin zuurstof als de laatste elektronenacceptor fungeert. In aanvulling op de MDH-enzymen maken ook glutamaat-oxaloacetaat transaminasen (GOT1 en GOT2), de malaat-2-oxoglutarate transporter (OGC) en de aspartaat-glutamaat transporter (AGC) deel uit van de MAS-cyclus. Naast de rol van de MAS in indirect elektronentransport, vervult het ook een belangrijke functie bij het handhaven van de NAD^+ /NADH verhouding in de cel. Deze balans is belangrijk voor het voortzetten van diverse metabole routes in de cel.

Aandoeningen van de MAS

De tot nu toe beschreven erfelijke MAS-aandoeningen zijn onder andere AGC2 (Citrine) deficiëntie en AGC1 (Aralar) deficiëntie, welke respectievelijk tot expressie komen in de lever en hersenen. Recentelijk zijn er ook patiënten beschreven met deficiënties in de mitochondriële enzymen GOT2 en MDH2. In dit proefschrift beschrijven we de eerste patiënten met een MDH1-deficiëntie (**hoofdstuk 2**). Met behulp van untargeted metabolomics hebben we glycerol 3-fosfaat (G3P) als biomarker in bloedspots van deze twee patiënten vastgesteld, die nu kan worden gebruikt als indicatie voor

een MDH1-deficiëntie. Beide patiënten vertoonden neurologische symptomen, algemene ontwikkelingsachterstand, epilepsie en progressieve microcefalie. Deze klinische verschijnselen vertonen overeenkomsten met andere neurologische MAS-aandoeningen, zoals de AGC1, MDH2 en GOT2-deficiënties. In een literatuuroverzicht hebben we de klinische en biochemische bevindingen van de MAS-aandoeningen met elkaar vergeleken om de klinische herkenning te vergemakkelijken (**hoofdstuk 3**). Omdat de symptomen vaak niet uniek zijn, is het moeilijk om een aandoening uitsluitend te identificeren op basis van fenotypische kenmerken. Een meer gerichte diagnose kan worden gesteld door het combineren van zowel fenotype als biochemie. Echter, MAS-aandoeningen vertonen zowel fenotypische als biochemische overeenkomsten met andere erfelijke metabole ziekten die verband houden met het energie- en aminozuurmetabolisme. Een dieper inzicht in de onderliggende oorzaak van biochemische veranderingen en pathofysiologie kan substantieel bijdragen aan het monitoren van deze complexe aandoeningen.

De pathofysiologie van MAS-defecten

Om inzicht te krijgen in de pathofysiologie van de verschillende MAS-aandoeningen op cellulair niveau, hebben we gebruik gemaakt van celmodellen. Hierbij hebben we een genetische verstoring aangebracht in de individuele MAS componenten in verschillende cellijnen. In deze MAS-deficiënte cellijnen hebben we vervolgens de omzettingen van een stabiel glucose-isotoop door het metabolisme getraceerd.

Serine is een belangrijk aminozuur in de hersenen en dient als voorloper van onder andere neuronale membraanlipiden en neurotransmitters zoals D-serine en glycine. Wanneer de serine-aanmaak verstoord is, kunnen neurologische aandoeningen het gevolg zijn. De synthese van serine is onder andere afhankelijk van de NAD⁺/NADH balans, en eerdere bevindingen tonen aan dat bij patiënten met een GOT2-deficiëntie een secundair defect in de serine biosynthese optreedt. Hierbij bleek serinesuppletie een effectieve behandeling voor het verlichten van het neurologische fenotype. We vroegen ons daarom af of de verstoorde NAD⁺/NADH balans in andere MAS-defecten eveneens leidt tot een verstoorde serinesynthese. Ons onderzoek laat inderdaad zien dat alle MAS-deficiënte cellen een verminderde serinesynthese hebben (**hoofdstuk 4**). Dit impliceert dat patiënten met andere MAS-aandoeningen ook gebaat kunnen zijn bij serinesuppletie.

Bij ons onderzoek kwam naar voren dat naast een verstoorde serinesynthese ook de gehele glycolyse in MAS-deficiënte cellen verstoord was, resulterend in een verhoogd G3P. Deze stof maakt deel uit van de glycerol fosfaat shuttle, een andere NADH shuttle waarin NAD⁺ gegenereerd wordt in het cytosol. De verhoogde

omzetting naar G3P kan duiden op een gunstig effect op de NAD^+/NADH balans. In MDH1-deficiënte cellen vonden we dat er naast de verhoogde omzetting ook een ophoping plaatsvond van de precursor van G3P, wat suggereert dat de glycerol fosfaat shuttle mogelijk niet in staat is om deze metabolietaanvoer effectief te verwerken (**hoofdstuk 5**). Daarnaast zijn er aanwijzingen dat de opstapeling van de precursor van G3P mogelijk een effect heeft op de serinesynthese, hoewel verder onderzoek vereist is om dit volledig te begrijpen.

De MAS is nauw verweven met de mitochondriële citroenzuurcyclus, ook wel bekend als de tricarbonzuur (TCA) cyclus, via MDH2. De TCA-cyclus speelt ook een belangrijke rol in het elektronentransport door de vorming van NADH , waar behalve malaat, ook glutamaat en pyruvaat belangrijke substraten zijn. Daarnaast is pyruvaat, het eindproduct van de glycolyse, een belangrijke elektronenacceptor die, na omzetting naar lactaat in het cytosol NAD^+ genereert. Het toevoegen van pyruvaat aan MDH1-deficiënte cellen heeft inderdaad een herstellend effect op het verloop van verstoorde NAD^+ -afhankelijke processen, zoals de glycolyse en serinesynthese, en fungeert eveneens als substraat voor de voortgang van de TCA cyclus (**hoofdstuk 5**). Daarnaast hebben we andere verstoorde routes in MDH1-deficiënte cellen geïdentificeerd, waaronder een verhoogde metaboliëflux naar de pentosefosfaatroute, resulterend in een accumulatie van ribitol. Deze verhoging van ribitol was tevens terug te vinden in de bloedspots van MDH1-deficiënte patiënten. De omzetting van sorbitol naar fructose in de polyolroute is NAD^+ -afhankelijk en een blokkade in deze route kan eveneens bijdragen aan de pathomechanismen van MDH1-deficiëntie.

De MAS speelt dus een integrale rol in tal van metabole processen, en een ontregeling ervan kan leiden tot energietekorten, met name in het centrale zenuwstelsel. Onze bevindingen bieden een fundament voor therapeutische strategieën die zich kunnen richten op herstel van zowel het energiemetabolisme als de NAD^+/NADH balans. Het ketogeen dieet, gekenmerkt door een hoog gehalte aan vetzuren en een laag gehalte aan koolhydraten, is momenteel de meest gevestigde en veilige behandelingsstrategie voor het aanpakken van een energietekort, waarbij tegelijkertijd de mogelijk toxische opstapeling van enkele metaboliëten vanuit glucose worden vermeden. Andere therapeutische mogelijkheden voor MAS-aandoeningen vereisen aanvullend onderzoek.

Deel 2 – Metabole fenotypering in zeldzame erfelijke anemieën

Erfelijke anemie

Bloedarmoede, ook wel bekend als anemie, is een aandoening waarbij er onvoldoende rode bloedcellen of hemoglobine in het bloed aanwezig zijn. Rode bloedcellen, de meest voorkomende cellen in ons lichaam, vervullen een belangrijke functie: het transporteren van zuurstof naar weefsels en het afvoeren van koolstofdioxide. Deze functie wordt mogelijk gemaakt door het aanwezige zuurstofbindende eiwit, hemoglobine. Tijdens hun rijping ontdoen rode bloedcellen zich van alle andere celorganellen om ruimte te maken voor hemoglobine. Hierdoor hebben ze slechts beperkte metabole activiteit en zijn ze voornamelijk afhankelijk van de anaërobe glycolyse voor energieproductie en de pentosefosfaatroute om hun antioxidant afweer te behouden. Daarnaast bevatten rode bloedcellen een unieke metabole route, de Rapoport-Luebering-shunt, waarbij de stof 2,3-bisfosfoglyceraat (2,3-DPG) wordt gegenereerd ter bevordering van de zuurstofafgifte aan weefsels. Anemie leidt tot vermoeidheid, kortademigheid en diverse andere symptomen, doordat het bloed minder efficiënt zuurstof kan transporteren. Erfelijke anemie omvat zeldzame aandoeningen die worden veroorzaakt door verschillende genetische afwijkingen in het functioneren of de aanmaak van rode bloedcellen. Dit proefschrift spitst zich toe op drie verschillende typen erfelijke anemie: Pyruvaat kinase deficiëntie, Diamond Blackfan anemie en erfelijke sferocytose.

1. Pyruvaat kinase deficiëntie (PKD) is een aandoening waarbij het enzym pyruvaat kinase (PK) niet goed werkt in de rode bloedcel. Omdat rode bloedcellen geen mitochondriën bevatten, is PK essentieel voor de productie van ATP. De verminderde ATP-productie leidt tot voortijdige afbraak van rode bloedcellen in de lever of milt. De behandeling bestaat voornamelijk uit bloedtransfusies.
2. Diamond Blackfan anemie (DBA) is een aandoening waarbij mutaties leiden tot een verstoring in de aanmaak van de rode bloedcellen. Patiënten hebben onder andere aangeboren misvormingen en een verhoogd risico op kanker. De behandeling bestaat uit toediening van glucocorticoïden en bloedtransfusies. Momenteel is stamceltransplantatie de enige curatieve behandeling voor DBA.
3. Erfelijke sferocytose (HS) ontstaat door mutaties die de membraaneiwitten in rode bloedcellen aantasten. Deze membraaneiwitten zijn cruciaal voor de flexibiliteit van rode bloedcellen terwijl ze door het vaatstelsel circuleren. De verstoring van membraaneiwitten resulteert in sferisch rode bloedcellen die

vastlopen en voortijdig worden afgebroken in de milt. Patiënten lijden hierdoor aan anemie, geelzucht, een vergrote milt en galstenen. De behandeling omvat regelmatige bloedtransfusies en in ernstige gevallen een verwijdering van de milt, geheel of gedeeltelijk.

Metabole fenotypering met een klinische toepassing

Om zeldzame erfelijke anemieën beter te begrijpen en de behandelingen ervan te verbeteren is aanvullend onderzoek noodzakelijk. In ons onderzoek hebben we untargeted metabolomics gebruikt als een nieuw onderzoeksinstrument voor erfelijke anemie, dat kan bijdragen aan zowel het versnellen van diagnostische procedures als het ontrafelen van de complexiteit van deze aandoeningen. We verzamelden bloedspots van patiënten met PKD, DBA en HS en gebruikten untargeted metabolomics om metabole vingerafdrukken vast te stellen. Binnen de medische gemeenschap wint machine-learning aan populariteit voor de analyse van omvangrijke datasets, dat door het ontdekken van patronen voorspellingen kan doen over patiënt uitkomsten, waarmee de snelheid en nauwkeurigheid van diagnoses kunnen worden verbeterd. In ons onderzoek hebben we laten zien dat met behulp van een machine-learning model patiënten met PKD en DBA te differentiëren zijn van gezonde controlepersonen op basis van hun metabole vingerafdruk (**hoofdstuk 6 en 7**). Daarnaast vonden we een verschil in de metabole vingerafdruk van DBA en congenitale dyserythropoëtische anemie (CDA), een klinisch en diagnostisch vergelijkbare ziekte. Deze bevindingen suggereren dat het mogelijk is om een onderscheidende diagnose te stellen op basis van een specifiek metabool profiel voor deze aandoeningen. Het vergroten van het aantal patiënten zou de statistische kracht van deze modellen versterken. Ondanks dat markeert het gebruik van metabolomics als middel voor het voorspellen van diagnostische resultaten een veelbelovend onderzoeksgebied dat kan bijdragen aan het verbeteren van diagnostiek en de uitkomsten voor de patiënt.

Naast een potentieel instrument voor ziektevoorspelling kan metabolomics ook worden ingezet ter ondersteuning van klinische besluitvorming. Zo ontdekten we een onderscheidende metabole signatuur bij DBA-patiënten die verschillende behandelingen ondergingen, wat mogelijkheden biedt om de respons op behandeling te monitoren of zelfs te voorspellen (**hoofdstuk 7**). Verder konden we onderscheid maken tussen patiënten met verschillende gradaties van klinische ernst bij HS (**hoofdstuk 8**). Idealiter kan metabolomics dus worden toegepast om voorspellers van behandelingseffectiviteit of klinische ernst te identificeren, waarmee individueel de effectiviteit van behandelingen kan worden verbeterd en de risico's op bijwerkingen kunnen worden verminderd.

Metabole inzichten in de pathofysiologie van RHA

Naast de mogelijkheden die een complete metabole vingerafdruk biedt, kan untargeted metabolomics ook dienen als instrument om hypothesen te formuleren voor toekomstig onderzoek, zoals het identificeren van pathofysiologische aanknopingspunten. Zowel HS als PKD worden gekenmerkt door hemolytische anemie, waarbij het openbreken van de RBC's resulteert in de afgifte van cel inhoud in het bloed. Enkele overeenkomsten tussen de metabole vingerafdrukken van beide ziekten waren verhoogde niveaus van polyamines en acylcarnitines. Bovendien vonden we een correlatie tussen deze metabolieten en het aantal RBC's en voorloper RBC cellen. Deze bevindingen suggereren dat deze metabolieten wellicht een rol spelen in de pathofysiologie van de ziekte of dat ze een indicatie zijn van de ernst van de aandoening.

Bloedspots in erfelijke anemie

Hoewel bloedspots al sinds de jaren zestig worden gebruikt in de hielprikscreening voor pasgeborenen, vinden ze tegenwoordig bredere toepassing in diverse onderzoeksvelden, zoals behandelingsmonitoring en farmacokinetiek. De niet-invasieve en snelle aard van het verkrijgen van bloedspots biedt tal van voordelen voor opslag en transport in diagnostische setting. Echter, bij het gebruik van bloedspots in de context van erfelijke anemie zijn er belangrijke overwegingen die verder onderzocht moeten worden. De veranderde bloedsamenstelling in anemie kan invloed hebben op de bloedverspreiding in de bloedspot en daarmee de gemeten metabolietconcentraties beïnvloeden. Het is nog onduidelijk of corrigeren voor bloedcel- of hemoglobinegehalte daadwerkelijk resulteert in een verbeterde interpretatie van de data.

Toepassingen van untargeted metabolomics in zeldzame ziekten

Dit proefschrift heeft zich gericht op het bestuderen van zowel metabole profielen in cellen als bij patiënten met zeldzame ziekten om de pathofysiologische kennis van deze ziekten te vergroten, wat potentieel kan bijdragen aan verbeterde diagnose- en behandelingsmogelijkheden. Maar hoe dragen deze inzichten nu uiteindelijk bij aan verbeterde patiëntenzorg? Een voorbeeld hiervan is dat het gebruik van untargeted metabolomics kan leiden tot de ontdekking van een biomarkerprofiel dat anders niet gedetecteerd zou worden, zoals G3P in MDH1-deficiëntie. Daarnaast hebben we inzichten verkregen in de onderliggende pathofysiologie van diverse zeldzame ziekten. Het is echter belangrijk te benadrukken dat de bevindingen van celmodellen verder moeten worden onderzocht in patiëntmateriaal om de klinische relevantie ervan te bevestigen. Daarnaast kan een ziekte-specifieke context, zoals een het gebruik van geavanceerde modellen zoals organoïden, organ-on-a-chip of diermodellen, helpen om de dynamische interacties tussen weefsels beter te begrijpen en de pathofysiologie van patiënten nauwkeuriger na te bootsen.

Hoewel untargeted metabolomics veel potentieel biedt voor toekomstig onderzoek vanwege zijn hypothese-genererende aard, zijn er nog steeds technische en data-gerelateerde uitdagingen, zoals de interpretatie van data. Integratie van metabolomics data met kennis uit het metabole netwerk of andere 'omics'-data kan het potentieel verder vergroten en daarmee de betekenisvolle interpretatie voor zowel diagnostiek als onderzoek verbeteren. Dit proefschrift toont aan dat untargeted metabolomics tal van toepassingen heeft, waaronder het ontdekken van biomarkers, het identificeren van nieuwe pathofysiologische aanknopingspunten, het vinden van therapeutische aangrijpingspunten, het evalueren van de klinische ernst en het beoordelen van respons op behandeling. Dankzij de veelzijdige aspecten van deze toepassingen heeft untargeted metabolomics het potentieel om het veld van zeldzame erfelijke ziekten te transformeren en zo een positieve impact te hebben op de patiëntenzorg.

LIST OF ABBREVIATIONS

AGC = aspartate glutamate carrier
Asp = aspartate
ATP = adenosine triphosphate
AUC = area under the curve
CDA = congenital dyserythropoietic anemia
CMST = cell membrane stability test
CoA = coenzyme A
DBA = Diamond Blackfan anemia
DBS = dried blood spots
DI-HRMS= direct infusion high resolution mass spectrometry
DHAP = dihydroxyacetone phosphate
EDTA = ethylenediaminetetraacetic acid
ETC = electron transport chain
FC = fold change
FH = fumarate hydratase
F1,6BP = fructose 1,6 bisphosphate
GAPDH = glyceraldehyde 3-phosphate dehydrogenase
GA3P= glyceraldehyde 3-phosphate
GC-MS = Gas chromatography mass spectrometry
GDH = glutamate dehydrogenase
Glu = glutamate
GOT = glutamate-oxaloacetate transaminase
GPD1 = glycerol phosphate dehydrogenase
G3P = glycerol 3-phosphate
Hb = hemoglobin
HC = healthy control
HMDB = human metabolome database
HEK293 = human embryonic kidney 293
HPO = human phenotype ontology
HS = hereditary spherocytosis
HSCT = hematopoietic stem cell transplantation
IEM = inborn errors of metabolism
IMD = inherited metabolic disease
KD = ketogenic diet
KO = knockout
LC-MS = liquid chromatography mass spectrometry
Mal = malate

MAS = malate-aspartate shuttle
MDH = malate dehydrogenase
MS = mass spectrometry
MRI = magnetic resonance image
MRS = magnetic resonance spectroscopy
m/z = mass to charge ratio
NAD(H) = nicotinamide adenine dinucleotide
OAA = oxaloacetate
OGC = oxoglutarate malate carrier
OGDH = oxoglutarate dehydrogenase
OMIM = online mendelian inheritance in man
PCA = principle component analysis
PEP = phosphoenolpyruvate
PHGDH = phosphoglycerate dehydrogenase
PLS-DA = partial least square discriminant analysis
PK = pyruvate kinase
PKD = pyruvate kinase deficiency
PPP = pentose phosphate pathway
Pyr = pyruvate
RBC = red blood cell
Rib5P = Ribose 5-phosphate
RHA = rare hereditary anemia
ROC = receiver operating characteristic
RP = ribosomal protein
RPE = ribulose phosphate epimerase
RPI = ribose 5-phosphate isomerase
RPS = ribosomal protein of the small subunit
RPL = ribosomal protein of the large subunit
R5P = ribulose 5-phosphate
SVM = support vector machine
S7P = sedoheptulose 7-phosphate
TALDO = transaldolase
TCA = tricarboxylic acid
THF = tetrahydrofolate
TKT = transketolase
WES = whole-exome sequencing
WT = wild type

X5P = Xylulose 5-phosphate

2-KB = 2-ketobutyrate

2-OG = 2-oxoglutarate

2,3-DPG = 2,3-diphosphoglyceric acid

3-PG = 3-phosphoglycerate

LIST OF PUBLICATIONS

Thesis

Broeks MH, Shamseldin HE, Alhashem A, Hashem M, Abdulwahab F, Alshedi T, Alobaid I, Zwartkruis F, Westland D, Fuchs S, Verhoeven-Duif NM, Jans JJM, Alkuraya FS. MDH1 deficiency is a metabolic disorder of the malate-aspartate shuttle associated with early onset severe encephalopathy. *Hum Genet.* 2019 Dec;138(11-12):1247-1257. doi: 10.1007/s00439-019-02063-z. Epub 2019 Sep 19. PMID: 31538237.

Broeks MH, van Karnebeek CDM, Wanders RJA, Jans JJM, Verhoeven-Duif NM. Inborn disorders of the malate-aspartate shuttle. *J Inher Metab Dis.* 2021 Jul;44(4):792-808. doi: 10.1002/jimd.12402. Epub 2021 May 24. PMID: 33990986; PMCID: PMC8362162.

Van Dooijeweert B*, **Broeks MH***, Verhoeven-Duif NM, Van Beers EJ, Nieuwenhuis EES, Van Solinge WW, Bartels M, Jans JJ, Van Wijk R. Untargeted metabolic profiling in dried blood spots identifies disease fingerprint for pyruvate kinase deficiency. *Haematologica.* 2021 Oct 1;106(10):2720-2725. doi: 10.3324/haematol.2020.266957. PMID: 33054133; PMCID: PMC8485668.

van Dooijeweert B*, **Broeks MH***, Verhoeven-Duif NM, van Solinge WW, van Beers EJ, Rab MAE, Nieuwenhuis EES, Jans JJM, Bartels M, van Wijk R. Metabolic Fingerprint in Hereditary Spherocytosis Correlates With Red Blood Cell Characteristics and Clinical Severity. *Hemasphere.* 2021 Jun 12;5(7):e591. doi: 10.1097/HS9.0000000000000591. PMID: 34131631; PMCID: PMC8196084.

van Dooijeweert B*, **Broeks MH***, van Beers EJ, Verhoeven-Duif NM, van Solinge WW, Nieuwenhuis EES, Jans JJ, van Wijk R, Bartels M. Dried blood spot metabolomics reveals a metabolic fingerprint with diagnostic potential for Diamond Blackfan Anaemia. *Br J Haematol.* 2021 Jun;193(6):1185-1193. doi: 10.1111/bjh.17524. Epub 2021 May 17. PMID: 33997957; PMCID: PMC8251760.

Broeks MH, Meijer NWF, Westland D, Bosma M, Gerrits J, German HM, Ciapaite J, van Karnebeek CDM, Wanders RJA, Zwartkruis FJT, Verhoeven-Duif NM, Jans JJM. The malate -aspartate shuttle is important for de novo serine biosynthesis. *Cell Rep.* 2023 Aug 29;42(9):113043. doi: 10.1016/j.celrep.2023.113043. PMID: 37647199.

In preparation

Broeks MH, Gerrits J, German HM, Zwartkruis FJT, Verhoeven-Duif NM, Jans JJM. Pyruvate reverses the metabolic consequences of malate dehydrogenase 1 deficiency.

Other

Jans JJM, **Broeks MH**, Verhoeven-Duif NM. Metabolomics in diagnostics of inborn metabolic disorders. *Curr Opin Syst Biol.* 2020 Mar;29:100409. doi:10.1016/j.coisb.2021.100409

Haijes HA, van der Ham M, Prinsen HCMT, **Broeks MH**, van Hasselt PM, de Sain-van der Velden MGM, Verhoeven-Duif NM, Jans JJM. Untargeted Metabolomics for Metabolic Diagnostic screening with automated data interpretation using a knowledge-based algorithm. *Int J Mol Sci.* 2020 Feb 1;21(3):979. doi: 10.3390/ijms21030979. PMID: 32024143; PMCID: PMC7037085

Willems HLDM, Silva Santos Ribeiro P, **Broeks MH**, Meijer N, Versteeg S, Malecki J, Falnes PO, Jans JJM, Eijkelkamp N. Inflammation-induced mitochondrial and metabolic disturbances in sensory neurons control the switch from acute to chronic pain. Submitted.

Edridge A, Abd-Elfarag G, Deijs M, **Broeks MH**, Cristella C, Sie B, Vaz F, Jans JJM, Calis J, Verhoef H, Demir A, Poppert S, Nickel B, van Dam A, Sebit B, Titulaer M, Verweij JJ, de Jong MD, van Gool T, Faragher B, Verhoeven-Duif NM, Elledge SJ, van der Hoek L, Boele van Hensbroek M. Parasitic, bacterial, viral, immune-mediated, metabolic, and nutritional factors associated with Nodding syndrome. *Brain Communications.* 2023 Aug 17. doi: 10.1093/braincomms/fcad223.

Lollinga WT*, **Broeks MH***, Abdulahad WH, Bijma T, Diepstra A, van den Born J, Hepkema BG, Heeringa P, Sanders JS. B-cell phenotyping before renal transplantation associates with cytomegalovirus infection, but not with biopsy-proven acute rejection. Lollinga, W.T. (2017). *The impact of cytomegalovirus in renal transplant recipients: From patient to cell.* [Thesis fully internal (DIV), University of Groningen].

*Authors contributed equally

Presentations

- 2019 Oral presentation, SSIEM, Rotterdam, The Netherlands: MDH1 deficiency is a metabolic disorder of the Malate-Aspartate Shuttle associated with early onset severe encephalopathy
- 2021 Oral presentation, European Metabolic Group, Online edition: Malate dehydrogenase deficiencies and serine biosynthesis (awarded)
- 2021 Podcast JIMD: inborn errors of the malate-aspartate shuttle. Accessible via: <https://soundcloud.com/user-109006120/malate-aspartate-shuttle-draft>

- 2021 Invited lecture ESN Najaars Symposium, Online edition: Fluxomics in cell models of the malate-aspartate shuttle
- 2022 Oral presentation, SSIEM, Freiburg, Germany: Inborn disorders in the malate-aspartate shuttle lead to disturbed NAD^+/NADH redox balance, glycolysis and defective serine biosynthesis

DANKWOORD/ACKNOWLEDGEMENTS

Na een uitdagende periode is dit proefschrift eindelijk tot stand gekomen. Ik wil dan ook van harte de vele mensen bedanken die mij hebben bijgestaan en gesteund gedurende dit promotietraject. Zonder jullie zou dit niet mogelijk zijn geweest!

Allereerst wil ik mijn oprechte dank uitspreken aan prof. dr. Nanda Verhoeven-Duif en dr. Judith Jans. Bedankt voor de kans om mijn promotieonderzoek onder jullie begeleiding uit te voeren. Dit heeft mij niet alleen de ruimte gegeven om te groeien als onderzoeker, maar ook als persoon. Met beperkte kennis van metabole ziekten en diagnostiek heb ik me volledig kunnen onderdompelen in een voor mij compleet nieuwe wereld met zeldzame single patients, metabole artsen, spoedjes, uitslagbrieven, massaspectrometrie, medische terminologie en 'praatbiochemie'. Jullie adviezen, vertrouwen en humor hebben mij erg geholpen. Nanda, jouw gerichte inzichten vormden een belangrijke leidraad wanneer door alle untargeted data het bos soms niet meer zichtbaar was. Dank ook voor het inspirerende voorbeeld dat je als vrouw in de wetenschap bent. Judith, jouw warme en enthousiaste begeleiding is het fundament van mijn traject geweest, en je enthousiasme en passie voor ons onderzoek werkte erg aanstekelijk. Jouw openheid over je eigen uitdagingen en lessen heeft me eveneens veel geleerd. Het was fijn om jou als mentor en klankbord te hebben, en bovendien ontzettend gezellig!

Ik wil mijn dank uitspreken aan de leden van de beoordelingscommissie - prof. dr. Hans Waterham, dr. Eva Brilstra, prof. dr. Roger Schutgens, prof. dr. Saskia van Mil en prof. dr. Riekelt Houtkooper – voor hun bereidheid om dit proefschrift te beoordelen, waarbij ik Hans en Eva ook wil bedanken voor de zitting in mijn PhD begeleidingscommissie. Prof. dr. Celia Berkers, prof. dr. ir. Boudewijn Burgering en prof. dr. Rob Scholten bedankt voor het zitting nemen in de promotiecommissie.

Gedurende mijn promotietraject heb ik de kans gehad om met velen samen te werken, en ik wil hen allemaal van harte bedanken. Allereerst veel dank aan de metabole artsen, patiënten en familieleden, want zonder hen verhaal en toestemming was dit onderzoek niet mogelijk geweest. Prof. dr. Fowzan Alkuraya and Hanan, thank you for your collaboration on the case of MDH1-deficiency, which laid a crucial foundation for future projects. Prof. dr. Ronald Wanders, gedurende onze samenwerking aan de malaat-aspartaat shuttle onderzoeken, zijn jouw enthousiasme voor het vak en eindeloze biochemische kennis van onschatbare waarde geweest. Dank daarvoor. Ook hartelijk dank aan prof. dr. Clara van Karnebeek voor de klinische inzichten in deze MAS-projecten. Graag bedank ik de sectie hematologie van het

CDL, met name dr. Richard van Wijk en dr. Marije Bartels. Ik ben dankbaar voor jullie samenwerking waarbij leuke en gezellige meetings een feit waren. Ook prof. dr. Edward Nieuwenhuis, prof. dr. Wouter van Solinge en prof. dr. Eduard Beers bedankt voor jullie waardevolle bijdrage aan de hematologie studies. Mijn grootste dank gaat hier uit naar mijn 'hemato-maatje' dr. Birgit van Dooijeweert. Terugdenkend aan onze live- en of Zoom meetings, waarbij we soms uren konden afdwalen in een of andere pathway, kon ik ook onze persoonlijke gesprekken erg waarderen. Ik ben trots op onze gezamenlijke prestaties en heel dankbaar dat jij mij als paranimf bij wil staan!

Mijn grote dank gaat ook uit naar dr. Fried Zwartkruis en Denise, een aanzienlijk deel van dit proefschrift is te danken aan de MASsa's cellijnen die jullie hebben gemaakt! Denise, bedankt voor de gigantische hoeveelheid celkweek die je zowel individueel als samen in ons MASTerplan hebt uitgevoerd. Wanneer je weer met de boodschappentas kwam shoppen op het metabole lab was jouw vrolijke aanwezigheid een feit. Fried, veel dank voor je scherpe blik en kritische inzichten. Daarnaast kon ik onze koffiegesprekken over wat data ook erg waarderen! Ook Susan wil ik bedanken voor haar bijdrage.

Kamergenoten van de donkere kamer! Gedurende mijn jaren op de afdeling is het daglicht op onze werkkamer zelden binnengedrongen, maar gedeelde smart is halve smart. Lennart, na anderhalf jaar in mijn promotietraject kwam jij als kamergenoot de kamer verlichtten met veel gezelligheid en gesprekken over de uitdagingen van het lab (en andere frustraties). Veel dank voor deze uitlaatklep en onze gesprekken over de 'mwah' van het leven. Ik hoop oprecht dat ook jij spoedig je PhD titel mag behalen (en het toch gaat vieren)! Nils, naast de gezellige en serieuze gesprekken, heel veel dank voor jouw hulp met alles. Hannah, ontzettend leuk dat jij verder gaat werken aan de malaat-aspartaat shuttle. Ook veel dank voor jouw hulp. Ik wens jullie beiden heel veel succes met de afronding van jullie promotie! Het was erg gezellig met jullie bij de borrels, pubquizes en het Freiburg congres. Ilja, ik was blij dat iemand mijn passie voor mooie plotjes deelde, maar daarnaast bleken we ook veel andere gedeelde interesses te hebben. Ik ben dankbaar voor onze vriendschap die is ontstaan en verdiept tijdens het afronden van mijn promotietraject, en dankbaar dat jij vandaag als paranimf naast me staat!

Ook wil ik de andere metabole mede-promovendi bedanken. Hanneke, bedankt voor je hulp bij mijn eerste stappen in mijn promotietraject, waarin je me erg op weg hebt geholpen. Bedankt voor al je wijze raad! Also Ruben, thank you for your support during the first part of my PhD. Loek, Marit en Suzan, ontzettend bedankt voor de gezellige lunch-wandelingen, het delen van ervaringen en de leuke uitjes. De

overnachting op unieke locatie (lees: 2-sterrenhotel met douche in de gang) tijdens ons eerste SSIEM congres in Rotterdam blijft toch een interessante herinnering. Sigrid en Titine, bedankt voor de gezelligheid en heel veel succes met het afronden van jullie promotietraject!

Heel veel dank aan alle medewerkers van het laboratorium metabole ziekten. Marjolein, veel dank voor je hulp en bijdrage bij het opzetten van het meten van alle flux-experimenten. Johan, jij bent onmisbaar voor vele projecten. Jouw vermogen om MS-methoden op verzoek te ontwikkelen en je 'eerste hulp bij massaspectrometrie' zijn van onschatbare waarde gebleken. Jolita, ik kon vaak bij je terecht met even een 'kort vraagje' tussendoor. Bedankt voor je hulp en waardevolle inzichten! Yuen-Fung en Maria, bedankt voor jullie hulp bij het werken met de DIMS. Nienke en Fini, bedankt voor de bio-informatische hulp. Daarnaast ook veel dank aan alle anderen: Ans, Mirjam, Gerda, Birgit, Raymond, Ramon, Deena, Isa, Helma, Karen, Harald, Martina, Wenru, Astrid, Suzana, Daniela, Arda, Aafke, Yvon, Monique, Berthil en Anke. De herfst, kerst en paas-lunches, buitendag, spelletjesavonden, pubquizes en borrels hebben stuk voor stuk bijgedragen aan de gezelligheid gedurende jaren. Ik heb veel geleerd van vele van jullie en kan terugkijken op een leuke tijd!

Studenten Gerben en Marieke bedankt voor jullie inzet in het ophelderen van de MDH1 pathofysiologie. Marieke, het was erg leuk om met je samen te werken. Ik ben blij dat je je weg naar een PhD positie hebt kunnen vinden en wens je veel succes met je traject! Daarnaast ook Sjoukje bedankt, ook al was je niet mijn student, de tijd die we samen doorbrachten was erg leuk!

Ook wil ik mijn nieuwe collega's in Leiden bedanken voor hun warme welkom en steun bij de laatste loodjes van mijn promotietraject. Prof. dr. Onno Meijer en dr. Jan Kroon, bedankt voor de kans om mijn postdoc bij jullie te doen. Ik kijk er naar uit om verder met jullie samen te werken.

Aniek, Lianne, Kim en Karin, fijn dat we na zoveel jaren vriendschap elkaar nog regelmatig zien. Ons (bijna) jaarlijkse uitstapje naar de Zwarte Cross is altijd een feestje! Karin, tafeltennismaatje sinds de basisschool, met jou uitgaan is een feest opzich. Veel dank voor je interesse en steun tijdens mijn promotietraject. Lisette, mijn fijne jumbo-collega! Na jarenlang wekelijks lief en leed gedeeld te hebben als collega's op de broodafdeling, is dat gelukkig niet gestopt toen ik vertrok. Ik ben dankbaar voor onze vriendschap.

Femke, vanaf de eerste week waren we maatjes toen we begonnen aan onze opleiding Life Science and Technology in Groningen. Hoewel onze paden leken te scheiden toen jij je PhD in Rotterdam begon, kwamen ze al snel weer samen met jouw verhuizing naar het PMC Utrecht en het begin van mijn PhD in het UMC Utrecht. Wonend in dezelfde flat in Zeist was ons leven weer herenigd en daar ben ik dankbaar voor. Bedankt voor je vriendschap, steun en het samen (poging tot) sporten en borrelen, die ik toch wel mis nu je inmiddels al bijna twee jaar aan je postdoc in Stockholm werkt. Ik ben blij dat je inmiddels bent gepromoveerd na een uitdagend traject! Ook Marjolein en Rosanne, bedankt voor jullie vriendschap. Rosanne, mooi hoe ook jij na je PhD je weg naar Zweden hebt gevonden voor je postdoc. Marjolein, alleen maar bewondering over hoe avontuurlijk je je leven invult. Ik hoop op een snelle 'croc's'-reunie!

Christian, zonder jou had dit proefschrift er hoogstwaarschijnlijk niet gelegen. Ook al zijn onze wegen sinds kort gescheiden, heel veel dank voor je onvoorwaardelijke steun gedurende mijn PhD traject.

Justin en Sarell, ik ben blij met de warme band die we als broer en zus hebben. Dank dat jullie er voor mij zijn.

Pap en Mam, bedankt voor alle kansen en het vertrouwen die jullie mij in het leven gegeven hebben. Jullie onvoorwaardelijke liefde en steun zijn onmisbaar.

CURRICIULUM VITAE



Melissa Henrike Broeks was born on September 23rd, 1994, in Zwolle, the Netherlands, to Martin and Herma Broeks. After obtaining her gymnasium diploma at the Thomas a Kempis College in Zwolle in 2012, she pursued a Bachelor's degree in Life Science and Technology, followed by a Master's degree in Biomedical Sciences at the University of Groningen. During her master's internship, she worked at the Rheumatology and Clinical Immunology group of the University medical Centre Groningen (UMCG), where she studied predictive insights in B-cells of renal transplant recipients. For her second internship, she worked at the Experimental Cardiology group in the UMCG, investigating biomarkers for heart failure with preserved ejection fraction. These internships raised a broad interest in biomedical sciences.

After obtaining her Master degree's, Melissa continued her academic career and started with her PhD in May 2018 at the Metabolic Diagnostic Lab at the UMC Utrecht. Under the supervision of Dr. Judith Jans and Prof. dr. Nanda Verhoeven-Duif, she focused on the application of untargeted metabolomics in rare inherited diseases, particularly disorders of the malate-aspartate shuttle and rare hereditary anemias. During her PhD, the analysis of untargeted metabolomics and stable isotope tracing data developed into a passion for puzzling with complex data. The results of her research were presented in this thesis and published in various peer-reviewed journals. Additionally, she presented her work at international conferences within the metabolic disease community and discussed her review about malate-aspartate shuttle disorders in a podcast.

Starting from April 2023, Melissa has been working as a postdoctoral researcher in the group led by Prof. dr. Onno Meijer at the Endocrinology Department of Leiden University Medical Centre, focusing on novel ligands for glucocorticoid receptors and transcriptomics.

